AIX-MARSEILLE UNIVERSITÉ
UNIVERSITÀ DEGLI STUDI DI GENOVA

ED 352 - PHYSIQUE ET SCIENCES DE LA MATIÈRE

DIPARTIMENTO DI FISICA
CENTRE DE PHYSIQUE THÉORIQUE

Thèse présentée pour obtenir le grade universitaire de docteur
Discipline: Physique Théorique

Flavio RONETTI

TRANSPORT DE CHARGE ET CHALEUR DANS LES SYSTÈMES TOPOLOGIQUES

Soutenance le 17/12/2018 devant le jury:

Maura SASSETTI	Università di Genova	Directeur de thèse
Thierry MARTIN	Université d'Aix-Marseille	Co-directeur de thèse
Laurent RAYMOND	Université d'Aix-Marseille	Examinateur
Fabio CAVALIERE	Università di Genova	Examinateur
Thomas SCHMIDT	Université du Luxembourg	Examinateur
Ludger WIRTZ	Université du Luxembourg	Examinateur

Contents

Résumé

Dans cette thèse, j'adresse le sujet fascinant et attirant du transport de charge électrique et de chaleur dans les systèmes Hall quantiques, qui sont parmi les exemples les plus célèbres des phases topologiques de la matière, en présence de potentiels électriques dépendantes du temps. L'intérêt de la communautè de physique de la matière condensée vers les systèmes topologiques a considérablement augmenté ces dernières années. Par exemple, il vaut la peine de se rappeler le prix Nobel pour la physique 2016 attribué aux Professeurs Thouless, Kosterlitz et Haldane pour leur contribution à l'étude des états topologiques de la matière. Ces états sont phases exotiques de matière, dont les propriétés sont décrites en termes des quantités qui ne dépendent pas des détails d'un système et qui sont très robuste contre des défauts et des perturbations.

En outre, l'intérêt pour les systèmes topologiquement protégés ne se limite pas à la physique de la matière condensée seulement, mais s'étend également à le domaine de l'informatique quantique: au fait, une nouvelle branche de cette discipline est apparue récemment, connu sous le nom de informatique quantique topologique, qui vise à tirer profit des propriétés émergents des systèmes topologiques pour coder et manipuler l'information quantique de façon plus robustes que avec des autres systèmes. Le premier et certainement un des exemples les plus célébres est l'effet Hall quantique, que l'on a découvert presque il y a quarante ans et attire toujours beaucoup d'attention du point de vue théorique et expérimental. Ce phénomène physique remarquable se produit dans des systèmes électroniques bidimensionnels dans la limite de forts champs magnétiques perpendiculaires. Après avoir imposé un courant le long d'une direction de l'échantillon, on mesure une tension dans la direction transversale qui aux tournants a provoqué une résistance transversale, linéairement proportionnelle au champ magnétique. Le comportement de la résistance transversale, généralement définie résistance de Hall, était conforme à la théorie classique du transport électronique diffusif de Drude et a permis d'examiner la nature de transporteurs de charge dans des métaux. Presque cent ans plus tard, cette sorte de mesure de Hall a été faite avec des électrons limités une région spatiale dans deux dimensions, connu comme des gaz électroniques bidimensionnels, qui se forme, par exemple, à l'interface de deux semi-conducteurs. En particulière, les expériences ont révélé que, dans des systèmes Hall quantiques, la résistance de Hall manifeste une quantification en termes de la unité minimale de résistance $R_K = h/e^2$, ainsi montrant des plateaux bien définis en fonction du champ magnétique, en forte contraste avec le comportement linéaire prévu selon la théorie classique.

La constant de proportionnalité est un numéro entier avec une exactitude plus grande qu'une partie par milliard. De façon intéressante, cette résistance n'est pas affecté par les propriétés spécifiques du système, puisqu'il dépend exclusivement de deux constants fondamentaux, la constante de Planck h et la charge électronique e.

La quantité $R_K = h/e^2$ est appelée résistance de Von Klitzing et, en raison de la précision extraordinaire de cette sorte de mesures, il est maintenant utilisé comme l'unité standard de résistance. Dans ce sens, on doit considérer la valeur de n un nombre entier par définition. Ce phénomène, connu comme l'effet Hall quantique entier, peut être compris d'une façon satisfaisante en recourant à une description quantique. Le résultat principal de ce traitement quantique-mécanique est que les niveaux d'énergie d'un électron placé dans un champ magnétique sont discrets et également espacés par un écart qui augmente linéairement avec le champ magnétique. Ces niveaux sont appelés niveaux de Landau, depuis le physicien russe L. Landau qui les a premièrement découverts. Le nombre de niveaux de Landau occupés est appelé facteur de remplissage. Une particularité des systèmes Hall quantique entiers est l'apparition des états de bord métalliques unidimensionnels sur les frontières du système. Le long de ce bord les particules se propagent avec une direction bien définie. Pour comprendre pourquoi, considérez une image semi-classique d'électrons contraints dans une région finie du plan. En présence d'un fort champ magnétique perpendiculaire la trajectoire est circulaire, avec un rayon qui diminue avec l'augmentation du champ magnétique. Pour des champs magnétiques suffisamment hauts, les particules décrivent des très petites orbites circulaires dont le rayon est beaucoup plus petit que les dimensions linéaires du système et aucune conduction ne peut avoir lieu. Aux bords, les électrons frappent le mur avant l'achèvement d'un cycle complet et, en conséquence des collisions multiples avec la frontière, ils se déplacent le long du bord décrivant des orbites sautantes. En effet, tant que nous restons loin des bords, pour chaque valeur possible du niveau de Fermi la bande occupée la plus haute est toujours séparée de la bande vide la plus basse par l'écart d'énergie. Cependant, la situation est trés différente prés du bord du système. Ici le spectre est changé en ce qui concerne les niveaux de Landau, en raison du fait que la fonction d'onde doit disparaître au bord. En conséquence, le niveau de Fermi croise toujours le spectre d'énergie tant sur le côté droite que sur le côté gauche d'une barre Hall quantique, provoquant des états de bord métalliques. Il est clair que chaque niveau de Landau remplis induit un état sur chaque bord, signifiant qui existe une correspondance biunique entre des niveaux de Landau remplis et des états de bord. Quand le facteur de remplissage est égal à n, un nombre total de n états de bord émerge. Ainsi, la résistance totale d'un bar Hall quantique est $R = nh/e^2$.

Un rôle clé dans la physique de l'effet Hall quantique est joué par le désordre, qui a souvent un effet dramatique sur des propriétés de transport. Le résultat important est que cette image intuitive d'états de bord n'est pas significativement changée par le désordre. Au contraire, le désordre est même utile dans ce cas, comme il aide la localisation des états loin des bords en correspondance des plateaux de résistance de Hall, tandis que les états de bord restent étendus et portent un courant même en présence de désordre dans le système.

La robustesse d'états de bord des systémes Hall quantiques peut être comprise en regardant la résistance de Hall d'une autre perspective. Observons que la résistance de Hall est directement liée au facteur de remplissage, qui est une propriété globale du bar de Hall, signifiant qu'il n'est pas possible de le décrire en termes d'un paramètre d'ordre local. Ce point, ensemble avec le fait qu'aucune symétrie n'est cassée pendant la transition entre les plateaux différents, aidé dans la compréhension même si les phases du effet Hall quantique décrites par des facteurs de remplissage différents ne pouvaient pas être classifiées en termes de la théorie de Landau-Ginzburg de transitions de phase. États de la matière qui sont caractérisés par des paramètres

globaux et qui sont au-delà du paradigme de Landau-Ginzburg sont appelés des états topologiques: l'effet Hall quantique entier était juste le premier exemple de beaucoup de systèmes topologiques qui ont été successivement découverts.

Le concept de topologie est emprunté aux mathématiques, oú toutes les structures avec un certain nombre de trous sont appelées topologiquement équivalentes et définissent des certaines classes topologiques: une figure géométrique peut être transformée en objet topologiquement distinct seulement par une transformation brusque qui modifie son nombre de trous. Par analogie, les plateaux différents, séparés par un écart et associés aux valeurs différentes de la résistance de Hall, peuvent être interprétés comme des phases quantiques topologiquement différentes. Une transition entre les classes topologiques, appelées la transition de phase topologique, est possible seulement après la fermeture de cet écart. C'est exactement ce qui arrive quand la résistance de Hall saute d'un plateau à l'autre.

L'interprétation topologique des états des systèmes Hall quantique fournit aussi un autre point de vue sur les canaux de bord précédemment discutés. Quand deux phases topologiques distinctes sont réunie, à leur interface une transition de phase topologique doit arriver: l'écart doit fermer. En particulier ceci arrive à l'interface entre une phase de Hall quantique et le vide: ceci explique l'existence d'états sur la frontière d'une barre de Hall quantique d'un point de vue topologique. De plus, le nombre de ces états de bord est déterminé par le facteur de remplissage. Cela signifie que la structure et la robustesse des états de bord sont profondément liées aux propriétés de la phase Hall quantique correspondante.

En 1982 D. C. Tsui, H. L. Stormer et des collègues ont rapporté un comportement inhabituel de la résistance de Hall. Pour un échantillon avec la mobilité plus haute et soumis à un champ magnétique plus intense que ceux utilisés par von Klitzing, ils ont observé l'apparition d'un plateau à un facteur de remplissage fractionnaire. Plus tard les plateaux ont été mesurés en correspondance à beaucoup d'autres valeurs fractionnaires de remplissage de niveau de Landau : cette phénoménologie particulière, que l'on ne peut pas expliquer en termes de l'image physique donnée pour l'effet Hall quantique entier, a été appelée l'effet Hall quantique fractionnaire. Contrairement au cas entier, l'explication physique d'effet de Hall quantique fractionnaire ne peut pas négliger la corrélation entre les électrons. Une première interprétation théorique de ces résultats expérimentaux a été publiée par Laughlin en 1983. Il s'est rendu compte que l'ingrédient manquant dans l'interprétation théorique d'effets Hall quantiques était les interactions entre électrons et que l'effet Hall quantique fractionnaire doit provenir d'un état quantique fortement corrélé. Comptant sur les propriétés analytiques de la fonction d'onde d'un électron dans le plus bas niveau de Landau et surtout sur une intuition physique brillante, il a mis au point une fonction d'onde variationnelle pour décrire la formation d'un nouveau type de liquide quantique pour un sous-ensemble spécifique de facteurs de remplissage fractionnaires, nommé "l'ordre de Laughlin". Une compréhension qualitative pour la stabilité d'états au facteur de remplissage fractionnaire peut être dessinée recourant à une image simple d'électrons interagissant. Dans niveaux de Landau partiellement remplis, il y a une liberté énorme de remplir la barre de Hall d'électrons. En présence de répulsion entre des électrons, notre liberté de les distribuer est réduite. Commençons à nous concentrer sur le cas idéal d'un champ magnétique infini. La longueur magnétique est zéro et les états sont localisés : les électrons ont donc la tendance à cristalliser en minimisant leur énergie d'interaction. Un état unique est formé, appelé le cristal de Wigner, qui est radicalement distinct de la phase Hall fractionnaire. Quand le

champ magnétique est baissé aux valeurs finies, les fonctions d'onde électroniques superposent et ils ne peuvent pas former désormais une structure cristalline. Pour certains facteurs de remplissage, ils forment un liquide quantique fortement corrélé, qui peut être décrit en termes d'une fonction d'onde unique à plusieurs corps. Une des conséquences de grande portée qui ont été présentées par l'idée de Laughlin est la prédiction que les excitations élémentaires de systèmes de Hall quantiques fractionnaires sont quasi-particules avec charge et statistique fractionnaire. Dans trois dimensions, les particules quantiques identiques peuvent être distinguées dans deux classes principales selon la statistique de change de leur fonction d'onde à plusieurs corps: bosons et fermions. Dans le premier cas, la fonction d'onde est inchangée par l'échange de deux particules; dans le deuxième, la fonction d'onde choisit simplement un signe moins. En deux dimensions, une troisième classe de particules existe, qui ne sont ni bosons, ni fermions, et qui sont appelé anyons. Quand deux anyons sont échangés la fonction d'onde à plusieurs corps des systèmes est multipliée par un numéro complexe de module un, avec une phase qui peut acquérir tout valeurs. En considérant toute la fonction d'onde à plusieurs corps possible dans deux dimensions, on peut distinguer entre deux classes séparées. Quand l'ordre d'échanges n'affecte pas la phase acquise par ces fonctions d'onde à plusieurs corps, nous traitons anyons abelian. Au contraire, si l'état final obtenu après plusieurs échanges dépend de cet ordre, anyons est appelé non-abelian. La statistique fractionnaire de quasi-particules de Laughlin et des quasi-trous est dictée par le facteur de remplissage spécifique de la correspondant état. Les états appartenant à l'ordre de Laughlin sont tout anyons abelian. Remarquablement, des états de bord unidimensionnels surgissent aussi dans l'effet de Hall quantique fractionnaire et leurs excitations héritent la charge et les propriétés statistiques du système. Un grand effort théorique a été fait pour décrire l'effet de Hall quantique fractionnaire en termes de théories efficaces des champs basées sur la théorie de champ de jauge topologique de Chern-Simon abelian. Ces théories efficaces contiennent les propriétés particulières des états, comme le facteur de remplissage, la charge et la statistique des excitations. Ce rapport profond entre la physique de matière condensée et des théories quantiques topologiques des champs représente une occasion unique de valider des concepts exotiques typiquement présentés dans la physique d'haute énergie au moyen des expériences effectuées dans des conditions qu'on peut obtenir facilement dans les laboratoires. En limitant ces théories sur la frontière, présentée par la taille finie de l'échantillon, on a une description efficace pour les états de bord du système. Les excitations héritent la charge et les propriétés statistiques de celui dans la plupart. Pour le facteur se remplissage que nous considérerons les états de bord sont décrits en termes de champs bosonic, conformément à la théorie de Tomonaga-Luttinger pour des électrons interagissant dans une dimension. Dans ce modèle, il est possible de calculer les propriétés de transport à travers le formalisme des fonctions de Green hors de l'équilibre en tenant compte de la présence des interactions électroniques. Pour décrire le système en l'absence d'interactions j'utiliserai le formalisme de la matrice de diffusion stationnaire ou dépendant du temps, que peut constituer une technique polyvalente pour l'étude des propriétés de transport. La longueur de cohérence assurée par la protection topologique garantit d'avoir accès à la nature ondulatoire des électrons. Cette enquête peut être poussée à sa limite fondamentale en explorant le transport quantique au niveau d'électrons individuels. Cette idée incarne le coeur d'un nouveau domaine de la recherche, connu comme la l'optique quantique électronique. Ce champ naissant vise à manipuler des électrons un à un dans des conducteurs

balistiques, cohérents. De cette façon il est possible de reproduire des expériences quantiques-optiques et des configurations dans des dispositifs de matière condensée, utilisant des fermions (des électrons dans des systèmes mesoscopic) au lieu des bosons (des photons dans des guides d'ondes et des cavités optiques). Á cette fin un effort énorme a été fait vers la réalisation des source à d'électrons individuels, qui représentent clairement un bloc de construction crucial pour réaliser chaque expérience quantique-optique avec des systèmes électroniques. La première proposition pour extraire un électron individuel de la mer de Fermi remplie a été théoriquement discutée par Buttiker et des collaborateurs: le condensateur mesoscopic. Il consiste de un point quantique connecté à un gaz électronique bidimensionnel par un contact quantique, où le contrôle périodique des niveaux d'énergie mène à l'injection alternée d'un électron et un trou dans le système pendant chaque période. Un protocole polyvalent pour émettre d'une façon contrôlable des électrons individuels le long des canaux des conducteurs quantiques peut être mis en oeuvre en recourant au principe apparemment simple d'appliquer un potentiel dépendant de temps à un conducteur quantique. Les électrons peuvent être émis dans un système mesoscopic aussi en employant un potentiel indépendant du temps. Néanmoins, ce potentiel ne peut pas être utilisé comme une source réglable des électrons individuels. Dans ce sens, on doit déclencher l'émetteur d'électrons individuels avec une tension dépendante du temps pour réaliser la manipulation contrôlable d'électrons exigés pour des buts expérimentaux. Le défi principal, dans ce cas, a consisté en ce qu'une tension dépendant du temps exciterait généralement des paires d'électron-trou neutres indésirables, gâtant ainsi à son coeur l'idée d'une source d'électrons individuels. Le tournant pour surmonter cette question était la prédiction théorique par Levitov et ses collaborateurs qu'un train périodique d'impulsions Lorentzian, portant un nombre entier de particules par période, peut injecter des excitations électroniques minimales exemptes des paires d'électron-trou supplémentaire, en ensuite nommé levitons. Pour leurs propriétés fascinantes, levitons a été proposé comme qubits pilotant et comme une source d'intrication quantique avec des applications attirantes pour le traitement d'informations quantique. De plus, les protocoles de tomographie quantiques capables de reconstruire leurs fonctions d'onde ont été proposés et réalisés expérimentalement. Tandis que la mise en oeuvre de sources d'électrons individuels n'a pas été une tâche insignifiante, les analogues en matière condensés des les composants expérimentaux de l'optique quantique peuvent être trouvés d'une façon plus naturelle. Comme discuté, les guides d'ondes pour des photons peuvent être remplacés par les états de bord balistiques de systèmes de Hall quantiques. De plus, le rôle de séparateur de rayon électronique, qui devrait imiter le miroir semi-argenté d'optique conventionnelle, peut être joué par un contact de point quantique, où les électrons sont reflétés ou transmis avec une probabilité contrôlable. Un accomplissement fondamental de l'électronique optique quantique a été la mise en oeuvre de l'interféromètre Hong-Ou-Mandel, où les électrons empiètent de l'autre côté d'un QPC avec un retard réglable. En exécutant cette sorte d'expérimente, il est possible de rassembler des informations sur les formes des paquets d'onde électroniques empiétant et mesurer leur caractère non distinguable. Par exemple, quand deux états électroniques indiscernables et cohérents entrent en collision simultanément au QPC le bruit de charge disparaître, montrant ainsi le "dip" de Pauli. Ce dip peut être interprétée en termes d'effets d'anti-bunching liés á la statistique Fermi d'électrons. L'interféromètre Hong-Ou-Mandel peut ainsi être employé pour tester si la decoherence et le déphasage, induit par des interactions électroniques-électroniques, ré-

duisent le caractère non distinguable d'électrons entrants en collision. Malgré des analogies évidentes et des ressemblances avec l'optique quantique photonique traditionnelle, l'optique quantique électronique apporte deux nouvelles caractéristiques qui sont á la base des caractéristiques d'une systèmes électroniques. Premièrement, les états de photon individuel sont d'habitude créés sur un vide quantique vrai (c'est-á-dire l'état avec zéro particules), tandis que des états d'électron individuel sont toujours produits au-dessus d'un état complètement différent avec sa propre dynamique, la mer de Fermi remplie. Néanmoins, un analogue fermionique de la théorie de cohérence optique de Roy J. Glauber peut être développé. Même ce qui est plus important, des systèmes de matière condensée peut être lourdement affecté par des interactions et l'état d'un système fermionique peut montrer des corrélations.

Par exemple, l'effet Hall quantique fractionnaire est un exemple paradigmatique des conséquences dramatiques des interactions entre électrons. Dans un travail récent on a montré que les conditions pour des excitations électroniques minimales ne sont pas affectées dans l'effet Hall quantique fractionnaire. Ici la notion de leviton a été étendue aux systèmes interagissant de la séquence de Laughlin et il a été démontré que des impulsions Lorentzian portant charge entière représentent le potentiel le plus propre malgré les porteurs fondamentaux étant des quasi-particules avec la charge et la statistique fractionnaire.

Ce fait prouve que les levitons sont robustes même à la présence d'interaction entre électrons. En regardant ce résultat d'une autre perspective, cela signifie que nous n'avons pas toujours identifié de caractéristique qui marque une différence saisissante dans les propriétés de levitons entre la phases non interagissant ou les phases fortement corrélées. Une des parties originales de cette thèse s'est concentrée sur le problème lié à l'effet de fortes interactions sur la propagation en temps de paquets d'onde des levitons dans l'effet Hall quantique fractionnaire. En effet, en raison de leur nature solitonique, les levitons sont des particules assez indépendantes. De la même façon de solitons, plusieurs levitons différent sont libre de se propager le long des états de bord électroniques unidimensionnels et peuvent être superposé de façon contrôlable, formant ainsi des états à plusieurs corps appelés le multi-levitons. Néanmoins, des configurations auto-organisés et corrélés de solitons ont été récemment rapportées dans le domaine optique. Une question fascinante est si un phénomène semblable peut être observé aussi pour levitons dans des états de bord de l'effet Hall quantique entier. Il est bien connu que, dans un système électronique unidimensionnel, l'interaction entre électrons affecte considérablement les propriétés de particules, induisant, par exemple, l'arrangement d'électrons dans une configuration régulière et statique dans l'espace. Ce phénomène est connu comme la cristallisation à et son homologue de taille fini est nommé la molécule de Wigner. De tels états fortement corrélés se manifestent comme un arrangement régulier de la densité électronique qui oscille autour des positions fixes pour minimiser l'énergie d'électrons. En particulier un système contenant des électrons exposera, en présence d'une forte interaction, un modèle oscillant avec exactement N maxima. De plus, quand la force d'interaction est augmentée, l'amplitude d'oscillation est améliorée aussi. Dans des états de bord d'effet Hall quantique fractionnaire, la connexion entre le temps et l'espace donné par la chiralité ouvre la voie à la réalisation possible de la version en temps réel de cette cristallisation induite par interaction en appliquant des impulsions de tension dépendant de temps directement aux canaux de bord. De toute façon, la densité électronique pourrait exposer des oscillations même dans le cas non-interagissant, par exemple, en raison des effets de taille finis (un phénomène

connu comme les oscillations de Friedel). Pour identifier la formation d'une configuration d'une molécule de Wigner, il est ainsi nécessaire d'examiner directement les corrélations électroniques, en se concentrant sur le corrélateur densité-densité. Un comportement oscillant dans un tel correlator est considéré une preuve catégorique pour la formation d'une molécule de Wigner. Néanmoins, les observations expérimentales de la cristallisation de Wigner sont tout à fait difficiles, puisqu'ils exigent pour explorer un arrangement statique d'électrons sans le perturber. Une image de la structure réelle-spatiale d'une molécule de Wigner a été réalisée seulement dans une expérience récente. Pour réaliser cette observation, une sonde faite par un nanotube carbonique a été employée. La taille microscopique de cette sonde et le grand contrôle expérimental de cela a permis d'obtenir un balayage imperceptiblement invasif d'une molécule de Wigner. De toute façon, le corrélateur densité-densité ne pouvait pas être évaluée. Nous proposons des états appartenant à la séquence de Laughlin, où un seul mode existe sur chaque bord, comme un banc d'essai pour observer la cristallisation des multi-levitons dans des systèmes de matière condensés. Ici, la densité de charge reflétée par un contact de point quantique montre une structure pointue en conséquence du réarrangement induit par interaction dans le domaine de temps, dans le contraste ouvert avec le profil sans traits distinctifs observé dans le cas d'entier. Pour confirmer le caractère corrélé de l'état de cristal, nous démontrons que ces caractéristiques produisent des minima inattendues dans le corrélateur courant-courant (qui est proportionnel à le corrélateur densité-densité) dans un interféromètre Hong-Ou-Mandel, qui sont observable avec la technologie contemporaine. Remarquablement, la densité de paquet d'onde des multi-levitons avant le tunnelling au QPC ne montre pas de différence qualitative entre le cas entier et le cas fractionnaire. On attend cependant que le tunnelling non-linéaire, typique de la phase fractionnaire interagissant, influence la propagation de levitons après la dispersion au QPC. En effet, en raison du contexte fortement corrélé, le multi-levitons que passent par le QPC sont réarrangés dans une configuration oscillant avec un certain nombre de maxima égale exactement au nombre de particules composant l'état, indépendamment de chaque autre paramètre. L'amplitude des oscillations augmente avec la diminution du facteur se remplissant (c'est-à-dire pour des corrélations plus fortes). Dans l'analogie avec d'autres phases fortement corrélées dans la matière condensée, nous interprétons cette structure comme une cristallisation de l'état de multi-levitons. Cependant, par contraste avec la cristallisation de Wigner, l'arrangement induit par interaction ne montre pas un profil statique, mais plutôt l'apparition d'une structure régulière dans le temps et non seulement dans l'espace. En raison de la nature de levitons, ce processus présente une analogie fascinante avec la formation de cristal de solitons optiques en présence d'un environnement non-linéaire, bien que dans un contexte complètement différent.

Une observation directe de la densité oscillante exigerait une mesure en temps réel du courant avec une résolution temporelle extrêmement haute. De plus, cette observation seule ne serait pas la preuve conclusive du processus de cristallisation. Pour indubitablement relier les oscillations de la densité à la cristallisation de levitons, on doit examiner le corrélateur densité-densité ou courant-courant. La nature très spéciale du cristal de multi-levitons, qui n'est pas limité à une région spatiale finie, mais se déplace plutôt rigidement le long des bords, nous laisse prévoir un test expérimental basé sur les corrélations de deux états cristallisés. Nous proposons d'exécuter une mesure, beaucoup plus faisable, du bruit à fréquence zéro dans une configuration expérimentale Hong-Ou-Mandel. Dans cette configuration, deux trains

identiques de levitons entre en collision au QPC retardé par un décalage de temps réglable. On attend à ce qu'un processus de cristallisation véritable se manifeste comme des oscillations dans le bruit analysé comme une fonction du retard. Comme note à côté, nous observons que les mesures de corrélateur intensité-intensité sont de façons analogues exécutées pour explorer la cristallisation de solitons dans le domaine optique.

Nous remarquons d'abord que l'interférence complètement destructive entre les deux signaux arrive toujours au retard zéro, que le système interagisse ou non. Cela montre que les interactions entre électrons dans les états de Laughlin n'incitent pas d'effets de decoherence. Pour l'état composé par un levition individuel, le corrélateur densitè-densitè expose le même comportement pour facteurs de remplissage entiers et fractionnaires. Ceci est lié au fait que le tunneling de un seul leviton produit un signal simple sans structure de sommet/vallée interne. Pour l'état de multi-levitons, le réarrangement de levitons produit des caractéristiques particulières qui distinguent entre la phase non interagissant et la phase fortement corrélée. Ces caractéristiques identifient les effets de la phase fractionnaire fortement corrélée sur les excitations des levitons, dans la frappe du contraste avec la phase non corrélée. Ici nous soutenons que le réarrangement de levitons doit être lié au processus non autrefois rapporté de cristallisation de multi-levitons dans des états de bord fractionnaire. Donc, l'apparence de maximums locaux et de minimums dans le corrélateur courant-courant aux facteurs de remplissage fractionnaires prouve l'existence d'un cristal des levitons dans le domaine de temps induit par des interactions. En augmentant le ratio entre la largeur des impulsions et la période, l'amplitude maximale-à-vallée d'oscillations est améliorée pour des facteurs de remplissage fractionnaires, tandis que pour le cas d'entier la situation est qualitativement inchangée. L'inconvénient principal est que certaines des oscillations qui sont clairement visibles pour des impulsions plus aigu« s sont maintenant perdues, puisque les impulsions appartenant aux périodes voisines commencent à se chevaucher significativement. Finalement, il vaut la peine de noter que le même comportement du ratio peut être observé pour tous les facteurs de remplissage dans l'ordre Laughlin. Une telle universalité nous dit que les interactions dans des états fractionnaire de Laughlin sont toujours assez fortes pour inciter une cristallisation complète.

Un deuxième sujet majeur que j'ai examiné dans cette thèse est relaté aux propriétés de transport de chaleur de levitons dans la séquence de Laughlin de l'effet de Hall quantique. L'intérêt dans des systèmes de Hall quantiques a été principalement consacré à ses propriétés électriques de transport, en raison des nombreux phénomènes physiques fascinants liés à ses états de bord chiral et des excitations fractionnaire. Néanmoins, la charge n'est pas le seul degré de liberté intéressant qui pourrait être examiné dans le transport quantique. Dans le passé, on a surtout considéré des flux de chaleur dans des petits conducteurs quantiques comme un effet nuisible dans des expériences. En effet, le contrôle expérimental de flux de chaleur dans des dispositifs mesoscopic a représenté un grand défi du point de vue technique, qui a été surmonté seulement ces dernières années. En effet, quelques expériences révolutionnaires récentes ont stimulé l'enquête aussi dans la direction du transport de chaleur au nanoscale. Des nouveaux défis fascinants posés en prolongeant des concepts comme la récolte d'énergie, la chaleur conduite et le transport d'énergie, l'échange d'énergie dans des systèmes ouverts et des théorèmes de dissipation de fluctuation au royaume quantique ont abouti à un grand progrès du champ de thermodynamique quantique. Dans ce contexte, l'enquête du transporte de chaleur dans

le régime balistique, où les électrons se propagent dans de canaux avec une transmission parfaite, est fondamental pour avoir accès à la limite quantique de phénomènes thermiques. Bien sûr, un rôle prédominant est joué par les états de bord de systèmes de Hall quantiques: le transport cohérent et la manipulation de flux de chaleur ont été rapportés dans des systèmes de Hall quantiques. De façon intrigante, la quantification de conductance de chaleur a été observée dans les systèmes Hall quantiques entiers et fractionnaires. De cette façon, des informations suffisantes et de valeur sur ces états particuliers de matière, complémentaire aux résultats bien établis associés au transport de charge, sont maintenant disponibles avec des implications intéressantes aussi pour le calcul quantique. Comme déjà discuté, l'optique quantique électronique a dû correctement réviser des expériences d'optique quantiques se concentrant sur les propriétés de transport de charge d'excitations électroniques individuels. Néanmoins, une nouvelle perspective sur l'optique quantique électronique a été aussi déclenchée par l'intérêt naissant pour les propriétés de transport de chaleur d'excitations électroniques individuels. L'étude des fluctuations est un outil extrêmement puissant pour examiner la réponse de canaux de bord de l'effet Hall quantiques aux sources des électrons individuels. En plus des fluctuations de courant de chaleur, aussi corrélateur entre la courant de charge et de chaleur a attiré beaucoup d'attention en raison de leur relation avec les propriétés thermoélectriques d'un système. Une question naturelle surgit immédiatement quand on considère la dynamique de chaleur dans l'électronique optique quantique: quel genre d'énergie de tension provoque des états d'excitation minimaux pour le transport de chaleur dans des conducteurs mesoscopic. À cette fin, nous étudions la conduction de chaleur le long des états de bord topologiquement protégés de l'effet Hall quantique. Nous analysons les fluctuations de courant de chaleur aussi bien que les corrélations de chaleur et charge mixte quand les types différents d'impulsions de tension périodiques sont envoyés au conducteur et divisés d'un QPC. Commençant du régime dc de tension, où des relations simples entre des bruits et des courants peuvent être tirées dans l'esprit de la formule célébré de Schottky, nous présentons les signaux d'excès pour des fluctuations de chaleur et mixtes, qui mesurent essentiellement la différence entre les bruits de fréquence zéro et leurs signaux de référence respectifs dans la configuration avec un potentiel indépendant de temps. La disparition des signaux d'excès du bruit mixte et de chaleur est ainsi utilisée pour garnir de signaler l'occurrence d'un état d'excitation minimal pour le transport de chaleur dans le régime de Hall quantique. Avec cet outil puissant nous manifestons que les états minimaux pour le transport de chaleur peuvent être réalisés seulement quand le potentiel de tension prend la forme d'impulsions Lorentzian portant un entier multiple de la charge électronique, c'est-à-dire quand levitons est injecté dans les états de bord de Hall quantiques. Nous étudions ce problème tant dans le régime entier que dans le régime fractionnaire. Nos résultats montrent une robustesse saisissante contre des interactions, puisque les levitons représente toujours des états d'excitation minimaux malgré la physique très non-linéaire arrivant au QPC en raison des excitations collectives particulières des états fractionnaire de Laughlin. Ayant reconnu les levitons comme le bloc de construction fondamental pour le transport de chaleur, nous nous tournons alors vers une deuxième question centrale, qui traite la robustesse comme des états d'excitation minimaux des multiples impulsions Lorentzian qui se superposent. En effet, Levitov et des collaborateurs ont démontré que N levitons voyageant par un conducteur quantique avec la transmission basse représente N tentatives indépendantes de passer la barrière, avec le bruit total non affecté par la

superposition. Ce n'est plus garanti quand nous cherchons les quantités qui, comme le courant et le bruit de chaleur, ont une dépendance non-linéaire au potentiel. De plus, d'autres non-linéarités surgissent comme une conséquence naturelle de la physique de l'effet Hall quantique fractionnaire, qui provoque des lois de pouvoir avec des exposent non entiers. Nous montrons que, tandis que les courants et les bruits sont sensibles au nombre réel de particules envoyées au QPC, les signaux d'excès disparaissent toujours pour la superposition arbitraire d'un nombre entier de levitons. On conclut alors que les levitons montrent une stabilité remarquable même en ce qui concerne des propriétés de transport de chaleur, combinées avec la robustesse également surprenante dans le liquide Hall fortement corrélé. Ceci fournit une nouvelle preuve de l'unicité de l'état de levitons dans le régime Hall quantique. Enfin, nous abordons le problème du bruit de chaleur produit par levitons injecté dans un interféromètre Hong-Ou-Mandel dans le régime Hall quantique fractionnaire. Nous démontrons que le bruit dans cette expérience de collision ne peut pas être reproduit dans une configuration avec un seul potentiel, par contraste avec ce qui a observé dans le casse de bruit de charge. Néanmoins, la collision simultanée de deux levitons identiques mène toujours à une suppression totale même pour le bruit de chaleur dans un interféromètre Hong-Ou-Mandel à tous les facteurs de remplissage, malgré la présence d'excitations de quasiparticule anyonic émergentes dans le régime fractionnaire. De façon intéressante, les corrélations fortes caractérisant la phase fractionnaire sont responsables d'une configuration oscillant remarquable du bruit de chaleur, qui est complètement absent dans le cas d'entier, en accorde avec la cristallisation de charge de multi-levitons.

Introduction

In recent years, a great interest has been addressed in the condensed matter community towards new phases of matter, whose properties are described in terms of quantities that do not depend on the details of a system. These new phases and their novel properties have been termed *topological*, a concept borrowed from the language of mathematics [1–4].

The first and certainly one of the most famous examples is the quantum Hall effect [5–8], which was discovered almost forty years ago and still attracts a lot of attention from the theoretical and experimental point of view. These remarkable physical phenomenon occurs in two-dimensional electron systems in the presence of strong perpendicular magnetic fields. In quantum Hall systems, the transverse resistance, which is commonly defined Hall resistance, manifests an intriguing pattern in terms of well-defined plateaus as the magnetic field is varied. This phenomenology is in striking contrast with the linear behaviour predicted by classical theory.

The earliest experimental evidence of the quantization of Hall resistance has been carried out by K. von Klitzing that, in 1980, observed the appearance of plateaus in the Hall resistance at integer values [9, 10]. This phenomenon, known as the integer quantum Hall effect, can be understood in a satisfying way by resorting to a single-particle quantum mechanical description. This explanation is fundamentally based on the discretization of energy spectrum for an electron in a magnetic field. These discrete energy levels are called Landau levels and the so-called filling factor ν indicates how many of them are occupied.

The hallmark of quantum Hall systems is the emergence of an one-dimensional metallic edge states on the boundaries of the system. Along these edge states particles propagate with a definite direction, i.e. chirally. As a result, they are topologically protected against backscattering and transport occurs in the ballistic regime.

The long coherence length ($> \mu$m) ensured by topological protection guarantees to access the wave-like nature of electrons, thus allowing the observation of unconventional and fascinating quantum phenomena. Intriguingly, this investigation can be pushed to its fundamental limit by exploiting quantum transport at the single-electron level [11–16]. This compelling idea embodies the core purpose of a new field of research, known as electron quantum optics [17]. The main purpose of electron quantum optics is to reproduce conventional optics experiments using single-electron [18–20]. The wave-guides where photons propagate in the vacuum are replaced by quantum Hall edge states in the condensed matter realm. Single-electron sources can be realized based on the prediction formulated by Levitov and co-workers that a periodic train of quantized Lorentzian-shaped pulses, carrying an integer number of particles per period, is able to inject minimal single-electron excitations, then termed levitons [21–23]. In order to realize quantum optics experiments using fermionic degree of freedom, the last required component is an electronic analogue of

the half-silvered mirror of conventional optics: its role can be played by a quantum point contact [24–27] generated by two negative tunable voltages, where electrons are reflected or transmitted. By combining these elements with the single-electron sources previously described, interferometric setup, originally conceived for optics experiments, can be implemented also in the condensed matter realm and quantum transport properties at the single-electron can be investigated [15, 16, 28–31].

Despite evident analogies and similarities with traditional photonic quantum optics, electron quantum optics brings into play two new features that are inherently characteristic of electronic systems. Firstly, single-photon states are usually created on a real quantum mechanical vacuum (i.e. zero-particle state), while single-electron states are always generated on top of a completely different ground state with its own dynamics, namely the filled Fermi sea. Nevertheless, a fermionic analogue of Roy J. Glauber's theory of optical coherence [32] can be developed circumventing this complication, and theoretical predictions are in excellent agreement with experiments [17, 33]. Even more importantly, solid state systems can be heavily affected by interactions, and the ground state of a fermionic system can show correlations [34–36].

The fractional quantum Hall effect is a paradigmatic example of the dramatic consequences of electron-electron interactions [37]. In this case, plateaus of the Hall resistance appear at fractional values of the filling factor ν. The first measurements of this fractional Hall resistance have been reported by D. C. Tsui and H. L. Stormer in 1982 [38]. Contrarily to the integer case, the physical explanation of fractional quantum Hall effect cannot neglect the correlation between electrons. With a great physical intuition, R. Laughlin introduced the first interpretation of strongly-correlated quantum Hall phases with fractional filling factors $\nu = \frac{1}{2n+1}$, with $n \in \mathbb{N}$. These phases form the so-called Laughlin sequence and their ground state can be described by means of a variational many-body wave-function. One of the most far-reaching consequences that have been introduced by Laughlin's idea is the prediction that elementary excitations of fractional quantum Hall systems are quasi-particle with fractional charge and statistics [39–45]. Remarkably, one-dimensional conducting edge states arise also in the fractional quantum Hall effect and their excitations inherit the charge and statistical properties of the one in the bulk [46–48].

In this thesis, we investigate the transport properties of levitons propagating along the edge states of a quantum Hall systems in the Laughlin sequence, thus taking into account the effect of Coulomb interaction. In one-dimensional systems, electron-electron interaction has dramatic effects on the transport properties of levitons [34, 49]. In particular, we will investigate the time-dependent dynamics of levitons, namely single-electron excitations travelling along quantum Hall edge states, and we will show how this is modified by the presence of strong correlations. Moreover, since some recent groundbreaking experiments has spurred the interest also in the direction of thermal transport at the nanoscale [50–53], we analyze also heat properties of levitons, thus considering electron quantum optics from a new perspective.

This thesis is divided in four Chapters.
In **Chapter 1** we will introduce the phenomenology of the integer and the fractional quantum Hall effect, by focusing on filling factors in the Laughlin sequence. The emergence of edge states in the integer regime is shown and their topological

protection from backscattering is discussed. An effective field theory for the bulk of the Laughlin sequence is derived following the seminal work of X. G. Wen. The restriction to the boundary of these models will lead to effective field theories for the edge states in terms of bosonic fields. By means of the bosonization technique we will give the operatorial description for the gapless excitations along the edge.

Chapter 2 is devoted to the introduction of the main concepts of electron quantum optics. The role of minimal excitations in the integer quantum Hall regime is established for levitons, by presenting the theoretical argument of Levitov and experimental evidence. Then, the electronic coherence theory, conceived in analogy with Glauber's coherence theory for photons, is presented and the form of leviton's wave-packets is derived. Finally, I present two main examples of single-electron interferometry with levitons, namely the Hanbury-Brown-Twiss and the Hong-Ou-Mandel interferometers, which are two crucial experimental setups of ordinary quantum optics.

In **Chapter 3**, the charge transport properties of levitons for fractional filling factors of the Laughlin sequence are taken into account. Firstly, we recall that levitons are minimal excitation states even in the presence of the strong correlation of fractional quantum Hall phases. Then, we demonstrate the crystallization of levitons in a quantum point contact geometry. Finally, we show that experimental evidence for the crystallization of levitons can be obtained in an Hong-Ou-Mandel setup where identical states of leviton collide at the quantum point contact.

In **Chapter 4**, we investigate also the heat transport properties in electron quantum optics setup with levitons. Levitons are shown to be minimal excitation states also for heat transport. This property is robust even with respect to an arbitrary overlap between them. The Hong-Ou-Mandel setup is also investigated from the point of view of heat transport, showing additional signatures of the crystallization of levitons.

Chapter 3 and **Chapter 4** contain the original parts of this work. Indeed, this thesis is based on the following paper co-authored by myself:

- L. Vannucci, F. Ronetti, J. Rech, D. Ferraro, T. Jonckheere, T. Martin, M. Sassetti, "Minimal excitation states for heat transport in driven quantum Hall systems", Phys. Rev. B **95**, 245415 (2017) [54] (Chapter 4)

- F. Ronetti, L. Vannucci, D. Ferraro, T. Jonckheere, J. Rech, T. Martin, M. Sassetti, "Crystallization of levitons in the fractional quantum Hall regime", Phys. Rev. B **98**, 075401 (2018) [55] (Chapter 3)

- D. Ferraro, F. Ronetti, L. Vannucci, M. Acciai, J. Rech, T. Jonckheere, T. Martin, M. Sassetti, "Hong-Ou-Mandel characterization of multiply charged levitons", invited paper on EPJ [56] (Chapter 3)

- F. Ronetti, L. Vannucci, D. Ferraro, J. Rech, T. Jonckheere, T. Martin, M. Sassetti, "Hong-Ou-Mandel heat interferometer in the fractional quantum Hall regime", in preparation (2017) (Chapter 4)

Other publications not included in this thesis are:

- L. Vannucci, F. Ronetti, G. Dolcetto, M. Carrega, M. Sassetti, "Interference induced thermoelectric switching and heat rectification in quantum Hall junctions", Phys. Rev. B **92**, 075446 (2015) [57]

- F. Ronetti, L. Vannucci, G. Dolcetto, M. Carrega, M. Sassetti, "Spin-thermoelectric transport induced by interactions and spin-flip processes in two dimensional topological insulators", Phys. Rev. B **93**, 165414 (2016) [58]

- F. Ronetti, M. Carrega, D. Ferraro, J. Rech, T. Jonckheere, T. Martin, M. Sassetti, "Polarized heat current generated by quantum pumping in two-dimensional topological insulators", Phys. Rev. B **95**, 115412 (2017) [59]

- L. Vannucci, F. Ronetti, D. Ferraro, J. Rech, T. Jonckheere, T. Martin, M. Sassetti, "Photoassisted shot noise spectroscopy at fractional filling factor", J. Phys.: Conf. Ser. **969**, 012143 (2018) [60]

- D. Ferraro, F. Ronetti, J. Rech, T. Jonckheere, M. Sassetti, T. Martin "Enhancing photon squeezing one Leviton at a time", Phys. Rev. B **97**, 155135 (2018) [61]

Chapter 1

Quantum Hall effect

In this Chapter, we introduce the main ideas and the theory behind the rich and fruitful discovery of the quantum Hall effect. In the first part, the phenomenology of the integer quantum Hall effect is presented. This peculiar physical phenomenon can be explained in terms of a non-interacting quantum mechanical treatment of an electron in a magnetic field. Then, we take into account the fractional quantum Hall effect, which can be explained only by taking into account electron-electron interactions [62]. For this reason, its theoretical description cannot be carried on in a non-interacting framework, but requires an effective field theory approach. For a specific set of fractional quantum Hall phases, known as Laughlin sequence, we will introduce in the last part of this Chapter a field theoretic description of edge states originally conceived by X. G. Wen [47].

1.1   Integer quantum Hall effect

The physics of a thin metallic plate subjected to a perpendicular magnetic field has been known for a long time, since the discovery by E. Hall in 1879 of the Classical Hall effect. After having imposed a current along one direction of the sample, he measured a voltage in the transverse direction which in turns gave rise to a transverse resistance, linearly proportional to the magnetic field. The behavior of the so called Hall resistance R_H was in accordance with the classical Drude theory of diffusive electron transport and allowed to investigate the nature of charge carriers in metals [5].

Around one hundred years later, this kind of Hall measurements were performed with electrons confined to a spatial region in two dimensions, known as two-dimensional electron gases (2DEG), which form, for instance, at the interface of two semiconductors. In 1980, K. Von Klitzing observed an anomalous behavior of the Hall resistance in a 2DEG put in a strong magnetic field B and at very low temperatures [9]. In particular, the experiments revealed that the proportionality to B was replaced by a quantization in terms of plateaus in which the Hall resistance remained constant over a certain range of the magnetic field (see Fig. 1.1). The transition between two plateaus is rather quick, but on each of them the resistance is extremely flat and assumes the values

$$R_H = \rho_{xy} = \frac{h}{e^2}\frac{1}{n} \quad n \in \mathbb{Z}. \tag{1.1}$$

The value n has been measured to be an integer number with an accuracy greater than one part over 10^9. Interestingly, this resistance is completely unaffected by
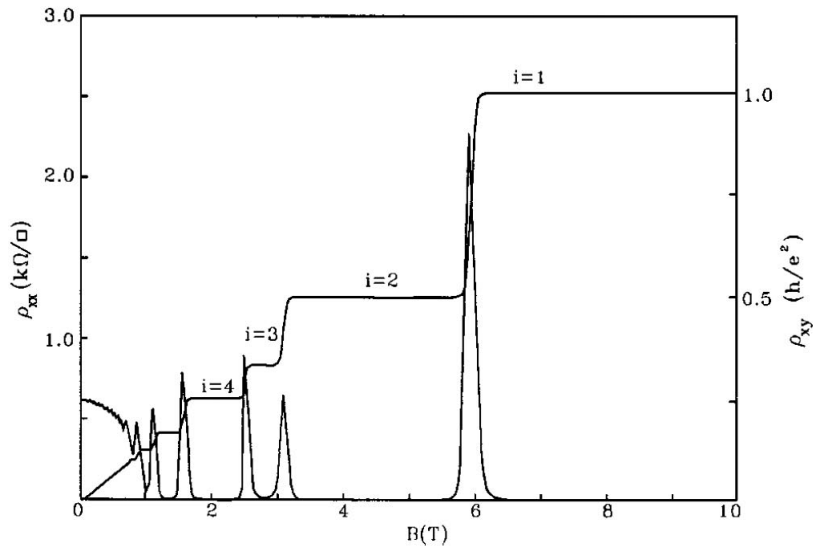
Figure 1.1: Von Klitzing's measurements of longitudinal resistivity ρ_{xx} and Hall resistivity ρ_{xy} as a function of the magnetic field for the states of the integer quantum Hall effect. The Hall resistance shows well defined plateaus, which correspond to integer fraction of $\frac{h}{e^2}$ with an greater than one part over 10^9. Taken from Ref. [9]

the specific properties of a sample, since it depends exclusively on two fundamental constants, i.e. the Planck constant h and the electron charge e. The quantity $R_K = \frac{h}{e^2}$ is called the quantum of resistance (or Von Klitzing resistance) and, due to the extraordinary precision of this kind of measurements, it is now used as the standard unit of resistances [10]. In this sense, the value of n has to be considered an integer number by definition.

Since this result violates the classical picture provided by the Drude model, it required a quantum mechanical framework in order to be fully understood. For this reason, the phenomenology so far described is termed the Integer Quantum Hall (IQH) effect. In the following, we will present a quantum mechanical treatment of electrons subjected to a perpendicular magnetic field in two dimensions in order to elucidate some fundamental properties of the IQH effect that will be crucial in the remainder of this thesis.

1.1.1 Electrons in a magnetic field

The physics of IQH effect can be understood by considering the properties of a two-dimensional electronic system in the presence of a magnetic field B. Moreover, one can come to a satisfactory explanation of this phenomenon even neglecting interactions among electron. In this single-particle picture, the only way that one particle knows about the presence of others is through the Pauli exclusion principle. Starting from the hamiltonian for a single electron

$$H_0 = \frac{\boldsymbol{p}^2}{2m},\tag{1.2}$$

one can introduce the effect of a magnetic field $\boldsymbol{B}$ using the substitution $(e > 0)$[63]

$$\mathbf{p} \to \mathbf{P} = \mathbf{p} + e\mathbf{A}(\boldsymbol{r}),\tag{1.3}$$

where **A** is the vector potential related to **B** by

$$\mathbf{B} = \nabla \times \mathbf{A}. \tag{1.4}$$

As a result, the hamiltonian of an electron subjected to a magnetic field is

$$H = \frac{\boldsymbol{P}^2}{2m} = \frac{(\mathbf{p} + e\mathbf{A}(\boldsymbol{r}))^2}{2m}. \tag{1.5}$$

We decided to consider the motion of electrons in free space, thus neglecting the presence of a crystalline environment of the background material (in the case of von Klitzing experiment, a semiconductor). It seems, at first sight, to be a very crude assumption. Nevertheless, it safely works as long as the lattice spacing is very small in comparison to the magnetic length [6]

$$l_B = \sqrt{\frac{\hbar}{eB}}. \tag{1.6}$$

It should be noted that this is indeed the case for any realistic value of magnetic field: for a lattice spacing of tenths of nanometer, the effect of a crystalline potential become relevant only for magnetic fields $B \gtrsim 45$ T.

The introduction of a vector potential bears the relevant consequence that the hamiltonian assumes a dependence on the spatial coordinates. For this reason, the different component of operator $\boldsymbol{P}$ do not commute with each other, in contrast with the usual momentum operator $\boldsymbol{p}$. By exploiting the canonical commutation relations $[x_k, p_j] = i\hbar\delta_{k,j}$, one can prove that

$$[P_x, P_y] = -i\hbar eB. \tag{1.7}$$

The calculation of this commutator returns a gauge-invariant quantity, since it is expressed directly in terms of the magnetic field. Interestingly, this result can be exploited to derive the spectrum of the hamiltonian in Eq. (1.5) without setting a specific form for **A**. This derivation requires to express Eq. (1.5) in terms of the following operators [63, 64]

$$a = \frac{l_B}{\sqrt{2}\hbar} \left(P_x + iP_y\right), \quad a^\dagger = \frac{l_B}{\sqrt{2}\hbar} \left(P_x - iP_y\right), \tag{1.8}$$

which satisfy, due to Eq. (1.7), the commutator $\left[a, a^\dagger\right] = 1$. The hamiltonian in Eq. (1.5) then becomes

$$H = \hbar\omega_B \left(a^\dagger a + \frac{1}{2}\right), \tag{1.9}$$

where $\omega_B = \frac{Be}{mc}$ is the cyclotron frequency. The above hamiltonian describes a quantum harmonic oscillator with frequency ω_B, whose spectrum is given by [63, 64]

$$E_n = \hbar\omega_B \left(n + \frac{1}{2}\right), \quad n \in \mathbb{N}. \tag{1.10}$$

The energy levels of an electron placed in a magnetic field are discretized and equally spaced by a gap which increases linearly with the magnetic field. These levels are called Landau levels, because they were firstly discovered by the Russian physicist L. Landau. Let us observe that the energy spectrum in Eq. (1.10) is labeled by a single quantum number. Nevertheless, since we consider a two-dimensional space,

we expect that two quantum numbers occur to fully characterize the system. As consequence, it can be easily understood that Landau levels in Eq. (1.10) are degenerate and that the wave-functions associated to these energy eigenvalues depend on an additional quantum number.

Since the wave-functions are gauge-dependent, we have to choose a specific form for the vector potential. An useful choice is the Landau gauge, where

$$\mathbf{A}(\boldsymbol{r}) = B(-y, 0, 0). \tag{1.11}$$

With this form of the vector potential, the hamiltonian in Eq. (1.5) does not depend on x. For this reason, the motion along $\hat{x}$ can be described in terms of plane waves, leading to an expression for the full wave-function of the form

$$\psi_{n,k}(x,y) = e^{ikx} f_{n,k}(y), \tag{1.12}$$

where k is a quantum number related to the transational invariance along $\hat{x}$. This latter expression leads to the hamiltonian

$$H = \frac{(k - eBy)^2}{2m} + \frac{p_y^2}{2m} = \frac{p_y^2}{2m} + \frac{1}{2}\omega_B \left(y - y_0(k)\right)^2, \tag{1.13}$$

where $y_0(k) = k l_B^2$. This hamiltonian describes a one-dimensional harmonic oscillator, whose eigenfunctions read

$$f_{n,k}(y) = e^{-\frac{(y - y_0(k)^2)^2}{4 l_B^2}} H_n(y - y_0(k)^2), \tag{1.14}$$

where $H_n(x)$ are the Hermite polynomials [64]. These eigenfunctions manifestly depend on two quantum numbers and are centered in $y_0(k)$.

The degeneracy of Landau levels can be easily computed for a finite size system with periodic boundaries along $\hat{x}$, where the quantum number k assumes discrete values. If we consider a rectangular sample with size L_x and L_y, the quantization condition for the values of k is

$$k = \frac{2\pi}{L_x} m \quad m \in \mathbb{N} \tag{1.15}$$

and the center of the harmonic oscillators has to satisfy the relation

$$0 < y_0(k) < L_y. \tag{1.16}$$

By combining these two conditions, the following restrictions are imposed on m

$$0 < m < \frac{L_x L_y}{2\pi l_B^2}, \tag{1.17}$$

such that the maximum number of degenerate state is equal, for each Landau level, to

$$N_{deg} = \frac{L_x L_y}{2\pi l_B^2} = \frac{\phi}{\phi_0}, \tag{1.18}$$

where $\phi = L_x L_y B$ is the total flux in the quantum Hall bar and $\phi_0 = \frac{h}{e}$ is the universal quantum of flux. In a system containing a total number of N electrons, the Landau levels are filled starting from the lowest one. In this sense, it is useful to introduce the *filling factor* of Landau levels as

$$\nu = \frac{N}{N_{deg}} = \frac{h n_e}{eB}, \tag{1.19}$$

where $n_e = \frac{N}{L_x L_y}$ is the electronic density in the sample.

1.1.2 Edge states

In order to understand the degeneracy of Landau levels, we mentioned the finiteness of the sample in our discussion. The presence of a confinement has a crucial effect on the properties of Landau levels, which can be clarified by a more quantitative treatment. For these reasons, we model the confinement of electrons to a finite region by introducing explicitly in the hamiltonian a potential $V_{conf}(y)$, which vanishes into the bulk but is finite on the boundaries. We consider a smoothly varying potential with respect to the magnetic length, meaning that $l_B|\partial_y V_{conf}(y)| \ll \hbar\omega_B$. This choice implies that, while along the $\hat{x}$ direction the system is still transationally invariant, along the $\hat{y}$ direction we expect that the confinement introduce a spatial dependence in the energy levels, in particular at the edges of the bar.

By recalling that the wave-functions without the confining potential are localized around $y_0 = kl_B^2$, the confining potential can be adiabatically approximated as

$$V_{conf}(y) = V_{conf}(y_0(k)) + \mathcal{O}\left(|\partial_y V_{conf}(y)|\right). \tag{1.20}$$

In the presence of confinement, the hamiltonian in Eq. (1.13), can thus be written as

$$H = \frac{p_y^2}{2m} + \frac{1}{2}\omega_B\left(y - y_0(k)\right)^2 + V_{conf}(y_0(k)). \tag{1.21}$$

The eigenvalues of this hamiltonian are simply given by the Landau levels in Eq. (1.10) shifted by the presence of the confinement

$$E_n(k) = \hbar\omega_B(n + \frac{1}{2}) + V_{conf}(y_0(k)), \tag{1.22}$$

thus acquiring a dependence on k. By considering that the center of eigenstates y_0 (see Eq. (1.14)) depends on the quantum number k, it is clear that the shift of Landau levels, given by V_{conf}, has significant consequences also in the real space (see Fig. 1.2). Since the confining potential is null inside the bulk of the system, eigenstates centered away from the edges are left unaffected. Nevertheless, the energy levels of states close to the ends of the bar in the $\hat{y}$ direction ($y = -\frac{L_y}{2}$ and $y = \frac{L_y}{2}$) are bent by the confining potential according to Eq. (1.22).

This bending of Landau levels has crucial consequence of the transport properties of a quantum Hall bar (see Fig. 1.2). When the Fermi energy lies between two Landau levels, transport of electrons is suppressed in the bulk since there exist an energetic cost $\hbar\omega_B$ to pay in order to reach the first unoccupied energy levels. Nevertheless, close to the edges, the Fermi level crosses the energy spectrum on both side of the sample (close to $y = -\frac{L_y}{2}$ and $y = \frac{L_y}{2}$). This means that gapless and conducting states arise at the edges of quantum Hall bar due to the magnetic field and the confining potential [65]. Moreover, since the Fermi level crosses the spectrum in a specific value of the axis $\hat{y}$ these states are considered one-dimensional (propagating only along $\hat{x}$). It is clear from Fig. 1.2 that any filled Landau levels would induce one gapless state on each edge, meaning that there exists a one-to-one correspondence between filled Landau levels and edge states. In the case that Fermi energy E_F lies between the first and the second Landau levels, i.e the filling factor is $\nu = 1$, a single edge channel emerges on the boundary (see upper panels of Fig. 1.2). By increasing the value of E_F, the filling factor switches to $\nu = 2$ and a second edge mode appears (see lower panels of Fig. 1.2). The properties of the bulk, in this case the filling factor of Landau levels, determine the behavior at the boundaries: this is a major
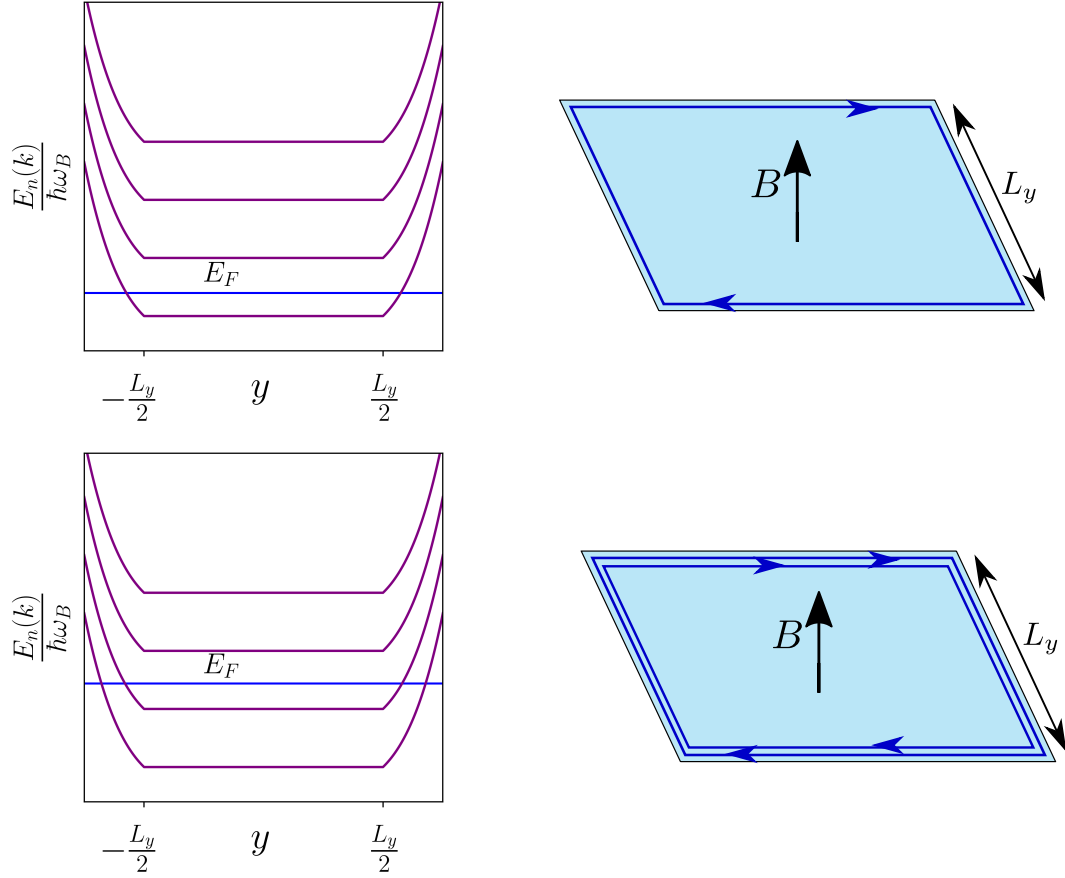
Figure 1.2: Energy levels in the presence of a confining potential $V_{conf}(y)$. In the bulk, Landau levels are unperturbed, while the confining potential modify the band profile close to the boundary. Gapless edge modes appear when the Fermi energy E_F is tuned between two Landau levels. For example, when Fermi energy E_F lies between the first and the second Landau levels, a single edge channel emerges on the boundary (upper panel). By increasing the value of E_F, a second edge mode appears (lower panel).

example of a general phenomenon known as bulk-boundary correspondence. The velocity of the excitations propagating in these edge states is given by

$$v_n(y_0(k)) = \frac{1}{\hbar} \frac{\partial E_n(y_0(k))}{\partial k} = \frac{1}{\hbar} \frac{\partial E_n(y_0(k))}{\partial y_0} \frac{\partial y_0(k)}{\partial k} = \frac{l_B^2}{\hbar} \frac{\partial E_n(y_0(k))}{\partial y_0}. \qquad (1.23)$$

As can deduced from Fig. 1.2,

$$v_n(y_0(k)) = -v_n(-y_0(k)). \qquad (1.24)$$

The velocities of excitations is different from zero only at the edges, where they are restricted to move in a definite direction. Particle that can propagate only in a single direction are called *chiral*. Due to Eq. (1.24), particles have opposite *chirality* on the two sides of the sample [1] and electrons are called left-movers or right-movers according whether the sign of their velocity is negative or positive.

1.1.3 Conductance of edge states

Since the bulk is gapped, the quantized value of the Hall resistance can be attributed exclusively to the presence of conducting states along the boundaries of the system. Let us consider a two-terminal quantum Hall bar, as depicted in Fig. 1.3. While the temperature θ if uniform along the sample, the chemical potentials in the left and right reservoirs assume two different values, respectively, μ_L and μ_R, thus generating an electrical bias given by

$$eV = \mu_R - \mu_L. \qquad (1.25)$$

According to the chirality of edge states, backscattering is forbidden and electron with opposite chirality never mix up. Therefore, when right-moving ($+$) and left-moving ($-$) electrons start propagating along the bar, they are still equilibrated to the Fermi distribution of left and right reservoir, given by

$$f_\pm(E) = \frac{1}{1 + e^{\frac{E - \mu_{L/R}}{k_B \theta}}}. \qquad (1.26)$$

The current flowing in response to the electrical bias can be obtained by summing over all the occupied states, labeled by n,

$$I = \frac{-e}{L_x} \left[\sum_n \sum_{k>0} v(k) f_+(E_n(k)) + \sum_n \sum_{k<0} v(k) f_-(E_n(k)) \right], \qquad (1.27)$$

where the contributions of right-movers and left-movers have been separated. It is convenient to replace the sums over k with an integral, thus obtaining

$$I = \frac{-e}{L_x} \frac{L_x}{2\pi\hbar} \sum_n \left[\int_0^{+\infty} dk \frac{\partial E_n(k)}{\partial k} f_+(E_n(k)) + \int_{-\infty}^0 dk \frac{\partial E_n(k)}{\partial k} f_-(E_n(k)) \right] =$$

$$= \frac{-e}{h} \sum_n \left[\int_{E_n(0)}^{+\infty} dE f_+(E) - \int_{E_n(0)}^{+\infty} dE f_-(E) \right], \quad (1.28)$$

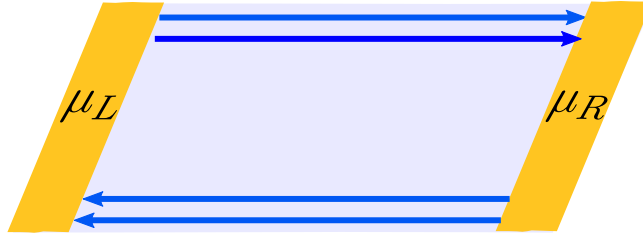[1] This is also a consequence of the fundamental property that current should vanish in the absence of an electric field.

Figure 1.3: The edge states of a quantum Hall bar in a two-terminal geometry. The chemical potentials of the two reservoirs are, respectively, μ_L and μ_R. Due to the chirality of edge states, electrons flowing along the channels are still equilibrated to the Fermi distribution of reservoirs.

where we used that $E_n(\pm\infty) = +\infty$. In the limit of zero temperature the Fermi distributions in Eq. (1.26) become

$$f_\pm(E) = \Theta(\mu_{L,R} - E),\tag{1.29}$$

where $\Theta(x)$ is the Heaviside step function. In this limit, the expression for the current is

$$I = -\frac{e}{h}\sum_n \int_{\mu_R}^{\mu_L} dE = -\nu\frac{e}{h}(\mu_L - \mu_R) = \tag{1.30}$$

$$= \nu\frac{e^2}{h}V,\tag{1.31}$$

when ν Landau levels are filled. Therefore, the Hall conductance is

$$G_H = \nu\frac{e^2}{h}.\tag{1.32}$$

By recalling that the resistance is simply the inverse of conductance, we find that the presence of chiral edge states is consistent with the observed quantized values of the Hall resistance.

It is interesting to compare the result of Eq. (1.32) with the conductance of quantum wires at zero temperature derived within the Landauer approach [66, 67]

$$G = \frac{e^2}{h}\sum_n T_n(E_F),\tag{1.33}$$

where the sum involve all one-dimensional channel in the wire and $T_n(E_F)$ is the transmission probability of n-th channel evaluated at the Fermi energy. In terms of Landauer formula for conductance, one can argue that each chiral edge state can be interpreted as a perfectly transmitting one-dimensional channel. The ideal transmission of quantum Hall edge states is again a consequence of their chirality: even in the presence of a scattering impurity, right-movers and left-movers cannot change their direction of motion because they are enforced by chirality to maintain the sign of their velocity.

Surprisingly, it turns out that disorder even plays an helpful role for the stability

of edge states [65, 68]. Indeed, a reduction of transmission could be induced by a tunneling from one edge to the other, as long as the width of the sample (L_y) is much greater than the magnetic length (l_B): nevertheless, impurities and disorder localize states belonging to the bulk in correspondence of plateaus of G_H and leaves unaffected the conductance of edge states [65, 69]. In this way, transfer of electrons in the transverse direction of the sample is forbidden.

The robustness of quantum Hall edge states can be understood by looking at the Hall conductance from another perspective [70, 71]. Let us observe that quantum Hall conductance in Eq. (1.32) is a directly related to the filling factor ν, which is a global property of the Hall bar, meaning that it is not possible to describe G_H in terms of a local order parameter. This point, together with the fact that no symmetry is broken during the transition between different plateaus, helped in understanding soon that the IQH phases described by different filling factors ν could not be classified in terms of the Landau-Ginzburg theory of phase transitions. States of matter, which are characterized by global parameters and that lie beyond the Landau-Ginzburg paradigm are called *topological states*: integer quantum Hall systems were just the first example of many topological systems that were successively discovered.

The concept of topology is borrowed from mathematics, where all the structure with a certain number of holes are called topologically equivalent and define certain topological classes: a geometrical figure can be transformed in a topologically distinct object only by an abrupt transformation that modifies its number of holes. By analogy, the different plateaus, separated by a gap $\hbar\omega_B$ and associated to different values of the Hall conductance, can be interpreted as topologically different quantum phases. A transition between topological classes, called *topological phase transition*, is possible only after the closing of this gap. This is exactly what happens when Hall conductance jumps from one plateau to the other.

The topological interpretation of integer quantum Hall states provide also another point of view on the gapless edge channels previously discussed. When two distinct topological phase are put together, at their interface a topological phase transition must occur, namely the gap must close. In particular, this happens at the interface between a quantum Hall phase and the vacuum: this explains the existence of gapless states on the boundary of a quantum Hall bar from a topological point of view. Moreover, the number of these edge states is determined by the filling factor of the bulk. This means that, according to Eq. (1.32), the structure and the robustness of the edge states are deeply rooted in the bulk property of the corresponding quantum Hall phase.

1.2   The fractional quantum Hall effect

In the previous Section, the main theoretical arguments describing the quantization of quantum Hall resistance at multiple integer values of $\frac{h}{e^2}$ were presented. Nevertheless, in 1982 D. C. Tsui, H. L. Stormer and coworkers reported an unusual behavior of the Hall resistance [38]. For a sample with higher mobility and subjected to a more intense magnetic field than those used by von Klitzing, they observed the appearance of a plateau at a fractional filling factor $\nu = \frac{1}{3}$. Later on plateaus were measured in correspondence to many other fractional values of Landau level filling: this peculiar phenomenology, which cannot be explained in terms of the physical picture given for the IQH effect, has been called fractional quantum Hall (FQH)
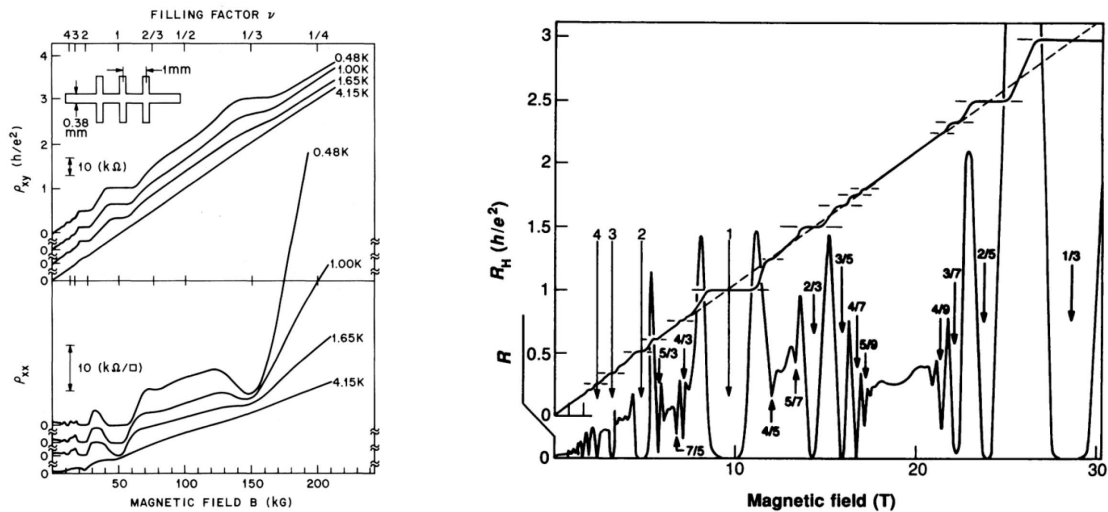
Figure 1.4: Fractional quantum Hall effect states. (Left panel) First observation of a plateau at $\nu = \frac{1}{3}$ in the Hall resistivity ρ_{xy}. Taken from [38]. (Right panel) Many others plateaus in the Hall resistance in correspondence of fractional values of filling factors. Taken from [68]

effect.

A theoretical explanation of the FQH effect is by far harder than for the IQH effect. Nevertheless, a subset of fractional filling factors received an insightful interpretation due to R. Laughlin in 1983, who won the Nobel Prize in 1998 together with D. C. Tsui and H. L. Stormer for this theoretical contribution [68, 72, 73]. This subsequence was named Laughlin sequence and contains all the filling factors of the form

$$\nu = \frac{1}{2n+1}, \quad n \in \mathbb{N}, \tag{1.34}$$

which includes $\nu = \frac{1}{3}$, the first observed FQH state. In the rest of this thesis, we will mainly focus on the Laughlin sequence in relation to FQH effect.

1.2.1 The Laughlin sequence

The theoretical framework that successfully explained the IQH effect has been entirely presented in terms of a single-particle picture. The great physical intuition of Laughlin was that the main element which gives rise to the FQH phenomenology is the Coulomb repulsion between electrons and that one should abandon the physical picture in terms of independent electrons used for the IQH effect [5].

A system of N interacting electrons in a magnetic field can be described by the following hamiltonian [2]

$$H = \sum_{i=1}^{N} \frac{\left(\mathbf{p}_i + \frac{e}{c}\mathbf{A}(\boldsymbol{r}_i)\right)^2}{2m} + \sum_{i \neq k}^{N} \frac{e^2}{\epsilon |\boldsymbol{r}_i - \boldsymbol{r}_k|}, \tag{1.35}$$

---

[2]We neglect the role of lattice potential and disorder, which turn out to be marginal in the description of FQH effect.

where ϵ is the dielectric constant of the material where the FQH state is realized. To deal with this additional contribution, one might think to proceed with a standard perturbative analysis. For a state like $\nu = \frac{1}{3}$, the degeneracy of the ground state would be $N_{deg} = 3N$. All the possible combination to fill the lowest Landau levels with N electrons are given by

$$\binom{3N}{N} = \frac{(3N)!}{N!(2N)!},\tag{1.36}$$

which for macroscopic N reaches really high values. In a degenerate perturbation theory, one should diagonalize a macroscopically large matrix, which is a task out of reach even for numerical algorithms.

Nevertheless, a qualitative understanding for the stability of states at fractional filling factor can be drawn resorting to a simple picture of interacting electrons. In partially filled Landau levels, there is a huge freedom to fill the Hall bar with electrons. In the presence of repulsion between electrons, our freedom to distribute them is reduced. Let us start focusing on the ideal case of an infinite magnetic field. The magnetic length goes to zero and states are localized: electrons behave like point charge and tend to crystallize by minimizing their interaction energy. A unique ground state is formed, called Wigner crystal [49], which is radically distinct from the FQH phase [3]. When the magnetic field is lowered to finite values, wave-functions of electron overlap and they cannot form anymore a crystalline structure. For some magic filling factors, they form a strongly correlated quantum liquid, which can be described in terms of an unique many-body wave-function.

The form of the ground state wave-function of Laughlin sequence states can be guessed based on generical considerations such as the symmetry of the problem and the Fermi statistics of electrons. The ansatz of Laughlin for the wave-function of the ground states is the following [62]

$$\Psi_{2n+1} = \mathcal{M} \prod_{i<j}^{N} (z_i - z_j)^m e^{-\sum_{k=1}^{N} |z_k|^2},\tag{1.37}$$

where $\mathcal{M}$ is a normalization factor and $z = x + iy$ is a complex spatial coordinate. This many-body wave-function is built from angular momentum eigenstates $\phi_m(z) \sim z^m e^{-|z|^2}$, in accordance with rotational invariance of Coulomb interaction. Moreover, it satisfies transational invariance with respect to the origin.

The Laughlin wave-function thus obtained has not been derived mathematically diagonalizing an hamiltonian. Actually, it is a variational wave-function that satisfy the symmetry and the constraints of the problem. The variational parameter is given by the integer number m, which is the only elements in Eq. (1.37) not already fixed. This variational wave-function efficiently approximates the ground state of a Laughlin state with filling factor ν when the value of m is chosen such that

$$m = 2n + 1, \quad n \in \mathbb{N},\tag{1.38}$$

which means that $m = \frac{1}{\nu}$. Indeed, by numerical simulations, it has been demonstrated that Laughlin wave-function overlaps at the 99% with the true ground states of the hamiltonian in Eq. (1.13). For such specific value of m, Laughlin wave-function satisfies Pauli exclusion principle: indeed, when two coordinates z_i and z_j

---

[3]It can be obtained more realistically for sample with a very low density [74].

are exchanged, the many-body wave-function acquires a minus sign, in accordance with Fermi statistics.

The presence of zeros with order $2n+1$ enforce a separation between electrons, which induces a strong correlation in the system ground state. This correlation increases for higher values of n, meaning that a lower filling factor corresponds to a stronger Coulomb interaction among electrons.

Before concluding this part, it is instructive to point out a relation between the order of zeros in the Laughlin wave-functions at filling factor ν and the corresponding degeneracy. The highest order zero in z_i in Eq. (1.37) has order $(2n+1)(N-1)$, which in the thermodynamic limit gives

$$(N-1)(2n+1) \simeq N(2n+1) = N_{deg}. \tag{1.39}$$

1.2.2 Laughlin's quasi-holes and quasi-particles

Starting from the Laughlin ansatz for the ground state, it is possible now to discuss the excitations of the system. There are two possibilities for adding charged excitations to the system. One way is to change directly the electron density. Another possibility is to vary the magnetic field, thus increasing or reducing the degeneracy, while keeping constant the filling factor ν.

As we have seen, the degeneracy N_{deg} is intimately related to the number of zeros in the Laughlin wave-function Therefore, we consider the following ansatz for an excited state with an additional zero in w of order N

$$\Psi_w^+ = \prod_{i=1}^{N}(z_i - w)\Psi_{2n+1}. \tag{1.40}$$

The introduction of an additional flux would lower the filling factor ν by a tiny amount. In order to keep ν fixed, one has to add some charge to compensate the extra magnetic flux quantum. The total charge when the degeneracy if modified by an unity is

$$Q = eN' = e\nu(N_{deg} + 1) = eN + \nu e, \tag{1.41}$$

which implies that the charge added due to the addition of a magnetic flux is given by

$$\Delta Q = e(N' - N) = \nu e. \tag{1.42}$$

This is a rather surprising result: the excitation of the Laughlin ground state must carry a fractional charge

$$e^* = \nu e = \frac{e}{2n+1}. \tag{1.43}$$

This fractionally charge excitation is called a quasi-hole

Similarly, it is possible to obtain an excited state also by removing an unit of flux. In this case, one would excite a quasi-particle with charge $-e^*$. A good variational wave-function for this type of excitation is

$$\Psi_w^- = \prod_{i=1}^{N}(2\partial_{z_i} - w)\Psi_{2n+1}. \tag{1.44}$$

Another fascinating properties of quasi-particles and quasi-holes is their exchange statistics, which is related more to the low dimensionality of the system rather than to the peculiar properties of the FQH effect.
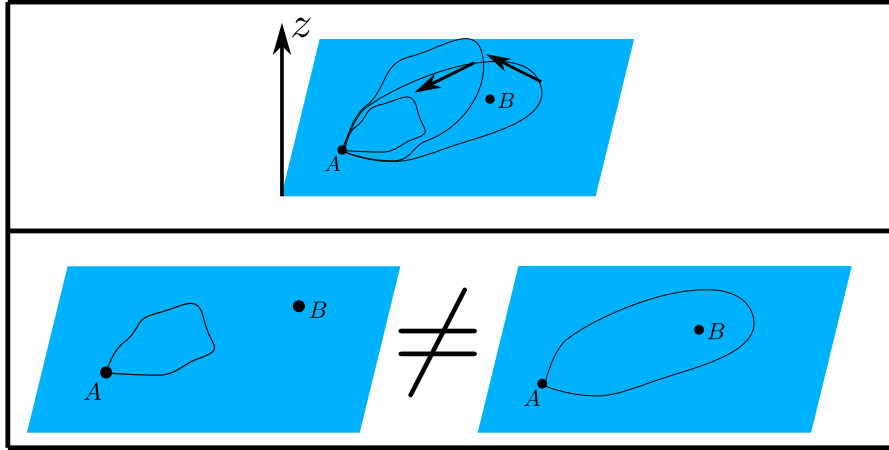
Figure 1.5: Upper panel: exchange of identical particles A and B in three dimensions. The third direction z allows to shrink the path into a single point. Thus, this path corresponds to the identity operator. Lower panels: Paths that enclosed particle B is topologically inequivalent to paths not including particle B.

Let us first review the usual argument about exchange statistics in three dimension [5].

Two identical particles A and B placed at the position $\boldsymbol{r}_A$ and $\boldsymbol{r}_B$ are described by a wave-function $\psi(\boldsymbol{r}_A, \boldsymbol{r}_B)$. When they are exchanged, all the probabilities must have remained the same, meaning that $|\psi(\boldsymbol{r}_A, \boldsymbol{r}_B)|^2 = |\psi(\boldsymbol{r}_B, \boldsymbol{r}_A)|^2$. This implies the final state must have picked up phase, at most, such that

$$\psi(\boldsymbol{r}_A, \boldsymbol{r}_B) = e^{i\pi\alpha}\psi(\boldsymbol{r}_B, \boldsymbol{r}_A). \tag{1.45}$$

When particles are exchanged again, one finds

$$\psi(\boldsymbol{r}_A, \boldsymbol{r}_B) = e^{i2\pi\alpha}\psi(\boldsymbol{r}_A, \boldsymbol{r}_B) \tag{1.46}$$

and, since the particles are returned to their initial states, it is necessary that $e^{i2\pi\alpha} = 1$. This latter condition leaves open only two possibilities, namely $\alpha = 0$ and $\alpha = 1$, which correspond respectively to bosons and fermions.

In a three-dimensional space, this argument works because, due to the presence of the $\hat{z}$ direction any winding path of A around B can always be shrunk into a single point, without even passing by the position $\boldsymbol{r}_B$ (see Fig. 1.5). As a consequence, any winding process is equivalent to leave particle 1 in its original position.

In two dimensions, the winding path of A cannot be reduced to a single point without touching particle B and, therefore, it is always distinct from the path that leaves A in its initial position. For this reason a third class of particles exist, which are neither bosons nor fermions, which obey the exchange statistics

$$\psi(\boldsymbol{r}_A, \boldsymbol{r}_B) = e^{i\theta}\psi(\boldsymbol{r}_B, \boldsymbol{r}_A), \tag{1.47}$$

where statistical angle θ can assume *any* real value. Particles satisfying the above relation are called *anyons* [5, 39] The statistics angle of Laughlin quasi-particles and quasi-holes always assume rational values, dictated by the specific filling factor of the corresponding FQH state. In Sec. 1.3, we will see a demonstration of the fractional statistics of Laughlin quasi-particles and quasi-holes.

31

Considering all the possible many-body wave-function in two dimensions, one can distinguish between two separate classes. When the order of exchanges does not affect the phase acquired by this many-body wave-functions, we are dealing with *abelian anyons*. On the contrary, if the final state obtained after several exchanges depends on this order, anyons are called *non-abelian* [39]. FQH states belonging to Laughlin sequence are all abelian anyons [5, 6].

1.2.3   Fractional charge conductance

The fractional quantization of conductance can be understood in terms of the existence of fractionally charged excitation through a gedanken experiment invented by Laughlin (see Fig. 1.6 and Ref. [62]). A Hall bar in the Laughlin sequence is threaded by a time-dependent flux $\phi(t)$. According to Faraday's law a voltage is induced by the flux variation

$$\oint_\Gamma \boldsymbol{E} \cdot d\boldsymbol{r} = -\frac{1}{c}\frac{d\phi}{dt}. \tag{1.48}$$

When the longitudinal conductance is zero, the electric field is given by

$$\boldsymbol{E} = \rho_{xy}\boldsymbol{J} \times \hat{z}. \tag{1.49}$$

By plugging this into Eq. (1.48), one finds

$$\rho_{xy}\frac{dq}{dt} = -\frac{1}{c}\frac{d\phi}{dt}, \tag{1.50}$$

where $\frac{dq}{dt}$ is the charge transfered in a unit of time along the radial axis.
Now, let us suppose that the flux is adiabatically changed from 0 to ϕ_0. The characteristic time τ_ϕ for this variation must satisfy $\tau_\phi \ll \frac{\hbar}{\Delta_-}$. Integrating Eq. (1.50) over time in an interval τ_ϕ, one finds

$$\rho_{xy}e^* = \frac{h}{e}, \tag{1.51}$$

since the flux is incremented exactly of an unit and, according to our previous discussion, the charge transfered in a radial direction is equal to $-e^*$. This means that the Hall resistivity is quantized as

$$\rho_{xy} = \frac{h}{\nu e^2}. \tag{1.52}$$

The interpretation of the fractional Hall conductance in terms of an edge state description is a bit more difficult than for IQH states. Since the states of Laughlin sequence lie within the first Landau, we expect that a single gapless channel arises on each edge for this particular values of filling factor. Nevertheless, due to the strongly correlated nature of FQH states a simple transport picture in terms of Fermi liquid is not possible and we have to introduce an effective field theory to describe them. This will be the purpose of next section.
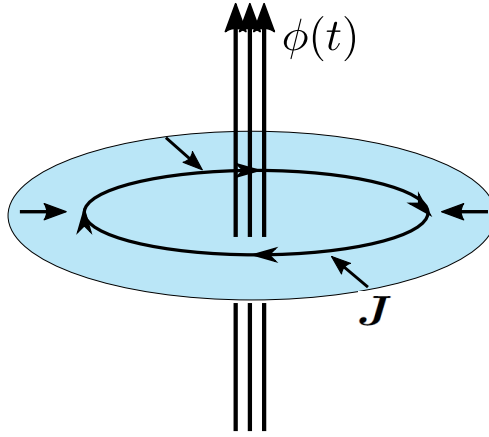
Figure 1.6: Laughlin gedanken experiment. The introduction of a magnetic flux $\phi(t)$ creates time-dependent electric field and a radial current density $\boldsymbol{J}(t)$.

1.3 Edge states in the Laughlin sequence

As we have seen in the previous Section, the FQH effect is a peculiar phase of matter whose description involves necessarily a many-body picture, in contrast with IQH effect, which can be completely understood in terms of independent electrons. As a result, the excitations of these states are not fermions, but exotic quasi-particles or quasi-holes with a fractional charge and a fractional statistics. Due to these peculiar characteristics of the FQH effect, its description in terms of a microscopic many-body model is an highly non-trivial problem. A common and powerful method to overcome this issue is to introduce low-energy effective field theories that capture all the essential properties of FQH states and disregard the microscopic degrees of freedom.

In this Section, we introduce a bulk effective field theory for Laughlin states that is able to reproduce the phenomenology previously described [47]. Subsequently, by restricting this effective field theory to the boundary, an edge state theory for the Laughlin sequence can be derived, which is of great interest for the remainder of this thesis. Interestingly, it turns out that FQH edge states allow for a description in terms of one-dimensional chiral bosonic modes. Then, starting from these bosonic modes, the bosonization identity, which we will introduce in the following, can be employed to construct a field operator for Laughlin quasi-particles.

1.3.1 Effective field theory for Laughlin states

In the following part, we derive an effective field theory for FQH states in the Laughlin sequence by following the seminal works by X. G. Wen [46, 47], who introduced this low-energy description for the first time. Here, we adopt the usual convention of field theory and we label with index 0 the temporal coordinates and with 1 and 2 the two spatial coordinates. We resort to Greek letters for index of three-dimensional vectors involving all the coordinates, while we employ Roman letters for indices of vectors with purely spatial components.

Let us consider a two-dimensional systems, whose electrons are coupled to an external electromagnetic field A_μ by the conserved current $J^\mu = (J^0, \boldsymbol{J})$, where J^0 and $\boldsymbol{J}$ are, respectively, the charge and current density of electrons. The Lagrangian

density assumes the following form

$$\mathcal{L}_A = A_\mu J^\mu, \tag{1.53}$$

where the summation over repeated index is considered. The physical quantities associated to this theory should behave in response to the external magnetic fields as those of a fractional state at a fixed filling factor ν. In the latter case, any variation in the magnetic field δB induces a variation in the charge density $\delta n_e = \frac{\delta J^0}{-e} \frac{\nu}{2\pi} \delta B$ in accordance with Eq. (1.19). Moreover, the presence of an electric field δE_i generates a current $\delta J^i = \sigma_{xy} \delta E_i$ in the transverse direction, where $\sigma_{xy} = \frac{\nu e^2}{2\pi}$ is the Hall resistivity. This two conditions can be resumed in a single expression involving the variation of current δJ^μ as

$$\delta J^\mu = -\frac{\nu e^2}{2\pi} \epsilon^{\mu\rho\sigma} \partial_\rho \delta A_\sigma, \tag{1.54}$$

where $\epsilon^{\mu\rho\sigma}$ is the anti-symmetric tensor in $2+1$ dimensions. A field theory that effectively describes a fractional quantum Hall states should produce a response to an external electromagnetic field corresponding to Eq. (1.54). Here, it is worth pointing out that the electromagnetic field A_μ does not include also the magnetic field that induces the quantum Hall effect.

The simplest way to implement such a theory is to introduce an additional vector field a, which is invariant under $U(1)$ transformations

$$a'_\mu = a_\mu + \partial_\mu g, \tag{1.55}$$

with $g = g(t, x, y)$ a generic function. A vector field that satisfies the transformation rule in Eq. (1.55) is called an *abelian field*. The only conserved current in $2+1$ dimensions that can be written in terms of a single abelian field and that satisfies gauge-invariance is [75]

$$J^\mu = -\frac{e}{2\pi} \epsilon^{\mu\rho\sigma} \partial_\rho a_\sigma. \tag{1.56}$$

In this phenomenological approach, a_μ can be viewed as an emergent field that stands for the collective behavior of many underlying electrons evolving according to an unspecified microscopic dynamics.

The following new term, including the abelian field a,

$$\mathcal{L}_a = \frac{k}{4\pi} a_\mu \epsilon^{\mu\rho\sigma} \partial_\rho a_\sigma \tag{1.57}$$

is added to the Lagrangian of the system, which now reads

$$\mathcal{L} = \mathcal{L}_a + \mathcal{L}_A = \frac{k}{4\pi} a_\mu \epsilon^{\mu\rho\sigma} \partial_\rho a_\sigma - \frac{e}{2\pi} A_\mu \epsilon^{\mu\rho\sigma} \partial_\rho a_\sigma, \tag{1.58}$$

where k is a real parameter. From the field-theoretical point of view, it is instructive to note that the new term $\mathcal{L}_a$ is an example of Chern-Simons Lagrangian [76]. They are the only relevant term in the low-energy limit (long-distance and large-time physics), which respect rotational symmetry and break time-reversal symmetry in $2+1$ dimensions. The value of parameter k can be fixed by imposing that the conserved current obtained from the Lagrangian in Eq. (1.58) assumes the form in Eq. (1.54). At this purpose, one can consider the Euler-Lagrange equations

$$\partial_\rho \frac{\delta \mathcal{L}}{\delta \partial_\rho a_\mu} - \frac{\delta \mathcal{L}}{\delta a_\mu} = 0, \tag{1.59}$$

which give the following result for the Lagrangian in Eq. (1.58)

$$\frac{1}{2\pi}\epsilon^{\mu\rho\sigma}\partial_\rho a_\sigma = \frac{e}{2\pi k}\epsilon^{\mu\rho\sigma}\partial_\rho A_\sigma. \tag{1.60}$$

By considering the definition of conserved current in Eq. (1.56), one finds the following relation

$$J_\mu = \frac{e}{2\pi k}\epsilon^{\mu\rho\sigma}\partial_\rho A_\sigma. \tag{1.61}$$

The form of current in Eq. (1.54), which is consistent with the phenomenology of a FQH state at filling factor ν, is thus recovered if the parameter is fixed to $k = \frac{1}{\nu}$. As a side comment, it is interesting to observe that the hamiltonian density obtained from Eq. (1.58) vanishes identically, namely

$$\mathcal{H} = \frac{\delta\mathcal{L}}{\delta\partial_t a_\mu}\partial_t a_\mu - \mathcal{L} = 0. \tag{1.62}$$

This result is a consequence of the fact that Chern-Simons theory are a particular example of a *topological quantum field theory* [5, 77].

1.3.2 Edge states

In general, Chern-Simons theory might include more than a single $U(1)$ gauge field or even $SU(n)$ gauge field. The choice of a single emergent gauge field imposes significant restriction on the phenomenology that can be described by this theory. In this case, as we will show in the following, the effective field theory with a single emergent field is a suitable description of a system with a single chiral mode at each boundary, i.e. a FQH state belonging to the Laughlin sequence. Indeed, for other filling factor, the structure of edge modes is more complicated and consists of several channels which might also have different chirality. The choice of states belonging to the Laughlin sequence with $\nu = \frac{1}{2n+1}$ simplifies drastically the structure at the edge, where a single edge mode arises at the boundary.

Starting from the total Lagrangian in Eq. (1.58), it is useful to construct the action

$$S = \int d^3x \mathcal{L} = \int d^3x \left(\frac{1}{4\pi\nu}a_\mu\epsilon^{\mu\rho\sigma}\partial_\rho a_\sigma - \frac{e}{2\pi}A_\mu\epsilon^{\mu\rho\sigma}\partial_\rho a_\sigma\right). \tag{1.63}$$

Let us observe that under the gauge transformation

$$\begin{cases} a'_\mu = a_\mu + \partial_\mu g, \\ A'_\mu = A_\mu + \partial_\mu f, \end{cases} \tag{1.64}$$

with $f = f(t,x,y)$ a real function, the action S transforms as

$$S' = S + \Delta S. \tag{1.65}$$

where the additional term is

$$\Delta S = \int d^3x \left(\frac{1}{4\pi\nu}\partial_\mu g\epsilon^{\mu\rho\sigma}\partial_\rho a_\sigma - \frac{e}{2\pi}\partial_\mu f\epsilon^{\mu\rho\sigma}\partial_\rho a_\sigma\right). \tag{1.66}$$

In order to obtain a gauge-invariant action S, the contribution ΔS must vanish. In a system without boundaries, all the integrals range from $-\infty$ to $+\infty$: since the
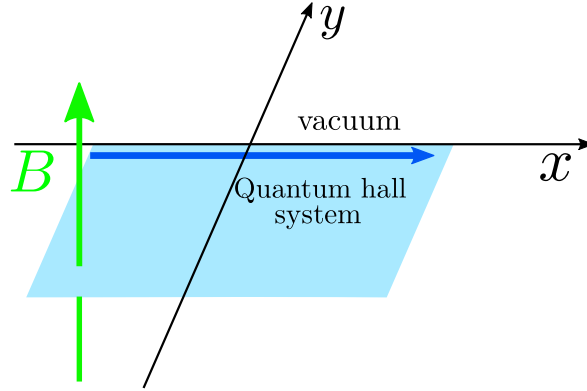
Figure 1.7: When a Laughlin system is confined to the lower region of the xy plane, a topologically protected edge state appears at the boundary between the quantum Hall system and the vacuum. This edge state propagates towards right for magnetic field pointing towards the positive semi-axis z.

integrand in ΔS contains only contributions including derivatives of the field a, the assumption that field a vanishes at infinite in time and space coordinates is sufficient to recover the gauge-invariance of the action S.

In the case of a finite system, the argument of gauge-invariance for the action S based on a field vanishing at infinite cannot hold true anymore. Nevertheless, the additional requirements to impose in order for the action S to be gauge-invariant will make us discover some new interesting physics. Indeed, as we have already seen for the IQH effect, the presence of a confinement is crucial for the emergence of chiral states at the boundary of a quantum Hall bar.

For definiteness, let us assume our system is confined to the lower part of the xy plane, as depicted in Fig. 1.7. In this case the integral over y in Eq. (1.66) is limited to the region $\{-\infty, 0\}$: the contribution ΔS becomes

$$\Delta S = \int_{-\infty}^{+\infty} dt \int_{-\infty}^{+\infty} dx \int_{-\infty}^{0} dy \left(\frac{1}{4\pi\nu} \partial_\mu g \epsilon^{\mu\rho\sigma} \partial_\rho a_\sigma - \frac{e}{2\pi} \partial_\mu f \epsilon^{\mu\rho\sigma} \partial_\rho a_\sigma \right) =$$

$$= \int_{-\infty}^{+\infty} dt \int_{-\infty}^{+\infty} dx \frac{1}{4\pi\nu} \left[g \left(\partial_t a_x - \partial_x a_t \right) \right]_{y=0}. \tag{1.67}$$

As a result, a sufficient condition for the gauge-invariance of the action S in this finite region is

$$\left[g \left(\partial_t a_x - \partial_x a_t \right) \right]_{y=0} = 0. \tag{1.68}$$

The simplest choice to satisfy this condition is to impose that the gauge transformation vanishes at the edge, such that $g(t, x, 0) = 0$. In this way, we do not have to restrict the gauge fixing of field a in any sense.

A possible choice to fix the gauge is to impose that the time component of a vanishes as

$$a_t = 0. \tag{1.69}$$

The equation of motion associated to this component are

$$\partial_x a_y = \partial_y a_x. \tag{1.70}$$

36

They are solved by introducing a new bosonic field $\Phi_R(t, x, y)$, which are linked to the emergent field a as

$$a_x(t, x, y) = -\sqrt{\nu}\partial_y\Phi_R(t, x, y), \quad a_y(t, x, y) = -\sqrt{\nu}\partial_x\Phi_R(t, x, y). \qquad (1.71)$$

This new bosonic field can be employed to define a $1 + 1$ boundary effective theory that is able to describe chiral edge states belonging to the Laughlin sequence. In order to find out the Lagrangian for this theory, we write the action S in terms of Φ_R as

$$S = \frac{1}{4\pi}\int_{-\infty}^{+\infty}dt\int_{-\infty}^{+\infty}dx\int_{-\infty}^{0}dy\,(\partial_y\Phi_R\partial_t\partial_x\Phi_R - \partial_x\Phi_R\partial_t\partial_y\Phi_R)\,, \qquad (1.72)$$

where we used the condition $a_t = 0$. The next step is to perform one integral, such that the remaining action would describe a $1 + 1$ system. Before doing that, we integrate by parts over x

$$S = \frac{1}{4\pi}\int_{-\infty}^{+\infty}dt\int_{-\infty}^{+\infty}dx\int_{-\infty}^{0}dy\partial_y\partial_t\Phi_R\partial_x\Phi_R, \qquad (1.73)$$

where we assumed that $\Phi_R(t, x = \pm\infty, y) = 0$. Now, the integral over y can be easily performed, thus obtaining

$$S = \frac{1}{4\pi}\int_{-\infty}^{+\infty}dt\int_{-\infty}^{+\infty}dx\partial_t\Phi_R\partial_x\Phi_R\Big|_{y=0}. \qquad (1.74)$$

This last equation allows us to define the following Lagrangian

$$\mathcal{L}_R = \frac{1}{4\pi}\partial_t\Phi_R\partial_x\Phi_R\Big|_{y=0}, \qquad (1.75)$$

such that

$$S = \int d^2x\mathcal{L}_R. \qquad (1.76)$$

Let us now observe that the field appearing in $\mathcal{L}_R$ are confined to the edge of the system, since they are evaluated for $y = 0$. Thus, we have found out a $1 + 1$ dimensional effective field theory that describes the emergent chiral states at the edge of FQH state in the Laughlin sequence. In this sense, it is useful to define the following notation for bosonic field Φ_R

$$\Phi_R(x, t) \equiv \Phi_R(t, x, 0), \qquad (1.77)$$

since they depend only on the coordinates x and t.

It is easy to demonstrate that the Lagrangian in Eq. (1.75) has a vanishing hamiltonian. This is a major problem for the description of edge states and for the derivation of their transport properties. An useful way to introduce a dynamics in the description of the edge states is to add a free parameter to the theory. This can be done by implementing a different gauge fixing condition with respect to (1.69), such as

$$a_t + va_x = 0, \qquad (1.78)$$

where v is a real parameter, without any constraint on its specific value. In the following, it will be clear that it represents the velocity of propagation along the FQH chiral states. This velocity is not an universal parameter and the determination of

its actual form is a non-trivial problem since it depends on the microscopic model for the confining potential of the edge.

Let us notice that it is not necessary to calculate the action S in this new gauge, since the condition in Eqs. (1.69) and (1.78) are related by the following change of variables

$$\left\{ \begin{array}{l} x' = x - vt \\ y' = y \\ t' = t \end{array} \right. \Rightarrow \left\{ \begin{array}{l} a'_x = a_x \\ a'_y = a_y \\ a'_t = a_t + v a_x \end{array} \right. . \tag{1.79}$$

In this new coordinates, the action in Eq. (1.76) becomes

$$S = -\frac{1}{4\pi} \int d^2 x \, \partial_x \Phi_R \left(\partial_t + v \partial_x \right) \Phi_R, \tag{1.80}$$

with a Lagrangian

$$\mathcal{L}_R = -\frac{1}{4\pi} \partial_x \Phi_R \left(\partial_t + v \partial_x \right) \Phi_R. \tag{1.81}$$

As anticipated, the dynamics of chiral edge states in the Laughlin sequence can be entirely described in terms of of a free bosonic mode propagating chirally in one dimension with velocity v. Since we are mainly interested in the transport properties of quantum Hall systems, it is useful to establish a connection between this bosonic field and electron charge density ρ_R on the edge. The latter quantity can be obtained by starting from the $\mu = 0$ component of the $2 + 1$-dimensional conserved current in Eq. (1.56)

$$\frac{J_0}{-e} = \frac{1}{2\pi} \left(\partial_x a_y - \partial_y a_x \right), \tag{1.82}$$

and integrating it on along the width of the edge λ, which is assumed to be very small along the $\hat{y}$ axis [78]. One finds

$$\rho_R(x) = \frac{1}{2\pi} \int_{-\lambda}^{0} \left(\partial_x a_y - \partial_y a_x \right). \tag{1.83}$$

The first contribution, in the limit $\lambda \to 0$, vanishes, since

$$\int_{-\lambda}^{0} \partial_x a_y \sim \lambda \partial_x a_y \Big|_{y=0} \to 0. \tag{1.84}$$

On the contrary, the remaining term is non-zero and can be evaluated as

$$\int_{-\lambda}^{0} \partial_y a_x = -a_x \Big|_{y=-\lambda} = \sqrt{\nu} \partial_x \Phi_R(x, t), \tag{1.85}$$

where we used that a_μ is zero outside the bar ($y \geq 0$). Thus, according to this relation, electron density at the edge is proportional to the space derivative of the bosonic field Φ_R

$$\rho_R = -\frac{1}{2\pi} \sqrt{\nu} \partial_x \Phi_R. \tag{1.86}$$

The edge Lagrangian in Eq. (1.81) generates the following equation of motion for the bosonic field Φ_R

$$\left(\partial_t + v \partial_x \right) \Phi_R = 0. \tag{1.87}$$

According to the relation in Eq. (1.86), one also finds the equation of motion for electron density

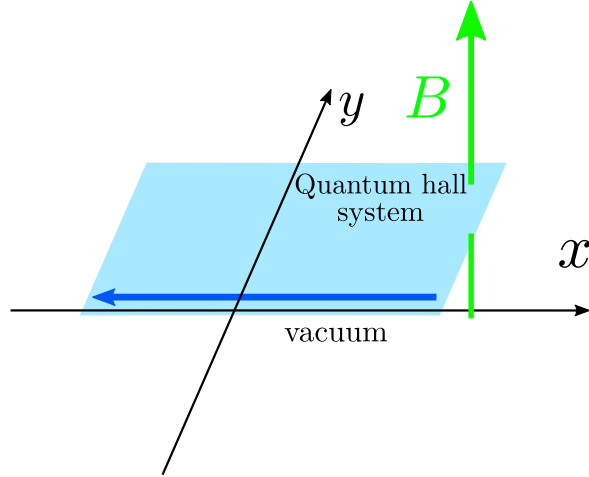$$\partial_t \rho_R + v \partial_x \rho_R = 0, \tag{1.88}$$

Figure 1.8: When a Laughlin system is confined to the upper region of the xy plane, a topologically protected edge state appears at the boundary between the quantum Hall system and the vacuum. This edge state propagates towards left for magnetic field pointing towards the positive semi-axis z.

which is solved by a generic function of the form $\rho_R(x,t) = f(x - vt)$. As a result, the density ρ_R propagates rigidly towards right as a wave with a constant speed v. The other alternative geometry, where the Hall fluid lies in the plane xy with $y > 0$, can be treated with a similar analysis (see Fig. 1.8). The emergent field a can be linked to a bosonic field Φ_L, as we did in Eq. (1.71). The edge Lagrangian for this bosonic field reads

$$\mathcal{L}_L = \frac{1}{4\pi} \partial_x \Phi_L \left(\partial_t - v \partial_x \right) \Phi_L, \tag{1.89}$$

which describes a bosonic mode propagating in the left (L) direction, i.e. a regressive mode. Notice that the same velocity v of right-moving has been chosen for symmetry reasons. An edge density ρ_L can be similarly introduced as

$$\rho_L = \frac{\sqrt{\nu}}{2\pi} \partial_x \Phi_L, \tag{1.90}$$

which propagates rigidly towards left, due to the equation of motion $(\partial_t - v \partial_x)\rho_L = 0$.

1.3.3 Edge hamiltonian

At this point, it is useful to express the bosonic theory in terms of an edge hamiltonian. We can evaluate the hamiltonian density $\mathcal{H}_R$ from Eq. (1.81), thus obtaining the edge hamiltonian

$$H_R = \int_{-\infty}^{+\infty} dx \mathcal{H}_R = \frac{v}{4\pi} \int_{-\infty}^{+\infty} dx \left(\partial_x \Phi_R \right)^2 . \tag{1.91}$$

It is convenient to recast the electron density ρ_R in terms of its Fourier components. By considering an edge with finite length L, the Fourier series for ρ_R is

$$\rho_R(x) = \frac{1}{L} \sum_{k=-\infty}^{+\infty} \rho_{R,k} e^{ikx}, \tag{1.92}$$

where we introduced

$$\rho_{R,k} = \int_{-\frac{L}{2}}^{\frac{L}{2}} dx \rho_R(x) e^{-ikx}. \tag{1.93}$$

Assuming periodic boundary conditions, the momentum k is quantized as $k = \frac{2\pi}{L}n$.

When expressed in term of this Fourier components, the edge hamiltonian becomes

$$H_R = \frac{2\pi v}{\nu L} \sum_{k=-\infty}^{+\infty} \rho_{R,k}\rho_{R,-k} + \frac{\pi v}{\nu L} N_R^2, \tag{1.94}$$

where we isolated the zero mode component of the density, that physically corresponds to the number of electrons in the systems respect to an average equilibrium value,

$$N_R = \rho_{R,0} = \int_{-\frac{L}{2}}^{\frac{L}{2}} \rho_R(x). \tag{1.95}$$

We define the variable $\pi_{R,k}$ conjugate to $\rho_{R,k}$ by imposing the following canonical commutation relation.

$$[\rho_{R,k}, \pi_{R,k'}] = i\delta_{k,k'}. \tag{1.96}$$

Through the hamiltonian in Eq. (1.94), it is immediate to show that the time derivative of this conjugate variable is proportional to $\rho_{R,k}$ as

$$\dot{\pi}_{R,k} = -\frac{\partial H_R}{\partial \rho_{R,k}} = \frac{2\pi v}{\nu L} \rho_{R,-k}, \tag{1.97}$$

when $k \neq 0$. Since the other Hamilton equation from Eq. (1.94) gives

$$\rho_{R,k} = -ikv\rho_{R,k}, \tag{1.98}$$

we find that for $k \neq 0$

$$\pi_{R,k} = i\frac{2\pi}{\nu k L} \rho_{R,-k}. \tag{1.99}$$

Given the direct proportionality between these two variables, the commutation relation in Eq. (1.96) becomes

$$[\rho_{R,k}, \rho_{R,k'}] = \frac{k\nu L}{2\pi} \delta_{k,-k'} \quad \text{if } k, k' \neq 0, \tag{1.100}$$

$$[\rho_{R,0}, \pi_{R,0}] = i. \tag{1.101}$$

This pair of commutation relations is known as Kac-Moody algebra [79], which typically determines the structure of all one-dimensional theories of interacting electrons, known as Tomonaga-Luttinger liquids [80–83].

Finally, we introduce this bosonic annihilation and creation operators for $k > 0$

$$b_{R,k} = \sqrt{\frac{2\pi}{k\nu L}} \rho_{R,k}, \quad b_{R,k}^\dagger = \sqrt{\frac{2\pi}{k\nu L}} \rho_{R,-k}, \tag{1.102}$$

which have to satisfy

$$\left[b_{R,k}, b_{R,k'}^\dagger\right] = \delta_{k,k'}. \tag{1.103}$$

The edge hamiltonian can now be separated in a zero-mode contributions related to the number of electrons in the system and in a contribution which is diagonal in the bosonic operator $b_{R,k}$

$$H_R = \sum_{k>0} vk b_{R,k}^\dagger b_{R,k} + \frac{\pi v}{\nu L} N_R^2. \tag{1.104}$$

40

Interestingly, we obtained for the bosonic part of the edge hamiltonian an exactly linear dispersion relation $\epsilon(k) = vk$.

The corresponding edge hamiltonian for left-moving modes is

$$H_L = \frac{v}{4\pi} \int_{-\infty}^{+\infty} dx \, (\partial_x \Phi_L(x))^2. \tag{1.105}$$

The corresponding Kac-Moody algebra for the left-moving density components is

$$[\rho_{L,k}, \rho_{L,k'}] = -\frac{k\nu L}{2\pi} \delta_{k,-k'}, \tag{1.106}$$

which has an opposite sign with respect to Eq. (1.100). By introducing left-moving bosonic annihilation and creation operators

$$b_{L,k} = \sqrt{\frac{2\pi}{k\nu L}} \rho_{L,-k}, \quad b_{L,k}^\dagger = \sqrt{\frac{2\pi}{k\nu L}} \rho_{L,k}, \tag{1.107}$$

the edge hamiltonian for left-movers in Eq. (1.105) can be written in a form similar to Eq. (1.104)

$$H_L = \frac{v}{4\pi} \int_{-\infty}^{+\infty} dx \, (\partial_x \Phi_L(x))^2 = \sum_{k>0} vk b_{L,k}^\dagger b_{L,k} + \frac{\pi v}{\nu L} N_L^2, \tag{1.108}$$

where $N_L = \rho_{L,0} = \int_{-\frac{L}{2}}^{\frac{L}{2}} dx \rho_L(x)$.

In conclusion, let us observe that the bosonic nature of collective excitations of fermionic systems is a typical characteristic of one-dimensional interacting quantum systems [34]. Indeed, this physical picture fits into the paradigm of the Tomonaga-Luttinger liquid [35, 83], which is effectively and powerfully employed to tackle low-energy physics of interacting fermions in one dimension. Through this theory, it is possible to find an exact solution of the interacting problem, a remarkable feature that has not analogies in higher dimensions. In particular, since the edge states of a FQH fluid are chiral, the theory just described is known as chiral Luttinger liquid theory [46].

In the following, we consider the limit $L \to \infty$: in this way, we can safely disregard the zero mode terms $\sim \frac{1}{L}$ in H_R and H_L. This is a good approximation, since, due to the remarkable coherence length of quantum Hall edge states, the Hall bar employed in transport experiments have edges with typical dimensions of the order of several μm [4]. Under this assumption, we obtain the following expansion of bosonic field $\Phi_{R/L}$ in terms of bosonic operators $b_{R/L,k}$

$$\Phi_{R/L}(x) = i\sqrt{\frac{2\pi}{L}} \sum_{k>0} \frac{e^{-\frac{ak}{2}}}{\sqrt{k}} \left(e^{\pm ikx} b_{R/L,k} - e^{\mp ikx} b_{R/L,k}^\dagger \right). \tag{1.109}$$

1.3.4 Bosonization for the Laughlin sequence

The derivation of the one-dimensional theory describing FQH edge states shows that a system of interacting fermions in one-dimension behave as collective bosonic modes propagating chirally along the edge. Here, we provide the connection between

---

[4]A careful treatment of the terms $\sim \frac{1}{L}$ becomes meaningful in strongly confined structures, where the finite size effects cannot be neglected, such as quantum dots

the bosonic fields $\Phi_{R/L}$ and the excitations of a FQH state, which are electrons or quasi-particle with fractional charge $e^* = \nu e$, in the framework of the so-called bosonization approach.

First of all, one has to understand how to add or remove charge at the edge. We introduce the electronic annihilation operators $\Psi_{R/L}^{(e)}$, which eliminate a charge e from the R or L edge state. To implement this operation, they must satisfy the following commutation relations with electron density operators

$$\left[\rho_{R/L}(x), \Psi_{R/L}^{(e)}(y)\right] = -\delta(x-y)\Psi_{R/L}^{(e)}(y). \tag{1.110}$$

As pointed out by X. G. Wen, from the Kac-Moody relations in Eq. (1.100) and (1.106) one finds the following commutators involving $\rho_{R/L}$ and $\Phi_{R/L}$

$$\left[\Phi_{R/L}(x), \Phi_{R/L}(y)\right] = \pm i\pi \text{sign}(x-y), \tag{1.111}$$

$$\left[\rho_{R/L}(x), \Phi_{R/L}(y)\right] = \mp i\sqrt{\nu}\delta(x-y)\Psi_{R/L}^{(e)}(y). \tag{1.112}$$

By comparing commutators in Eqs. (1.110) and (1.112), the density operators seem to behave as functional derivatives for the electronic fields $\Psi_{R/L}^{(e)}(x)$. Inspired by this analogy, Wen postulated that the form of fermionic fields should be $\Psi_{R/L}^{(e)} \propto e^{\frac{i}{\sqrt{\nu}}\Phi_{R/L}(x)}$. This is called bosonization identity. The exact expression for fermionic fields is [46]

$$\Psi_{R/L}^{(e)} = \frac{\mathcal{F}_{R/L}^{(e)}}{\sqrt{2\pi a}} e^{\pm ik_F x} e^{-\frac{i}{\sqrt{\nu}}\Phi_{R/L}(x)}, \tag{1.113}$$

where a is a finite length cut-off, k_F is the Fermi momentum and $\mathcal{F}_{R/L}^{(e)}$ are ladder operators, called Klein factors, that change the numbers of electrons on the edge R or L [34–36]. Their presence is fundamental to ensure that fermionic fields obey the correct commutation relations and the right statistical properties between electrons on different edges. Let us note that the role of the phase factor $e^{\pm ik_F x}$ is to take into account that excitations are built on the top of a Fermi sea [83].

In order to show the validity of the postulated form for fermionic fields, we check whether they satisfy Eq. (1.110). By using the following operatorial identity

$$\left[e^A, B\right] = [A, B]e^A, \tag{1.114}$$

which is valid only if $[A, B]$ a c-number, we can easily prove that

$$\left[\mp\partial_x\Phi_{R/L}(x), \frac{\mathcal{F}^{(e)}}{\sqrt{2\pi a}} e^{\frac{i}{\sqrt{\nu}}\Phi_{R/L}(y)}\right] = -\delta(x-y)\Psi_{R/L}^{(e)}(y), \tag{1.115}$$

where the commutation relations in Eq. (1.111) have been used.

Fermionic fields must satisfy also the following anti-commutators

$$\left\{\Psi_{R/L}^{(e)}(x), \Psi_{R/L}^{(e)}(y)\right\} = 0. \tag{1.116}$$

Indeed, fermionic operators in Eq. (1.113) provide the right anti-commutator only if ν belongs to the Laughlin sequence. The Baker-Hausdorff relation, that holds for two operators A and B, whose commutator $[A, B]$ is a c-number,

$$e^A e^B = e^{A+B} e^{\frac{1}{2}[A,B]}, \tag{1.117}$$

can be used to show that

$$\Psi_{R/L}^{(e)}(x)\Psi_{R/L}^{(e)}(y) = \frac{1}{2\pi a}e^{\frac{i}{\sqrt{\nu}}\left[\Phi_{R/L}(x)+\Phi_{R/L}(y)\right]}e^{\frac{i\pi}{2\sqrt{\nu}}\left[\pm 2(x+y)-\text{sign}(x-y)\right]}, \qquad (1.118)$$

$$\Psi_{R/L}^{(e)}(x)\Psi_{R/L}^{(e)}(y) = \frac{1}{2\pi a}e^{\frac{i}{\sqrt{\nu}}\left[\Phi_{R/L}(x)+\Phi_{R/L}(y)\right]}e^{\frac{i\pi}{2\sqrt{\nu}}\left[\pm 2(x+y)+\text{sign}(x-y)\right]}, \qquad (1.119)$$

where we employed again the commutation relations in Eq. (1.111). From these equations,

$$\Psi_{R/L}^{(e)}(x)\Psi_{R/L}^{(e)}(y) = \Psi_{R/L}^{(e)}(y)\Psi_{R/L}^{(e)}(x)e^{\frac{i\pi}{\sqrt{\nu}}\text{sign}(x-y)}, \qquad (1.120)$$

which gives the correct anti-commutator in Eq. (1.116) only if $\nu = \frac{1}{2n+1}$, with $n \in \mathbb{N}$. The other anti-commutator relations of fermionic statistics

$$\left\{\Psi_{R/L}^{(e)}(x), \Psi_{R/L}^{(e)}{}^{\dagger}(y)\right\} \qquad (1.121)$$

requires a more complicated demonstration, which is behind the aim of this thesis and can be found in full detail in Ref. [36]. It is instructive to mention that the presence Klein factors $\mathcal{F}_{R/L}^{(e)}$ and the normalization constant $\frac{1}{\sqrt{2\pi a}}$, with $a \to 0$ are crucial in order to ensure the validity of Eq. (1.121).

As we already mentioned, electrons are not the only possible excitations of a FQH fluid. Indeed, Laughlin quasi-particles with fractional charge and statistics also exist in this strongly correlated phase of matter. The form for the quasi-particle field operators can be guessed by the previous discussion on fermion field operators and by the additional requirement that they add or remove from the edge a fraction of the electronic charge νe. For these reasons, we postulate that the field operators for quasi-particles is implemented by an operator $\Psi_{R/L}^{(qp)}(x) \propto e^{-i\sqrt{\nu}\Phi_{R/L}(x)}$. Indeed, field operators with such a form satisfy

$$\left[\rho_{R/L}(x), e^{-i\sqrt{\nu}\Phi_{R/L}(y)}\right] = -i\sqrt{\nu}\left[\rho_{R/L}(x), \Phi_{R/L}(y)\right]e^{-i\sqrt{\nu}\Phi_{R/L}(y)} =$$
$$= -\nu\delta(x-y)e^{-i\sqrt{\nu}\Phi_{R/L}(y)}, \qquad (1.122)$$

meaning that they correctly change the total density by a charge νe. Moreover, we can show that they satisfy also the anyonic statistical exchange properties. Indeed, one has that

$$e^{-i\sqrt{\nu}\Phi_{R/L}(x)}e^{-i\sqrt{\nu}\Phi_{R/L}(y)} =$$
$$= e^{-i\sqrt{\nu}\Phi_{R/L}(y)}e^{-i\sqrt{\nu}\Phi_{R/L}(x)}e^{-\nu\left[\Phi_{R/L}(x),\Phi_{R/L}(y)\right]} =$$
$$= e^{-i\sqrt{\nu}\Phi_{R/L}(y)}e^{-i\sqrt{\nu}\Phi_{R/L}(x)}e^{\mp i\nu\pi\text{sign}(x-y)}. \qquad (1.123)$$

Thus, these quasi-particle fields return the fractional statistical angle $\nu\pi$ for anyons. The complete bosonized expression for quasi-particle fields is

$$\Psi_{R/L}^{(qp)}(x) = \frac{\mathcal{F}_{R/L}^{(qp)}}{\sqrt{2\pi a}}e^{\pm ik_F x}e^{-i\sqrt{\nu}\Phi_{R/L}(x)}, \qquad (1.124)$$

where $\mathcal{F}_{R/L}^{(qp)}$ is the Klein factor for quasi-particle, defined in analogy with fermionic ones.
It is useful to point out the existence of a duality between electron and quasi-particle

fields, which can be understood by looking at Eqs. (1.113) and (1.124). The exponents of these fields, containing the bosonic fields are related by the transformation $\nu \leftrightarrow \frac{1}{\nu}$. This duality allows to immediately obtain the transport properties of electrons in presence of tunneling in terms of those of quasi-particles [84]. Let us notice that the difference between Klein factors of quasi-particles and electrons can be neglected, since Klein factors will play no role in our calculations.

Fermionic operators and hamiltonian at $\nu = 1$

As a conclusion, let us comment on the connection between electronic and quasi-particle fields derived in the bosonized for the unique integer filling factor of the Laughlin sequence, namely $\nu = 1$. Indeed, field operators in Eqs. (1.113) and (1.124) coincide at $\nu = 1$, such that one can use a single notation for that specific filling factor

$$\Psi_{R/L}(x) \equiv \Psi_{R/L}^{(qp)}(x)\Big|_{\nu=1} = \Psi_{R/L}^{(el)}(x)\Big|_{\nu=1}. \tag{1.125}$$

In addition, one can show that the bosonic description of low-energy excitations is completely equivalent to a one-dimensional fermionic model of non-interacting electrons with linear spectrum (see Appendix A). The hamiltonian for this system reads

$$H_{R/L} = \int_{-\infty}^{+\infty} dx : \Psi^\dagger(x)(\mp iv\partial_x - \mu)\Psi_{R/L}(x) :, \tag{1.126}$$

where $\mu = vk_F$ is the chemical potential. The contribution proportional to μ is fundamental in order to fix the ground state charge and energy (see the work of Haldane in Ref. [83]). The notation $: \cdots :$ stands for the normal ordering of operators with respect to the ground state: for fermionic systems the ground state is the filled Fermi sea. At $\nu = 1$, fermionic fields $\Psi_{R/L}(x)$ admit the following representation

$$\Psi_{R/L}(x) = \frac{1}{\sqrt{2\pi v}} \int_{-\infty}^{+\infty} d\epsilon\, e^{\mp i\epsilon \frac{x}{v}} a_{R/L}(\epsilon), \tag{1.127}$$

where $a_{R/L}(\epsilon)$ is a fermionic annihilation operator that satisfies the anti-commutation relation

$$\left\{ a_{R/L}(\epsilon), a_{R/L}^\dagger(\epsilon') \right\} = \delta(\epsilon - \epsilon'). \tag{1.128}$$

Given Eq. (1.128), it is easy to show that also $\Psi_{R/L}(x)$ satisfy fermionic anti-commutation relations

$$\left\{ \Psi_{R/L}(x), \Psi_{R/L}^\dagger(x') \right\} = \delta(x - x'). \tag{1.129}$$

Finally, in this fermionic picture, it is also possible to show that the electronic density assumes the following form (see Appendix A)

$$\rho_{R/L}(x) =: \Psi_{R/L}^\dagger(x)\Psi_{R/L}(x) : . \tag{1.130}$$

Chapter 2

Electron quantum optics

Due to the emergence of chiral and protected channels at the edges of a quantum Hall bar, experiments able to explore quantum phenomena associated with the wave-like nature of electrons can be realized. The idea of pushing this investigation down to the single-electron level gave rise to the new field of electron quantum optics (EQO). The wave nature of electrons traveling in one-dimensional edge states of quantum Hall systems bears strong analogies with the propagation of photons in wave-guide. Using analogs of beam-splitters and optical fibers, the electronic equivalents of optical setups can be implemented in a solid state system and used to investigate mesoscopic transport in the single-electron limit. These optical-like experiments provide a powerful tool to improve the understanding of electron propagation in quantum conductors. Inspired by the controlled manipulations of the quantum state of light, the recent development of single electron emitters has opened the way to the controlled preparation, manipulation and characterization of single to few electronic excitations that propagate in electron quantum optics setups. However, these experiments go beyond the simple transposition of optics concepts in electronics as several major differences occur between electron and photons, as we will demonstrate in the remainder of this thesis.

2.1 Introduction to electron quantum optics

In the context of EQO, a remarkable effort has been put forth by the condensed matter community to implement on-demand sources of electronic wave-packets in mesoscopic systems. After seminal theoretical works and groundbreaking experimental results, two main methods to realize single-electron sources assumed a prominent role in the field of EQO [85–89]. The first injection protocol relies on the periodic driving of the discrete energy spectrum of a quantum dot, which plays the role of a mesoscopic capacitor [11, 12, 90]. In this way, it is possible to achieve the periodic injection of an electron and a hole along the ballistic channels of a system coupled to this mesoscopic capacitor through a quantum point contact (QPC) [13, 15, 91, 92].

A second major step has been the recent realization of an on-demand source of electron through the application of a time-dependent voltage to a quantum conductor [31, 56, 87, 88, 93]. The main challenge to face, in this case, has been that an ac voltage would generally excite unwanted neutral electron-hole pairs, thus spoiling at its heart the idea of a single-electron source. The turning point to overcome this issue was the theoretical prediction by Levitov and co-workers that a periodic train

of quantized Lorentzian-shaped pulses, carrying an integer number of particles per period, is able to inject minimal single-electron excitations devoid of any additional electron-hole pair, then termed *levitons* [21–23]. Indeed, this kind of single-electron source is simple to realize and operate, since it relies on usual electronic components, and potentially provides a high level of miniaturization and scalability. For their fascinating properties [94], levitons have been proposed as flying qubits [95] and as source of entanglement [96–98] with appealing applications for quantum information processing. Moreover, quantum tomography protocols able to reconstruct their single-electron wave-functions have been proposed [99–101] and experimentally realized [28].

These single-electron sources allow the on-demand injection of individual excitations into mesoscopic devices mimicking the conventional photonic quantum optics with quantum Hall edge channels behaving as waveguides. Topological protection of edge states guarantees long electronic coherence lengths, which ensure the coherent manipulation of this individual electronic excitations over several μm. Moreover, the role of electronic beam splitter, which should mimic the half-silvered mirror of conventional optics, can be played by a quantum point contact (QPC), where electrons are reflected or transmitted with a tunable probability. By combining these elements with the single-electron sources previously described, interferometric setup, originally conceived for optics experiments, can be implemented also in the condensed matter realm [102, 103]. One famous example is the Hanbury-Brown-Twiss (HBT) interferometer [19], where a stream of electronic wave-packets is excited along ballistic channels and it is partitioned against a QPC [15]. The shot noise signal, generated due to the granular nature of electrons [104, 105], was employed to probe the single-electron nature of levitons in a non-interacting two-dimensional electron gas [14, 31].

A fundamental achievement of EQO has been the implementation of the Hong-Ou-Mandel (HOM) interferometer [18], where electrons impinge on the opposite side of a QPC with a tunable delay [14, 16, 88]. By performing this kind of collisional experiments, it is possible to gather information about the forms of the impinging electronic wave-packets and to measure their degree of indistinguishability [56, 92, 106]. For instance, when two indistinguishable and coherent electronic states collide simultaneously (zero time delay) at the QPC charge current fluctuations are known to vanish at zero temperature, thus showing the so called Pauli dip [14, 88, 107]. This dip can be interpreted in terms of anti-bunching effects related to the Fermi statistics of electrons [29, 30, 101, 108, 109].

In this Chapter, we restrict ourselves to consider only quantum Hall edge states at filling factor $\nu = 1$: due to the presence of a single non-interacting channel, this is the simplest system for the theoretical description of EQO fundamental concepts and results.
While many interesting and fascinating results have been obtained with the mesoscopic capacitor [15, 29, 30], we focus on the single-electron source based on Lorentzian voltage pulses for the rest of this thesis.

2.2   Single-electron voltage sources

A versatile protocol to emit in a controllable way single electrons along the channels of quantum conductors can be implemented by resorting to the apparently simple principle of applying a time-dependent voltage drive to a quantum conductor.
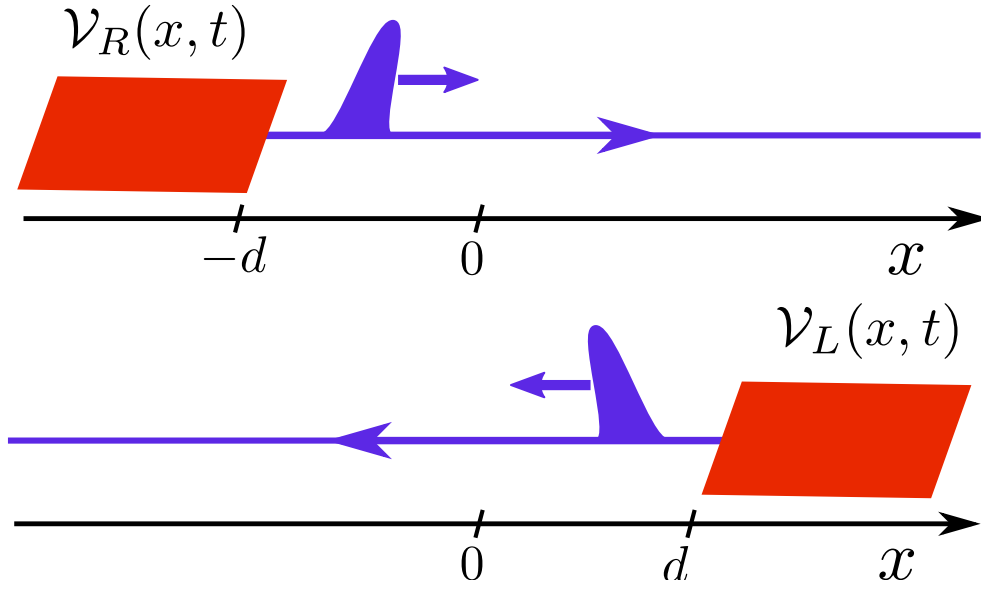
Figure 2.1: (Upper panel) A right-moving channel emerging on the edge of quantum Hall bar. This edge state is connected to a reservoir driven by a time-dependent drive. This configuration is modeled by a space- and time- dependent potential $\mathcal{V}_R(x,t)$. (Lower panel) The same situation for a left-moving channel. This configuration is modeled by a space- and time- dependent potential $\mathcal{V}_L(x,t)$.

Electrons can be emitted into a mesoscopic system also by employing dc biased contact. Nevertheless, a dc bias cannot be used as an on-demand and tunable source of electron. In this sense, one has to trigger the single-electron emitter with a time-dependent voltage to achieve the controllable manipulation of electrons required for experimental and applicative purposes.

Let us consider the right-moving edge of a quantum Hall bar at filling factor $\nu = 1$, connected to a reservoir driven by a time-dependent voltage $V_R(t)$, as in Fig. 2.1. For the following discussion, it does not matter on which chirality we focus on. The total charge $\mathcal{C}$ emitted by this time-dependent voltage into the edge states can be written as the integral over all times of the right-moving current in Eq. (B.22)

$$\mathcal{C} = \int_{-\infty}^{+\infty} dt\, J_R(x,t) = \frac{e^2}{2\pi} \int_{-\infty}^{+\infty} dt\, V_R(t). \qquad (2.1)$$

For a generic ac voltage, electrons are emitted into the edge state together with other neutral excitations, such as electron-hole pairs. The main challenge to face is to get rid of this unwanted neutral electron-hole pairs, that spoil at its heart the idea of a single-electron source. In the following, we exploit the time-dependent transport theory developed in Sec. B.1 of Appendix B in order to find out the form of the optimal drive that is able to inject minimal single-electron excitations devoid of any additional electron-hole pair.

2.2.1 Fermionic fields in presence of time-dependent voltage

A single right-moving edge state of a quantum Hall bar at $\nu = 1$ is described by the edge hamiltonian

$$H_{R/L} = \int_{-\infty}^{+\infty} dx : \Psi^{\dagger}(x)(\mp iv\partial_x - \mu)\Psi_{R/L}(x) :, \tag{2.2}$$

where $\mu = vk_F$ is the chemical potential and

$$\Psi_{R/L}(x) = \frac{1}{\sqrt{2\pi v}} \int_{-\infty}^{+\infty} d\epsilon \, e^{\mp i\epsilon\frac{x}{v}} a_{R/L}(\epsilon). \tag{2.3}$$

Let us comment that operators $a_R(\epsilon)$ satisfy the following average values over the equilibrium configuration at temperature θ

$$\tag{2.4}$$

$$\langle a_R^{\dagger}(\epsilon)a_R(\epsilon')\rangle = \delta(\epsilon - \epsilon')f(\epsilon), \tag{2.5}$$

$$\langle a_R(\epsilon)a_R^{\dagger}(\epsilon')\rangle = \delta(\epsilon - \epsilon')\left(1 - f(\epsilon)\right), \tag{2.6}$$

where $f(\epsilon) = \frac{1}{1+e^{\frac{\epsilon-\mu}{\theta}}}$ is the Fermi distribution function at temperature θ.

The spectrum of hamiltonian in Eq. (2.3) is linear, namely $\epsilon(k) = vk$ (see upper panel of Fig. 2.2), where k represents the momentum of electrons. As demonstrated in detail in Appendix B, when a right-moving channel is connected to a time-dependent voltage $V_R(t)$, electrons that exit the contact and enter into the conducting channels have acquired a time-dependent phase $e^{i\chi(t)}$, with

$$\chi(t) = e \int_{-\infty}^{t-\frac{x}{v}} dt' V_R(t'). \tag{2.7}$$

This time dependence reflects the fact that electrons are not emitted in quantum states with definite energy. It is useful to introduce the Fourier transform of this voltage phase, which reads

$$p(\epsilon) = \int_{-\infty}^{+\infty} dt \, e^{i\chi(t)} e^{i\epsilon t}. \tag{2.8}$$

The right-moving fermionic field operator in Eq. (B.23) can be recast in terms of this Fourier transform as

$$\Psi_R(x,t) = \psi_R(x,t)e^{i\chi(t)}e^{i\epsilon t} =$$

$$= \frac{1}{\sqrt{2\pi v}} \int_{-\infty}^{+\infty} d\epsilon \, e^{-i\epsilon\left(t-\frac{x}{v}\right)} \tilde{a}(\epsilon), \tag{2.9}$$

where we defined

$$\tilde{a}_R(\epsilon) = \int_{-\infty}^{+\infty} d\epsilon_1 p(\epsilon_1)a_R(\epsilon - \epsilon_1), \tag{2.10}$$

which are expressed as a superposition of fermionic operators $a(\epsilon)$ weighted by the Fourier transform of the voltage phase.

In the presence of a time-dependent drive electrons is excited above the chemical potential and holes are generated below, with respect to the equilibrium situation. In the following, we employ this description of fermionic fields in presence of an external voltage to find out the drive able to emit on-demand single-electron excitations.
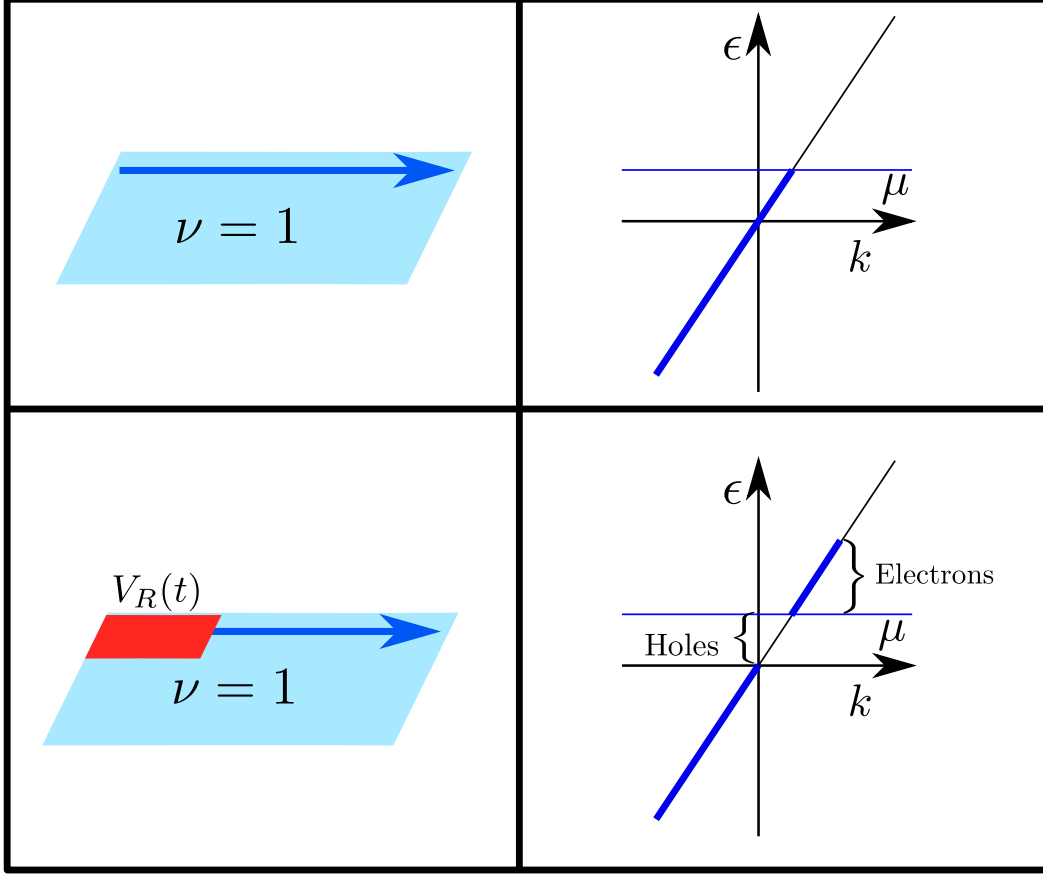
Figure 2.2: (Upper panel) A right-moving channel on the edge of quantum Hall bar. Its energy dispersion $\epsilon(k)$ is linear according to the edge hamiltonian.
(Lower panel) A right-moving channel on the edge of quantum Hall bar connected to a time-dependent voltage. Electrons are excited above the chemical potential μ and holes are generated below.

2.2.2 Single-electron voltage source

In the lower part of Fig. 2.2, the linear dispersion $\epsilon(k)$ of edge states is plotted in the presence of $V_R(t)$. The optimal condition for a time-dependent voltage is to generate no hole at all. In order to find out the optimal drive for the on-demand generation of single-electron excitations, we use the formalism to relate the property of a specific voltage, encoded in the function $p(\epsilon)$, to the number of holes N_h that it generates. This quantity can be calculated in terms of fermionic operators $\tilde{a}_R(\epsilon)$ as

$$N_h = \int_{-\infty}^{\mu} d\epsilon \left\langle \tilde{a}_R(\epsilon)\tilde{a}_R^\dagger(\epsilon) \right\rangle, \tag{2.11}$$

where the average is taken with respect to the equilibrium configuration. Let us observe that the integration is performed exclusively over energy *below* the chemical

potential. By using Eq. (2.10), one finds that

$$N_h = \int_{-\infty}^{\mu} d\epsilon \int_{-\infty}^{+\infty} d\epsilon_1 \int_{-\infty}^{+\infty} d\epsilon_2 p(\epsilon_1) p^*(\epsilon_2) \left\langle a(\epsilon) a^\dagger(\epsilon) \right\rangle =$$

$$= \int_{-\infty}^{\mu} d\epsilon \int_{-\infty}^{+\infty} d\epsilon_1 \int_{-\infty}^{+\infty} d\epsilon_2 p(\epsilon_1) p^*(\epsilon_2) \delta(\epsilon_1 - \epsilon_2) \left(1 - f(\epsilon - \epsilon_1)\right), \qquad (2.12)$$

where we used the average value of operators $a(\epsilon)$ given in Eq. (2.6). Since finite temperature effects can generate particle-hole pairs, we restrict our discussion to the zero temperature limit, where holes can exist only due to the presence of the ac voltage. In this limit, $f(\epsilon) = \theta(\mu - \epsilon)$ and one finds

$$N_h = \int_{-\infty}^{\mu} d\epsilon \int_{-\infty}^{\epsilon-\mu} d\epsilon_1 |p(\epsilon_1)|^2 = \int_{-\infty}^{0} d\epsilon \int_{-\infty}^{\epsilon} d\epsilon_1 |p(\epsilon_1)|^2., \qquad (2.13)$$

Notice that in the last step we performed the shift $\epsilon \to \epsilon + \mu$. Since ϵ is restricted to negative values by the first integral in Eq. (2.13), it is necessary that $p(\epsilon) = 0$ for $\epsilon < 0$ in order to ensure that no unwanted electron-hole pair is generated. By looking at Eq. (2.8), it is clear that this condition imposes a constraint on the structure of $e^{-i\chi(t)}$, when prolongate to the complex plane. In particular, it must have no pole in the lower half plane, in order to vanish for negative energy displacement, but at least one pole in the upper half plane, since it has to be non-zero somewhere. The simplest function that fulfills this requirement is

$$e^{i\chi(t)} = \frac{t + iW}{t - iW}, \qquad (2.14)$$

where W is a positive and real parameter. As a consequence, the corresponding voltage is

$$V(t) = -i\frac{1}{e}\frac{d}{dt} \ln\left(e^{i\chi(t)}\right). \qquad (2.15)$$

By applying this last equation to Eq. (2.14), one finds that the optimal drive is a Lorentzian voltage pulse with width at mid-height equal to $2W$

$$V_{lor}(t) = \frac{1}{(-e)}\frac{2W}{t^2 + W^2}. \qquad (2.16)$$

In addition, notice that the parameter of this voltage pulse are already set in order to give (see Eq. (2.1))

$$\mathcal{C} = \int_{-\infty}^{\infty} \frac{e^2}{2\pi} V_R(t) = -e. \qquad (2.17)$$

Thus, we demonstrated that the voltage in Eq. (2.15) emit into a quantum conductor a single charge. This minimal single-electron excitation, devoid of any additional electron-hole pair, emitted by the Lorentzian-shaped voltage in Eq. (2.16) is termed *leviton* [14, 23, 31].

Levitov generalized this result to the injection of multiple levitons at different time and with different width, such that the voltage

$$V_{lor}(t) = \sum_{k=1}^{N} \frac{1}{(-e)} \frac{2W_k}{(t - t_k)^2 + W_k^2} \qquad (2.18)$$

is a source of N pure electronic excitations. Let us point out that this result is analogous the properties of solitons in non-integrable systems, which can be arbitrarily

superimposed without losing their solitonic nature. In this way, also the simultaneous and on-demand emission of many electronic excitations can be easily achieved. On the experimental side, a single-electron source based on levitons is simple to realize, since it relies on usual electronic components. Anyway, for a realistic implementation one has to considered periodic voltage pulses. The expression for a train of quantized Lorentzian pulses with period $\mathcal{T}$ is

$$V_{lor}(t) = \sum_{k=-\infty}^{\infty} \frac{1}{(-e)} \frac{2W}{(t-k\mathcal{T})^2 + W^2},$$
(2.19)

which is nothing but a particular case of Eq. (2.18), thus proving that levitons are single-electron excitations even in the periodic case.

2.3 Electron coherence and levitons wave-functions

The single-electron source previously introduced can be employed to investigate the properties of electronic quantum states traveling along the edge states of quantum Hall systems. A single leviton that propagates along an edge channel can be properly characterized in terms of a wave-function that represents a single-particle quantum state placed on the top of the Fermi sea. In the following, our goal is to extract the expression for this wave-function. For this reason, we focus on the electronic correlations in energy space, where it is easy to discriminate the nature of excitations induced into the edge states by the presence of a voltage. The best way to find out levitons wave-function is to work at zero temperature, condition that we will assume in the following.

2.3.1 Correlation in energy space

It is useful to start by describing the effect of a generic time-dependent voltage $V_R(t)$ on the occupation number of electrons in the energy space. At this purpose, we define the correlation function for fermionic operators $\tilde{a}_R(\epsilon)$

$$\tilde{G}_R(\epsilon, \epsilon') = \left\langle \tilde{a}_R^\dagger(\epsilon) \tilde{a}_R(\epsilon') \right\rangle.$$
(2.20)

Indeed, the function $\tilde{G}_R(\epsilon, \epsilon')$ takes into account all the electronic correlations, including those due to the driving voltage and those related to the presence of a filled Fermi sea. At the equilibrium, i.e. when $V_R(t) = 0$, Eq. (2.20) reduces to

$$\tilde{G}_{0,R}(\epsilon, \epsilon') = \left\langle a_R^\dagger(\epsilon) a_R(\epsilon') \right\rangle.$$
(2.21)

It is convenient to subtract this equilibrium contribution to $\tilde{G}_R(\epsilon, \epsilon')$, thus defining the following excess correlation function in the energy space

$$\Delta\tilde{G}_R(\epsilon, \epsilon') = \tilde{G}_R(\epsilon, \epsilon') - \tilde{G}_{0,R}(\epsilon, \epsilon'),$$
(2.22)

which provides information about the distribution in energy of electronic states exclusively related to the voltage drive. The off-diagonal contribution ($\epsilon \neq \epsilon'$) corresponds to the coherence between electronic states at different energies. By exploiting it, one can discriminate the nature of fermionic excitations by inspecting their energy properties. In Fig. 2.3, we present the Fourier plane corresponding to the
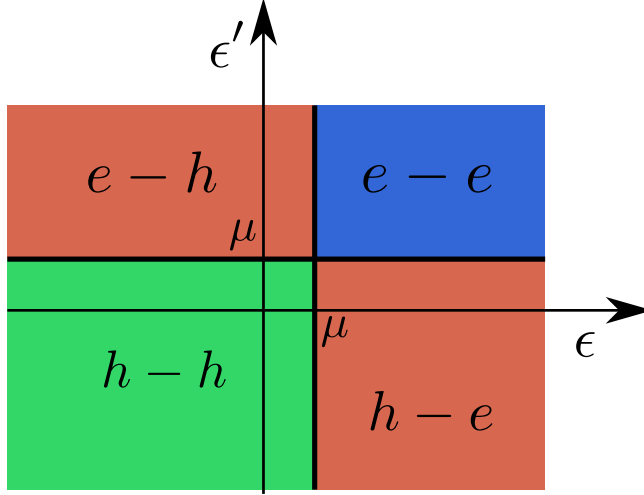
Figure 2.3: Scheme of electronic correlations in Fourier space. Single-electron excitations ($e-e$) contributes to the upper-right quadrant, while single-hole excitations ($h-h$) to the lower-left quadrant ($\epsilon < \mu$, $\epsilon' < \mu$). The remaining quadrants, defined by $\epsilon < \mu \epsilon' > \mu$ or $\epsilon > \mu, \epsilon' < \mu$ correspond to the coherence between electronic and hole excitations ($e-h$ or $h-e$).

electronic correlation function $\Delta \tilde{G}_R(\epsilon, \epsilon')$. The upper-right quadrant, defined by $\epsilon > \mu$ and $\epsilon' > \mu$ contains the contribution of excitations having positive energies, that correspond to single-electron excitations ($e-e$ quadrant). Similarly, the lower-left quadrant ($\epsilon < \mu$, $\epsilon' < \mu$) contains the contribution of single-hole excitations with negative energies ($h-h$ quadrant). Finally, notice that, since the coherence functions depends on two time variables (which correspond to two energy variables in Fourier space), correlations of electron and hole excitations are possible. Therefore, the remaining quadrants, defined by $\epsilon < \mu \epsilon' > \mu$ or $\epsilon > \mu, \epsilon' < \mu$ correspond to the coherence between electronic and hole excitations. Let us observe that an optimal drive, injecting exclusively single-electron excitations, should have non-vanishing contribution solely from the $e-e$ quadrant. In order to connect Eq. (2.33) directly to the property of a particular drive $V_R(t)$, it is convenient to express Eq. (2.20) in terms of fermionic field Ψ_R, which contains the voltage phase $e^{i\chi(t)}$, by using

$$\tilde{a}_R(\epsilon) = \sqrt{\frac{v}{2\pi}} \int_{-\infty}^{+\infty} dt e^{i\epsilon t} \Psi_R(0, t). \tag{2.23}$$

Indeed, one finds

$$\tilde{G}_R(\epsilon, \epsilon) = \int_{-\infty}^{+\infty} dt \int_{-\infty}^{+\infty} dt' e^{i\epsilon t} e^{-i\epsilon t'} \langle \Psi_R^\dagger(0, t) \Psi_R(0, t') \rangle =$$
$$= \frac{1}{2\pi} \int_{-\infty}^{+\infty} dt \int_{-\infty}^{+\infty} dt' e^{i\epsilon t} e^{-i\epsilon t'} G_R^<(t, t'), \tag{2.24}$$

where we defined the Green's function

$$G_R^<(t, t') = \langle \Psi_R^\dagger(0, t) \Psi_R(0, t') \rangle. \tag{2.25}$$

$$\tag{2.26}$$

Let us comment, that, in analogy with Glauber's coherence theory of photons [32], Eq. (2.25) can be also termed electron coherence function. This object is the central quantity of the *electron coherence theory*, which aims at extending the theory of coherence originally conceived for photons to the case of electrons in mesoscopic systems [33, 86, 100]. While for photons a single coherence functions is sufficient, in mesoscopic systems one needs two types of coherence functions, respectively, for electrons and holes. Therefore, in addition to Eq. (2.25), one has to introduce

$$G_R^>(t, t') = \langle \Psi_R(0, t) \Psi_R^\dagger(0, t') \rangle. \tag{2.27}$$

Similarly to $\tilde{G}_R(\epsilon, \epsilon')$, also the equilibrium contribution $\tilde{G}_{0,R}(\epsilon, \epsilon')$ can be connected to fermionic operators ψ_R as

$$\tilde{G}_{0,R}(\epsilon, \epsilon') = \int_{-\infty}^{+\infty} dt \int_{-\infty}^{+\infty} dt' e^{i\epsilon t} e^{-i\epsilon t'} \langle \psi_R^\dagger(0, t) \psi_R(0, t') \rangle =$$
$$= \frac{1}{2\pi} \int_{-\infty}^{+\infty} dt \int_{-\infty}^{+\infty} dt' e^{i\epsilon t} e^{-i\epsilon' t'} G_{0,R}^<(t - t'), \tag{2.28}$$

where we identified the Green's function of the system at equilibrium

$$G_{0,R}^<(t - t') = \langle \psi_R^\dagger(0, t) \psi_R(0, t') \rangle, \tag{2.29}$$

$$\tag{2.30}$$

that corresponds to Eq. (2.27) when $V_R(t) = 0$. By plugging Eqs. (2.24) and (2.28) into Eq. (2.22), one obtains

$$\Delta \tilde{G}_R(\epsilon, \epsilon') = \int_{-\infty}^{+\infty} dt \int_{-\infty}^{+\infty} dt' e^{i\epsilon t} e^{-i\epsilon' t'} e^{-i\mu(t - t')} \Delta G_R^<(t, t'), \tag{2.31}$$

where we introduced the excess electron coherence function

$$\Delta G_R^<(t, t') = e^{i\mu(t - t')} \left(G_R^<(t, t') - G_{0,R}^<(t - t') \right) =$$
$$= e^{i\mu(t - t')} e^{i(\chi(t') - \chi(t))} \psi_R^\dagger(0, t) \langle \psi_R(0, t') \rangle, \tag{2.32}$$

which encodes all the effects of electron coherence due to the presence of a time-dependent drive.

The diagonal part ($\epsilon = \epsilon'$) of $\Delta \tilde{G}_R$ defines the following function

$$\Delta \tilde{f}_R(\epsilon) = \Delta \tilde{G}_R(\epsilon, \epsilon'), \tag{2.33}$$

which represents the probability distribution of electrons in energy space associated solely with the presence of the voltage. For a generic time-dependent drive, $\Delta \tilde{f}_R(\epsilon)$ can be different from zero for energies below or above the chemical potential, thus showing that unwanted electron-hole pairs are generated. On the contrary, when a voltage emits single-electron minimal excitations, the quantity in Eq. (2.33) must vanish for $\epsilon < \mu$, since hole-like states cannot be occupied. In this sense, $\Delta \tilde{f}_R(\epsilon)$ is related to the occupation probability for single-electron states. In terms of Eq. (2.32), the probability distribution $\Delta \tilde{f}_R(\epsilon)$ becomes

$$\Delta \tilde{f}_R(\epsilon) = \int_{-\infty}^{+\infty} dt \int_{-\infty}^{+\infty} dt' e^{i\epsilon t} e^{-i\epsilon t'} \Delta G_R^<(t, t'), \tag{2.34}$$

This expression holds true for a generic time-dependent drive: in the following, we evaluate it for the Lorentzian-shaped pulse in Eq. (2.89) and we use it to derive the explicit expression for the single-leviton wave-function.

2.3.2   Levitons wave-functions

The time-dependent phase for this Lorentizan-shaped pulse is given in Eq. (2.14). For completeness, we report here its expression

$$e^{i\chi(t)} = \frac{t + iW}{t - iW}. \tag{2.35}$$

Using this result, we can express Eq. (2.32) as

$$\Delta G_R^<(t,t') = e^{i\mu(t-t')} \left(\frac{t' - iW}{t' + iW} \frac{t + iW}{t - iW} - 1 \right) \langle \psi^\dagger(0,t)\psi(0,t') \rangle. \tag{2.36}$$

At zero temperature, the Fermi sea contribution is

$$\langle \psi^\dagger(0,t)\psi(0,t') \rangle = \frac{i}{2\pi v} \frac{e^{-i\mu(t-t')}}{t - t' - i0^+}. \tag{2.37}$$

By plugging this result into (2.36), one has that

$$\Delta G_R^<(t,t') = \frac{i}{2\pi v} \left(\frac{t' - iW}{t' + iW} \frac{t + iW}{t - iW} - 1 \right) \frac{1}{t - t' + i0^+}$$
$$= \frac{i}{2\pi v} \frac{1}{tt' + W^2 - iW(t' - t)} \frac{2iW(t' - t)}{t - t' + i0^+} = \frac{W}{\pi v} \frac{1}{t' + iW} \frac{1}{t - iW}. \tag{2.38}$$

Let us observe that $\Delta G_R^<(t,t')$ has factorized into a function depending only on t and one depending only on t'. This factorization does not occur for any kind of driving voltage and it is a consequence of the peculiar form of the voltage phase for levitons reported in Eq. (2.14). By inserting the specific expression for the voltage phase of a single-leviton, appearing in Eq. (2.38), into Eq. (2.31), one finds

$$\Delta \tilde{f}_R(\epsilon) = \frac{W}{\pi v} \int_{-\infty}^{+\infty} dt \frac{1}{t - iW} \int_{-\infty}^{+\infty} dt' e^{i\epsilon t} e^{-i\epsilon t'} \frac{1}{t' + iW} =$$
$$= |\tilde{\varphi}_e(\epsilon)|^2, \tag{2.39}$$

where we identified the function

$$\tilde{\varphi}_e(\epsilon) = \frac{1}{\sqrt{2\pi}} \int_{-\infty}^{\infty} dt e^{-i(\epsilon-\mu)t} \sqrt{\frac{W}{\pi}} \frac{1}{t + iW} =$$
$$= \frac{1}{\sqrt{2\pi}} \sqrt{\frac{W}{\pi}} e^{-W(\epsilon-\mu)} \int_{-\infty}^{\infty} dt e^{-i(\epsilon-\mu)t} \frac{1}{t} = i\sqrt{2W} e^{-W(\epsilon-\mu)} \Theta(\epsilon - \mu), \tag{2.40}$$

where we recognized the integral representation of a Θ function [110]. The possibility to write $\Delta \tilde{f}_R(\epsilon)$ as a squared module of $\tilde{\varphi}_e(\epsilon)$ is a direct consequence of the factorization obtained in Eq. (2.39) and, therefore, it is a special property of levitons, which does not hold true for a generic time-dependent voltage. Notice that $\tilde{\varphi}_e(\epsilon) \neq 0$, only for $\epsilon > \mu$. For this reason, we interpret $\tilde{\varphi}_e(\epsilon)$ as the probability density for electronic states, namely as the wave-function of the single-leviton state in energy space. It represents the probability density for a single electron, in the sense that the probability to fill an electronic state (above the chemical potential) between two given energies ϵ_1 and ϵ_2 is given by

$$P_e(\epsilon_1, \epsilon_2) = \int_{\epsilon_1}^{\epsilon_2} |\tilde{\varphi}_e(\epsilon)|^2. \tag{2.41}$$
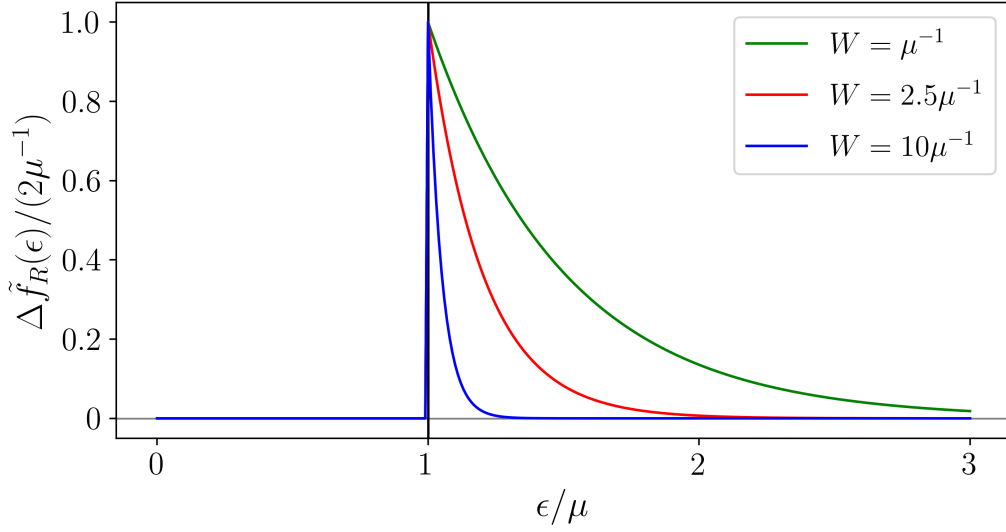
Figure 2.4: $\Delta \tilde{f}_R(\epsilon)$ in units of $2\mu^{-1}$ as a function of energy for a single leviton. The width of the Lorentzian pulse assume the values $W = \mu^{-1}, 2.5\mu^{-1}, 10\mu^{-1}$.

In addition, this wave-function satisfies the normalization condition $\int_{-\infty}^{+\infty} |\tilde{\varphi}_e(\epsilon)|^2 = 1$. According to this result, the wave-function of a single leviton in time space is

$$\varphi_e(t) = \sqrt{\frac{W}{\pi}} \frac{1}{t + iW}. \tag{2.42}$$

such that the excess Green's function $\Delta G^<(t, t')$ in presence of a single leviton can be written as

$$v\Delta G_R^<(t, t') = \varphi_e^*(t)\varphi_e(t'), \tag{2.43}$$

This example illustrates that electron excess coherence function provides a direct way to access the wave-function of the single-electron emitted state. By using the expression for the single-leviton wave-function in Eq. (2.40), one can plot the distribution function $\Delta \tilde{f}_R(\epsilon)$. In Fig. 2.4, one can see that up to $\epsilon = \mu$ its value is zero, according to the fact that all the states are filled: deviations from the equilibrium situations occur only for $\epsilon > \mu$ and correspond to the presence of a single excitations on the top of the Fermi sea. This electronic excitations has an exponential distribution in energy which is related to the width of the Lorentizan pulse.

Since the simultaneous emission of many electrons is perfectly accessible using Lorentzian shaped voltage pulse, one could also look for the expression of the excess coherence function of a state made by q electronic excitations emitted simultaneously. It can be shown that the excess coherence function for such generic state is given by [33, 86, 100]

$$v\Delta G_R^<(t, t') = \sum_{k=1}^{q} \varphi_k^*(t)\varphi_k(t'), \tag{2.44}$$

where

$$\varphi_k(t) = \sqrt{\frac{W}{\pi}} \frac{(t - iW)^{k-1}}{(t + iW)^k}, \quad k = 1, ..., q, \tag{2.45}$$

where we identified $\varphi_1 \equiv \varphi_e$. The wave-functions φ_k form a complete and orthonormal set. Indeed, one can convince himself of the correctness of this result by noticing

that the diagonal part of (2.44) exactly describes the probability density of the many body state found from the Slater determinant of $\{\varphi_k, \quad k = 1, ..., q\}$ [31, 86]. The analogous result for the hole coherence function is

$$v\Delta G_R^>(t,t') = ve^{-i\mu(t-t')} \left(G_R^>(t,t') - G_{0,R}^>(t,t') \right) = \sum_{k=1}^{q} \varphi_k(t)\varphi_k^*(t'), \qquad (2.46)$$

For completeness, we report also the generalization of this orthonormal set of wavefunctions to the case of a periodic train of Lorentzian pulses that has been given in Ref. [111]. In this case, the expressions for the excess Green's functions are [31]

$$\Delta G_R^<(t,t') = \frac{1}{\pi v} \frac{\sin\left(\pi\frac{t-t'}{\mathcal{T}}\right)}{t'-t} \sum_{k=1}^{+\infty} \varphi_k^*(t)\varphi_k(t'), \qquad (2.47)$$

$$\Delta G_R^>(t,t') = -\frac{1}{\pi v} \frac{\sin\left(\pi\frac{t-t'}{\mathcal{T}}\right)}{t'-t} \sum_{k=1}^{+\infty} \varphi_k(t)\varphi_k^*(t'), \qquad (2.48)$$

with

$$\varphi_k(t) = \sqrt{\frac{\sinh\left(2\pi\frac{W}{\mathcal{T}}\right)}{2}} \frac{\sin^{k-1}\left(\pi\frac{t-iW}{\mathcal{T}}\right)}{\sin^k\left(\pi\frac{t+iW}{\mathcal{T}}\right)}, \quad k = 1, ..., q. \qquad (2.49)$$

2.4 Single-electron interferometry

Before entering the discussion about the real implementation of single-electron interferometers, we illustrate a schematic view of the concept of quantum interferometry of few-particle states, which is a central concept of quantum optics with both photons and electrons [112]. We consider an experimental scheme with four different arms, presented in the upper panel of Fig. 2.5, which contains two coherent sources at the beginning of arms 1 and 2 of *indistinguishable* particles and two ideal detectors at the end of arms 3 and 4. In the condensed matter domain, the waveguides for photons can be replaced by ballistic edge channels of integer quantum Hall systems. The central scatter is assumed to reflect or transmit incident states with probability amplitudes r and t, respectively. For photons, this scatter corresponds to a beam splitter, which can be implemented using an half-silvered mirror (see left lower panel of Fig. 2.5). In order to implement an electronic analog of a beam splitter, such that electrons can be controllably reflected or transmitted as photons, one can a quantum point contact (QPC) [24, 25]. This device consists of a pair of electrostatic gates deposited on the surface of a Hall bar, as shown in the lower panel of Fig. 2.5. Its working principle is simple: when a negative voltage V_G is applied to each gate, a potential barrier is formed, which tends to repel incoming electrons. In general, one assign to a QPC a certain transmission probability T (and a corresponding reflection probability $R = 1 - T$) in a phenomenological way for each edge channel. According to Landauer formula, the conductance for a quantum Hall system at filling factor $\nu = 1$ in a QPC geometry is $G_H = T\frac{e^2}{h}$. This result allows to determine experimentally the relation between the gate voltage and the transmission amplitude measuring the conductance G_H of a sample as a function of V_G.

We describe the incident states propagating in the i-th arm ($i = 1, 2$) with annihilation operators a_i and creation operators $a_i^\dagger$. Similarly, outgoing states scattered into
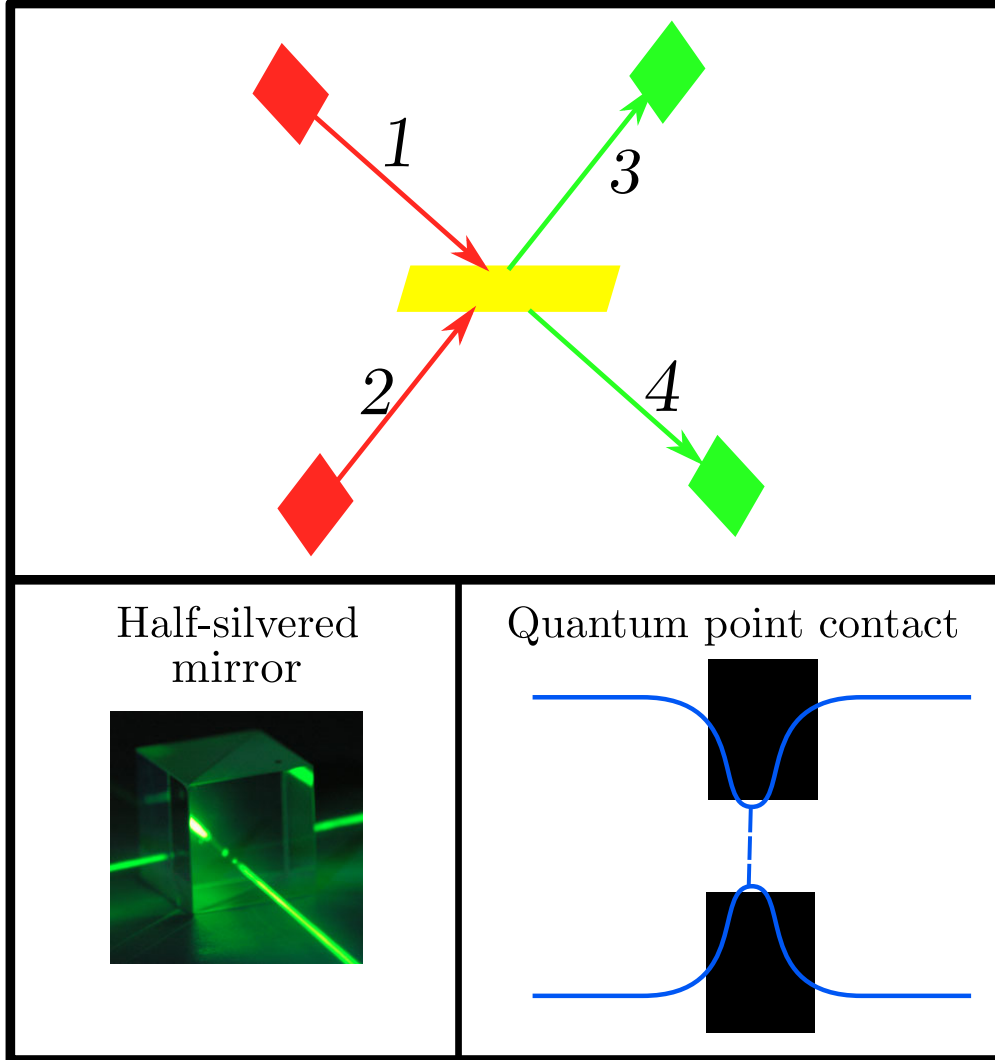
Figure 2.5: (Upper panel) Setup for two-particle interferometry. Incoming particles, traveling in input channels 1 and 2, impinge on the beam splitter in the middle (yellow layer). They are either transmitted (with probability T) or reflected (with probability $R = 1 - T$) into output channels 3 and 4. Two detectors are placed at the end of output arms 3 and 4. (Lower panel)Half-silvered mirrors (left) and quantum point contacts (right) play the role of beam splitter for bosons and fermions, respectively geometry. In a quantum point contact geometry, two negative gate voltages V_G generates a narrow constriction by repelling incoming electrons.

the $j-th$ channel ($j = 3, 4$) are described by annihilation operators b_j and creation operators $b_j^\dagger$. Due to the probabilistic nature of scattering processes, the incoming and the out-coming states are related by a scattering matrix s as

$$\begin{pmatrix} b_3 \\ b_4 \end{pmatrix} = \begin{pmatrix} r & t \\ t & r \end{pmatrix} \begin{pmatrix} a_1 \\ a_2 \end{pmatrix}. \tag{2.50}$$

The occupation number of input and output arms are $n_i = a_i^\dagger a_i$ and $n_j = b_j^\dagger b_j$. The occupation number of output channels are given by

$$n_3 = Rn_1 + Tn_2 + t^* r a_2^\dagger a_1 + tr^* a_1^\dagger a_2, \tag{2.51}$$

$$n_4 = Rn_2 + Tn_1 + t^* r a_1^\dagger a_2 + tr^* a_2^\dagger a_1, \tag{2.52}$$

where we introduce the reflection coefficient $R = |r|^2$ and the transmission coefficient $T = |t|^2$. The probabilistic scattering of particles induce fluctuations in the occupation number of output arms. For instance, by using Eq. (2.51) and applying repeatedly Wick's theorem, one can compute the auto-correlators and cross-correlator of number occupations in arms 3 and 4, which are

$$\langle \Delta n_3^2 \rangle \equiv \langle n_3^2 \rangle - \langle n_3 \rangle^2 = R^2 \langle n_1 \rangle^2 + RT \langle n_1 \rangle \langle a_2 a_2^\dagger \rangle - R^2 \langle n_1 \rangle^2 = RT, \tag{2.53}$$

where the average is performed over the initial state $|\Psi\rangle = a_1^\dagger |0\rangle$ and we introduced $\Delta n_k = n_k - \langle n_k \rangle$.

The correlations in the occupation numbers in transmitted and reflected beams are called *partition noise*. Let us observe that the partition noise does not provide information about the statistics of impinging particles, i.e. whether they are fermions or bosons. To distinguish between the different character of bosonic and fermionic statistics, multi-particle states have to be scattered. For this reason, we take into exam in the following two-particle interference.

The relevant situation for the observation of statistical properties of fermions and bosons is the simultaneous scattering of two identical particles at the beam-splitter. The initial state can be expressed as $|\Psi\rangle = a_1^\dagger a_2^\dagger |0\rangle$. In this case, a particle is present in each input arm, such that $\langle n_1 \rangle = \langle n_2 \rangle = 1$. As a consequence, the average values of number occupation in the output arms are $\langle n_3 \rangle = R\langle n_1 \rangle + T\langle n_2 \rangle = 1$ and $n_4 = R\langle n_2 \rangle + T\langle n_1 \rangle = 1$.

The average values of $\langle n_3^2 \rangle$ is

$$\langle n_3^2 \rangle = R^2 \langle n_1^2 \rangle + T^2 \langle n_2^2 \rangle + 2RT \langle a_1^\dagger a_1 a_2^\dagger a_2 \rangle + RT \left(\langle a_1^\dagger a_1 a_2 a_2^\dagger \rangle + \langle a_2^\dagger a_2 a_1 a_1^\dagger \rangle \right) =$$

$$= R^2 + T^2 + 2RT \langle n_1 n_2 \rangle + RT \left(\langle n_1 (1 \pm n_2) \rangle + \langle n_2 (1 \pm n_1) \rangle \right) =$$

$$= (R + T)^2 + (2 \pm 2)RT = 1 + (2 \pm 2)RT, \tag{2.54}$$

where the upper and lower signs refer to bosons and fermions, respectively. This difference arises because, according to the statistical properties,

$$a_i a_i^\dagger = \begin{cases} 1 + a_i^\dagger a_i & \text{for bosons} \\ 1 - a_i^\dagger a_i & \text{for fermions} \end{cases}. \tag{2.55}$$

Similarly, one can repeat an analogous calculation for the other output arm, thus finding that $\langle n_3^2 \rangle = \langle n_4^2 \rangle$. The correlation between the occupation number of different

output channels can be obtained from the particle conservation $n_1 + n_2 = n_3 + n_4$ and its final value is

$$\langle n_3 n_4 \rangle = 1 - RT(2 \pm 2). \tag{2.56}$$

By using these results, the fluctuations of the occupation number are

$$\langle \Delta n_3^2 \rangle = \langle \Delta n_4^2 \rangle = -\langle \Delta n_3 n_4 \rangle = RT(2 \pm 2). \tag{2.57}$$

Interestingly, for fermions the fluctuations in Eq. (2.57) vanish, regardless of reflection and transmission coefficient.

The physical explanation for this result is deeply rooted in the statistics of bosons and fermions. Let us notice that the probability to observe both particles scattered into arm j is $P_{j,j} = \frac{1}{2} |b_j^\dagger b_j^\dagger |\Psi\rangle|^2$, where the prefactor $\frac{1}{2}$ is needed to normalize the probability. These probabilities can be recast as

$$P_{j,j} = \frac{1}{2} |b_j^\dagger b_j^\dagger |\Psi\rangle|^2 = \pm \frac{1}{2} \langle \Delta n_j^2 \rangle, \quad P_{3,4} = \langle n_3 n_4 \rangle. \tag{2.58}$$

In the case of bosons, when $R = T = \frac{1}{2}$, they are forced to exit on the same output arm, since $P_{3,4} = 0$: this effect is called *bosons (or photons) bunching* (see left panel of Fig. 2.6).

For fermions, we find that $P_{j,j} = 0$ and $P_{3,4} = 1$, independently of the barrier transmission. This result is a strict consequence of Pauli exclusion principle, which enforce two indistinguishable fermions to occupy different positions. In this way, the two fermions *always* exit on opposite output arms, thus generating no fluctuations in the occupation numbers. This result is usually termed *fermion anti-bunching*, presented in the right panel of Fig. 2.6.

2.4.1 Noise in interferometric setup

By using IQH edge states as electronic wave-guides and QPC as electronic beam-splitter, we can implement EQO experiments. As we have just understood, the fluctuations in the occupation numbers encode valuable and interesting information intimately related to the nature of particles involved into these experiments. This is the reason way many photonic experiments, employing photo-detectors, were focused on their measurement. In condensed matter system, it is not easy to obtain direct information on electrons entering a certain reservoir, since particles are embedded in a solid state system. Nevertheless, one can focus on the fluctuations of electrical current, which are experimentally accessible by measuring the current noise [104, 112].

Let us consider a quantum Hall bar at filling factor $\nu = 1$ in a two-terminal QPC geometry, presented in Fig. 2.7. Two time-dependent voltage $V_R(t)$ and $V_L(t)$, which are both function with period $\mathcal{T} = \frac{2\pi}{\omega}$, are applied to reservoirs 1 and 2, respectively. In this setup, reservoir 1 plays simultaneously the role of source for right-movers and detector for left-movers. The opposite situation occurs for reservoir 2. The derivation of current noise will be carried out for generic periodic voltages $V_{R/L}$. At the end of calculations, we will focus on specific configurations for the external drive and we will specify the form for $V_{R/L}$.

The tunneling at the QPC is treated within the *Scattering Matrix Theory* [104, 112–114], whose principles have been introduced in the schematic example presented at the beginning of this section. This kind of approach provides a phenomenological description of tunneling processes in presence of a QPC, without resorting to a
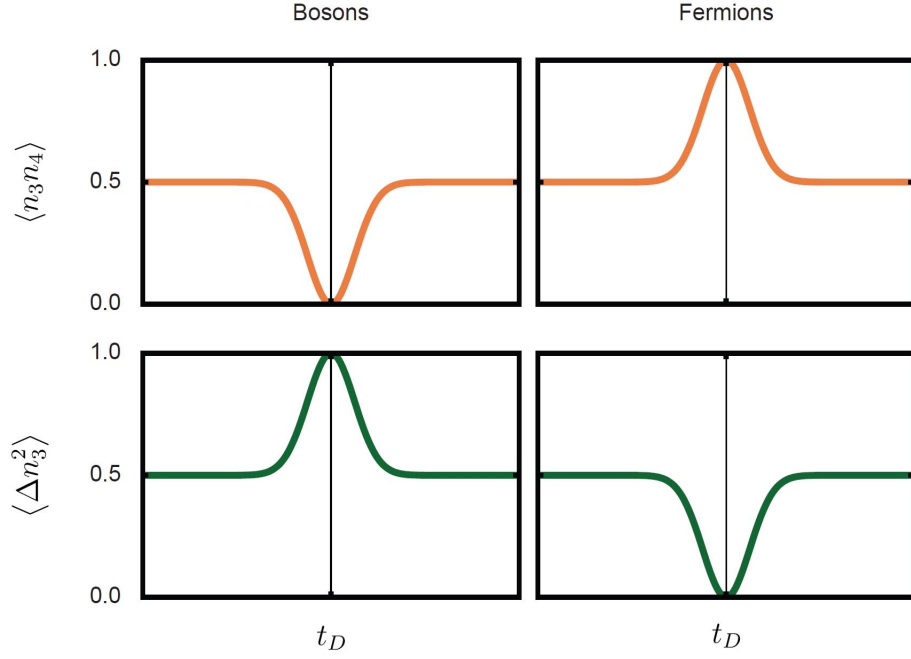
Figure 2.6: Comparison between boson bunching and fermion anti-bunching in a symmetric interferometer with $T = R = \frac{1}{2}$. When two wave-packets with finite temporal extension collide at the beam splitter, different scenarios may emerge depending on the statistics and the time delay t_D between arrivals. At $t_D = 0$, the number of coincidence counts $\langle n_3 n_4 \rangle$ for bosons gets suppressed, while the one for fermions is enhanced. Fluctuations in the particle number $\langle \Delta n_3^2 \rangle$ measured by a single detector behave the opposite way: bosonic fluctuations are enhanced near $t_D = 0$, while fermionic ones are suppressed.
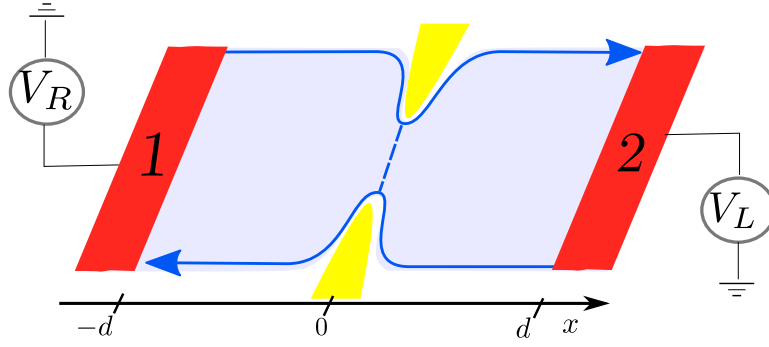
Figure 2.7: Quantum Hall bar at filling factor $\nu = 1$ in a two-terminal QPC geometry. Two time-dependent potential V_R and V_L are applied to left and right reservoirs, respectively.

microscopic model. We remark that this theory is valid only for free electrons and, when in the next Chapters we will deal with interacting systems, it could no longer be applied. Fermionic fields incoming into the edge states from the two reservoirs are given by

$$\Psi_{in,R/L}(x,t) \equiv \Psi_{R/L}(x,t) = e^{i\chi_{R/L}(t\mp\frac{x}{v})}\psi_{R/L}(x,t), \tag{2.59}$$

where $\chi_{R/L}(t) = e\int_{-\infty}^{t}dt V_{R/L}(t)$. Electronic fields outgoing from the QPC are termed $\Psi_{out,R/L}(x,t)$, whether they enter into reservoir 2 or 1. They are connected to fermionic fields in Eq. (2.59) by a matrix, which model the scattering at the QPC between the two edge states. In this way, the fermionic fields $\Psi_{out,R/L}$ are expressed as a simple linear combination of $\Psi_{in,R/L}$, weighted by the appropriate probability transmission and reflexion, T and R, determined by the voltage gate of the QPC. Thus, one has

$$\begin{pmatrix} \Psi_{out,L} \\ \Psi_{out,R} \end{pmatrix} = \begin{pmatrix} \sqrt{T} & i\sqrt{R} \\ -i\sqrt{R} & \sqrt{T} \end{pmatrix} \begin{pmatrix} \Psi_{in,L} \\ \Psi_{in,R} \end{pmatrix}. \tag{2.60}$$

As argued before, we are interested in using this scattering matrix approach to compute the current noise in single-electron interferometric setup. The zero-frequency current noise is defined as (α and β can assume the value 1 or 2)

$$\mathcal{S}_{\alpha\beta} = \int_{-\frac{\mathcal{T}}{2}}^{\frac{\mathcal{T}}{2}} dt \int_{-\infty}^{+\infty} dt' \langle J_\alpha(x_\alpha,t)J_\beta(x_\beta,t')\rangle - \langle J_\alpha(x_\alpha,t)\rangle\langle J_\beta(x_\beta,t')\rangle =$$

$$= \int_{-\frac{\mathcal{T}}{2}}^{\frac{\mathcal{T}}{2}} dt \int_{-\infty}^{+\infty} dt' \langle J_\alpha(0,t-\xi_\alpha\frac{x_\alpha}{v})J_\beta(0,t'-\xi_\beta\frac{x_\beta}{v})\rangle +$$

$$- \langle J_\alpha(0,t-\xi_\alpha\frac{x_\alpha}{v})\rangle\langle J_\beta(0,t'-\xi_\beta\frac{x_\beta}{v})\rangle, \tag{2.61}$$

where $\xi_{1/2} = \pm 1$, $J_\alpha(x_\alpha,t)$ is the chiral current operator incoming into reservoir α and x_α indicates the position of such reservoir. The current operator can be easily expressed as a balance of fermionic operators entering or exiting reservoirs as

$$J_1(x,t) = -ev\left(: \Psi_{out,L}^\dagger(x,t)\Psi_{out,L}(x,t) : - : \Psi_{in,R}^\dagger(x,t)\Psi_{in,R}(x,t) :\right), \tag{2.62}$$

$$J_2(x,t) = -ev\left(: \Psi_{out,R}^\dagger(x,t)\Psi_{out,R}(x,t) : - : \Psi_{in,L}^\dagger(x,t)\Psi_{in,L}(x,t) :\right), \tag{2.63}$$

where the notation $: \cdots :$ indicates the normal ordering with respect to the Fermi sea.

The current fluctuations associated to the same reservoir ($\alpha = \beta$) are called auto-correlators, while for different reservoirs ($\alpha \neq \beta$) they are called cross-correlators. The current operator associated to terminal 1 and 2 can be recast using Eq. (2.60), thus obtaining

$$J_1(x,t) = -ev\Big[T\left(-:\Psi^\dagger_{in,L}(x,t)\Psi_{in,L}(x,t):+:\Psi^\dagger_{in,R}(x,t)\Psi_{in,R}(x,t):\right)+$$
$$-i\sqrt{RT}\left(\Psi^\dagger_{in,R}(x,t)\Psi_{in,L}(x,t)-\Psi^\dagger_{in,L}(x,t)\Psi_{in,R}(x,t)\right)\Big], \qquad (2.64)$$

$$J_2(x,t) = -ev\Big[T\left(:\Psi^\dagger_{in,L}(x,t)\Psi_{in,L}(x,t):-:\Psi^\dagger_{in,R}(x,t)\Psi_{in,R}(x,t):\right)+$$
$$+i\sqrt{RT}\left(\Psi^\dagger_{in,L}(x,t)\Psi_{in,R}(x,t)-\Psi^\dagger_{in,R}(x,t)\Psi_{in,L}(x,t)\right)\Big]. \qquad (2.65)$$

Let us notice that the two current are related as $J_1(x,t) = -J_2(x,t)$, which is consistent with charge conservation. As a consequence, the auto-correlators are related to the cross-correlators according to

$$\mathcal{S}_{11} = \mathcal{S}_{22} = -\mathcal{S}_{12} = -\mathcal{S}_{21}. \qquad (2.66)$$

In the following, for definiteness we focus on the cross-correlator of reservoirs 1 and 2, namely $\mathcal{S}_{12}$, and we use the shorthand notation $\mathcal{S} = \mathcal{S}_{12}$.

By using the definition of current noise in Eq. (2.61) and the expression for the current J_2 just derived, one finds for the zero-frequency auto-correlator of reservoir 2

$$\mathcal{S} = -e^2v^2T^2\int_{-\frac{\mathcal{T}}{2}}^{\frac{\mathcal{T}}{2}}dt\int_{-\infty}^{+\infty}dt'\sum_{r=L,R}G^<_{0,r}(t,t')G^>_{0,r}(t,t')+$$
$$-e^2v^2RT\int_{-\frac{\mathcal{T}}{2}}^{\frac{\mathcal{T}}{2}}dt\int_{-\infty}^{+\infty}dt'\left(G^<_R(t,t')G^>_L(t,t')+G^<_L(t,t')G^>_R(t,t')\right), \qquad (2.67)$$

where we eliminate the dependence on x_1 and x_2, by using the chirality of fermionic fields and we recall the expression for Green's functions

$$G^<_{R/L}(t,t') = \langle\Psi^\dagger_{in,R/L}(0,t)\Psi_{in,R/L}(0,t')\rangle, \qquad (2.68)$$

$$G^>_{R/L}(t,t') = \langle\Psi_{in,R/L}(0,t)\Psi^\dagger_{in,R/L}(0,t')\rangle, \qquad (2.69)$$

and the equilibrium Green's functions

$$G^<_{0,R/L}(t,t') = \langle\psi^\dagger_{in,R/L}(0,t)\psi_{in,R/L}(0,t')\rangle = \int_{-\infty}^{+\infty}\frac{d\epsilon}{2\pi v}e^{i\epsilon(t-t')}f(\epsilon), \qquad (2.70)$$

$$G^>_{0,R/L}(t,t') = \langle\psi_{in,R/L}(0,t)\psi^\dagger_{in,L/R}(0,t')\rangle = \int_{-\infty}^{+\infty}\frac{d\epsilon}{2\pi v}e^{-i\epsilon(t-t')}\left(1-f(\epsilon)\right). \qquad (2.71)$$

While the second contribution in Eq. (2.67) encodes the effects of interplay between the two edge channels, the first contribution is given by fluctuations of current in each single channel. By exploiting Eqs. (2.70) and (2.71), a straightforward calculation can show that this last contribution is given by

$$e^2v^2T^2\int_{-\frac{\mathcal{T}}{2}}^{\frac{\mathcal{T}}{2}}dt\int_{-\infty}^{+\infty}dt'\sum_{r=L,R}G^<_{0,r}(t,t')G^>_{0,r}(t,t') = 2T^2\frac{e^2}{2\pi}k_B\theta. \qquad (2.72)$$

The second contribution is strongly dependent on the type of configurations chosen for the voltage drive. In the following, we focus on two specific experimental configurations with a QPC geometry in order to further simplify the expression for $\mathcal{S}$. In the first case, a single voltage drive is turned on, namely

$$V_R(t) = V(t), \quad V_L(t) = 0, \tag{2.73}$$

where $V(t) = V_{dc} + V_{ac}(t)$, with V_{ac} a generic function with period $\mathcal{T}$ and satisfying $\int_{-\frac{\mathcal{T}}{2}}^{\frac{\mathcal{T}}{2}} \frac{dt}{\mathcal{T}} V_{ac}(t) = 0$. This configuration is called *Hanbury-Brown-Twiss* (HBT) setup, in analogy with the HBT experiment performed with photons. Indeed, when a source of levitons is applied to the driven reservoir, a stream of single electrons is partitioned against the QPC. The first experimental evidence of the existence of levitons were reported by performing noise measurements in this setup. The second configuration, is the *Hong-Ou-Mandel* (HOM) setup. In this configuration, two identical trains of levitons are generated and delayed by a tunable time shift t_D. We describe the HOM setup by setting

$$V_R(t) = V_{lor}(t), \quad V_L(t) = V_{lor}(t + t_D). \tag{2.74}$$

Hanbury-Brown-Twiss setup

In the HBT setup, the noise in Eq. (2.67) becomes

$$\mathcal{S}^{HBT} = -2T^2 \frac{e^2}{2\pi} k_B \theta - e^2 v^2 RT \int_{-\frac{\mathcal{T}}{2}}^{\frac{\mathcal{T}}{2}} dt \int_{-\infty}^{\infty} dt' \Big(G_R^<(t,t') G_{0,L}^>(t,t') +$$
$$+ G_{0,L}^<(t,t') G_R^>(t,t') \Big). \tag{2.75}$$

In this configuration, the Green's functions for right-movers are

$$G_R^{</>}(t,t') = e^{\pm ie \int_t^{t'} d\tau V(\tau)} \langle \psi_{in,R}^\dagger(0,t) \psi_{in,R}(0,t') \rangle. \tag{2.76}$$

In order to conveniently deal with voltage phases, we introduce the following Fourier decomposition [85]

$$e^{i\chi_{ac}(t)} = \sum_{l=-\infty}^{+\infty} p_l e^{-il\omega t}, \tag{2.77}$$

where $\chi_{ac}(t) = e \int_0^t dt' V_{ac}(t')$ is a function with period $\mathcal{T}$. Here, we have introduced the Fourier coefficients

$$p_l = \int_{-\frac{\mathcal{T}}{2}}^{\frac{\mathcal{T}}{2}} dt e^{i\phi_{ac}(t)} e^{il\omega t} = \int_{-\frac{\mathcal{T}}{2}}^{\frac{\mathcal{T}}{2}} dt e^{i\phi(t)} e^{i(l+q)\omega t}, \tag{2.78}$$

where we defined q, the number of particle emitted by $V(t)$ in a period as

$$q = -\frac{e}{h} \int_{-\frac{\mathcal{T}}{2}}^{\frac{\mathcal{T}}{2}} dt V(t) = -\frac{eV_{dc}}{\omega}. \tag{2.79}$$

Eq. (2.78) is the probability amplitude for particles to absorb or emit an energy $l\omega$. This discretization of energy shifts can be interpreted in terms of emission or absorption of finite quanta of energy corresponding to photons of the electromagnetic field generated by V_{ac}. This kind of energy transfers due to an ac drive are called

photo-assisted processes and expressions in Eq,. (2.78) are called *photo-assisted coefficients* [31, 85].

By expressing $G_R^{</>}$ in Fourier space as

$$G_R^<(t,t') = \sum_{l,k} p_k^* p_l e^{-i(l+q)\omega t'} e^{i(k+q)\omega t} \int_{-\infty}^{+\infty} \frac{d\epsilon}{2\pi v} e^{i\epsilon(t-t')} f(\epsilon), \tag{2.80}$$

$$G_R^>(t,t') = \sum_{l,k} p_k p_l^* e^{i(l+q)\omega t'} e^{i-(k+q)\omega t} \int_{-\infty}^{+\infty} \frac{d\epsilon}{2\pi v} e^{i\epsilon(t-t')} (1 - f(\epsilon)), \tag{2.81}$$

one can further simplify the expression in Eq. (2.75). The zero-frequency noise at finite temperature θ due to a QPC with transmission T is

$$\mathcal{S}^{HBT} = -2T^2 \frac{e^2}{2\pi} k_B \theta - \frac{e^2}{2\pi} RT \sum_l |p_l|^2 (l+q)\hbar\omega \coth\left(\frac{(q+l)\hbar\omega}{2k_B\theta}\right). \tag{2.82}$$

The second contribution is called photo-assisted shot noise and carries information about the properties of the driving voltage due to the presence of the coefficients p_l. At zero temperature, the noise in Eq. (2.82) becomes

$$\mathcal{S}^{HBT} = -S_0 \sum_l |p_l|^2 |l+q|, \tag{2.83}$$

where we introduced $S_0 = \frac{e^2}{T} RT$.

The noise in the HBT geometry was used by the group of D. C. Glattli at CEA Saclay in 2013 to provide the first experimental signatures of the correctness of Levitov's theoretical prediction [14]. In particular, they defined an excess noise

$$\Delta\mathcal{S} = \mathcal{S}^{HBT} - \mathcal{S}_{dc}, \tag{2.84}$$

where $\mathcal{S}_{dc}$ is the noise due solely to V_{dc} (equivalent to set $p_l = \delta_{l,0}$), whose expression at finite temperature is

$$\mathcal{S}_{dc} = -\frac{e^2}{2\pi} RTeV_{dc} \coth\left(\frac{eV_{dc}}{2k_B\theta}\right). \tag{2.85}$$

At zero temperature, the excess noise reads

$$\Delta\mathcal{S} = -S_0 \sum_{l<-q} |p_l|^2 |l+q|. \tag{2.86}$$

It is possible to demonstrate that $\Delta\mathcal{S}$ object quantifies exactly the number of unwanted electron-hole pairs generated at zero temperature by a generic time-dependent drive [23]. Its usefulness can be also intuitively understood as follows. When a time-dependent voltage $V(t) = V_{dc} + V_{ac}(t)$ works correctly as a single-electron source only electrons are expected to be generated and partitioned against the QPC, as for a dc bias V_{dc}. Therefore, the partition noise $\mathcal{S}^{HBT}$ should be equivalent to $\mathcal{S}_{dc}$ and the corresponding excess noise $\Delta\mathcal{S}$ should vanish.

Before presenting the experimental results, we give the theoretical predictions for the excess noise for some experimentally relevant voltage drive. In particular, we choose a sinusoidal drive, a square drive and a Lorentizan drive, given respectively
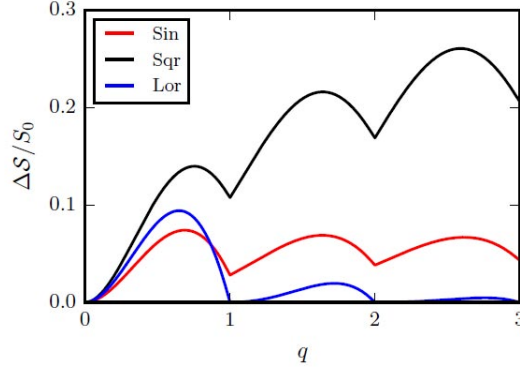
Figure 2.8: Theoretical expectation for the excess-noise $\Delta \mathcal{S}$ as a function of q for a cosine drive (red line), a square drive (black line) and a Lorentzian drive (blue line), in units of S_0, at zero temperature. The width of Lorentzian pulses is $W = 0.1\mathcal{T}$.

by

$$V_{sin}(t) = V_{dc}(1 - \cos(\omega t)), \tag{2.87}$$

$$V_{sqr}(t) = 2V_{dc} \sum_{k=-\infty}^{\infty} \Theta(t - k\mathcal{T}) \Theta\left(\frac{\mathcal{T}}{2} - t + k\mathcal{T}\right), \tag{2.88}$$

$$V_{lor}(t) = \frac{V_{dc}}{\pi} \sum_{k=-\infty}^{+\infty} \frac{W}{W^2 + (t - k\mathcal{T})^2}. \tag{2.89}$$

The corresponding form for the p_l coefficients can be calculated (see Appendix C) and, subsequently, the excess noise associated to each particular drive is reported in Fig. 2.8 for the case of zero temperature. A common features to all voltages is the appearance of minima in correspondence of integer values of $q = -\frac{eV_{dc}}{\omega}$, showing that an integer amount of charge always minimize the generation of extra electron-hole pairs. More interestingly, only the excess noise of the Lorentzian voltage pulse exactly vanishes at zero temperature: both the sinusoidal and the square drive stay well above zero even for integer value of q.

We now address the experiment that demonstrated the existence of levitons, performed by the group of D. C. Glattli. The measurement outcomes are presented in Fig. 2.9. The dashed line corresponds to the value for Lorentzian pulses expected at finite temperature (the difference between Eq. (2.82) and Eq. (2.85)). Let us observe that this in a realistic setup the limit $\theta \to 0$ is forbidden. The Lorentzian curve matches almost exactly the dashed level, indicating that no additional noise is generated by the train of voltage pulses. The right panel of Fig. 2.9 shows another set of data for sharper Lorentzian pulses and higher-frequency sinusoidal drive. This time the finite temperature contributions are different, but we still observe that the sinusoidal voltage generates some extra noise which is due to the excitation of particle-hole pairs, while the Lorentzian one does not. All these features point toward the observation of the minimal excitation state predicted by Levitov.

Hong-Ou-Mandel setup

In the quantum optics implementation of the HOM experiment, indistinguishable photons collide at a beam splitter and the coincidence counts between detectors are
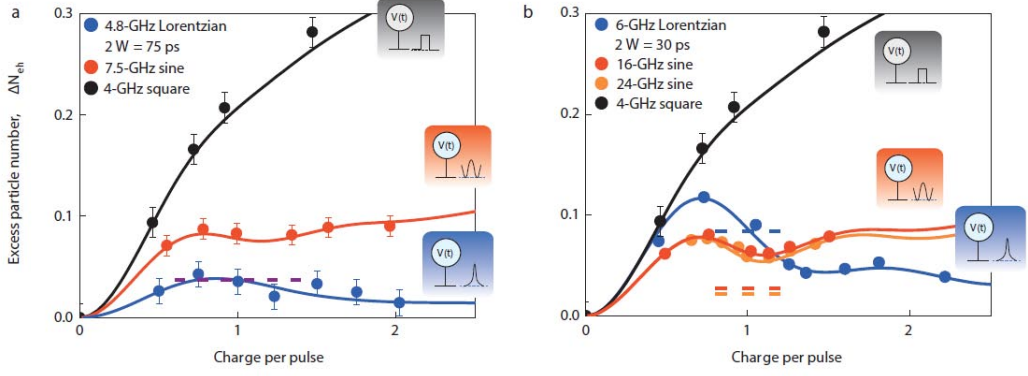
Figure 2.9: Experimental evidence of the leviton (from Ref. [14]). The excess particle number, given by $\frac{\Delta \mathcal{S}}{S_0}$, is measured as a function of q. Square, sinusoidal and Lorentzian voltages with different frequency are considered. The dashed lines correspond to the contributions at finite temperature $\theta = 39$ mK due to thermal excitations at equilibrium for the sinusoidal and Lorentzian drives. Lorentzian pulses in left and right panels have width $W = 0.18\mathcal{T}$ and $W = 0.09\mathcal{T}$ respectively.

measured. In this way, one can extract information about the statistical properties of the colliding particles (observing the photon bunching effect) and the shape of their wave-functions. A solid state analogue of the HOM experiment can be realized in the context of EQO using a single-electron voltage pulses for emitting indistinguishable electrons. Information about statistical properties of electrons are rooted in the current noise, given by Eq. (2.67), for the particular choice of voltage drive, namely $V_L(t) = V_{lor}(t)$ and $V_R(t) = V_{lor}(t+t_D)$. In this case, the number of particles emitted per period by each Lorentzian drive is equal to q (see Eq. (2.89)).

For simplicity, we consider the limit of zero temperature, where the quantum interference effects dominate over the thermal fluctuations: in particular, the thermal noise contribution in Eq. (2.67) vanishes. By using the relation

$$G_R^{</>} = e^{\pm i\mu(t-t')}\Delta G_R^{</>}(t,t') + G_{0,R}^{</>}(t-t'), \tag{2.90}$$

$$G_L^{</>} = e^{\pm i\mu(t-t')}\Delta G_L^{</>}(t,t') + G_{0,L}^{</>}(t-t'), \tag{2.91}$$

one finds

$$\mathcal{S}^{HOM} = -e^2 RT \int_{-\frac{\mathcal{T}}{2}}^{\frac{\mathcal{T}}{2}} dt \int_{-\infty}^{+\infty} dt' \left(\Delta G_R^<(t,t')\Delta G_L^>(t,t') + \Delta G_L^<(t,t')\Delta G_R^>(t,t') \right) +$$

$$- 2e^2 v^2 RT \int_{-\frac{\mathcal{T}}{2}}^{\frac{\mathcal{T}}{2}} dt \int_{-\infty}^{+\infty} dt' \left(G_R^<(t,t')G_{0,L}^>(t,t') + G_L^<(t,t')G_{0,R}^>(t,t') \right). \tag{2.92}$$

This expression for noise in the case of $q = 1$ can be recast in terms of single-leviton wave-functions in Eq. (2.49), using the expression for Green's function in Eq. (2.38) and for the single-leviton wave-function in the periodic case given. The expression for the HOM current noise becomes

$$\mathcal{S}^{HOM} = 2\mathcal{S}^{HBT} - \mathcal{I}(t_D), \tag{2.93}$$

66

where $\mathcal{S}_{LR}^{HBT}$ is the zero temperature limit of the HBT noise given in Eq. (2.75) and

$$\mathcal{I}(t_D) = -e^2 v^2 RT \int_{-\frac{\mathcal{T}}{2}}^{\frac{\mathcal{T}}{2}} \frac{dt}{\mathcal{T}} \int_{-\infty}^{+\infty} dt' \frac{\sin^2\left(\pi\frac{t'-t}{\mathcal{T}}\right)}{(t'-t)^2} \left(\varphi_{1,L}(t)\varphi_{1,L}^*(t')\varphi_{1,R}(t')\varphi_{1,R}^*(t) + \text{h.c.}\right),$$

(2.94)

encodes the interference between the wave-packets of levitons emitted by the two reservoir, respectively, $\varphi_{1,L}(t) = \varphi_1(t)$ and $\varphi_{1,R}(t) = \varphi_1(t + t_D)$. By exploiting the following relation

$$\int_{-\infty}^{+\infty} dt' \frac{\sin^2\left(\pi\frac{(t'-t)}{\mathcal{T}}\right)}{(t'-t)^2} F(t') = \int_{-\frac{\mathcal{T}}{2}}^{\frac{\mathcal{T}}{2}} dt' F(t'),$$

(2.95)

which is valid for a generic function $F(t')$ of period $\mathcal{T}$, the interference term can be further simplified as

$$\mathcal{I}(t_D) = -2S_0 \left| \int_{-\frac{\mathcal{T}}{2}}^{\frac{\mathcal{T}}{2}} \frac{dt}{\mathcal{T}} \varphi_1(t)\varphi_1^*(t + t_D) \right|.$$

(2.96)

This last formula shows that the HOM current noise is directly related to the overlap between the two wave-functions of levitons impinging at the QPC.
It is useful to introduce the following ratio

$$\mathcal{R}(t_D) = \frac{\mathcal{S}^{HOM}}{2\mathcal{S}^{HBT}}.$$

(2.97)

From the vanishing of excess noise $\Delta\mathcal{S}$ for levitons at zero temperature (see the discussion about HBT setup), we know that the HBT contribution becomes

$$\mathcal{S}^{HBT} = \mathcal{S}_{dc} = S_0 q = S_0,$$

(2.98)

where in the last step we explicited that $q = 1$. By using these results the HOM ratio of two single-leviton states colliding at the QPC becomes

$$\mathcal{R}(t_D) = 1 - \left| \int_{-\frac{\mathcal{T}}{2}}^{\frac{\mathcal{T}}{2}} \frac{dt}{\mathcal{T}} \varphi_1(t)\varphi_1^*(t + t_D) \right|^2.$$

(2.99)

Let us notice that for $t_D = 0$, the overlap integral of the single-leviton wave-function is nothing but the normalization condition for the wave-function $\varphi_1(t)$, which is therefore equal to 1. In this case, the HOM ratio vanishes, in accordance with the expected anti-bunching effect of fermions. With the analytical form of $\varphi_1(t)$, given in Eq. (2.49), the overlap integral for a single-leviton can be calculated using standard complex analysis method. The result is [106]

$$\mathcal{R}(t_D) = \frac{\sin^2\left(\pi\frac{t_D}{\mathcal{T}}\right)}{\sin^2\left(\pi\frac{t_D}{\mathcal{T}}\right) + \sinh^2\left(2\pi\frac{W}{\mathcal{T}}\right)}.$$

(2.100)

This HOM ratio is plotted in Fig. 2.10. Clearly, the interference effects that lead to the total suppression of noise at $t_D = 0$ are reduced for greater delay times, when the distinguishability of the two levitons is increased. In this case, the ratio is close to 1, meaning that the HOM current noise is similar to the sum of the partitioning HBT noise of two uncorrelated levitons. Moreover, the shape of this HOM ratio is
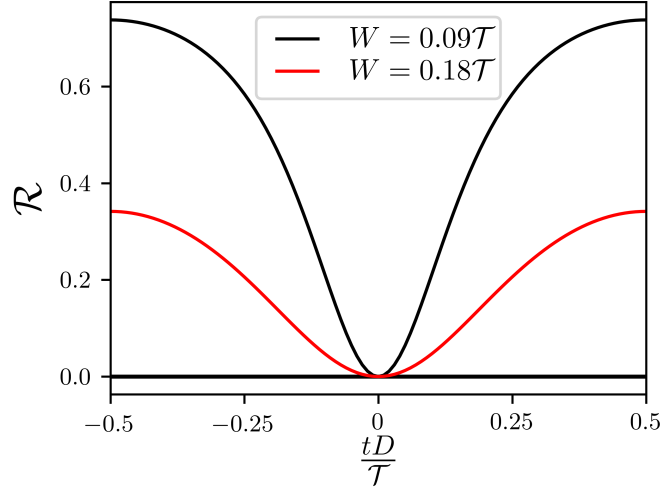
Figure 2.10: HOM ratio $\mathcal{R}$ as a function of $t_D/\mathcal{T}$ for $q = 1$, $\nu = 1$ and two values of the width of the Lorentzian pulse, $W = 0.09\mathcal{T}$ (black line) and $W = 0.18\mathcal{T}$ (red line). The single smooth dip at $t_D = 0$ demonstrates fermion anti-bunching.

Lorentzian and it is plotted for two different values of the width $W = 0.09$ (black line) and $W = 0.18$ (red line): by comparing these two curves, one can argue that the HOM ratio is extremely sensitive to the shape of the overlapping wave-packets. The HOM current noise can be generalized to the case when q levitons are emitted by each source, by using all the set of wave-functions given in Eq. (2.49). By repeating the same procedure using as excess Green's function those in Eqs. (2.47) and (2.48), one finds

$$\mathcal{R}(t_D) = 1 - \frac{1}{q} \sum_{k,k'} \left| \int_{-\frac{\mathcal{T}}{2}}^{\frac{\mathcal{T}}{2}} \frac{dt}{\mathcal{T}} \varphi_k(t) \varphi_{k'}^*(t + t_D) \right|^2. \tag{2.101}$$

It is interesting to point out that a peculiar property of the ratio for $q = 1$ when a finite temperature is considered. When thermal effects are relevant, one has to provide a more general definition of the HOM ratio, where equilibrium thermal noise $\mathcal{S}_{vac}$ has to be subtracted from signals. Indeed, for a finite temperature HOM ratio is defined as

$$\mathcal{R}(t_D) = \frac{\mathcal{S}^{HOM} - \mathcal{S}_{vac}}{2\mathcal{S}^{HBT} - 2\mathcal{S}_{vac}}. \tag{2.102}$$

Interestingly, when a single leviton is emitted by each source, this ratio has exactly the same expression of the zero temperature limit given in Eq. (2.100). The proof of this result will be given in the next Chapter, where we will deal with fractional filling factors of Laughlin sequence.

Chapter 3

Levitons in the fractional regime

In this Chapter, we take advantage of the edge transport theory developed in Chapter 1 in order to compute charge current and noise in EQO-like configurations for fractional filling factors in the Laughlin sequence. We will show that Lorentzian pulses carrying integer charge represent the cleanest voltage drive even for the FQH case [115], despite the presence of strong interactions and quasi-particles with fractional charge and statistics.

At this purpose, by considering the simultaneous emission of multiple levitons, we investigate the charge density backscattered off the QPC in the FQH regime. In this case, a regular pattern of peaks and valleys emerges, reminiscent of analogous self-organization recently observed for optical solitons in non-linear environments. This rearrangement of the density of levitons can be interpreted as a real-time version of the Wigner crystallization occurring in Luttinger liquids confined by a potential well. This crystallization phenomenon is confirmed by additional side dips in the Hong-Ou-Mandel noise, a feature that can be observed in nowadays EQO experiments [55, 56].

3.1   Transport properties in the QPC geometry

We consider a four-terminal FQH bar in the presence of a QPC, as shown in the Fig. 3.1. For a quantum Hall system with filling factor ν in the Laughlin sequence $\nu = 1/(2n + 1)$ [62], with $n \in \mathbb{N}$, a single chiral mode emerges at each edge of the sample. As derived in Sec. 1.3, the effective bosonic hamiltonian for edge states reads ($\hbar = 1$) [47]

$$H_0 = \sum_{r=R,L} \frac{v}{4\pi} \int_{-\infty}^{+\infty} dx \left[\partial_x \Phi_r(x)\right]^2 . \tag{3.1}$$

The presence of two voltage drives applied to reservoirs 1 and 4 is modeled by the hamiltonian

$$H_g = -e \sum_{r=R,L} \int_{-\infty}^{+\infty} dx \, \Theta(\mp x - d) V_r(t) \rho_r(x), \tag{3.2}$$

which couples densities $\rho_{R/L}(x) = \mp \frac{\sqrt{\nu}}{2\pi} \partial_x \Phi_{R/L}(x)$ with two voltage gates acting separately on the right and left moving excitations. Here, the step function $\Theta(\mp x - d)$ describes the experimentally relevant situation of infinite, homogeneous contacts,
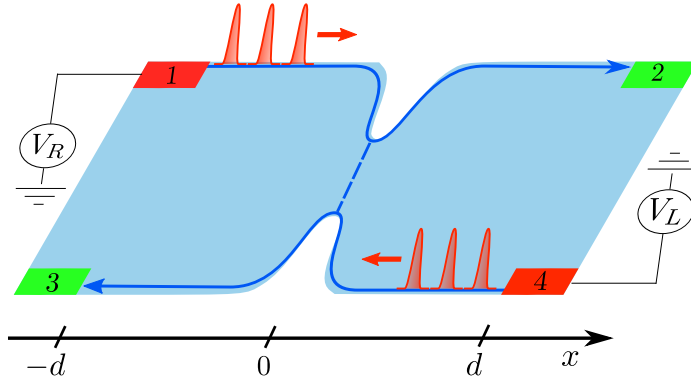
Figure 3.1: Four-terminal setup for Hong-Ou-Mandel interferometry in the FQH regime. Contact 1 and 4 are used as input terminals, while contact 2 and 3 are the output terminals where current and noise are measured.

introduced in Sec. B.1. The corresponding time-evolution of bosonic modes reads (see Eq. (B.17) in Appendix B)

$$\Phi_{R/L}(x,t) = \phi_{R/L}\left(t \mp \frac{x}{v}\right) - e\sqrt{\nu}\int_{-\infty}^{t \mp \frac{x}{v}} dt' V_{R/L}(t'). \tag{3.3}$$

This characteristic chiral dynamics is a consequence of the linear dispersion of edge states for all filling factors in the Laughlin sequence.

Finally, the tunneling between the two edges occurs through a QPC at $x = 0$. In Chapter 2, tunneling at the QPC in the IQH regime has been treated within the scattering matrix approach. We remark that this approach relies on the approximation of non-interacting electrons, which does not hold true in the FQH phase. In order to deal with tunneling processes we introduced in the main text an hamiltonian approach. A QPC at the position $x = 0$ can be effectively described by the following tunneling hamiltonians [36, 116]

$$H_T^{(qp)} = \Lambda \Psi_R^{(qp)\dagger}(0)\Psi_L^{(qp)}(0) + \text{h.c.}, \tag{3.4}$$

$$H_T^{(el)} = \Lambda \Psi_R^{(el)\dagger}(0)\Psi_L^{(el)}(0) + \text{h.c..} \tag{3.5}$$

We will assume that the QPC weakly couples the two edges in the weak backscattering regime, which means that the barrier is almost transparent and only a small amount of particles are reflected back into the opposite chiral mode. In this tunneling regime, which is called weak-backscattering, tunneling hamiltonian can be treated as a small perturbation with respect to the hamiltonian $H_0 + H_g$. As a consequence, the time evolution of quantum operators can be constructed in terms of perturbative series in the parameter Λ (see Appendix D).

In general, contributions coming both from electrons and fractional quasi-particles tunneling should be taken into account. In the following, charge current and noise are perturbatively evaluated at lowest order in the tunneling amplitude and we will focus on the case of quasi-particles tunneling. The results for electrons tunneling will be given at the end of calculations by exploiting the substitution $\nu \to \frac{1}{\nu}$, as discussed in Sec. 1.3.4. Indeed, we will see in the following that only quasi-particles tunneling contribution has to be considered in the weak backscattering regime, since this is the only relevant process in the renormalization group sense [117].

3.1.1 Charge current

Charge current operators for right- and left-moving modes can be defined by resorting to the continuity equation of densities $\rho_{R/L}(x,t)$, namely

$$\partial_t \rho_{R/L}(x,t) + \partial_x J_{R/L}(x,t) = 0. \tag{3.6}$$

According to chirality of edge states, one finds

$$J_{R/L}(x,t) = \mp ev\rho_{R/L}(x,t), \tag{3.7}$$

where $\rho_{R/L}(x,t)$ are density operators evolving with respect to the whole hamiltonian $H_0 + H_g + H_T^{(qp)}$, whose exact expression we are not interested in.

Starting from the definition of chiral current operator, we can define the operators for charge current entering reservoir 2 and 3 as

$$J_{2/3}(t) = J_{R/L}(\pm d, t), \tag{3.8}$$

where we recall that the interfaces between edge states and contacts 2 and 3 are placed in $x = \pm d$ respectively. The expansion of $J_{2/3}$ in terms of the parameter Λ is presented in detail in Appendix D. Here, we simply quote the result, which reads

$$J_{2/3}(t) = J_{2/3}^{(0)}(t) + J_{2/3}^{(1)}(t) + J_{2/3}^{(2)}(t) + \mathcal{O}(\Lambda^3), \tag{3.9}$$

where

$$J_{2/3}^{(0)}(t) = \frac{ev\sqrt{\nu}}{2\pi}\left(\partial_x \Phi_{R/L}(x,t)\right)_{x=\pm d}, \tag{3.10}$$

$$J_{2/3}^{(1)}(t) = \pm i\Lambda e\nu \Psi_R^\dagger\left(0, t - \frac{d}{v}\right)\Psi_L\left(0, t - \frac{d}{v}\right) + \text{h.c.}, \tag{3.11}$$

$$J_{2/3}^{(2)}(t) = \pm i \int_{-\infty}^{t-\frac{d}{v}} dt'' \left[H_T^{(qp)}(t''), +i\Lambda e\nu \Psi_R^{(qp)\dagger}\left(0, t - \frac{d}{v}\right)\Psi_L^{(qp)}\left(0, t - \frac{d}{v}\right) + \text{h.c.}\right]. \tag{3.12}$$

Let us observe that tunneling contribution entering reservoirs 2 and 3 are connected by the simple relation

$$J_2^{(1/2)}(t) = -J_3^{(1/2)}(t). \tag{3.13}$$

Now, the different contributions to the expansion of charge current operators have been expressed in a suitable form for calculating their average values. The thermal average of current operators will be performed over the initial equilibrium condition, i.e. in the absence of driving voltages and tunneling. Let us observe that terms involving a different number of annihilation or creation field operators with a defined chirality have a vanishing average value: indeed, this is the case for $J_{2/3}^{(1)}(x,t)$. Therefore, the average values of charge current operators are

$$\langle J_{2/3}(t)\rangle = \langle J_{2/3}^{(0)}(t)\rangle + \langle J_{2/3}^{(2)}(t)\rangle + \mathcal{O}(\Lambda^3), \tag{3.14}$$

where

$$\langle J_{2/3}^{(0)}(t)\rangle = \frac{e^2\nu}{2\pi}V_{R/L}\left(t - \frac{2d}{v}\right), \tag{3.15}$$

$$\langle J_{2/3}^{(2)}(t)\rangle = \pm ie\nu v \int_{-\infty}^{t-\frac{d}{v}} dt'' \langle\left[H_T^{(qp)}(t''), +i\Lambda \Psi_R^{(qp)\dagger}(d-vt,0)\Psi_L^{(qp)}(d-vt,0) + \text{h.c.}\right]\rangle. \tag{3.16}$$

Since we will focus only on quasi-particles contribution, we will omit the index (qp) from now on.

The first term corresponds to the charge current emitted by reservoirs 1 and 4, which constitutes the main contribution to the detected currents in reservoirs 2 and 3. In the absence of tunneling processes ($\Lambda = 0$), these zero-order contributions would correspond to periodic current signals generated by the two voltages. For this reason, their integral over one period $\mathcal{T}$ gives the total charge $\mathcal{C}_{R/L}$ emitted by $V_{R/L}$ into the edge states

$$
\mathcal{C}_{R/L} = \int_{-\frac{\mathcal{T}}{2}}^{\frac{\mathcal{T}}{2}} dt \langle J_{2/3}^{(0)}(t) \rangle = \frac{e^2 \nu}{2\pi} \int_{-\frac{\mathcal{T}}{2}}^{\frac{\mathcal{T}}{2}} dt V_{R/L}\left(t - \frac{2d}{v}\right) = \frac{e^2 \nu}{\omega} V_{dc}^{(R/L)} = -e q_{R/L},
$$

(3.17)

where we defined

$$
V_{dc}^{(R/L)} = \int_{-\frac{\mathcal{T}}{2}}^{\frac{\mathcal{T}}{2}} \frac{dt}{\mathcal{T}} V_{R/L}(t),
$$

(3.18)

and where $q_{R/L} = -\frac{e \nu V_{dc}^{(R/L)}}{\omega}$ are the numbers of electronic charges injected by $V_{R/L}$. Due to the QPC, some of the particles emitted into the edge states are backscattered: $\langle J_{2/3}^{(2)}(t) \rangle$ are the current due to the reflection of particles incoming from reservoirs 1 and 4, respectively. These currents are usually termed backscattering currents [116, 118]. Due to the relation in Eq. (3.13), backscattering currents are equal up to a sign, such that we can define

$$
J_{BS}(t) = \langle J_3^{(2)}(t) \rangle = -\langle J_2^{(2)}(t) \rangle.
$$

(3.19)

This backscattering current can be evaluated by expanding the tunneling hamiltonian in Eq. (3.16) in terms of quasi-particles fields as

$$
J_{BS}(t) = -ie\nu \int_{-\infty}^{t-\frac{d}{v}} dt'' \left\langle \left[\Lambda \Psi_R^\dagger(0,t'') \Psi_L(0,t'') + \text{h.c.}, +i\Lambda \Psi_R^\dagger(d-vt,0)\Psi_L(d-vt,0) + \text{h.c.} \right] \right\rangle =
$$

$$
= -e|\Lambda|^2 \nu \int_{-\infty}^{t-\frac{d}{v}} dt'' \left\langle \left[\Psi_R^\dagger(0,t'') \Psi_L(0,t'') \Psi_L^\dagger\left(0, t-\frac{d}{v}\right) \Psi_R\left(0, t-\frac{d}{v}\right) + \right.\right.
$$

$$
- \Psi_L^\dagger(0,t'') \Psi_R(0,t'') \Psi_R^\dagger\left(0, t-\frac{d}{v}\right) \Psi_L\left(0, t-\frac{d}{v}\right) +
$$

$$
- \Psi_L^\dagger\left(0, t-\frac{d}{v}\right) \Psi_R\left(0, t-\frac{d}{v}\right) \Psi_R^\dagger(0,t'') \Psi_L(0,t'') +
$$

$$
\left.\left. + \Psi_R^\dagger\left(0, t-\frac{d}{v}\right) \Psi_L\left(0, t-\frac{d}{v}\right) \Psi_L^\dagger(0,t'') \Psi_R(0,t'') \right] \right\rangle =
$$

$$
= -e|\Lambda|^2 \nu \int_{-\infty}^{t-\frac{d}{v}} dt'' \left[G_R^<\left(t'', t-\frac{d}{v}\right) G_L^>\left(t'', t-\frac{d}{v}\right) - G_L^<\left(t'', t-\frac{d}{v}\right) G_R^>\left(t'', t-\frac{d}{v}\right) + \right.
$$

$$
\left. - G_R^<\left(t-\frac{d}{v}, t''\right) G_L^>\left(t-\frac{d}{v}, t''\right) + G_L^<\left(t-\frac{d}{v}, t''\right) G_R^>\left(t-\frac{d}{v}, t''\right) \right],
$$

(3.20)

where, in the intermediate step, we used again that average values with a different number of annihilation or creation field operators with a defined chirality must

72

vanish and, in the last step, we introduced the quasi-particles Green's functions

$$G^{<}_{R/L}(t',t) = \langle \Psi_{R/L}{}^{\dagger}(0,t')\Psi_{R/L}(0,t)\rangle = e^{-i\nu e \int_t^{t'} d\tau V_{R/L}(\tau)}\langle \psi_{R/L}{}^{\dagger}(0,t')\psi_{R/L}(0,t)\rangle,$$
(3.21)

$$G^{>}_{R/L}(t',t) = \langle \Psi_{R/L}(0,t')\Psi_{R/L}{}^{\dagger}(0,t)\rangle = e^{i\nu e \int_t^{t'} d\tau V_{R/L}(\tau)}\langle \psi_{R/L}(0,t')\psi_{R/L}{}^{\dagger}(0,t)\rangle.$$
(3.22)

In order to proceed with the calculations of J_{BS}, we have to derive the expressions for the equilibrium Green's functions involving quasi-particle fields $\psi_{R/L}$. We start by considering those in Eq. (3.21). By using the Baker-Hausdorff formula

$$e^A e^B = e^{A+B}e^{C/2},$$
(3.23)

and bosonization identity, one finds

$$\left\langle \psi_{R/L}{}^{\dagger}(0,t')\psi_{R/L}(0,t)\right\rangle =$$
$$= \frac{e^{-ik_F v(t'-t)}}{2\pi a}\left\langle e^{i\sqrt{\nu}[\phi_{R/L}(0,t')-\phi_{R/L}(0,t)]}\right\rangle e^{\frac{\nu}{2}[\phi_{R/L}(0,t),\phi_{R/L}(0,t')]}.$$
(3.24)

It is useful to recast the above expression such that the average values involve polynomials function of $\phi_{R/L}$: in this way, we will be able to evaluate thermal averages over the bosonic edge hamiltonian. This can be achieved by exploiting the relation

$$\left\langle e^O\right\rangle = e^{\frac{1}{2}\langle O^2\rangle},$$
(3.25)

which is valid for operators which are linear combinations of $b_{R/L,k}$ and $b_{R/L,k}^{\dagger}$. Inserting this relation in Eq. (3.24), one obtains

$$\left\langle \psi_{R/L}{}^{\dagger}(0,t')\psi_{R/L}(0,t)\right\rangle =$$
$$= \frac{e^{ik_F v(t'-t)}}{2\pi a}e^{-\frac{\nu}{2}\left\langle \phi^2_{R/L}(0,t')+\phi^2_{R/L}(0,t)-\phi_{R/L}(0,t)\phi_{R/L}(0,t')-\phi_{R/L}(0,t')\phi_{R/L}(0,t)\right\rangle}e^{\frac{\nu}{2}[\phi_{R/L}(0,t),\phi_{R/L}(0,t')]} =$$
$$= \frac{e^{ik_F v(t'-t)}}{2\pi a}e^{\left\langle \phi_{R/L}(0,t)\phi_{R/L}(0,t')-\phi^2_{R/L}(0,0)\right\rangle},$$
(3.26)

where we commuted $\phi_{R/L}(0,t')$ and $\phi_{R/L}(0,t)$, thus eliminating the commutator in the other exponential, and we used the transational invariance of the thermal average to write $\left\langle \phi^2_{R/L}(0,t')\right\rangle = \left\langle \phi^2_{R/L}(0,t)\right\rangle = \left\langle \phi^2_{R/L}(0,0)\right\rangle$. As a result, we managed to write these expressions as an average involving solely polynomial functions of $\phi_{R/L}$. These average values are evaluated in Appendix C and read [59, 119]

$$W(t-t') = \left\langle \phi_{R/L}(0,t)\phi_{R/L}(0,t') - \phi^2_{R/L}(0,t)\right\rangle =$$
$$= \ln\left[\frac{\left|\Gamma\left(1+\frac{\theta}{\omega_c}+i\theta(t-t')\right)\right|^2}{\left|\Gamma\left(1+\frac{\theta}{\omega_c}\right)\right|^2(1+i\omega_c(t-t'))}\right] \simeq \ln\left[\frac{\pi(t-t')\theta}{\sinh\left(\pi(t-t')\theta\right)(1+i\omega_c(t-t'))}\right],$$
(3.27)

where we introduce the temperature θ and the high energy cut-off $\omega_c = \frac{v}{a}$: the approximation in the above equation is valid as long as $\omega_c \gg \theta$. Let us observe that

73

these expressions are equal for right- and left-movers and, therefore, we omitted any label R or L. Moreover, W depends only on the difference between t and t' and it is a single-argument function.

One can perform a very similar calculations for the case of $G^>_{R/L}$. In the end, the expressions for the Green's functions in Eqs. (3.21) and (3.22) are

$$G^<_{R/L}\left(t',t\right) = \langle \Psi_{R/L}{}^\dagger(0,t')\Psi_{R/L}(0,t)\rangle = e^{-i\nu e \int_t^{t'} d\tau V_{R/L}(\tau)}\frac{e^{ik_F v(t'-t)}}{2\pi a}\mathcal{P}_\nu(t-t'),$$
(3.28)

$$G^>_{R/L}\left(t',t\right) = \langle \Psi_{R/L}(0,t')\Psi_{R/L}{}^\dagger(0,t)\rangle = e^{i\nu e \int_t^{t'} d\tau V_{R/L}(\tau)}\frac{e^{-ik_F v(t'-t)}}{2\pi a}\mathcal{P}_\nu(t-t'),$$
(3.29)

where we defined the function

$$\mathcal{P}_g(\tau) = e^{gW(\tau)}.$$
(3.30)

By inserting these expression for the Green's functions into Eq. (3.20), one finds

$$J_{BS}(t) = 2i\nu e \left|\lambda\right|^2 \int_0^{+\infty} d\tau \sin\left[\nu e \int_{t-\tau}^t dt'' V_-(t'')\right] (\mathcal{P}_{2\nu}(\tau) - \mathcal{P}_{2\nu}(-\tau)),$$
(3.31)

where we introduced $V_-(t) = V_R(t) - V_L(t)$. Since V_R and V_L are time-dependent voltages with period $\mathcal{T} = \frac{2\pi}{\omega}$, we expect the current to satisfy $J_{BS}(t) = J_{BS}(t+\mathcal{T})$. One can check this property by noticing that

$$\sin\left[\nu e \int_{t+\mathcal{T}-\tau}^{t+\mathcal{T}} dt'' V_-(t''+\mathcal{T})\right] = \sin\left[\nu e \int_{t-\tau}^t dt'' V_-(t'')\right].$$
(3.32)

It is thus possible to perform an average over one period of the backscattering current

$$\overline{J_{BS}(t)} = \int_0^{\mathcal{T}} \frac{dt}{\mathcal{T}} J_{BS}(t) =$$

$$= 2i\nu e \left|\lambda\right|^2 \left\{ \int_0^{+\infty} d\tau \int_0^{\mathcal{T}} \frac{dt}{\mathcal{T}} \sin\left[\nu e \int_{t-\tau}^t dt'' V_-(t'')\right] \mathcal{P}_{2\nu}(\tau) + \right.$$

$$\left. + \int_{-\infty}^0 d\tau \int_{-\tau}^{\mathcal{T}-\tau} \frac{dt}{\mathcal{T}} \sin\left[\nu e \int_t^{t+\tau} dt'' V_-(t'')\right] \mathcal{P}_{2\nu}(\tau) \right\}.$$
(3.33)

Notice that we used the property valid for a generic periodic function that $\int_0^{\mathcal{T}} dt f(t) = \int_c^{\mathcal{T}+c} dt f(t)$. Then, one obtains a single term involving an integration over τ over the whole real axis by changing variable as $t' = t+\tau$ in the second term, thus finding

$$\overline{J_{BS}(t)} = 2i\nu e \left|\lambda\right|^2 \left\{ \int_0^{+\infty} d\tau \int_0^{\mathcal{T}} \frac{dt}{\mathcal{T}} \sin\left[\nu e \int_{t-\tau}^t dt'' V_-(t'')\right] \mathcal{P}_{2\nu}(\tau) + \right.$$

$$\left. + \int_{-\infty}^0 d\tau \int_0^{\mathcal{T}} \frac{dt'}{\mathcal{T}} \sin\left[\nu e \int_{t'-\tau}^{t'} dt'' V_-(t'')\right] \mathcal{P}_{2\nu}(\tau) \right\} =$$

$$= 2i\nu e \left|\lambda\right|^2 \int_0^{\mathcal{T}} \frac{dt}{\mathcal{T}} \int d\tau \sin\left[\nu e \int_{t'-\tau}^{t'} dt'' V_-(t'')\right] \mathcal{P}_{2\nu}(\tau).$$
(3.34)

The presence of a periodic voltage can be conveniently handled by resorting to the photo-assisted coefficient $\tilde{p}_l = \int_0^{\mathcal{T}} \frac{dt}{\mathcal{T}} e^{i(l+q_R-q_L)\omega t} e^{ie\int_0^t d\tau V_-(\tau)}$.

By using the following relation

$$\sin\left[\nu e \int_{t-\tau}^t dt'' V_-(t'')\right] = \frac{1}{2i} \sum_{l,m} \left[\tilde{p}_l^* \tilde{p}_m e^{-i(l-m)\omega t} e^{i(q_R-q_L+m)\omega\tau} - \text{h.c.}\right] \qquad (3.35)$$

the backscattering current assumes the final expression

$$\overline{J_{BS}(t)} = 2i\nu e |\lambda|^2 \sum_l |p_l|^2 \int_{-\infty}^{+\infty} d\tau \sin\left[(q_R - q_L + l)\omega\tau\right] \mathcal{P}_{2\nu}(\tau). \qquad (3.36)$$

Let us comment that now the backscattering current is directly related to the properties of a specific voltage drive through the coefficient $\tilde{p}_l$ and to the number of emitted particles q_R and q_L.

By moving to Fourier space, this current can be recast as a simple sum over l. At this purpose, we introduce the Fourier transform of $\mathcal{P}_g(t)$, which is calculated in Appendix F. It reads [34, 120, 121]

$$\tilde{\mathcal{P}}_g(E) = \int_{-\infty}^{+\infty} dt e^{iEt} P_g(t) = \left(\frac{2\pi\theta}{\omega_c}\right)^{g-1} \frac{e^{\frac{E}{2\theta}}}{\omega_c} \mathcal{B}\left(\frac{g}{2} - i\frac{E}{2\pi\theta}, \frac{g}{2} + i\frac{E}{2\pi\theta}\right) =$$

$$= \left(\frac{2\pi\theta}{\omega_c}\right)^{g-1} \frac{e^{\frac{E}{2\theta}}}{\Gamma(g)\omega_c} \left|\Gamma\left(\frac{g}{2} - i\frac{E}{2\pi\theta}\right)\right|^2. \qquad (3.37)$$

By substituting $P_g(t) = \int_{-\infty}^{+\infty} \frac{dE}{2\pi} e^{-iEt} \tilde{\mathcal{P}}_g(E)$ into Eq. (3.36), one finds

$$\overline{J_{BS}(t)} = \nu e |\lambda|^2 \sum_l |p_l|^2 \left\{\tilde{\mathcal{P}}_{2\nu}[(q_R - q_L + l)\omega] - \tilde{\mathcal{P}}_{2\nu}[-(q_R - q_L + l)\omega]\right\}. \qquad (3.38)$$

3.1.2 Charge current fluctuations

We recall that the dc component of the zero-frequency current noise is defined as

$$\mathcal{S}_{\alpha\beta} = \int_0^{\mathcal{T}} \frac{dt}{\mathcal{T}} \int_{-\infty}^{+\infty} dt' \langle J_\alpha(t) J_\beta(t')\rangle - \langle J_\alpha\rangle \langle (t) J_\beta(t')\rangle, \qquad (3.39)$$

where α and β may refer to reservoirs 2 or 3.

By exploiting the expansion of current operator in Eq. (3.9), one can evaluate the lowest order contribution in Λ of $S_{\alpha\beta}$, which read

$$\mathcal{S}_{\alpha\beta} = \mathcal{S}_{\alpha\beta}^{(02)} + \mathcal{S}_{\alpha\beta}^{(11)} + \mathcal{S}_{\alpha\beta}^{(20)} + \mathcal{O}\left(\Lambda^3\right), \qquad (3.40)$$

with

$$\mathcal{S}_{\alpha\beta}^{(ij)} = \int_0^{\mathcal{T}} \frac{dt}{\mathcal{T}} \int_{-\infty}^{+\infty} dt' \left[\left\langle J_\alpha^{(i)}(t) J_\beta^{(j)}(t')\right\rangle - \left\langle J_\alpha^{(i)}\right\rangle \left\langle (t) J_\beta^{(j)}(t')\right\rangle\right]. \qquad (3.41)$$

Let us observe that, according to the relation in Eq. (3.13), auto-correlators and cross-correlators are connected as [104, 112]

$$\mathcal{S}_{22} = \mathcal{S}_{33} = -\mathcal{S}_{23} = -\mathcal{S}_{32}. \qquad (3.42)$$

Moreover, it is possible to demonstrate that the only term that contributes at lowest order in Λ in the above expansion is $\mathcal{S}_{\alpha\beta}^{(11)}$ (see Appendix G).

For the following discussions, due to the relation in Eq. (3.42), we focus on the auto-correlator of reservoirs 2, namely $\mathcal{S}_{22}$, and we use the shorthand notation $\mathcal{S}_C \equiv \mathcal{S}_{22}$. At lowest order in tunneling it reads

$$\mathcal{S}_C = (\nu e)^2 |\Lambda|^2 \int_0^{\mathcal{T}} \frac{dt}{\mathcal{T}} \int_{-\infty}^{+\infty} dt' \left\{ G_R^<(t,t') G_L^>(t,t') + G_L^<(t,t') G_R^>(t,t') \right\}, \quad (3.43)$$

where we used the definitions of quasi-particle Green's functions. By using their explicit expressions contained in Eqs. (3.28) and (3.29), the auto-correlator can be recast as

$$\mathcal{S}_C = 2(\nu e)^2 |\Lambda|^2 \int_0^{\mathcal{T}} \frac{dt}{\mathcal{T}} \int_{-\infty}^{+\infty} dt' \cos\left[\nu e \int_{t'}^t V_-(t'') dt'' \right] \mathcal{P}_{2\nu}(t'-t) =$$

$$= 2(\nu e)^2 |\Lambda|^2 \int_0^{\mathcal{T}} \frac{dt}{\mathcal{T}} \int_{-\infty}^{+\infty} d\tau \cos\left[\nu e \int_{t+\tau}^t V_-(t'') dt'' \right] \mathcal{P}_{2\nu}(\tau), \quad (3.44)$$

where we changed variable as $\tau = t' - t$.

Even though this charge noise is generated in a double-drive configuration, it is interesting to point out that it actually depends only on the single effective drive $V_-(t)$. Therefore, the charge noise presented in Eq. (3.44) is the same as the one generated in a single-drive configuration, where reservoir 4 is grounded ($V_L(t) = 0$) and reservoir 1 is contacted to the periodic voltage $V_-(t)$, such that

$$S_C (V_R, V_L) = S_C (V_-, 0). \quad (3.45)$$

Here, the arguments in brackets indicate the voltage applied to reservoirs 1 and 4, respectively. One might consider Eq. (3.45) as a consequence of a trivial shift of both voltages by a value corresponding to V_L. Nevertheless, such a result cannot be obtained by means of a gauge transformation (see Appendix B). In this sense, Eq. (3.45) implies that the charge noise *incidentally* acquires the same expression in these two physically distinct experimental setups. As will be clearer in the following, for the charge case this is a consequence of the presence of a single local (energy independent) QPC. Generally, we expect that the double-drive and the single-drive ($V_R(t) = V_-(t)$ and $V_L(t) = 0$) configurations return different outcomes for other physical observables, such as heat noise, as discussed in the next Chapter.

The function $\cos\left[\nu e \int_{t+\tau}^t V_-(t'') dt'' \right]$ can be expanded into a Fourier series by exploiting the coefficient $\tilde{p}_l$

$$\cos\left[\nu e \int_{t+\tau}^t V_-(t'') dt'' \right] = \frac{1}{2} \sum_{l,m} \left[\tilde{p}_l^* \tilde{p}_m e^{-i(l-m)\omega t} e^{-i(q_R - q_L + m)\omega \tau} + \text{h.c.} \right]. \quad (3.46)$$

By inserting this result into Eq. (3.44), one has

$$\mathcal{S}_C = 2(\nu e)^2 |\lambda|^2 \sum_l |\tilde{p}_l|^2 \int_{-\infty}^{+\infty} d\tau \cos\left[(q_R - q_L + l)\omega \tau \right] \mathcal{P}_{2\nu}(\tau). \quad (3.47)$$

Finally, it is again useful to obtain an expression in the Fourier space by using the Fourier transform of $\mathcal{P}_g(t)$. Indeed, one finds

$$\mathcal{S}_C = 2(\nu e)^2 |\lambda|^2 \sum_l |\tilde{p}_l|^2 \left[\tilde{\mathcal{P}}_{2\nu}[(q_R - q_L + l)\omega] + \tilde{\mathcal{P}}_{2\nu}[(q_R - q_L + l)\omega] \right]. \quad (3.48)$$

3.2 Particular limits

The expressions for charge current and noise that we have just derived are valid for a generic temperature θ [1] and for all kind of periodic voltage drive. Before moving on with our discussion, it is useful to present some specific limits of these expression. The first one is the zero-temperature limit, where the temperature is assumed to be the lowest energy scale in the problem. In the other case, we assume to apply to reservoir 1 a constant dc bias V_{dc} and to connect reservoir 4 to the ground.

Zero-temperature current and noise

The limit of zero-temperature for expressions in Eqs. (3.38) and (3.48) can be readily obtained by observing that at $\theta \to 0$, the function $\tilde{\mathcal{P}}_g(E)$ becomes

$$\tilde{\mathcal{P}}_g(E) = \frac{2\pi}{\Gamma(g)\omega_c^g} E^{g-1}\Theta(E), \tag{3.49}$$

where we exploited the asymptotic relation $|\Gamma(x+iy)| \sim \sqrt{2\pi}|y|^{x-\frac{1}{2}}e^{-\pi|y|/2}$, which is valid for $|y| \to \infty$ [110]. Difference and sum of functions $\tilde{\mathcal{P}}_g(E)$ appearing in Eqs. (3.38) and (3.48) are in the zero-temperature limit

$$\tilde{\mathcal{P}}_g(E) - \tilde{\mathcal{P}}_g(E) = \frac{2\pi}{\Gamma(g)\omega^g}|E|^{2\nu-1}\mathrm{sign}(E), \tag{3.50}$$

$$\tilde{\mathcal{P}}_g(E) + \tilde{\mathcal{P}}_g(E) = \frac{2\pi}{\Gamma(g)\omega^g}|E|^{2\nu-1}. \tag{3.51}$$

By substituting these asymptotic expressions into Eqs. (3.38) and (3.48), one finds

$$\overline{J_{BS}(t)}\Big|_{\theta=0} = \frac{\nu e}{\omega}|\lambda|^2 \frac{2\pi}{\Gamma(2\nu)}\left(\frac{\omega}{\omega_c}\right)^{2\nu}\sum_l |p_l|^2 |q_R - q_L + l|^{2\nu-1}\mathrm{sign}(q_R - q_L + l), \tag{3.52}$$

$$\mathcal{S}_C\Big|_{\theta=0} = \frac{(\nu e)^2}{\omega}|\lambda|^2 \frac{4\pi}{\Gamma(2\nu)}\left(\frac{\omega}{\omega_c}\right)^{2\nu}\sum_l |p_l|^2 |q_R - q_L + l|^{2\nu-1}. \tag{3.53}$$

In the fractional case, each contribution to the sum are non-linear in $q_R - q_L + l$, since they follow a power law with exponent $2\nu - 1$. The appearance of such power-law behavior in tunneling contributions at $\theta = 0$ is a typical feature of Luttinger liquid physics [34, 35, 118, 122] (in particular of chiral Luttinger liquid, since the exponent is a function of the filling factor ν).

Current and noise in the presence of a dc bias

Let us now discuss the situation where $V_R(t) = V_{dc}$ and $V_L(t) = 0$. This particular configuration entails that the photo-assisted coefficient reduce to $\tilde{p}_l = \delta_{l,0}$. Thus, current and noise become

$$J_{BS} = \frac{2\nu e}{\omega_c}|\lambda|^2 \frac{1}{\Gamma(2\nu)}\left(\frac{2\pi\theta}{\omega_c}\right)^{2\nu-1}\left|\Gamma\left(\nu - i\frac{\nu e V_{dc}}{2\pi\theta}\right)\right|^2 \sinh\left(\frac{\nu e V_{dc}}{2\theta}\right), \tag{3.54}$$

$$\mathcal{S}_C = \frac{2(\nu e)^2}{\omega_c}|\lambda|^2 \frac{1}{\Gamma(2\nu)}\left(\frac{2\pi\theta}{\omega_c}\right)^{2\nu-1}\left|\Gamma\left(\nu - i\frac{\nu e V_{dc}}{2\pi\theta}\right)\right|^2 \cosh\left(\frac{\nu e V_{dc}}{2\theta}\right), \tag{3.55}$$

---

[1]Anyway, the temperature θ must be much smaller than the energy cut-off ω_c.

where $q\omega = \nu eV_{dc}$. These expressions are valid both at zero and finite temperature θ. It is instructive to discuss the limit $\theta \to 0$ of Eqs. (3.54) and (3.55), which read [2]

$$J_{BS}\Big|_{\theta=0} = \frac{\nu e}{\omega_c} |\lambda|^2 \frac{2\pi}{\Gamma(2\nu)} \left| \frac{\nu eV_{dc}}{\omega_c} \right|^{2\nu-1} \text{sign}(V_{dc}), \tag{3.56}$$

$$\mathcal{S}_C\Big|_{\theta=0} = \frac{(\nu e)^2}{\omega_c} |\lambda|^2 \frac{4\pi}{\Gamma(2\nu)} \left| \frac{\nu eV_{dc}}{\omega_c} \right|^{2\nu-1}. \tag{3.57}$$

The duality between electron and quasi-particle fields, introduced in Sec. 1.3 can be exploited to straightforwardly obtain backscattering current and noise due to the tunneling of electrons at the QPC (i.e., when current operators evolve in time with respect to $H_T^{(el)}$). At this purpose, the parameter ν has to be replaced with $\frac{1}{\nu}$ in the power laws appearing in Eqs. (3.56) and (3.57) [57]. By operating this substitution, one can write the ratio between transport properties of tunneling electrons and quasi-particles

$$\frac{J_{BS}^{(el)}}{J_{BS}} \sim \left| \frac{\nu eV_{dc}}{\omega_c} \right|^{\frac{2}{\nu}-2\nu}, \qquad \frac{\mathcal{S}_C^{(el)}}{\mathcal{S}_C} \sim \left| \frac{\nu eV_{dc}}{\omega_c} \right|^{\frac{2}{\nu}-2\nu}, \tag{3.58}$$

where these exponents are always positive for $\nu = \frac{1}{2n+1}$. Since $eV_{dc} \ll \omega_c$, tunneling electrons always generate negligible backscattering current and noise with respect to tunneling quasi-particles in the weak-backscattering regime. This discussion for the dc limit can be immediately extended to the ac case, since each contribution in the sum appearing in Eqs. (3.52) and (3.53) exhibits the same power-law behavior of dc contributions in Eqs. (3.56) and (3.57). Indeed, the relevance of tunneling processes of quasi-particles in the weak-backscattering regime is a general result which can be rigorously proven in the framework of renormalization group theory [117]. For this reason, we will only focus on quasi-particle tunneling in the rest of this thesis.

In the dc case, a general relation can be found by comparing the backscattering current and the noise in the low transmission regime of the QPC. From Eqs. (3.54) and (3.55), one can easily deduce that

$$\mathcal{S}_C = \nu e \coth\left(\frac{\nu eV_{dc}}{2\theta} \right) \overline{J_{BS}(t)}, \tag{3.59}$$

by noticing that $\cosh(x) = \sinh(x)\coth(x)$. In particular, in the zero-temperature limit, one has [3]

$$\mathcal{S}_C = \nu e \overline{J_{BS}(t)}, \tag{3.60}$$

which is the well-known Schottky result for noise in the weak-backscattering regime [123]. Interestingly, noise and backscattering current are directly proportional in this regime and the constant of proportionality is exactly the charge of tunneling quasi-particles. Indeed, this holds true even in the non-interacting case at $\nu = 1$, where, in that case, the tunneling charge correspond exactly to e. This property of the low-transmission current noise has been exploited in many experiments to test the fractional values of quasi-particles charges in different FQH phases [40, 124].

---

[2]Since the backscattering current is time-independent for a constant bias, we simply indicate it as J_{BS}.
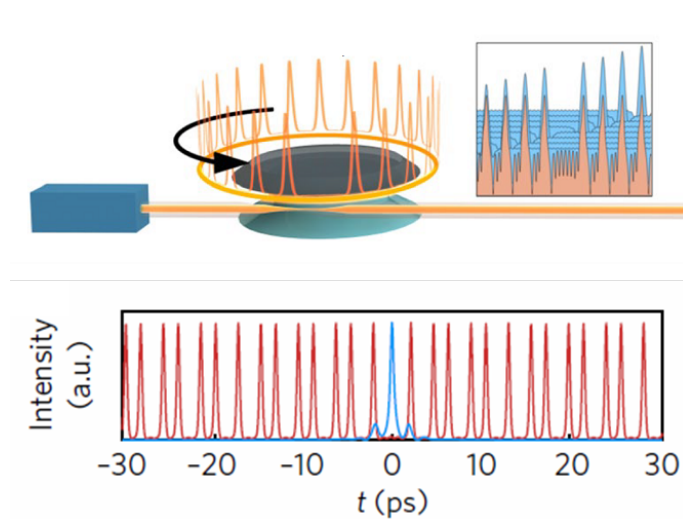
[3]We assume $V_{dc} > 0$.

Figure 3.2: (Upper panel) Depiction of the generation of a soliton crystal. (Lower panel) Simulation of the intensity pattern of the soliton crystal as a function of time. Optical solitons present a regular and ordered structure in the time domain. Taken from Ref. [126]

3.3 Crystallization of levitons in the FQH regime

In the first part of this section, we will employ the result for charge current and noise previously derived in order to demonstrate that levitons are minimal excitation states for both integer and fractional filling factors of the Laughlin sequence, as confirmed by the vanishing of the excess noise for integer value of q in the case of a Lorentizan-shaped voltage. In this way, it will be clear that that levitons are robust even to the presence of electron-electron interaction.

By looking at this result from another perspective, this means that we have not still identified any feature that marks a striking difference in the properties of levitons in non-interacting or strongly-correlated phases. In this sense, an appealing problem to investigate is the effect of strong interactions on the time-resolved propagation of leviton wave-packets in the FQH effect. Indeed, due to their solitonic nature already discussed in Sec. 2, levitons are fairly independent particles [21]. Similarly to solitons, q different levitons travel unhindered along one-dimensional electronic edge states and can be controllably superimposed, thus forming many-body states called multi-electron levitons or, simply, q-levitons [31, 125]. Nevertheless, self-organized and correlated patterns of solitons have been recently reported in the optical domain(see Fig. 3.2 and Refs. [126–128]). An intriguing question is whether a similar phenomenon can be observed also for levitons in FQH edge states. It is well known that, in one dimensional electronic systems, electron-electron interaction drastically affect the properties of particles, inducing, for instance, the arrangement of electrons in a static regular pattern in space. This phenomenon is known as Wigner crystallization and its finite size counterpart is termed Wigner molecule [49, 129–135]. Such strongly correlated states manifest as a regular arrangement of the electronic density which oscillates around fixed positions in order to minimize the energy of electrons. In particular, a system containing N electrons will exhibit, in presence of a strong interaction, an oscillating pattern with exactly N peaks. Moreover, when the strength of interaction is increased, the amplitude of oscillation is enhanced as
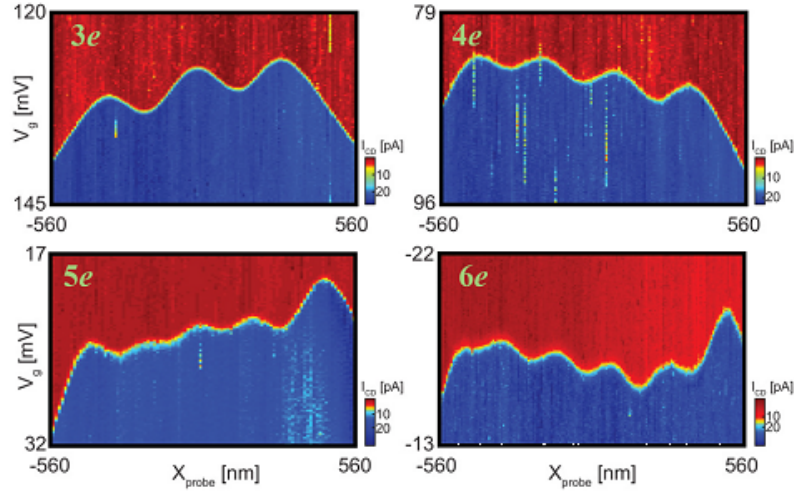
79

Figure 3.3: Imaging in the real-space of Wigner molecule formed by $3, 4, 5$ or 6 electrons. Taken from Ref. [137].

well. In FQH edge states, the connection between time and space given by chirality opens the way to the possible realization of the real-time version of this interaction-induced crystallization by applying time dependent voltage pulses directly to the edge channels.

Anyway, the electronic density could exhibit oscillations even in the non-interacting case, for instance, due to finite size effects (a phenomenon known as Friedel oscillations). In order to identify the pattern formation of a Wigner molecule, it is thus necessary to investigate directly the electronic correlations, by focusing on the density-density correlator [136]. An oscillating behavior in such correlator is considered a smoking gun evidence for the formation of a Wigner molecule.

Nevertheless, experimental observations of Wigner crystallization are quite challenging, since they require to probe a static arrangement of electrons without perturbing it. An imaging of the real-space structure of a Wigner molecule has been realized only in a recent experiment (see Fig. 3.3). In order to perform this observation, a probe made by a carbon nanotube has been employed. The microscopic size of this probe and the great experimental control over it allowed to perform a minimally-invasive scanning of a Wigner molecule. Despite of this remarkable experimental achievement, the density-density correlator could not be assessed anyway.

In the second part of this section, we propose FQH states belonging to the Laughlin sequence [62], where a single mode exists on each edge, as a testbed to observe the crystallization of robust q-Leviton excitations in condensed matter systems. Here, the charge density reflected by a quantum point contact (QPC) shows a q-peaked structure as a consequence of the interaction-induced rearrangement in the time domain, in open contrast to the featureless profile observed in the integer case. To confirm the correlated character of the crystal state, we demonstrate that these features generate unexpected side dips in the current-current correlator (which is proportional to the density-density correlator) in a HOM collisional experiments, which are within reach for the nowadays technology [14, 16, 29, 30, 108].

3.3.1 Levitons as minimal excitations in the FQH effect

Charge current and noise previously evaluated for a generic drive can now be employed to test whether quantized Lorentzian pulses or other kind of driving voltages are minimal excitations even in the FQH regime. At this purpose, the suitable experimental configuration is the HBT setup, as for the integer case in Chap. 2. Here, a drive is applied only to reservoir 1 and reservoir 4 is grounded, such that $V_R(t) = V(t)$ and $V_L(t) = 0$, with $V(t)$ a generic periodic drive. Notice that, in this case, the emitted numbers of particles are $q_R = q$ and $q_L = 0$.

In this light, one should find an extension to the concept of excess noise introduced in the IQH case. The idea to extend the definition of excess noise to the FQH effect is based on the Schottky result in Eq. (3.60). In general, time-dependent drives do not satisfy that relation in contrast with a dc constant bias. The combination of transport properties that we use to define the excess noise is given by

$$\Delta \mathcal{S} = \mathcal{S}_C - \nu e \overline{J_{BS}(t)}, \tag{3.61}$$

where the noise is measured with respect to a reference value given by the average value of ac current. First of all, let us observe that this definition is consistent with the case at $\nu = 1$, where the excess noise has been defined as $\Delta \mathcal{S} = \mathcal{S}_{22} - \mathcal{S}_{dc}$. Indeed, by putting $\nu = 1$ in Eqs. (3.52) and (3.53)

$$\mathcal{S}_C \Big|_{\theta \to 0} = \frac{|\Lambda|^2}{v^2} \frac{e^2}{2\pi} e V_{dc} = e J_{BS} \Big|_{\theta \to 0}. \tag{3.62}$$

By identifying the transmission as $T = \frac{|\Lambda|^2}{v^2}$, the expression in Eq. (3.62) coincide with $\mathcal{S}_{dc}$ (see Eq. (2.85)) in the weak-backscattering regime ($T \ll 1$). As a result, according to Eq. (3.62), the reference subtracted from $\mathcal{S}_C$ at $\nu = 1$ can be viewed as $\mathcal{S}_{dc}$ or as the backscattered current.

Another physical explanation for the choice of defining the excess noise as in Eq. (3.61) is due to the relation between the excess noise and the number of particle-hole pairs [23]. In this light, let us focus on the non-interacting case at $\nu = 1$ and count the number of electrons generated above the Fermi level (that we set to $E_F = 0$) or holes below it on a single right-moving edge channel. At $\theta = 0$, these quantities are defined as

$$N_e(t) = \int_{-\infty}^{+\infty} \frac{d\epsilon}{2\pi} f(-\epsilon) \left\langle \tilde{a}_R^\dagger(\epsilon, t) \tilde{a}_R(\epsilon, t) \right\rangle, \tag{3.63}$$

$$N_h(t) = \int_{-\infty}^{+\infty} \frac{d\epsilon}{2\pi} f(\epsilon) \left\langle \tilde{a}_R(\epsilon, t) \tilde{a}_R^\dagger(\epsilon, t) \right\rangle, \tag{3.64}$$

where $f(E) = \Theta(\mu - E)$ and we introduced the operator

$$\tilde{a}_R(\epsilon, t) = \frac{1}{\sqrt{2\pi v}} \int_{-\infty}^{+\infty} dx e^{-i\frac{\epsilon}{v}x} \Psi_R(x, t), \tag{3.65}$$

which annihilates an electron with energy ϵ. Notice that we dropped all the index R and L, which refer to a specific edge channel.

Here, our goal is to evaluate N_h, which corresponds to the number of unwanted holes generated by a generic drive, and show that it is related to the excess noise as defined in Eq. (3.61). At this purpose, let us observe that the Fermi function $f(E)$ can be written, at $\nu = 1$, in terms of the function $\tilde{\mathcal{P}}_{\nu=1}(E) = \frac{2\pi}{\omega_c} f(E)$. By

substituting this relation and the definition of operators c_k into Eq. (3.64), thus finding

$$N_h(t) = \frac{v^2}{(2\pi a)^2} \int_{-\infty}^{+\infty} d\tau' \int_{-\infty}^{+\infty} d\tau \exp\left[ie \int_{\tau'-\tau}^{\tau'} dt' V(t')\right] \mathcal{P}_{2\nu}(t). \qquad (3.66)$$

A similar form for the excess noise at $\theta = 0$ can be obtained by combining Eqs. (3.33) and (3.44) according to the definition in Eq. (3.61)

$$\Delta\mathcal{S} = 2(\nu e)^2 |\lambda|^2 \int_{-\infty}^{+\infty} d\tau' \int_0^{\mathcal{T}} \frac{dt}{\mathcal{T}} \exp\left[i\nu e \int_{\tau'-\tau}^{\tau'} dt' V(t')\right] \mathcal{P}_{2\nu}(t), \qquad (3.67)$$

which is proportional to N_h in Eq. (3.66) at $\nu = 1$.

This relation can be used to prove that levitons are minimal excitation states at $\nu = 1$. For our discussion, we extend this result to FQH edge states, meaning that, for minimal excitations in the FQH effect, the following quantity should be zero [115]

$$\mathcal{N} = \frac{v^2}{(2\pi a)^2} \int_{-\infty}^{+\infty} d\tau' \int_{-\infty}^{+\infty} d\tau \exp\left[i\nu e \int_{\tau'-\tau}^{\tau'} dt' V(t')\right] \mathcal{P}_{2\nu}(t). \qquad (3.68)$$

The latter expression is proportional to the excess noise in Eq. (3.67) for a generic ν belonging to the Laughlin sequence. As a consequence, a voltage drive which emit clean pulses in the FQH regime must fulfill the condition $\Delta\mathcal{S} = 0$, where the excess noise has been defined according to Eq. (3.61).

By using this definition of excess noise, at $\theta = 0$, one can consider the expressions for current and noise in Eqs. (3.52) and (3.53) and write

$$\Delta\mathcal{S} = \frac{(\nu e)^2}{\omega} |\lambda|^2 \frac{4\pi}{\Gamma(2\nu)} \left(\frac{\omega}{\omega_c}\right)^{2\nu} \sum_{l<-q} |p_l|^2 |q+l|^{2\nu-1}. \qquad (3.69)$$

This expression is directly related to the properties of a generic voltage: by substituting the proper form for the photo-assisted coefficient p_l, one can directly inspect whether a certain drive give rise to a vanishing excess noise.

Let us observe that the vanishing of the excess noise for Lorentzian pulses carrying an integer number of particles can be proven mathematically. Equation (3.69) depends directly on the Fourier coefficients p_l with $l < -q$. Let us also remark that the Lorentzian pulse is the only drive showing this striking feature. In such case, the analytical behavior of $e^{-i\nu e \int_0^t d\tau V(t)}$ as a function of the complex variable $z = e^{i\omega t}$ guarantees that $p_{l<-q} = 0$ when q is an integer, as shown in Appendix C. This immediately leads to the simultaneous vanishing of the excess noise at integer charge q, as all contributions of the sum in Eq. (3.69) are positive terms and can thus *only* vanish if $|p_l|^2$ is zero for all l below $-q$.

In order to confirm the validity of this analytical result, we plot the excess noise for a Lorentzian-shaped voltage

$$V_{lor}(t) = \frac{V_{dc}}{\pi} \sum_{k=-\infty}^{+\infty} \frac{W}{W^2 + (t - k\mathcal{T})^2}, \qquad (3.70)$$
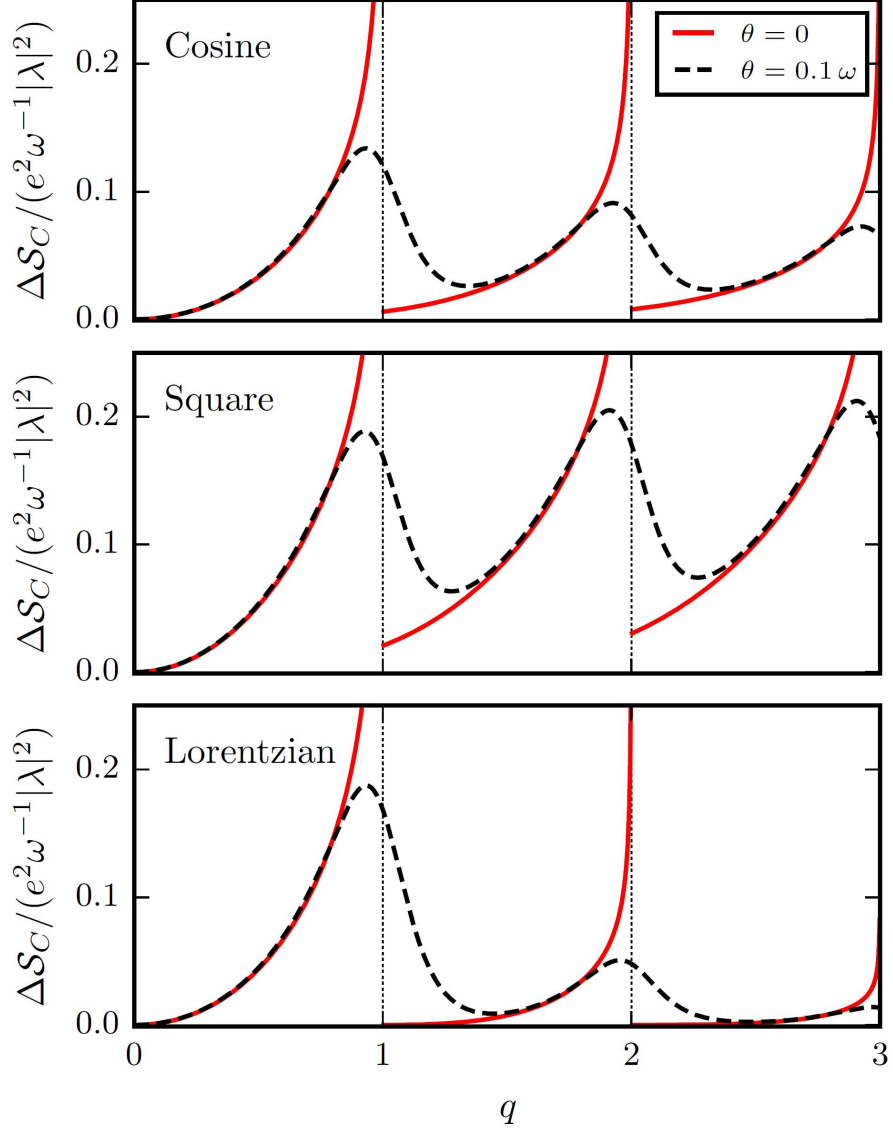
Figure 3.4: Excess noise $\Delta \mathcal{S}_C$ in units of $\frac{e^2}{\omega}|\lambda|^2$ at filling factor $\nu = \frac{1}{3}$ as a function of q. We compare the sinusoidal, square and Lorentzian voltages at $\theta = 0$ (solid curves) and $\theta = 0.1$ (dashed curves). The width of Lorentzian pulses is $W = 0.1\mathcal{T}$.

83

and we compare it with other relevant voltage drives, as we did in Sec. 2, such as a cosine and a square drive

$$V_{sin}(t) = V_{dc}(1 - \cos(\omega t)), \tag{3.71}$$

$$V_{sqr}(t) = 2V_{dc} \sum_{k=-\infty}^{\infty} \Theta(t - k\mathcal{T}) \Theta\left(\frac{\mathcal{T}}{2} - t + k\mathcal{T}\right). \tag{3.72}$$

The excess noise corresponding to these drives are presented in Fig. 3.4 in the zero-temperature limit for filling factor $\nu = \frac{1}{3}$, which is the most stable FQH plateau of the Laughlin sequence. All the curves show local minima in correspondence of integer value of q. In particular, the signal for the Lorentzian drive at $\theta = 0$ vanishes exactly for $q = 1, 2, 3, ...$, in accordance with the quantization condition already discussed in Chapter 1 in the framework of the non-interacting edge states of the IQH effect. Again, cosine and square voltages always generate a finite excess noise, even in correspondence of integer values of q. As proven analytically, integer Lorentzian voltage pulses still generate minimal excitation states even in the Laughlin FQH regime. Moreover, fractional values of q do not present any remarkable feature, despite the presence of quasi-particles with a fractional charge.

Interestingly, all the curves show a diverging behavior right before integer values of q. This feature is connected to the orthogonality catastrophe argument discussed by Levitov: non-optimal pulses generate a quantum state that is orthogonal to the unperturbed ground state, and this manifests as a huge number of particle-hole pairs contributing to the transport [21]. Nevertheless, apart from the power-law divergent behavior, the excess noise is qualitatively similar to the case of a normal metal.

At finite temperature, one can modify the excess noise as follows

$$\Delta\mathcal{S} = \mathcal{S}_C - \nu e \overline{J_{BS}(t)} \coth\left(\frac{q\omega}{2\theta}\right), \tag{3.73}$$

where the reference value $\nu e \overline{J_{BS}(t)} \coth\left(\frac{q\omega}{2\theta}\right)$ has been changed accordingly to Eq. (3.59). Black dashed curves in Fig. 3.4 are plotted for $\theta = 0.1\omega_c$. Here, the diverging behavior is smoothed by finite temperature effects. For a non-zero temperature, the excess noise is always finite, a fact that was already observed in the Fermi liquid case. Nevertheless, at finite temperature the excess noise is not expected to vanish even for an optimal drive, since electron-hole pairs would be additionally generated by thermal effects.

3.3.2 Density and Leviton crystallization

In the following, we focus only on Lorentzian-shaped voltage $V_{lor}(t)$ carrying an integer number of emitted particles. The formation of a multi-leviton crystal can be seen from the behavior of the excess charge density, defined as

$$\Delta\rho_{R/L}(x,t) = -e\left(\langle\rho_{R/L}(x,t)\rangle - \langle\rho_{R/L}^{(eq)}(x,t)\rangle\right). \tag{3.74}$$

Here, $\rho_{R/L}^{(eq)}(x,t) = \mp\frac{\sqrt{\nu}}{2\pi}\partial_x\phi_{R/L}(x,t)$ is the charge density operator at equilibrium ($V_R = V_L = 0$). Thermal averages are performed over the initial equilibrium density matrix in the absence of tunneling.

Since the density will be perturbatively evaluated at lowest order in tunneling, calculations are usefully carried out in terms of quasi-particle correlation functions

$G^<_{R/L}(t', t)$ and $G^>_{R/L}(t', t)$, presented in Eqs. (3.28) and (3.29). Contrarily to ordinary optics, these correlators do not vanish even at equilibrium, due to the different nature of the ground state in condensed matter systems. Since one is mainly interested in characterizing deviations from equilibrium introduced by the voltage drives, it is useful to define the excess quasi-particle and quasi-hole correlators as

$$\Delta G^{(qp)}_{R/L}(t', t) = e^{-ik_F v(t'-t)} \left(G^<_{R/L}(t', t) - G^<_{0,R/L}(t' - t) \right), \qquad (3.75)$$

$$\Delta G^{(qh)}_{R/L}(t', t) = e^{ik_F v(t'-t)} \left(G^>_{R/L}(t', t) - G^>_{0,R/L}(t' - t) \right), \qquad (3.76)$$

where we recall that the equilibrium Green's function ($V_L = V_R = 0$) are

$$G^<_{0,R/L}(t' - t) = \langle \psi^{(qp)\dagger}_{R/L}(0, t') \psi^{(qp)}_{R/L}(0, t) \rangle = \frac{e^{ik_F v(t'-t)}}{2\pi a} \mathcal{P}_\nu(t' - t), \qquad (3.77)$$

$$G^>_{0,R/L}(t' - t) = \langle \psi^{(qp)}_{R/L}(0, t') \psi^{(qp)\dagger}_{R/L}(0, t) \rangle = \frac{e^{-ik_F v(t'-t)}}{2\pi a} \mathcal{P}_\nu(t' - t). \qquad (3.78)$$

The expression for the excess correlators can be explicited by inserting Eqs. (3.28) and (3.29),

$$\Delta G^{(qp)}_{R/L}(t', t) = \frac{1}{2\pi a} \left(e^{-i\nu e \int_t^{t'} d\tau V_{R/L}(\tau)} - 1 \right) \mathcal{P}_\nu(t' - t), \qquad (3.79)$$

$$\Delta G^{(qh)}_{R/L}(t', t) = \frac{1}{2\pi a} \left(e^{i\nu e \int_t^{t'} d\tau V_{R/L}(\tau)} - 1 \right) \mathcal{P}_\nu(t' - t). \qquad (3.80)$$

Interestingly, it can be shown that the phases containing the voltages $V_{R/L}$ is independent of the filling factor. Indeed, for a Lorentzian-shaped voltage, one finds

$$e^{\pm i\nu e \int_t^{t'} d\tau V_{R/L}(\tau)} = \left(\frac{\sin\left(\frac{\pi}{\mathcal{T}}(t \pm iW)\right)}{\sin\left(\frac{\pi}{\mathcal{T}}(t - \mp iW)\right)} \right)^q. \qquad (3.81)$$

In the following we focus on the HBT experimental configuration, where we create only right-moving excitations, by imposing $V_R(t) = V_{lor}(t)$ and $V_L(t) = 0$. In this case, the Green's functions for left-moving modes are simply $\Delta G^{(qp/qh)}_L(t', t) = \frac{1}{2\pi a} \mathcal{P}_\nu(t', t)$ and the excess correlators vanish. Moreover, the number of emitted particles by reservoir 1 will be labeled as q. By exploiting the result in Eq. (3.81), excess quasi-particle and quasi-hole correlators for the right-moving modes become

$$\Delta G^{(qp)}_R(t', t) = -\frac{i}{\pi a} \mathcal{P}_\nu(t' - t) \sin\left(\frac{\pi(t' - t)}{T}\right) \sum_{k=1}^{q_{R/L}} \varphi_k(t) \varphi_k^*(t'), \qquad (3.82)$$

$$\Delta G^{(qh)}_R(t', t) = \frac{i}{\pi a} \mathcal{P}_\nu(t' - t) \sin\left(\frac{\pi(t' - t)}{T}\right) \sum_{k=1}^{q_{R/L}} \varphi_k^*(t) \varphi_k(t'). \qquad (3.83)$$

Here, we remind that the functions

$$\varphi_k(t) = \sqrt{\frac{\sinh\left(2\pi \frac{W}{\mathcal{T}}\right)}{2}} \frac{\sin^{k-1}\left(\pi \frac{t - iW}{\mathcal{T}}\right)}{\sin^k\left(\pi \frac{t + iW}{\mathcal{T}}\right)} \qquad (3.84)$$

are the periodic wave functions with period $2\mathcal{T}$, already defined in Eq. (2.49). [31, 138]. We recall that they form a complete orthonormal basis, thus satisfying the
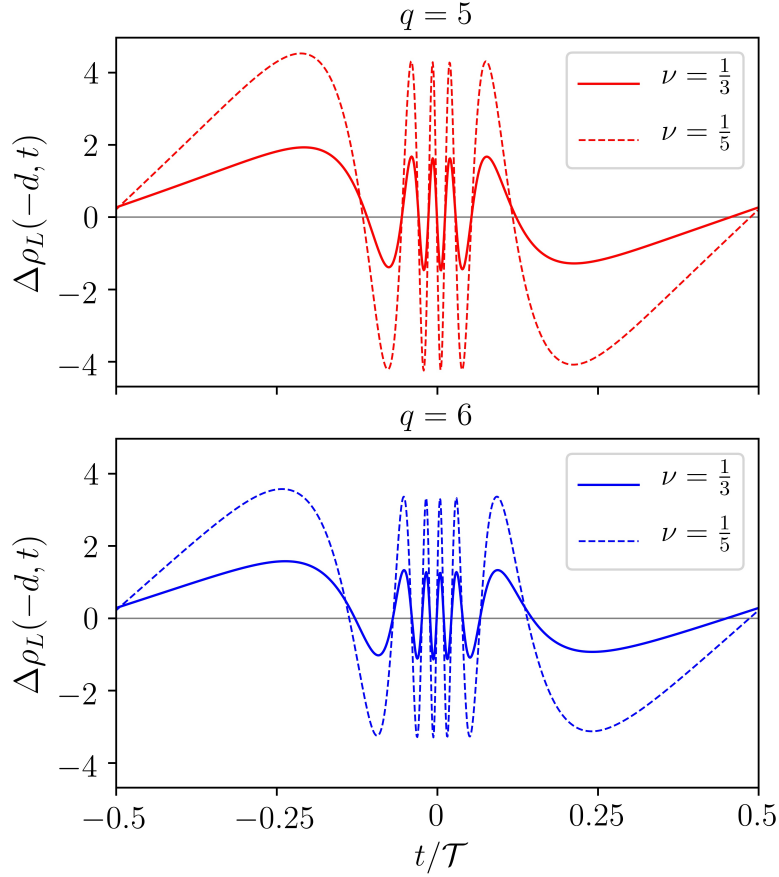
Figure 3.5: Excess charge density $\Delta\rho_L(-d, t)$ evaluated in terminal 2 (i.e. $x = -d$), in the presence of a single source for $q = 5$ and $q = 6$, in units of $\frac{e|\Lambda|^2\omega_c}{2\pi v^3}$. Two different filling factors are considered: $\nu = \frac{1}{3}$ (solid lines) and $\nu = \frac{1}{5}$ (dashed lines). The other parameters are $W = 0.04\mathcal{T}$, $k_B\theta = 10^{-3}\omega$ and $\omega = 0.01\omega_c$.

condition $\int_0^{\mathcal{T}} \frac{dt}{\mathcal{T}} \varphi_k(t)\varphi_{k'}^*(t) = \delta_{k,k'}$. Let us notice that Eq. (3.98) reduces to single-electron and single-hole coherence functions in the limit of free fermions ($\nu = 1$) and infinite period [86, 100].

The excess density in Eq. (3.74) varies significantly if evaluated *before* or *after* the scattering of injected particles at the QPC. Indeed, before the scattering we have $\Delta\rho_L(x, t)=0$, while $\Delta\rho_R(x, t)$ can be readily obtained by evaluating the excess quasi-particle correlator at equal times and positions. In the region $-d < x < 0$ (that is, downstream of the contact but still before the QPC) we find

$$\Delta\rho_R(x, t) = -\frac{e}{v\mathcal{T}} \sum_{k=1}^{q} |\varphi_k(t_-)|^2 = -\frac{e^2\nu}{2\pi v} V(t_-), \tag{3.85}$$

since $|\varphi_k(t)|^2 = \frac{e\nu V(t)}{q\omega}$ for each k. We note that Eq. (3.85) is nothing but the single-particle density of a q-particle state described by a Slater determinant formed by the set of wave functions $\{\varphi_k\}, k = 1, ..., q$ [86]. Remarkably, this excess density does not display any qualitative difference between the integer and the fractional case.

Non-linear tunneling, typical of the interacting FQH phase, is however expected to influence the propagation of levitons *after* the scattering at the QPC [116, 117]. We

thus focus on the excess density backscattered into the left-moving channel, namely $\Delta\rho_L(x,t)$, with $x < 0$. Since the QPC is assumed to work in the weak backscattering regime, we are allowed to set up a perturbative expansion in the tunneling amplitude Λ for the charge density operator $\rho_L(x) = -\frac{e\sqrt{\nu}}{2\pi}\partial_x\Phi_L(x)$, which reads (see Eqs. (D.16) in Appendix D)

$$\rho_L(x,t) = \rho_L^{(0)}(x,t) + \rho_L^{(1)}(x,t) + \rho_L^{(2)}(x,t) + o(\Lambda^3). \tag{3.86}$$

The different contributions are written in Eqs. (D.17), (D.27) and (D.28): we quote here their expressions

$$\rho_L^{(0)}(x,t) = \frac{\sqrt{\nu}}{2\pi}\partial_x\Phi_L(x,t), \tag{3.87}$$

$$\rho_L^{(1)}(x,t) = i\Theta(\pm x)\frac{\Lambda\nu}{v}\Psi_R^{(qp)\dagger}\left(0,t+\frac{x}{v}\right)\Psi_L^{(qp)}\left(0,t+\frac{x}{v}\right) + \text{h.c.}, \tag{3.88}$$

$$\rho_L^{(2)}(x,t) = i\Theta(\mp x)\int_{-\infty}^{t\mp\frac{x}{v}}dt''\left[H_T^{(qp)}(t''), +i\frac{\Lambda\nu}{v}\Psi_R^{(qp)\dagger}\left(0,t+\frac{x}{v}\right)\Psi_L^{(qp)}\left(0,t+\frac{x}{v}\right) + \text{h.c.}\right]. \tag{3.89}$$

Note that the step function in $\rho_L^{(1)}(x,t)$ is directly related to the effect of backscattering at $x = 0$.

We thus get the excess charge density to lowest non-vanishing order in the tunneling expressed in terms of quasi-particles and quasi-holes Green's functions, by repeating similar steps that led to Eq. (3.20). One finds

$$\Delta\rho_L(x,t) = \frac{e|\Lambda|^2\nu}{2\pi av}\int_{-\infty}^{t+\frac{x}{v}}dt''\left[G_R^<\left(t'',t+\frac{x}{v}\right)G_{0,L}^>\left(t'',-t+\frac{x}{v}\right) +\right.$$

$$- G_{0,L}^<\left(t''-t+\frac{x}{v}\right)G_R^>\left(t'',t+\frac{x}{v}\right) +$$

$$- G_R^<\left(t+\frac{x}{v},t''\right)G_{0,L}^>\left(t+\frac{x}{v}-t''\right) +$$

$$\left. + e^{ik_F(t''-t+\frac{x}{v})}G_{0,L}^<\left(t+\frac{x}{v}-t''\right)G_R^>\left(t-\frac{d}{v},t''\right)\right]. \tag{3.90}$$

By inserting the excess correlators in Eqs. (3.82) and (3.83) into the above expression, one finds

$$\Delta\rho_L(x,t) = \frac{e\nu|\Lambda|^2}{2\pi av}\int_{-\infty}^{t_+}dt'\left[\Delta G_R^{(qp)}(0,t';0,t_+) +\right.$$

$$\left. - \Delta G_R^{(qh)}(0,t';0,t_+)\right]\mathcal{P}_\nu\left(t'-t_+\right) + \text{h.c.}. \tag{3.91}$$

According to the completeness of the set $\{\varphi_k\}$, the above result can be recast in the more compact and physically insightful form

$$\Delta\rho_L(x,t) = \frac{e|\Lambda|^2}{v^3\mathcal{T}}\sum_{k=1}^{q}\sum_{p=1}^{+\infty}\Re[c_{k,p}\varphi_k(t_+)\varphi_p^*(t_+)], \tag{3.92}$$

where coefficients $c_{k,p}$ depend on the temperature θ and the filling factor ν. In terms of the overlap integrals $g_{kp}(\bar{t}) = \int_0^{\mathcal{T}}\frac{dt}{\mathcal{T}}\varphi_k(t+\bar{t})\varphi_p^*(t)$, they are given by

$$c_{k,p} = \frac{4\nu v^2}{\pi a^2\omega}\int_{-\infty}^{0}dt'g_{kp}^*(t')\sin\left(\frac{\pi t'}{\mathcal{T}}\right)\Im\left[\mathcal{P}_{2\nu}(t')\right]. \tag{3.93}$$

In an ordinary metallic system ($\nu = 1$), they reduce to $c_{k,p} = \delta_{k,p}$, so that Eq. (3.92) becomes simply $\Delta\rho_L(x,t) = -\frac{e^2\nu}{2\pi v}V(t_+)$. Thus backscattered pulses at $\nu = 1$ maintain the same Lorentzian shape as the injected ones.

Conversely, the excess density in a Laughlin FQH system departs strongly from the trivial metallic result, as we show in Fig. 3.5, for $\nu = \frac{1}{3}$ and $\nu = \frac{1}{5}$ and different values of q. Here we focus on the excess density measured in terminal 2, i.e. for $x = -d$ [139]. Due to the strongly correlated background, the q-Leviton state backscattered off the QPC is rearranged into an oscillatory pattern with a number of peaks exactly equal to q, regardless of any other parameter. The amplitude of the oscillations increases with decreasing filling factor (that is, for stronger correlations). These patterns suggest that scattering at the QPC creates a correlated structure of q separated and co-moving levitons. In analogy with other strongly correlated phases in condensed matter [130, 136, 140], we interpret this structure as a *crystallization* of the q-Leviton state. However, in contrast to Wigner crystallization, the arrangement induced by interaction does not show a static profile but rather a propagating one, thus leading to the emergence of a regular structure in time and not only in space. Due to the soliton-like nature of levitons [21], this process presents an intriguing analogy with the formation of optical soliton crystal in the presence of a non-linear environment [126], albeit in a completely different context.

In passing, let us comment about the parity of excess density shown in Fig. 3.5. In this light, it is useful to further manipulate Eq. (3.91) in such a way that

$$\Delta\rho_L(x,t) = \frac{e|\Lambda|^2}{v^3\mathcal{T}} \sum_{k=1}^{q} \sum_{p=1}^{+\infty} \Big\{ \Re[c_{k,p}]\Re[\varphi_k(t_+)\varphi_p^*(t_+)] +$$

$$- \Im[c_{k,p}]\Im[\varphi_k(t_+)\varphi_p^*(t_+)] \Big\}. \tag{3.94}$$

Here, $\Re[\varphi_k(\tau)\varphi_p^*(\tau)]$ and $\Im[\varphi_k(\tau)\varphi_p^*(\tau)]$ are, respectively, an even function and an odd function of τ, since $\varphi_k(\tau) = -\varphi_k^*(-\tau)$ (see Eq. (3.84)). It is thus clear that the excess density has not a definite parity with respect to $t_+ = t + \frac{x}{v}$ for a generic value of ν, as both an even term and an odd component are present in Eq. (3.94). In the non-interacting case ($\nu = 1$), the coefficients $c_{k,p}$ are real-valued and the excess density reduces to an even function of t_+.

3.3.3 Experimental signatures in current noise

A direct observation of the oscillating density would require a real-time measurement of the backscattered current with extremely high temporal resolution. Moreover, this observation alone would not be the conclusive proof of the crystallization process. In order to indubitably relate the oscillations of the density to the crystallization of levitons, one has to further investigate the density-density or current-current correlators [131, 141]. The very special nature of the q-Leviton crystal, which is not confined to a finite spatial region, but rather moves rigidly along the edges, lets us envisage an experimental test based on the cross-correlations of two flying crystallized patterns. In this light, we propose to perform a much more feasible zero-frequency measurement of current noise in a HOM experimental setup [16, 18, 85]. In this configuration, a second train of levitons (identical to the first one) is generated in terminal 4 and delayed by a tunable time shift t_D. We describe the HOM setup by setting $V_R(t) = V(t)$ and $V_L(t) = V(t + t_D)$. A genuine crystallization process is expected to manifest as oscillations in the current noise analyzed as a function

of the delay t_D. As a side note, let us observe that intensity-intensity correlation measurements are analogously performed to probe the crystallization of solitons in the optical domain [126].

We thus focus on the zero-frequency cross-correlation between terminals 2 and 3, defined as

$$\mathcal{S}_{23} = \int_0^{\mathcal{T}} \frac{dt}{\mathcal{T}} \int_{-\infty}^{+\infty} d\tau \left[\langle J_2(t+\tau) J_3(t) \rangle - \langle J_2(t+\tau) \rangle \langle J_3(t) \rangle \right], \tag{3.95}$$

which can be put in a form manifestly related to a density-density correlators

$$\mathcal{S}_{23} = -v^2 e^2 \int_0^{\mathcal{T}} \frac{dt}{\mathcal{T}} \int_{-\infty}^{+\infty} d\tau \left[\langle \rho_R(d, t+\tau) \rho_L(-d, t) \rangle - \langle \rho_R(d, t+\tau) \rangle \langle \rho_L(-d, t) \rangle \right], \tag{3.96}$$

by using the connection between density operator and chiral current operators.

In the following, we use the notation $\mathcal{S}_C^{HOM} \equiv -\mathcal{S}_{23}$. Due to the relation $\mathcal{S}_C = -\mathcal{S}_C^{HOM}$, the expression for the HOM current noise in terms of Green's functions in Eqs. (3.28) and (3.29) can be obtained directly from Eq. (3.43)

$$\mathcal{S}_C^{\mathrm{HOM}} = -(\nu e)^2 |\Lambda|^2 \int_0^{\mathcal{T}} \frac{dt}{\mathcal{T}} \int_{-\infty}^{+\infty} d\tau \left[G_R^<(t+\tau, t) G_L^>(t+\tau, t) + G_R^<(t+\tau, t) G_L^>(t+\tau, t) \right]. \tag{3.97}$$

It is interesting to recast the current noise directly in terms of the excess correlation functions $\Delta G_{R/L}^{(qp)}$ and $\Delta G_{R/L}^{(qh)}$, which encode all the information about levitons. Let us observe that in the HOM configuration they are given by

$$\Delta G_{R/L}^{(qp)}(t', t) = -2i G_0(t' - t) \sin\left(\frac{\pi(t' - t)}{\mathcal{T}} \right) \sum_{k=1}^{q_{R/L}} \varphi_{k,R/L}(t) \varphi_{k,R/L}^*(t'), \tag{3.98}$$

$$\Delta G_{R/L}^{(qh)}(t', t) = 2i G_0(t' - t) \sin\left(\frac{\pi(t' - t)}{\mathcal{T}} \right) \sum_{k=1}^{q_{R/L}} \varphi_{k,R/L}^*(t) \varphi_{k,R/L}(t'), \tag{3.99}$$

where $\varphi_{k,R}(t) = \varphi_k(t)$ and $\varphi_{k,L}(t) = \varphi_k(t + t_D)$. By using the relations $G_{R/L}^<(t', t) = e^{ik_F v(t' - t)} \Delta G_{R/L}^{(qp)}(t', t) + G_{0,R/L}^<(t' - t)$ and $G_{R/L}^>(t', t) = e^{-ik_F v(t' - t)} \Delta G_{R/L}^{(qh)}(t', t) + G_{0,R/L}^>(t' - t)$ (we omitted here the time dependence for notational convenience), one finds

$$\mathcal{S}_C^{\mathrm{HOM}} = -\mathcal{S}_C^{(0)} + \mathcal{S}_{C,R}^{\mathrm{HBT}} + \mathcal{S}_{C,L}^{\mathrm{HBT}} +$$
$$- (\nu e)^2 |\Lambda|^2 \int_0^{\mathcal{T}} \frac{dt}{\mathcal{T}} \int_{-\infty}^{+\infty} d\tau \Big[\Delta G_R^{(qp)}(t+\tau, t) \Delta G_L^{(qh)}(t+\tau, t) +$$
$$+ \Delta G_R^{(qh)}(t+\tau, t) \Delta G_L^{(qp)}(t+\tau, t) \Big], \tag{3.100}$$

where we have used the expressions of the equilibrium noise $\mathcal{S}_{32}^{(0)}$ and the HBT noise $\mathcal{S}_{32,R/L}^{\mathrm{HBT}}$ in terms of Green's functions, which read

$$\mathcal{S}_C^{(0)} = -\frac{(\nu e)^2 |\Lambda|^2}{2(\pi a)^2} \int_{-\infty}^{+\infty} d\tau \mathcal{P}_{2\nu}(\tau), \tag{3.101}$$

$$\mathcal{S}_{C,R/L}^{\mathrm{HBT}} = -(\nu e)^2 |\Lambda|^2 \int_0^{\mathcal{T}} \frac{dt}{\mathcal{T}} \int_{-\infty}^{+\infty} d\tau \left[G_{R/L}^{(qp)}(t+\tau, t) G_{0,R/L}^>(\tau) + G_{R/L}^{(qh)}(t+\tau, t) G_{0,R/L}^<(\tau) \right]. \tag{3.102}$$

A standard procedure is to normalize the HOM signal with respect to the HBT one [16, 106]. We thus define the ratio

$$\mathcal{R} = \frac{\mathcal{S}_C^{\text{HOM}}(t_D) - \mathcal{S}_C^{(0)}}{\mathcal{S}_{C,R}^{\text{HBT}} + \mathcal{S}_{C,L}^{\text{HBT}} - 2\mathcal{S}_C^{(0)}}. \tag{3.103}$$

By using the previous results the HOM ratio becomes

$$\mathcal{R} = 1 - \frac{\mathcal{N}}{\mathcal{D}}, \tag{3.104}$$

with $\mathcal{N}$ and $\mathcal{D}$ given respectively by

$$\mathcal{N} = -\int_0^{\mathcal{T}} \frac{dt}{\mathcal{T}} \int_{-\infty}^{+\infty} d\tau \left[\Delta G_R^{(qp)}(t+\tau, t) \Delta G_L^{(qh)}(t+\tau, t) + \right.$$
$$\left. + \Delta G_R^{(qh)}(t+\tau, t) \Delta G_L^{(qp)}(t+\tau, t) \right], \tag{3.105}$$

$$\mathcal{D} = \frac{1}{2\pi a} \sum_{r=R,L} \int_0^{\mathcal{T}} \frac{dt}{\mathcal{T}} \int_{-\infty}^{+\infty} d\tau \left[\Delta G_r^{(qp)}(t+\tau, t) + \Delta G_r^{(qh)}(t+\tau, t) \right] \mathcal{P}_\nu(\tau). \tag{3.106}$$

By inserting equations (3.98) and (3.99) into the above equations, these two contributions can be further expressed in terms of the wave-functions $\{\varphi_k\}$ as

$$\mathcal{N} = \frac{1}{(2\pi a)^2} \int_0^{\mathcal{T}} \frac{dt}{\mathcal{T}} \int_{-\infty}^{+\infty} d\tau \left[\sum_{k=1}^{q_R} \sum_{k'=1}^{q_L} \varphi_k(t) \varphi_k^*(t+\tau) \varphi_{k'}^*(t+t_D) \varphi_{k'}(t+t_D+\tau) + \text{h.c.} \right] \times$$
$$\times \sin^2\left(\frac{\pi\tau}{T}\right) \mathcal{P}_{2\nu}(\tau), \tag{3.107}$$

$$\mathcal{D} = \frac{1}{2(2\pi a)^2} \sum_{r=R,L} \int_0^{\mathcal{T}} \frac{dt}{\mathcal{T}} \int_{-\infty}^{+\infty} d\tau \left[i \sum_{k=1}^{q_r} \varphi_k(t) \varphi_k^*(t+\tau) + \text{h.c.} \right] \sin\left(\frac{\pi\tau}{T}\right) \mathcal{P}_{2\nu}(\tau). \tag{3.108}$$

Finally, by introducing the overlap integrals of wave-functions $g_{kp}(t_D) = \int_0^{\mathcal{T}} \frac{dt}{\mathcal{T}} \varphi_k(t+t_D) \varphi_p^*(t)$, the ratio acquires the form

$$\mathcal{R} = 1 - \frac{\sum_{k=1}^{q_R} \sum_{k'=1}^{q_L} \sum_{p=1}^{+\infty} \sum_{p'=1}^{+\infty} \Re\left[w_{pp'}^k g_{k'p}(t_D) g_{k'p'}^*(t_D) \right]}{\frac{1}{2}\left(v_{q_R} + v_{q_L}\right)}, \tag{3.109}$$

where the coefficients are

$$w_{pp'}^k = \int_0^{\mathcal{T}} \frac{dt}{\mathcal{T}} \int_{-\infty}^{+\infty} d\tau \, \varphi_k(t) \varphi_k^*(t+\tau) \varphi_p(t) \varphi_{p'}^*(t+\tau) \sin^2\left(\frac{\pi\tau}{\mathcal{T}}\right) \mathcal{P}_{2\nu}(\tau), \tag{3.110}$$

$$v_{q_r} = \sum_{k=1}^{q_r} \int_{-\infty}^{+\infty} d\tau \sin\left(\frac{\pi\tau}{\mathcal{T}}\right) g_{kk}^*(\tau) \mathcal{P}_{2\nu}(\tau). \tag{3.111}$$

Finally, starting from equation (3.109) one also gets a simplified formula for the integer case at zero temperature, which reads

$$\mathcal{R} = 1 - \frac{2}{q_L + q_R} \sum_{k=1}^{q_R} \sum_{k'=1}^{q_L} |g_{k'k}(t_D)|^2, \tag{3.112}$$
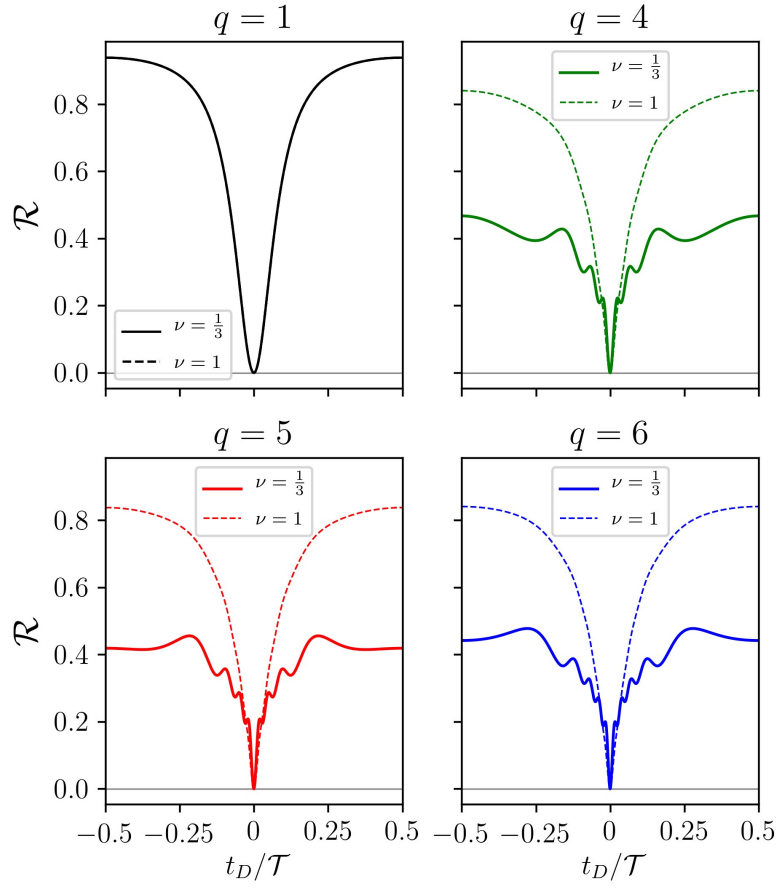
Figure 3.6: Ratio $\mathcal{R}$ as a function of the time delay t_D for $q = 1$, $q = 4$, $q = 5$, $q = 6$. The integer case (dashed lines) and the fractional case for $\nu = \frac{1}{3}$ (solid lines) are compared. The other parameters are $W = 0.04\mathcal{T}$, $k_\mathrm{B}\theta = 10^{-3}\omega$ and $\omega = 0.01\omega_c$.

in accordance with previous results [106, 111].

Let us start by analyzing the most interesting situation of collision between identical wave-packets, namely the case with $q_R = q_L = q$.

The HOM ratio at $\nu = 1$ consists of a single, smooth dip shown with dashed lines in Fig. 3.6 for different values of q. The absence of any additional structure at $\nu = 1$ confirms the uncorrelated nature of levitons in the Fermi-liquid state. Conversely, full lines in Fig. 3.6 show the behavior of $\mathcal{R}(t_D)$ at fractional filling $\nu = \frac{1}{3}$ for the same values of q. We first notice that completely destructive interference between the two signals always occurs at $t_D = 0$ (as demonstrated by the total central dip), whether the system is interacting or not. This shows that electron-electron interactions in single-edge-mode Laughlin states do not induce decoherence effects, in contrast with the role played by interactions in the $\nu = 2$ integer quantum Hall effect, where two co-propagating edge states exist [101, 108]. At $q = 1$, the ratio exhibits the same behavior for integer and fractional filling factors [115]. This is related to the fact that backscattering of a single Leviton generates a simple signal with no internal peak/valley structure. For higher values of q, rearrangement of q-Leviton excitations generates peculiar features that distinguish between the non-interacting and the strongly correlated phase. Plots at $\nu = \frac{1}{3}$ clearly show the presence of oscillations in the current-current correlators for $q > 1$, with $2q - 2$ new dips aside of the principal one at $t_D = 0$. It is interesting to notice that their arrangement bears similarities with the behavior of $\Delta\rho_L(x, t)$ shown in Fig. 3.5. Indeed, as for the excess density, the spacing between maxima/minima of $\mathcal{R}(t_D)$ tends to widen while approaching the ends of the period. These features unambiguously identify the effects of the strongly correlated FQH phase on Leviton excitations, in striking contrast with the uncorrelated Fermi liquid phase. A similar pattern was predicted in Ref. [108] and experimentally observed in Ref. [29], where the internal peak/valley structure is generated by a fractionalization effect in a $\nu = 2$ quantum Hall interferometer. Here we argue that the new side dips must be related to the unprecedentedly reported process of crystallization of q-levitons in FQH edge states, as no fractionalization occurs in the single-edge-mode Laughlin sequence. Therefore, the appearance of local maxima and minima in the current-current correlators at fractional filling factors proves the existence of a q-Leviton crystal in the time domain induced by interactions.

By increasing the ratio between the width of the pulses and the period, the peak-to-valley amplitude of oscillations is enhanced for fractional filling factors, while for the integer case the situation is qualitatively unchanged, as depicted in Fig. 3.7. The principal downside is that some of the oscillations that are clearly visible for sharper pulses are now lost, since pulses belonging to neighboring periods start to overlap significantly. Therefore, the choice of increasing the ratio $W/\mathcal{T}$ makes it easier to observe the presence of oscillations in the current-current correlators, even though some dips inevitably disappear. Complementary information can be drawn by fixing a value of the delay t_D and inspecting the shape of the ratio $\mathcal{R}$ as the ratio $W/\mathcal{T}$ is varied. The plots of $\mathcal{R}$ as a function of $W/\mathcal{T}$ for different values of q are shown in Fig. 3.8, where we set $t_D = 0.5\mathcal{T}$ since the signal is bigger and oscillations are more pronounced for such a value of the delay. Interestingly, the integer and the fractional cases show a dramatically different behavior. In the former case, the ratio is smoothly decreasing without any particular feature. In the latter, conversely, it oscillates for quite a large interval of $W/\mathcal{T}$, before eventually decreasing. Furthermore, the number of peaks appearing for fractional filling factors is exactly equal
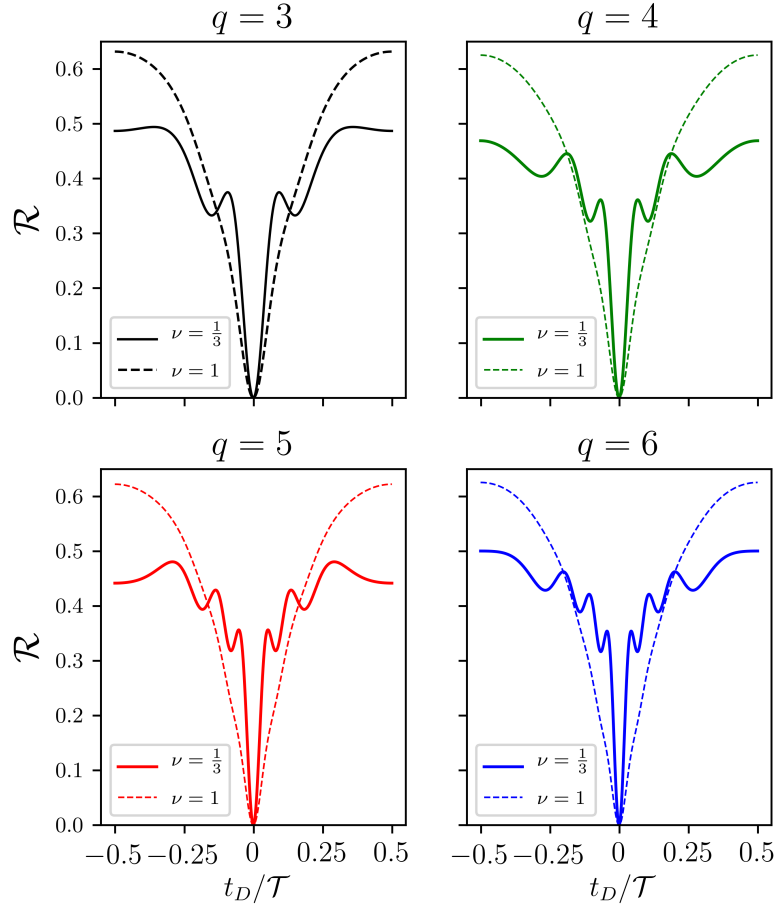
Figure 3.7: Ratio $\mathcal{R}$ as a function of the time delay t_D for $q = 3$, $q = 4$, $q = 5$, $q = 6$. The integer case (dashed lines) and the fractional case for $\nu = \frac{1}{3}$ (solid lines) are compared. The other parameters are $W = 0.1\mathcal{T}$ and $\omega = 0.01\omega_c$.

to q. This additional experimental investigation could significantly help in discriminating between the crystallized and the non-crystallized regime. Finally, it is worth noting that the same behavior of the ratio can be observed for all filling factors in the Laughlin sequence. Such an universality tells us that interactions in Laughlin FQH states are always strong enough to induce a complete crystallization.

3.3.4 Asymmetric collisions

We now examine what happens when wave-packets carrying different charges are injected in terminals 1 and 4 and sent to the collider. For simplicity, we inject integer Lorentzian pulses with $q_R = 1$ on the upper right-moving edge, while the opposite contact is driven with a generic Lorentzian drive with tunable q_L and t_D. Starting from the $\nu = 1$ case, we observe that the total suppression of HOM noise is achieved only for $q_L = q_R = 1$, as expected. However, different values of q_L still generate a partial dip in the noise whose value is given by

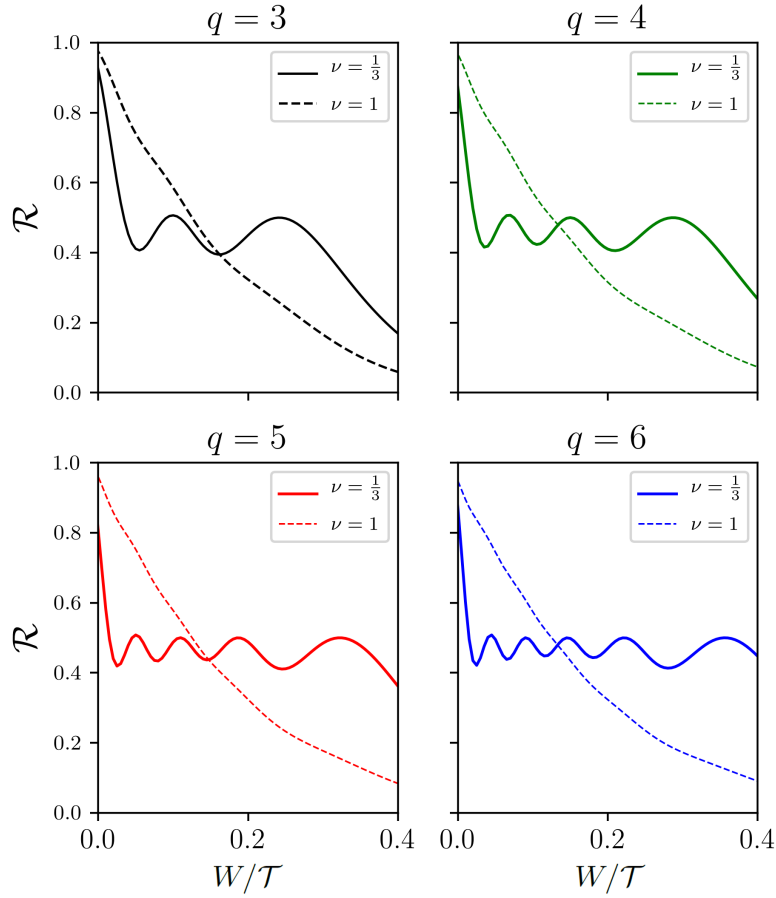$$\mathcal{R}(q_R, q_L, t_D = 0) = \frac{q_L - q_R}{q_L + q_R}, \tag{3.113}$$

Figure 3.8: Ratio $\mathcal{R}$ as a function of $W/\mathcal{T}$ for $q = 3$, $q = 4$, $q = 5$, $q = 6$. The integer case (dashed lines) and the fractional case for $\nu = \frac{1}{3}$ (solid lines) are compared. The other parameters are $t_D = 0.5\mathcal{T}$ and $\omega = 0.01\omega_c$.

as one can infer by looking at Figure 3.9a. For instance, by fixing the value of q_L we obtain the four curves shown in Figure 3.9b, which clearly demonstrate that the anti-bunching effect is not complete - although still present - when excitations with different charge collide at the QPC.

In the FQH regime the values of the ratio $\mathcal{R}$ at zero delay is slightly modified, while two unexpected sub-dips appear (see Figures 3.9c and 3.9d). Moreover, the distance between these two side-dips progressively increases by increasing q_L. As deduced previously from Figure 3.6, the q_L-levitons, with $q_L > 1$, are re-arranged in a crystallized structure, while the single Leviton wave-packet maintains a trivial pattern. Therefore, the latter is not suitable to resolve the more complicated crystal of q_L-levitons in the type of experiment presented in Figure 3.9. As a consequence, the number of side-dips is totally unrelated to the specific value of q_L, in contrast to the configuration with identical drives. A better resolution would require the injection of a very narrow Leviton wave-packet from terminal 1, ideally reaching the limit of a delta-like pulse: anyway, the generation of such a narrow pulse is beyond the state-of-art technology. Another possibility would be to increase the value of q_R, thus characterizing the crystal of q_L-levitons with a comparably complicated wave-packet: in this case, a total number of $2q_R$ side-dips would appear.
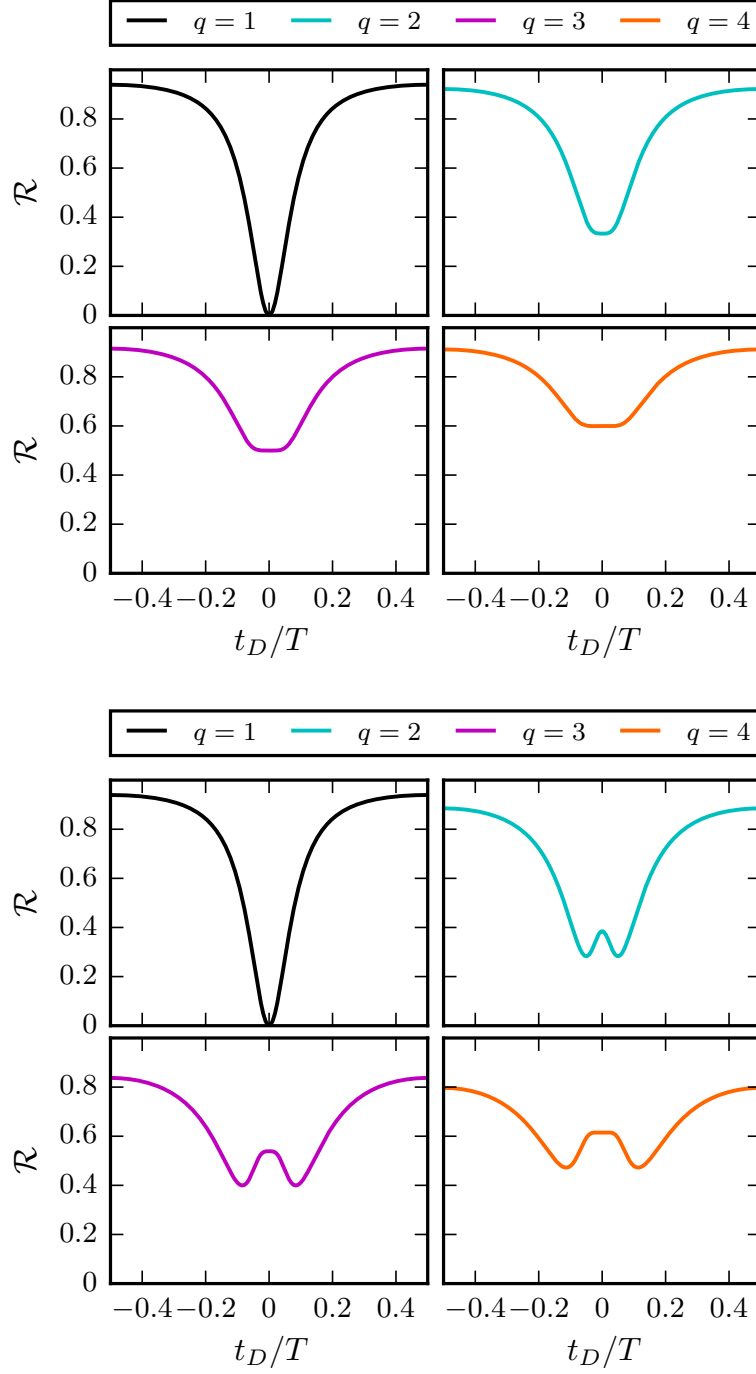
Figure 3.9: HOM ratio $\mathcal{R}$ for collisions of integer $(q_R = 1)$ and generic $(q_L = q)$ pulses as a function of the delay t_D and the charge q injected in the left-moving edge. The upper panels refers to the case of integer filling factor, while the lower panels corresponds to fractional filling $\nu = 1/3$. The temperature is $\theta = 0.01\,\omega$, the dimensionless width of the pulses is $W = 0.04\mathcal{T}$ and the high energy cut-off is $v/a = 10\omega$.

Chapter 4

Heat transport properties of levitons

In this Chapter we investigate heat transport properties of Lorentzian-shaped voltage pulses in the quantum Hall systems. Excitations are studied through heat and mixed noise generated by the random partitioning at the QPC. It is shown that levitons represent the cleanest states even for heat transport properties, since excess heat and mixed shot noise both vanish only when Lorentzian voltage pulses carrying integer electric charge are applied to the conductor. This happens in the integer QH regime and for Laughlin fractional states as well, with no signature associated to fractional excitations. In addition, we demonstrate the robustness of such excitations to the overlap of Lorentzian wave-packets. Even though mixed and heat noise have nonlinear dependence on the voltage bias, and despite the non-integer power-law behavior arising from the FQH physics, an arbitrary superposition of levitons always generates minimal excitation states. Finally, we investigate heat current fluctuations induced by levitons in a Hong-Ou-Mandel interferometer implemented in a quantum Hall bar in the Laughlin sequence. We demonstrate that the noise in this collisional experiment cannot be reproduced in a setup with a single drive, in contrast to what is observed in the charge noise case. Nevertheless, the simultaneous collision of two identical levitons always leads to a total suppression even for the Hong-Ou-Mandel heat noise at all filling factors, despite the presence of emergent anyonic quasi-particle excitations in the fractional regime. Interestingly, the strong correlations characterizing the fractional phase are responsible for a remarkable oscillating pattern in the HOM heat noise, which is completely absent in the integer case.

4.1 Introduction

The interest in quantum Hall systems has been mainly devoted to its electrical transport properties, due to the many fascinating physical phenomena related to its chiral edge states and fractionally charged excitations. Nevertheless, charge is not the only interesting degree of freedom that could be investigated in quantum transport. In the past, heat fluxes in small quantum conductors have been mostly considered as a detrimental effect in experiments. Indeed, the experimental control over heat fluxes in mesoscopic devices represented a great challenge from the technical point of view, which was overcome only in recent years. Indeed, some recent groundbreaking experiments has spurred the investigation also in the direction of heat transport at

the nanoscale [142–147]. New intriguing challenges posed by extending concepts like energy harvesting [148–152], driven heat and energy transport [59, 153–155], energy exchange in open systems [156, 157] and fluctuation-dissipation theorems [158–161] to the quantum realm resulted in a great progress of the field of quantum thermodynamics. In this context, the investigation of heat transport in the ballistic regime, where electrons propagate in ideally transmitting channels, is fundamental to access the quantum limit of thermal phenomena. Of course, a prominent role is played by chiral edge states of quantum Hall systems: the coherent transport and manipulation of heat fluxes have been reported in quantum Hall systems [162–164]. Intriguingly, the quantization of heat conductance has been observed in integer [51] and fractional quantum Hall systems [52, 53, 122]. In this way, ample and valuable information about these peculiar states of matter, complementary to the well-established results associated with quantized charge transport, is now available with interesting implications also for quantum computation [165–167].

As discussed in the previous Chapters, the main driving force behind EQO has been to properly revise quantum optics experiments focusing on charge transport properties of single-electron excitations. Nevertheless, a new perspective on EQO has been also triggered by the rising interest for heat transport properties of single-electron excitations. As described in Chapters 2 and 3, the study of noise is an extremely powerful tool to investigate the response of quantum Hall edge channels to single-electron sources. In addition to fluctuations of heat current, also correlators between charge and heat currents attracted a lot of attention due to their relation with thermoelectric properties of a system [168, 169]. Indeed, both heat and mixed noises started to be investigated also in the presence of single-electron voltage sources [170–172]. Moreover, heat current has revealed an useful resource in the context of EQO, since it might provide the full reconstruction of a single-electron wave-function [173].

A natural question immediately arises when one considers heat dynamics in EQO, namely what kind of voltage drive gives rise to minimal excitation states for heat transport in mesoscopic conductors. The first result of this Chapter will be exactly the answer to this question. To this end, we study heat conduction along the topologically-protected chiral edge states of the quantum Hall effect. We analyze heat current fluctuations as well as mixed charge-heat correlations [168, 169] when different types of periodic voltage pulses are sent to the conductor and partitioned off a QPC [14]. Starting from the dc regime of the voltage drive, where simple relations between noises and currents can be derived in the spirit of the celebrated Schottky's formula [112, 123], we introduce the *excess signals* for charge, heat and mixed fluctuations, which basically measure the difference between the zero-frequency noises in an ac-driven system and their respective reference signals in the dc configuration. The vanishing of excess heat and mixed noise is thus used to flag the occurrence of a minimal excitation state for heat transport in the quantum Hall regime. With this powerful tool we demonstrate that minimal noise states for heat transport can be achieved only when the voltage drive takes the form of Lorentzian pulses carrying an integer multiple of the electron charge, i.e. when levitons are injected into the quantum Hall edge states. We study this problem both in the integer regime and in the FQH regime, where strong interactions give rise to the fractional properties of quasi-particle excitations.

Having recognized levitons as the fundamental building block for heat transport, we then turn to the second central issue of this paper, which deals with the

robustness of multiple overlapping Lorentzian pulses as minimal excitation states. Indeed, Levitov and collaborators demonstrated that N levitons traveling through a quantum conductor with transmission $\mathcal{T} < 1$ represent N independent attempts to pass the barrier, with the total noise not affected by the overlap between their wave-packets. This is no more guaranteed when we look for quantities which, like heat current and noise, have a non-linear dependence on the voltage bias. In addition, other non-linearities arise as a natural consequence of FQH physics, which give rise to exotic power laws with non-integer exponents. We show that, while currents and noises are sensitive to the actual number of particles sent to the QPC, excess signals always vanish for arbitrary superposition of integer levitons. One then concludes that levitons show a remarkable stability even regarding heat transport properties, combined with the equally surprising robustness in the strongly-correlated FQH liquid. This provides further evidence of the uniqueness of the leviton state in the quantum Hall regime.

In the last part of this Chapter, we address the problem of the heat noise generated by levitons injected in a HOM interferometer in the fractional quantum Hall regime. We consider a four terminal quantum Hall bar in the Laughlin sequence [62], where a single channel arises on each edge. Two terminals are contacted to time-dependent voltages, namely V_L and V_R. Tunneling processes of quasi-particles are allowed by the presence of a QPC connecting the two edge states. In this case, charge noise generated in the HOM setup is identical to the one generated in a single-drive setup driven by the voltage $V_L - V_R$. Interestingly, we prove that this does not hold true anymore for heat noise, since it is possible to identify a contribution to HOM heat noise which is absent in a single-drive interferometer driven by $V_L - V_R$. In addition, we prove that the HOM heat noise always vanishes for a zero delay between the driving voltage, both for integer and fractional filling factors. Finally, we focus on the case of Lorentzian-shaped voltage carrying an integer number of electrons and we show that the HOM heat noise displays unexpected side dips in the fractional quantum Hall regime, which have no parallel in the integer regime. Intriguingly, the number of these side dips increases with the number of levitons injected per period. This result is consistent with the recently predicted phenomenon of charge crystallization of levitons in the fractional quantum Hall regime [55].

4.2 Heat current and noise in quantum Hall systems

In order to extend the concepts of EQO to heat transport, this section is devoted to the introduction and the definition of heat current operators and heat noise. We will refer to the model for time-dependent transport in the FQH effect described in Sec. B.1 of Appendix B. For a system, with hamiltonian density $\mathcal{H}$ and particle number density $\mathcal{N}$, heat density $\mathcal{Q}$ is defined as

$$\mathcal{Q} = \mathcal{H} - \mu\mathcal{N}, \tag{4.1}$$

where μ is the system chemical potential. This definition is motivated by the fact that the energy density depends on an arbitrary energy reference and, thus, it is not a well-defined experimental observable. On the contrary, heat is defined as the energy carried by particles with respect to the chemical potential in order to be a valid observable, thus motivating Eq. (4.1). For this reason, a correct heat transport quantity should be completely unaffected by chemical potential.

In a chiral Luttinger liquid hamiltonian density (see the integrand function in Eq.

(3.1)), the contributions proportional to μ is automatically subtracted [118, 122]: the presence of a chemical potential $\mu = vk_F$ is taken into account in the bosonized expression for field operators by inserting the exponential $e^{\pm ik_F x}$

$$\Psi_{R/L}^{(qp)}(x,t) = e^{-i\nu e \int_0^{t \mp \frac{x}{v}} dt' V_{R/L}(t')} \frac{\mathcal{F}_{R/L}^{(qp)}}{\sqrt{2\pi a}} e^{\pm ik_F(x \mp vt)} e^{-i\sqrt{\nu}\phi_{R/L}(x,t)}. \tag{4.2}$$

Therefore, one can define heat density as the hamiltonian densities (see Eqs. (1.91) and (1.89))

$$\mathcal{Q}_{R/L}(x,t) = \frac{v}{4\pi} \left(\partial_x \Phi_{R/L}(x,t) \right)^2. \tag{4.3}$$

The heat current operators of terminal 2 and 3 can be expressed in terms of heat density operators [118] as

$$\mathcal{J}_{2/3}(t) = \pm v \, \mathcal{Q}_{R/L}(\pm d, t), \tag{4.4}$$

due to the chirality of Laughlin edge states.

Analogously to charge current, one can expand heat current operators in power of the tunneling amplitude Λ, thus obtaining (see appendix D)

$$\mathcal{J}_{2/3}(t) = \mathcal{J}_{2/3}^{(0)}(t) + \mathcal{J}_{2/3}^{(1)}(t) + \mathcal{J}_{2/3}^{(2)}(t) + \mathcal{O}\left(|\Lambda|^3\right), \tag{4.5}$$

where

$$\mathcal{J}_{2/3}^{(0)}(t) = \pm v \mathcal{Q}_{R/L}^{(0)}(\pm d, t), \tag{4.6}$$

$$\mathcal{J}_{2/3}^{(1)}(t) = \pm iv \int_{-\infty}^t dt' \left[H_T^{(qp)}(t'), \mathcal{Q}_{R/L}^{(0)}(\pm d, t) \right], \tag{4.7}$$

$$\mathcal{J}_{2/3}^{(2)}(t) = \pm i^2 v \int_{-\infty}^t dt' \int_{-\infty}^{t'} dt'' \left[H_T^{(qp)}(t''), \left[H_t(t'), \mathcal{Q}_{R/L}^{(0)}(\pm d, t) \right] \right]. \tag{4.8}$$

In the above equations we have denoted with $\mathcal{Q}^{(0)}(x,t)$, the time evolution of heat density in the absence of tunneling, which can be obtained from the time evolution of bosonic fields in Eq. (B.17) and reads

$$\mathcal{Q}_{R/L}^{(0)}(x,t) = \frac{v}{4\pi} \left[\left(\partial_x \phi_{R/L}(x,t) \right)^2 \pm 2e\sqrt{\nu} \partial_x \phi_{R/L}(x,t) V_{R/L}\left(t \mp \frac{x}{v}\right) + \frac{e^2\nu}{v} V_{R/L}^2\left(t \mp \frac{x}{v}\right) \right]. \tag{4.9}$$

By exploiting bosonization identity and Baker-Hausdorff relation, the commutator involving $\mathcal{Q}_{R/L}^{(0)}(x,t)$ in Eqs. (4.7) and (4.8) can be recast into an expression in terms of quasi-particle fields, as we did for charge current operators, which will be useful for the following calculation of average values. It reads

$$\left[H_T^{(qp)}(t'), \mathcal{Q}_{R/L}^{(0)}(x,t) \right] = \left[\Lambda \Psi_R^{(qp)\dagger}(0,t') \Psi_L^{(qp)}(0,t') + \text{h.c.}, \frac{v}{4\pi} \left[\left(\partial_x \phi_{R/L}(x,t) \right)^2 + \right. \right.$$
$$\left. \pm \frac{e\sqrt{\nu}}{2\pi} \partial_x \phi_{R/L}(x,t) V_{R/L}\left(t \mp \frac{x}{v}\right) + \frac{e^2\nu}{v} V_{R/L}^2\left(t \mp \frac{x}{v}\right) \right] \right] =$$
$$= 2 \left[\Lambda \Psi_R^{(qp)\dagger}(0,t') \Psi_L^{(qp)}(0,t') + \text{h.c.}, \frac{v}{4\pi} \partial_x \phi_{R/L}(x,t) \right] \partial_x \phi_{R/L}(x,t) +$$
$$\pm \left[\Lambda \Psi_R^{(qp)\dagger}(0,t') \Psi_L^{(qp)}(0,t') + \text{h.c.}, \frac{e\sqrt{\nu}}{2\pi} \partial_x \phi_{R/L}(x,t) V_{R/L}\left(t \mp \frac{x}{v}\right) \right], \tag{4.10}$$

where we used that $V_{R/L}$ are c-numbers and commute with any operator. At this point, we can take advantage of the following commutator, derived in Eq. (D.25),

$$\left[\psi_{R/L}^{(qp)}(0,t'),\partial_x\phi_{R/L}(x,t)\right] = \pm 2\pi\sqrt{\nu}\delta(x \mp v(t-t'))\Psi_{R/L}^{(qp)}(0,t'), \tag{4.11}$$

in order to recast Eq. (4.10) as

$$\left[H_T^{(qp)}(t'),\mathcal{Q}_{R/L}^{(0)}(x,t)\right] = -iv\delta\left(x \mp v(t-t')\right)\dot{Q}_{R/L}(x,t), \tag{4.12}$$

where we introduced the following operators

$$\dot{Q}_R(x,t) = v\Lambda\left(\partial_x + ik_F\right)\Psi_R^{(qp)\dagger}(x,t)\Psi_L^{(qp)}(x,t) + \text{H.c.}, \tag{4.13}$$

$$\dot{Q}_L(x,t) = -v\Lambda\Psi_R^{(qp)\dagger}(x,t)\left(\partial_x + ik_F\right)\Psi_L^{(qp)}(x,t) + \text{H.c.}. \tag{4.14}$$

Eq. (4.12) can be used to recast Eqs. (4.7) and (4.8)

$$\mathcal{J}_{2/3}^{(1)}(t) = \pm\dot{Q}_{R/L}(\pm d,t), \tag{4.15}$$

$$\mathcal{J}_{2/3}^{(2)}(t) = \pm i\int_{-\infty}^{t-\frac{d}{v}}dt''\left[H_t(t''),\dot{Q}_{R/L}(\pm d,t)\right]. \tag{4.16}$$

Then, we can define mixed and heat noises as

$$\mathcal{S}_{X,\alpha\beta} = \int_0^{\mathcal{T}}\frac{dt}{\mathcal{T}}\int_{-\infty}^{+\infty}dt'\ \left[\langle J_\alpha(t')\mathcal{J}_\beta(t)\rangle - \langle J_\alpha(t')\rangle\langle\mathcal{J}_\beta(t)\rangle\right]\ , \tag{4.17}$$

$$\mathcal{S}_{Q,\alpha\beta} = \int_0^{\mathcal{T}}\frac{dt}{\mathcal{T}}\int_{-\infty}^{+\infty}dt'\ \left[\langle\mathcal{J}_\alpha(t')\mathcal{J}_\beta(t)\rangle - \langle\mathcal{J}_\alpha(t')\rangle\langle\mathcal{J}_\beta(t)\rangle\right]\ . \tag{4.18}$$

The perturbative expansion of charge and heat current operators in Eqs. (D.16) and (4.5) allows to express mixed and heat noises at lowest order as

$$\mathcal{S}_{X,\alpha\beta} = \mathcal{S}_{X,\alpha\beta}^{(02)} + \mathcal{S}_{X,\alpha\beta}^{(20)} + \mathcal{S}_{X,\alpha\beta}^{(11)} + \mathcal{O}\left(|\Lambda|^3\right), \tag{4.19}$$

$$\mathcal{S}_{Q,\alpha\beta} = \mathcal{S}_{Q,\alpha\beta}^{(02)} + \mathcal{S}_{Q,\alpha\beta}^{(20)} + \mathcal{S}_{Q,\alpha\beta}^{(11)} + \mathcal{O}\left(|\Lambda|^3\right), \tag{4.20}$$

where

$$\mathcal{S}_{X,\alpha\beta}^{(ij)} = \int_0^{\mathcal{T}}\frac{dt}{\mathcal{T}}\int_{-\infty}^{+\infty}dt'\left\{\langle J_\alpha^{(i)}(t')\mathcal{J}_\beta^{(j)}(t)\rangle - \langle J_\alpha^{(i)}(t')\rangle\langle\mathcal{J}_\beta^{(j)}(t)\rangle\right\}, \tag{4.21}$$

$$\mathcal{S}_{Q,\alpha\beta}^{(ij)} = \int_0^{\mathcal{T}}\frac{dt}{\mathcal{T}}\int_{-\infty}^{+\infty}dt'\left\{\langle\mathcal{J}_\alpha^{(i)}(t')\mathcal{J}_\beta^{(j)}(t)\rangle - \langle\mathcal{J}_\alpha^{(i)}(t')\rangle\langle\mathcal{J}_\beta^{(j)}(t)\rangle\right\}. \tag{4.22}$$

4.3 Minimal excitation states for heat transport

4.3.1 Calculations of heat transport in the HBT geometry

In this Section, our goal is to establish which drive gives rise to minimal excitations of heat transport. In analogy with the discussion for charge, we focus on a HBT geometry, where $V_R(t) = V(t)$ and $V_L(t) = 0$, with $V(t)$ a generic drive with period $\mathcal{T}$. In this case, a single stream of particles emitted from reservoir 1 is scattered off the QPC (see Fig. 3.5). Moreover, we will focus on the case of zero temperature, in order to get rid of thermal fluctuations that would hide the existence of minimal excitations for heat noise

Let us start by looking at the thermal average of heat current operators in Eq. (4.5), which reads

$$\left\langle \mathcal{J}_{2/3}(t) \right\rangle = \langle \mathcal{J}_{2/3}^{(0)} \rangle + \langle \mathcal{J}_{2/3}^{(2)} \rangle, \tag{4.23}$$

where

$$\langle \mathcal{J}_{2/3}^{(0)}(t) \rangle = \pm \langle v \mathcal{Q}_{R/L}^{(0)}(x,t) \rangle = \frac{v}{4\pi} \left[\left\langle \left(\partial_x \phi_{R/L}(x,t) \right)^2 \right\rangle + \frac{e^2 \nu}{4\pi v} V_{R/L}^2 \left(t \mp \frac{x}{v} \right) \right], \tag{4.24}$$

$$\langle \mathcal{J}_{2/3}^{(2)}(t) \rangle = \pm i \int_{-\infty}^{t-\frac{d}{v}} dt'' \langle \left[H_t(t''), \dot{Q}_{R/L}(\pm d, t) \right] \rangle. \tag{4.25}$$

Notice that the average value of $\mathcal{J}_{2/3}^{(1)}$ is zero due to the unbalance between annihilation and creation field operators of each chirality. The terms in Eq. (4.24) are the heat currents flowing along the edge states emitted from reservoirs 1 and 4, which would reach unmodified reservoirs 2 and 3 in the absence of any tunneling process between the two edges. The presence of a QPC tuned to the high transparency limit generates the other contribution in Eq. (4.25). For the following discussion, we are interested in the heat current that is backscattered by the QPC into reservoir 3. Therefore, we define backscattering heat current as

$$\mathcal{J}_{BS}(t) = \langle \mathcal{J}_3^{(2)}(t) \rangle. \tag{4.26}$$

The latter can be expressed in terms of Green's functions in Eqs. (3.28) and (3.29), by exploiting the explicit expression of $\dot{Q}_L(x,t)$ in Eq. (4.14) for $V_L(t) = 0$, thus finding

$$\mathcal{J}_{BS}(t) = i|\Lambda|^2 \int_{-\infty}^{t-\frac{d}{v}} d\tau \left[G_R^< \left(t', t - \frac{d}{v} \right) (\partial_t - ik_F v) G_L^< \left(t', t - \frac{d}{v} \right) + \right.$$

$$+ G_R^< \left(t', t - \frac{d}{v} \right) (\partial_t + ik_F v) G_L^< \left(t', t - \frac{d}{v} \right) +$$

$$- G_R^< \left(t - \frac{d}{v}, t' \right) (\partial_t - ik_F v) G_L^< \left(t - \frac{d}{v}, t' \right) +$$

$$\left. - G_R^< \left(t - \frac{d}{v}, t' \right) (\partial_t + ik_F v) G_L^< \left(t - \frac{d}{v}, t' \right) \right]. \tag{4.27}$$

By recalling the link between Green's functions and the function $\mathcal{P}_g(t)$, which, in this case, is

$$G_R^{</>}(t',t) = \frac{e^{\pm ik_F v(t'-t)}}{2\pi a} e^{\mp i\nu e \int_t^{t'} d\tau V_R(\tau)} \mathcal{P}_\nu(t'-t), \tag{4.28}$$

$$G_L^{</>}(t',t) = \frac{e^{\pm ik_F v(t'-t)}}{2\pi a} \mathcal{P}_\nu(t'-t), \tag{4.29}$$

$$\tag{4.30}$$

the contributions with k_F in Eq. (4.27) are exactly canceled by the derivative of the exponentials $e^{\pm ik_F v(t'-t)}$ and heat backscattering current becomes

$$\mathcal{J}_{BS}(t) = i|\lambda|^2 \int_0^{+\infty} d\tau \cos \left[\nu e \int_t^{t-\tau} dt'' V_R(t'') \right] \partial_\tau \left[\mathcal{P}_{2\nu}(\tau) - \mathcal{P}_{2\nu}(-\tau) \right]. \tag{4.31}$$

102

At this stage it is useful to recall the Fourier transform $\tilde{\mathcal{P}}_g(E) = \int_{-\infty}^{+\infty} d\tau e^{iE\tau}\mathcal{P}_g(\tau)$ at zero temperature, that reads [174, 175]

$$\tilde{\mathcal{P}}_g(E) = \frac{2\pi}{\Gamma(g)\omega_{\rm c}}\left|\frac{E}{\omega_{\rm c}}\right|^{g-1}\Theta(E). \tag{4.32}$$

Using Eq. (4.32) and averaging over one period of the voltage drive we get

$$\overline{\mathcal{J}_{BS}(t)} = |\lambda|^2\frac{\omega}{2}\sum_l |p_l|^2(q+l)\left\{\tilde{\mathcal{P}}_{2\nu}\left[(q+l)\omega\right] - \tilde{\mathcal{P}}_{2\nu}\left[-(q+l)\omega\right]\right\} \tag{4.33}$$

where the notation $\overline{\cdots}$ stands for $\int_0^{\mathcal{T}}\frac{dt}{\mathcal{T}}\langle\ldots\rangle$.

We now turn to the calculation of the noises defined in Eqs. (4.17) and (4.18). In particular, we focus exclusively on the auto-correlators of reservoir 3, namely $\mathcal{S}_{X,33}$ and $\mathcal{S}_{Q,33}$. For the sake of simplicity, we will use the shorthand notation $\mathcal{S}_X \equiv \mathcal{S}_{X,33}$ and $\mathcal{S}_Q \equiv \mathcal{S}_{Q,33}$.

Firstly, let us comment that in the perturbative expansions in Eqs. (4.19) and (4.20), the only surviving terms are $\mathcal{S}_X^{(11)}$ and $\mathcal{S}_Q^{(11)}$, since one can show that (see Appendix G)

$$\mathcal{S}_X^{(02)} = \mathcal{S}_X^{(20)} = 0, \tag{4.34}$$

$$\mathcal{S}_Q^{(02)} = \mathcal{S}_Q^{(20)} = 0. \tag{4.35}$$

Mixed and heat noises are obtained in terms of Green's functions as

$$\mathcal{S}_X = i\,|\Lambda|^2\int_0^{\mathcal{T}}\frac{dt}{\mathcal{T}}\int_{-\infty}^{+\infty}dt'\left[G_R^<(t',t)(\partial_t - ik_F v)G_L^<(t',t) - G_R^<(t',t)(\partial_t + ik_F v)G_L^<(t',t)\right], \tag{4.36}$$

$$\mathcal{S}_Q = |\Lambda|^2\int_0^{\mathcal{T}}\frac{dt}{\mathcal{T}}\int_{-\infty}^{+\infty}dt'\Big[G_R^<(t',t)(\partial_{t'} + ik_F v)(\partial_t - ik_F v)G_L^<(t',t)+$$
$$+ G_R^<(t',t)(\partial_{t'} - ik_F v)(\partial_t + ik_F v)G_L^<(t',t)\Big]. \tag{4.37}$$

Then, exploiting Eqs. (4.28) and (4.29), mixed and heat noises become

$$\mathcal{S}_X = 2\nu e|\lambda|^2\int_0^{\mathcal{T}}\frac{dt}{\mathcal{T}}\int_{-\infty}^{+\infty}dt'\sin\left[\nu e\int_{t'}^t dt''V(t'')\right]\mathcal{P}_\nu(t'-t)\partial_{t'}\mathcal{P}_\nu(t'-t), \tag{4.38}$$

$$\mathcal{S}_Q = 2|\lambda|^2\int_0^{\mathcal{T}}\frac{dt}{\mathcal{T}}\int_{-\infty}^{+\infty}dt'\cos\left[\nu e\int_{t'}^t dt''V(t'')\right]\mathcal{P}_\nu(t'-t)\partial_t\partial_{t'}\mathcal{P}_\nu(t'-t). \tag{4.39}$$

Using the series $e^{-i\varphi(t)} = \sum_l p_l e^{-il\omega t}$ and the Fourier transform for $\mathcal{P}_\nu(t'-t)$ one is left with

$$\mathcal{S}_X = \frac{\nu e\omega}{2}|\lambda|^2\sum_l |p_l|^2(q+l)\left\{\tilde{\mathcal{P}}_{2\nu}\left[(q+l)\omega\right] + \tilde{\mathcal{P}}_{2\nu}\left[-(q+l)\omega\right]\right\}, \tag{4.40}$$

$$\mathcal{S}_Q = \frac{|\lambda|^2}{2\pi}\sum_l |p_l|^2\int_{-\infty}^{+\infty}dE E^2\hat{P}_\nu(E)\left\{\tilde{\mathcal{P}}_\nu\left[(q+l)\omega - E\right] + \tilde{\mathcal{P}}_\nu\left[-(q+l)\omega - E\right]\right\}. \tag{4.41}$$

To perform the integral in the equation for $\mathcal{S}_Q$, we make use of the identity

$$\int_{-\infty}^{+\infty}\frac{dY}{2\pi}Y^2\tilde{\mathcal{P}}_{g_1}(Y)\tilde{\mathcal{P}}_{g_2}(X-Y) =$$
$$= \frac{\tilde{\mathcal{P}}_{g_1+g_2}(X)}{1+g_1+g_2}\left[g_1 g_2\pi^2\theta^2 + \frac{g_1(1+g_1)}{g_1+g_2}\omega^2\right]. \tag{4.42}$$

The latter leads to

$$\mathcal{S}_Q = |\lambda|^2 \sum_l |p_l|^2 \left[\frac{2\pi^2 \nu^2}{1 + 2\nu} \theta^2 + \frac{1 + \nu}{1 + 2\nu} (q + l)^2 \omega^2 \right] \times$$

$$\times \left\{ \tilde{\mathcal{P}}_{2\nu} \left[(q + l)\omega \right] + \tilde{\mathcal{P}}_{2\nu} \left[-(q + l)\omega \right] \right\}. \tag{4.43}$$

for the zero-frequency component of the noises. In particular, using the expression for $\mathcal{P}_g(E)$ at zero temperature one has

$$\tilde{\mathcal{P}}_g(E) = \frac{2\pi}{\Gamma(g)\omega_c} \left| \frac{E}{\omega_c} \right|^{g-1} \Theta(E), \tag{4.44}$$

with $\omega_c = v/a$ the high energy cutoff and $\Theta(E)$ the Heaviside step function. The noises then reduce to

$$\mathcal{S}_X = \nu e |\lambda|^2 \frac{\pi}{\Gamma(2\nu)} \left(\frac{\omega}{\omega_c} \right)^{2\nu} \sum_l |p_l|^2 |q + l|^{2\nu} \text{sign}(q + l), \tag{4.45}$$

$$\mathcal{S}_Q = \omega |\lambda|^2 \frac{\pi(1 + \nu)}{\Gamma(2\nu)(1 + 2\nu)} \left(\frac{\omega}{\omega_c} \right)^{2\nu} \sum_l |p_l|^2 |q + l|^{2\nu+1}. \tag{4.46}$$

Heat current at zero-temperature reads

$$\overline{\mathcal{J}_{BS}(t)} = |\lambda|^2 \frac{\pi}{\Gamma(2\nu)} \left(\frac{\omega}{\omega_c} \right)^{2\nu} \sum_l |p_l|^2 |q + l|^{2\nu}. \tag{4.47}$$

Equation (4.44) and subsequent Eqs. (4.40), (4.43) and (4.47) show the familiar power-law behavior of the Luttinger liquid [34, 176].

Constant bias limit

In the following, we present heat current, mixed and heat noises in the presence of a single constant bias, i.e. $V(t) = V_{dc}$, at zero temperature. Such a situation entails that photo-assisted Fourier coefficients reduce to $p_l = \delta_{l,0}$. In the dc case, a proportionality relation between charge backscattered current and noise in the weak backscattering limit, known as Schottky relation, has been introduced in Eq. (3.60). Interestingly, similar expressions can be derived relating mixed and heat noise to the heat current for a dc bias. From Eq. (4.33) and assuming $V_{dc} > 0$, one gets the following formula for the heat current

$$\mathcal{J}_{BS} = |\lambda|^2 \frac{\pi}{\Gamma(2\nu)} \left(\frac{e^* V_{dc}}{\omega_c} \right)^{2\nu}. \tag{4.48}$$

Similarly, mixed and heat noise are obtained from Eqs. (4.40) and (4.43) with the condition $p_l = \delta_{l,0}$. They read

$$\mathcal{S}_X = \nu e |\lambda|^2 \frac{\pi}{\Gamma(2\nu)} \left(\frac{e^* V_{dc}}{\omega_c} \right)^{2\nu}, \tag{4.49}$$

$$\mathcal{S}_Q = \nu e V_{dc} |\lambda|^2 \frac{\pi(1 + \nu)}{\Gamma(2\nu)(1 + 2\nu)} \left(\frac{e^* V_{dc}}{\omega_c} \right)^{2\nu}. \tag{4.50}$$

Comparing the last three results we immediately notice a proportionality between $\mathcal{S}_X$, $\mathcal{S}_Q$ and $\mathcal{J}_{BS}$, namely

$$\mathcal{S}_X = \nu e \mathcal{J}_{BS}, \tag{4.51}$$

$$\mathcal{S}_Q = \nu e \frac{1+\nu}{1+2\nu} V_{DC} \mathcal{J}_{BS}. \tag{4.52}$$

Equations (4.51) and (4.52) are generalizations of Schottky's formula to the heat and mixed noise. They show that the uncorrelated backscattering of Laughlin quasi-particles at the QPC leaves Poissonian signature in heat transport properties also. This holds both in a chiral Fermi liquid (i.e. at $\nu = 1$, when tunneling involves integer electrons only) and in the FQH regime, with proportionality constants governed by the filling factor ν. Similar relations for transport across a quantum dot were recently reported [168, 177].

4.3.2 Excess signals and noiseless drive

In general, the Schottky relation breaks down in the ac regime, since the oscillating drive excites particle-hole pairs contributing to transport. Nevertheless, when a single electron is extracted from the filled Fermi sea we expect the photon-assisted zero-frequency shot noise to match the lower bound set by Schottky's Poissonian dc relation, as already seen for charge excess-noise in Sec. 3.1.

We now address the central quantities of interest for the present Section. Equation (4.51), representing a proportionality between the mixed charge-heat correlator $\mathcal{S}_X$ and the heat current for a dc voltage drive governed by the charge νe, leads us to introduce the *excess mixed noise* given by

$$\Delta \mathcal{S}_X = \mathcal{S}_X - \nu e \overline{\mathcal{J}_{BS}(t)}. \tag{4.53}$$

As for $\Delta \mathcal{S}_C$, this quantity measures the difference between the noise in presence of a generic periodic voltage drive and the dc reference value. Using the results of Sec. 4.3.1 the excess mixed noise reads

$$\Delta \mathcal{S}_X = -\nu e |\lambda|^2 \frac{2\pi}{\Gamma(2\nu)} \left(\frac{\omega}{\omega_c} \right)^{2\nu} \sum_{l<-q} |p_l|^2 |q+l|^{2\nu}. \tag{4.54}$$

With a very similar procedure it is possible to extract the excess component of the zero-frequency heat noise due to the time dependent drive. Equation (4.52) states that $\mathcal{S}_Q$ is proportional to the heat current multiplied by the voltage bias in the dc limit. In view of this consideration we define the *excess heat noise*

$$\Delta \mathcal{S}_Q = \mathcal{S}_Q - 2e^* \frac{1+\nu}{1+2\nu} \overline{V(t)\mathcal{J}_{BS}(t)}. \tag{4.55}$$

The time-averaged value of $V(t)\mathcal{J}_{BS}(t)$ can be calculated from Eq. (4.31) using the relation $\nu e V(t) e^{-i\chi(t)} = (\omega q + i\partial_t) e^{-i\chi(t)}$. Then from the above definition we get

$$\Delta \mathcal{S}_Q = \omega |\lambda|^2 \frac{4\pi(1+\nu)}{\Gamma(2\nu)(1+2\nu)} \left(\frac{\omega}{\omega_c} \right)^{2\nu} \sum_{l<-q} |p_l|^2 |q+l|^{2\nu+1}. \tag{4.56}$$

Let us now look for the physics described by Eqs. (4.54) and (4.56). Once again, it is enlightening to start from the analogy with the charge shot noise. In the $\nu = 1$ quantum Hall state, described by a one-dimensional chiral Fermi liquid, the excess

charge noise $\Delta\mathcal{S}_C$ is proportional to the number of holes N_h induced in the Fermi sea by the voltage drive. One has

$$N_h(t) \propto \mathcal{S}_C - 2e\overline{\langle J_C(t)\rangle}, \tag{4.57}$$

where $n_{\mathrm{F}}(E) = \Theta(-E)$ is the Fermi distribution at zero temperature. Similarly, the number of quasi-holes in the FQH liquid reads

$$\mathcal{N} \propto \mathcal{S}_C - 2e^*\overline{\langle J_C(t)\rangle}. \tag{4.58}$$

It is worth noticing that Eqs. (4.57) and (4.58) hold in an unperturbed system without tunneling between opposite edges. The shot-noise induced by the presence of the QPC can thus be viewed as a probe for the number of holes (or quasi-holes in the case of a fractional filling) generated by the ac pulses.

We now consider the energy associated with hole-like excitations at $\nu = 1$, that reads

$$E_{qh} = -\int_{\infty}^{+\infty} \frac{d\epsilon}{2\pi} \frac{\omega_{\mathrm{c}}}{2\pi} f(\epsilon)\epsilon \left\langle \tilde{a}_R(\epsilon, t)\tilde{a}_R^\dagger(\epsilon, t)\right\rangle. \tag{4.59}$$

This quantity can be written as

$$\begin{aligned}
E_{qh} &= \frac{i}{2}\frac{v^2}{(2\pi a)^2}\int_{-\infty}^{+\infty} d\tau' \int_{-\infty}^{+\infty} d\tau\, e^{ie\int_{\tau'-\tau}^{\tau'} dt'V(t')}\partial_\tau \mathcal{P}_2(\tau)\\
&= \frac{1}{2}\frac{v^2}{(2\pi a)^2}\int_{-\infty}^{+\infty} d\tau' \int_{-\infty}^{+\infty} d\tau \left\{\sin\left[e\int_{\tau'-\tau}^{\tau'} dt'V(t')\right]\right.\\
&\quad \left. +i\cos\left[e\int_{\tau'-\tau}^{\tau'} dt'V(t')\right]\right\}\partial_\tau \mathcal{P}_2(\tau).
\end{aligned} \tag{4.60}$$

Then, comparing this result with Eqs. (4.38) and (4.31) we find that $\Delta\mathcal{S}_X$ measures the energy associated with the unwanted quasi-holes generated through the periodic voltage drive, namely

$$E_{qh} \propto -\mathcal{S}_X + 2e\overline{\mathcal{J}_{BS}(t)} = -\Delta\mathcal{S}_X. \tag{4.61}$$

This accounts for the negative value of $\Delta\mathcal{S}_X$ arising from Eq. (4.54).In analogy with what we have done in Sec. 3.3, one can generalize this relation to the fractional regime

$$E_{qh} \propto -\mathcal{S}_X + 2\nu e\overline{\mathcal{J}_{BS}(t)} = -\Delta\mathcal{S}_X. \tag{4.62}$$

The vanishing of $\Delta\mathcal{S}_X$ should highlight an energetically clean pulse, for which the mixed noise reaches the minimal value $\mathcal{S}_X = 2\nu e\overline{\langle J_Q(t)\rangle}$ expected from Schottky's formula for the mixed noise Eq. (4.51). A similar relation involving the sum of the squared energy for each value of k holds for $\Delta\mathcal{S}_Q$ at $\nu = 1$

$$\int_{-\infty}^{+\infty} \frac{d\epsilon}{2\pi} \frac{\omega_{\mathrm{c}}}{2\pi} f(\epsilon)\epsilon^2 \left\langle \tilde{a}_R(\epsilon, t)\tilde{a}_R^\dagger(\epsilon, t)\right\rangle \propto \Delta\mathcal{S}_Q. \tag{4.63}$$

In Fig. 4.1 we show the behavior of the excess mixed noise as a function of the charge q injected during one period T. Notice that we normalize $\Delta\mathcal{S}_X$ by a negative quantity, in order to deal with a positive function. Two types of bias are considered: a sinusoidal drive and a train of Lorentzian pulses given respectively by

$$V_{sin}(t) = V_{dc}[1 - \cos(\omega t)], \tag{4.64}$$

$$V_{lor}(t) = \frac{V_{dc}}{\pi}\sum_k \frac{\eta}{\eta^2 + (t/T - k)^2}, \tag{4.65}$$
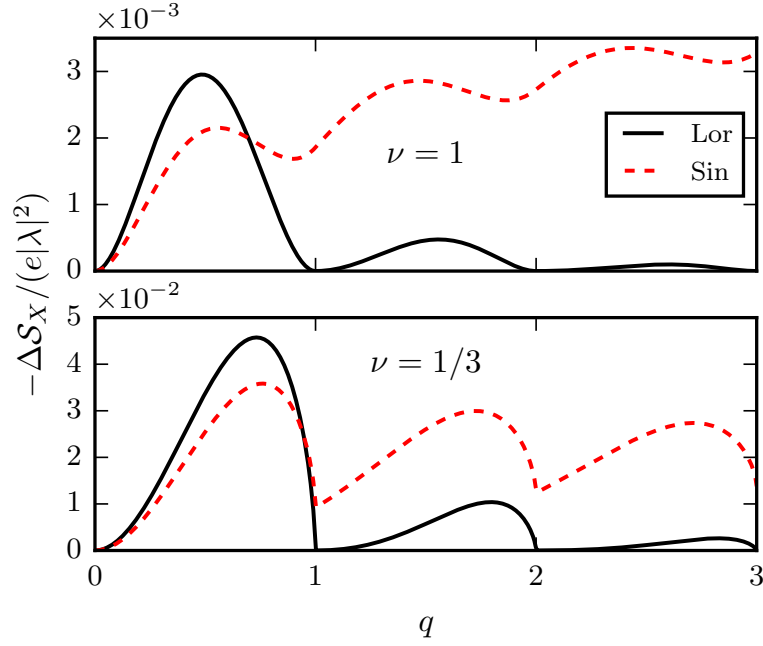
106

Figure 4.1: Excess mixed noise $-\Delta\mathcal{S}_X$ as a function of the charge per period q at zero temperature. The high energy cutoff is set to $\omega_c = 10\,\omega$. Behavior for Lorentzian pulses (full black line) and sinusoidal voltage drive (dashed red line) is reported.

with $\eta = W/T$ the ratio between the half width W at half maximum of the Lorentzian peak and the period T. The former is representative of all kinds of non-optimal voltage drive, while the latter is known to give rise to minimal charge noise both at integer [23] and fractional [115] fillings. We will set $\eta = 0.1$, a value lying in the range investigated by experiments [14]. At $\nu = 1$, both curves display local minima whenever q assumes integer values. However, while the sinusoidal drive always generates an additional noise with respect to the reference Schottky value $\nu e \overline{\mathcal{J}_{BS}}$, the Lorentzian signal drops to zero for $q \in \mathbb{N}$, indicating that the mixed noise $\mathcal{S}_X$ due to levitons exactly matches the Poissonian value set by Eq. (4.51). Since the excess mixed noise is linked to the unwanted energy introduced into the system as a result of hole injection [see Eq. (4.61)], Fig. 4.1 shows that there is no hole-like excitation carrying energy in our system. The bottom panel of Fig. 4.1 shows the same situation in a $\nu = 1/3$ FQH bar. The hierarchy of the $\nu = 1$ configuration is confirmed, with Lorentzian pulses generating minimal mixed noise for $q \in \mathbb{N}$ and sinusoidal voltage displaying non-optimal characteristics with non-zero $\Delta\mathcal{S}_X$. As for the charge excess noise no signature for fractional values of q arises, signaling once again the robustness of levitons in interacting fractional systems. This is markedly different from driven-quantum-dot systems, where a strategy to inject a periodic train of fractionally charged quasi-particles in the FQH regime has been recently discussed [92].

The same analysis can be carried out for the excess heat noise $\Delta\mathcal{S}_Q$. Equation (4.56) suggests that the excess heat noise vanishes for the very same conditions that determine the vanishing of $\Delta\mathcal{S}_C$ and $\Delta\mathcal{S}_X$, given that we get a similar structure with only a different power law behavior. This expectation is confirmed in Fig. 4.2, where we report the behavior of $\Delta\mathcal{S}_Q$ for both $\nu = 1$ and $\nu = 1/3$. Lorentzian pulses car-
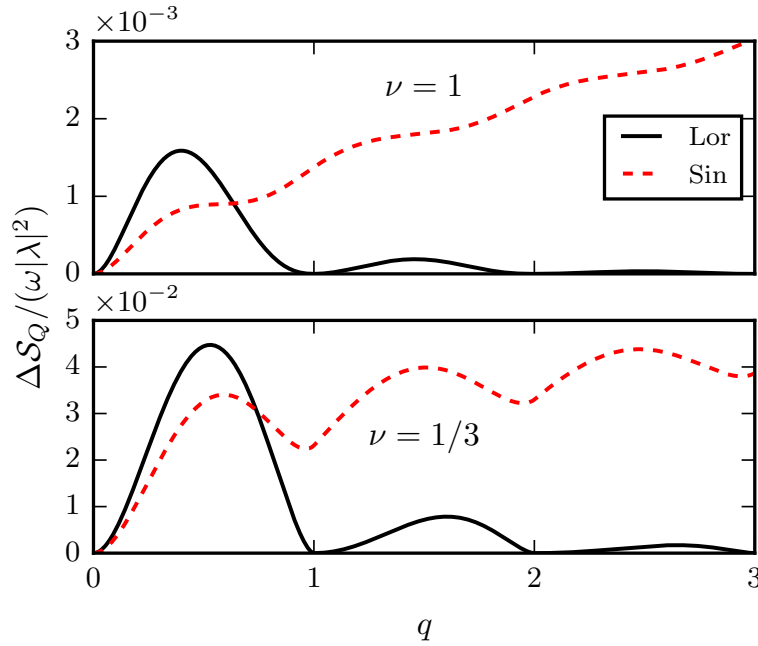
Figure 4.2: Excess heat noise $\Delta\mathcal{S}_Q$ as a function of the charge per period q. Full black and dashed red lines represent Lorentzian and sinusoidal drives respectively. The temperature is $\theta = 0$ and the cutoff is $\omega_{\mathrm{c}} = 10\,\omega$.

rying integer charge per period represent minimal-heat-noise states, independently of the filling factor.

4.3.3   Multiple Lorentzian pulses

In the previous section we demonstrated that quantized Lorentzian pulses with integer charge q represent minimal excitation states for the heat transport in the FQH regime, but this statement may potentially fail when different Lorentzian pulses have a substantial overlap. Indeed, nonlinear quantities such as $\mathcal{J}_{2/3}$, $\mathcal{S}_X$ and $\mathcal{S}_Q$ may behave very differently from charge current and noise, which are linear functions of the bias $V(t)$ in a Fermi liquid. For instance, at $\nu = 1$ one already sees a fundamental difference between average charge and heat currents in their response to the external drive, as $J_{2/3}$ is independent of V_{ac}, while $\mathcal{J}_{2/3}$ goes like $V(t)^2 = V_{\mathrm{dc}}^2 + \overline{V_{\mathrm{ac}}^2(t)}$. Then, one might wonder whether the independence of overlapping levitons survives when we look at such nonlinearity. In this regard Battista *et al.* pointed out that in Fermi liquid systems N levitons emitted in the same pulse are not truly independent excitations, since heat current and noise associated with such a drive are proportional to N^2 times the single-particle heat current and N^3 times the single-particle heat noise respectively. Nevertheless, well-separated levitons always give rise to really independent excitations with $\mathcal{J}_{2/3}$ and $\mathcal{S}_Q$ both equal to N times their corresponding single-particle signal, due to the vanishing of their overlap [171]. Moreover, an additional source of nonlinearity is provided by electron-electron interactions giving rise to the FQH phase, whose power-law behavior is governed by fractional exponents, thus strongly deviating from the linear regime.

In the following we study how nonlinearities due to heat transport properties and interactions affect the excess signals we introduced in Sec. 4.3.2. For this purpose,
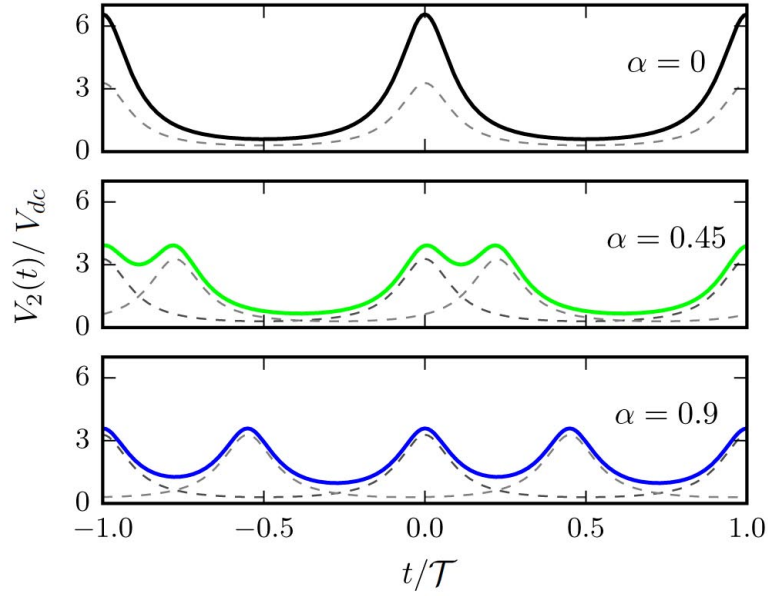
Figure 4.3: Time-periodic voltage drive given by Eq. (4.66) in the case of $N = 2$ Lorentzian-shaped pulses per period at total charge $q = 1$ (i.e. $1/2$ for each pulse). The top panel represents two completely overlapping pulses ($\alpha = 0$), for which we simply have $V_2(t) = 2\widetilde{V}(t)$. The central and bottom panels correspond to nontrivial cases $\alpha = 0.45$ and $\alpha = 0.9$ with finite overlap between pulses. In all cases the behavior of individual Lorentzian pulses $\widetilde{V}(t)$ and $\widetilde{V}\left(t - \frac{\alpha}{N}\mathcal{T}\right)$ are depicted with dashed, thin lines.

we consider a periodic signal made of a cluster of N pulses described by

$$V_N(t) = \sum_{j=0}^{N-1} \widetilde{V}\left(t - j\frac{\alpha}{N}\mathcal{T}\right), \tag{4.66}$$

where $\widetilde{V}(t)$ is periodic of period $\mathcal{T}$. We still consider the parameter q as the total charge injected during one complete period $\mathcal{T}$ of the drive $V_N(t)$, which means that each pulse in the cluster carries a fraction q/N of the total charge. Inside a single cluster, the N signals in Eq. (4.66) are equally spaced with a fixed time delay $\Delta t = \alpha\mathcal{T}/N$ between successive pulses. Note that $\alpha = 0$ corresponds to several superimposed pulses, giving $V_N(t)|_{\alpha=0} = N\widetilde{V}(t)$. Also, for $\alpha = 1$ we just get a new periodic signal with period $\mathcal{T}/N$. We thus restrict the parameter α to the interval $0 \leq \alpha < 1$. An example of such a voltage drive is provided in Fig. 4.3.

Fourier coefficients for a periodic multi-pulse cluster can be factorized in a convenient way (see Appendix C). Here we take as an example the simple case $N = 2$, whose coefficients are given by

$$p_l^{(2)}(q) = \sum_{m=-\infty}^{+\infty} e^{i\pi\alpha m} p_{l-m}\left(\frac{q}{2}\right) p_m\left(\frac{q}{2}\right). \tag{4.67}$$

Each pulse carries one half of the total charge q, a fact that is clearly reflected in the structure of Eq. (4.67).

Let us first focus on an integer quantum Hall effect with $\nu = 1$. It is easy to see that, at least in the DC regime, $\mathcal{S}_X$ and $\mathcal{S}_Q$ scale as V^2 and V^3 respectively. It is
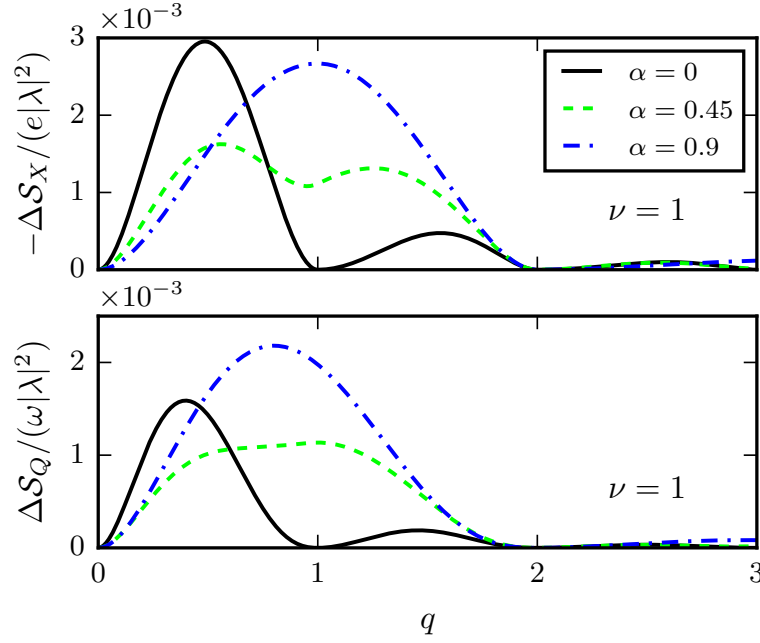
109

Figure 4.4: Excess signals $-\Delta\mathcal{S}_X$ (top panel) and $\Delta\mathcal{S}_Q$ (bottom panel) as a function of q for a cluster of two identical Lorentzian pulses separated by a time delay $\alpha\mathcal{T}/2$. All curves refer to the case of $\nu = 1$ and zero temperature. The cutoff is set to $\omega_c = 10\,\omega$.

then natural to wonder if a cluster of Lorentzian pulses still gives rise to minimal values of $\mathcal{S}_X$ and $\mathcal{S}_Q$ when the interplay of nonlinearities, AC effects and overlapping comes into play. We thus look for the excess mixed and heat noises for the case of $N = 2$ Lorentzian pulses per period, in order to shed light on this problem. The top and bottom panels of Fig. 4.4 show the excess mixed and heat noises respectively in presence of two pulses per period at $\nu = 1$. For $\alpha = 0$ we get a perfect superposition between pulses, and we are left with a single Lorentzian carrying the total charge q. This case displays zeros whenever the total charge reaches an integer value, as was already discussed in the previous Section. Higher values of α represent non-trivial behavior corresponding to different, time-resolved Lorentzian pulses. A Lorentzian voltage source injecting $q = 1/2$ electrons per period is not an optimal drive (and so is, a fortiori, an arbitrary superposition of such pulses). As a result, signals for $\alpha = 0.45$ and $\alpha = 0.9$ turn out to be greater than zero at $q = 1$. However $\Delta\mathcal{S}_X$ and $\Delta\mathcal{S}_Q$ still vanish at $q = 2$, where they correspond to a pair of integer levitons, showing the typical behavior of minimal excitation states with no excess noise. This demonstrates that integer levitons, *although overlapping*, always generate the Poissonian value for heat and mixed noises expected from their respective Schottky formulas. It is worth noticing that the blue curves in Fig. 4.4 (nearly approaching the limit $\alpha \to 1$) almost totally forget the local minimum in $q = 1$ and get close to a simple rescaling of the single-pulse excess noises $\Delta\mathcal{S}_X\left(\frac{q}{2}\right)$ and $\Delta\mathcal{S}_Q\left(\frac{q}{2}\right)$. This is because $\alpha \to 1$ is a trivial configuration corresponding to one pulse per period with $\mathcal{T}' = \frac{\mathcal{T}}{2}$, as was mentioned before.

It is even more remarkable, however, to still observe a similar qualitative behavior in the FQH regime, where one may expect this phenomenon to break down as a
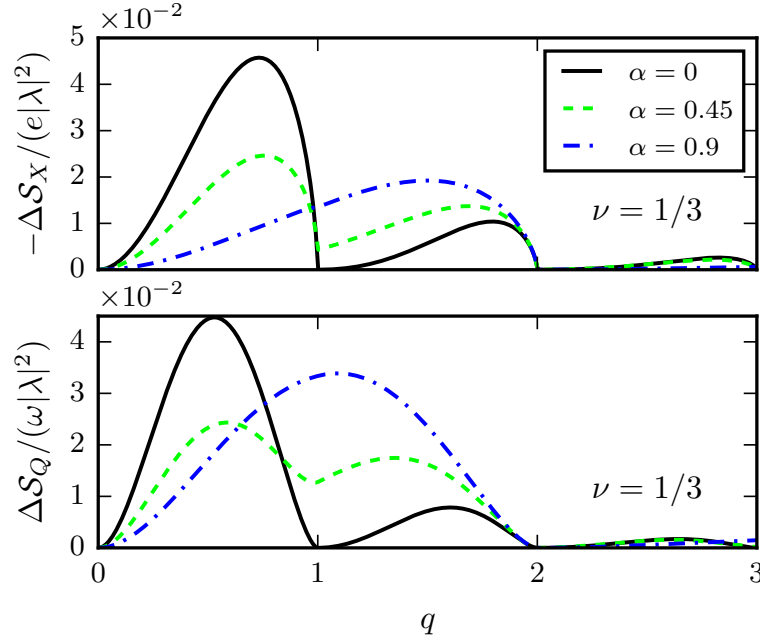
Figure 4.5: Excess signals $-\Delta \mathcal{S}_X$ and $\Delta \mathcal{S}_Q$ as a function of q for two identical Lorentzian pulses with time delay $\alpha \mathcal{T}/2$ at fractional filling $\nu = 1/3$ and zero temperature. The cutoff is set to $\omega_c = 10\,\omega$.

result of the strong nonlinearities due to the chiral Luttinger liquid physics. Figure 4.5 shows that both signals drop to zero for $q = 2$, representing a robust evidence for a minimal excitation state even in a strongly-interacting fractional liquid. We stress that such a strong stability of heat transport properties is an interesting and unexpected result both at integer and fractional filling factor. Indeed, the bare signals $\overline{\langle J_Q \rangle}$, $\mathcal{S}_X$ and $\mathcal{S}_Q$ are affected by the parameters governing the overlap between pulses, namely

$$\overline{\mathcal{J}_{BS}}^{(N)} \neq N \overline{\mathcal{J}_{BS}}^{(1)}, \tag{4.68a}$$

$$\mathcal{S}_X^{(N)} \neq N \mathcal{S}_X^{(1)}, \tag{4.68b}$$

$$\mathcal{S}_Q^{(N)} \neq N \mathcal{S}_Q^{(1)}, \tag{4.68c}$$

even at $q = N$, in accordance with Ref. [171]. Nonetheless, such differences are washed out when the DC Schottky-like signals are subtracted from $\mathcal{S}_X$ and $\mathcal{S}_Q$ in Eqs. (4.53) and (4.55), giving

$$\Delta \mathcal{S}_X^{(N)} = \Delta \mathcal{S}_X^{(1)} = 0, \tag{4.69}$$

$$\Delta \mathcal{S}_Q^{(N)} = \Delta \mathcal{S}_Q^{(1)} = 0. \tag{4.70}$$

While multiple levitons are not independent [in the sense of Eqs. (4.68)], they do represent minimal excitation states even in presence of a finite overlap between Lorentzian pulses. This is a remarkable property which seems to distinguish the Lorentzian drive from every other type of voltage bias.

Let us note that the robustness with respect to the overlap of Lorentzian pulses is an interesting result for the charge transport at fractional filling as well. Indeed $\overline{J_{BS}}$ and $\mathcal{S}_C$ do not show a trivial rescaling at $\nu \neq 1$. Nevertheless, we have checked
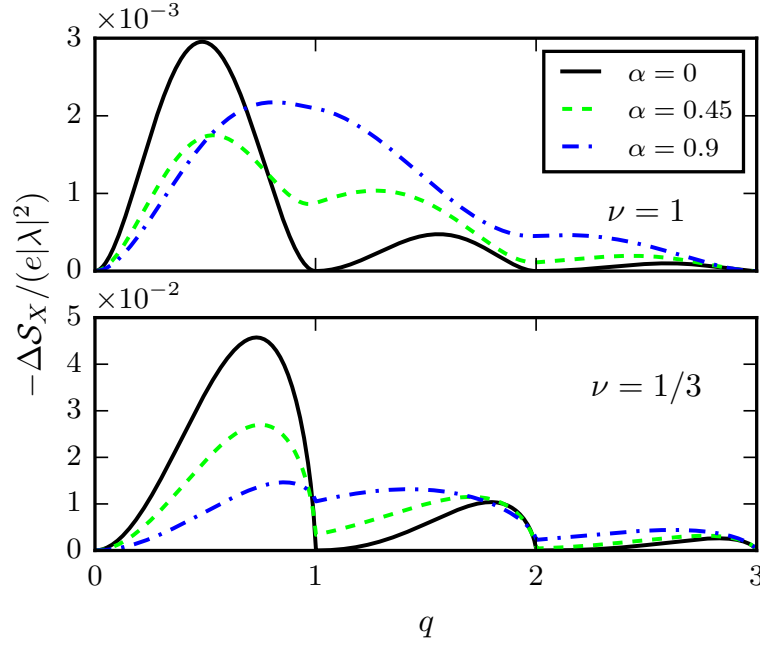
Figure 4.6: Excess mixed noise $-\Delta \mathcal{S}_X$ as a function of q for a cluster of two Lorentzian pulses. Here q is partitioned asymmetrically, with the two pulses carrying respectively $1/3$ and $2/3$ of the total charge per period. One should compare this figure with Figs. 4.4 and 4.5, where $-\Delta \mathcal{S}_X$ for identical pulses is plotted. The time delay between pulses is $\alpha \mathcal{T}/2$, with different values of α according to the legend. The cutoff is set to $\omega_c = 10\,\omega$ and the temperature is $\theta = 0$.

that the excess charge noise $\Delta \mathcal{S}_C$ is insensitive to different overlap between levitons as it vanishes when exactly one electron is transported under each pulse, i.e. when $q = N$. Note that a very similar behavior was described for the excess charge noise in Ref. [86], where multiple pulses were generated as a result of fractionalization due to inter-channel interactions in the integer quantum Hall regime at $\nu = 2$.

To provide a further proof for our results, we analyze a two-pulse configuration with an asymmetrical charge distribution, namely a case in which the first pulse carries $1/3$ of the total charge q while the second pulse takes care of the remainder. It is straightforward to verify that the voltage phase associated with such a drive is represented by a Fourier series with coefficients

$$p_l^{(2)}(q) = \sum_{m=-\infty}^{+\infty} e^{i\pi\alpha m} p_{l-m}\left(\frac{q}{3}\right) p_m\left(\frac{2q}{3}\right), \qquad (4.71)$$

where the asymmetry in the charge distribution is manifest, as opposed to the symmetric case in Eq. (4.67). In view of previous considerations, we expect this signal to be an optimal voltage drive when both pulses carry an integer amount of charge. This condition is obviously fulfilled when $q = 3$, so that the total charge can be divided into one and two electrons associated with the first and second pulse respectively. Figure 4.6 confirms our prediction, showing the first universal vanishing point shared by all three curves at $q = 3$ instead of $q = 2$.

In passing, it is worth remarking that the choice of multiple Lorentzian pulses with identical shape was only carried out for the sake of simplicity. A generalization

to more complicated clusters with different width W gives rise to a very similar qualitative behavior (not shown).

4.4 Heat interferometry with single-electron in fractional edge states

The main purpose of EQO is to reproduce conventional optics interferometric experiments using electronic wave-packets propagating in condensed matter systems instead of photons traveling along waveguides. While this issue has been widely investigated in relation to charge transport, in condensed matter systems one can figure out interferometric experiments even in the heat transport domain. Here, we address the problem of the heat noise generated by levitons injected in a HOM interferometer in the FQH effect. We consider a four terminal quantum Hall bar in the Laughlin sequence, where a single channel arises on each edge, as presented in Fig. 4.7. Since, we are interested in the effect of the overlap between right-moving and left-moving states at the QPC on heat noise, our focus is put on the cross-correlation noise between reservoirs 2 and 3, namely $\mathcal{S}_{Q,23}$. In this section, we derive its expressions exploiting the model introduced in Chapter 3, focusing on the regions downstream of the voltage contacts, namely $-d < x < d$.

The perturbative expansion of heat current operator in Eq. (4.5) allows to express heat correlation noise at lowest order as

$$\mathcal{S}_{Q,23} = \mathcal{S}_{Q,23}^{(02)} + \mathcal{S}_{Q,23}^{(20)} + \mathcal{S}_{Q,23}^{(11)} + \mathcal{O}\left(|\Lambda|^2\right), \tag{4.72}$$

where

$$\mathcal{S}_{Q,23}^{(ij)} = \int_0^{\mathcal{T}} \frac{dt}{\mathcal{T}} \int dt' \left\{ \langle \mathcal{J}_2^{(i)}(t') \mathcal{J}_3^{(j)}(t) \rangle - \langle \mathcal{J}_2^{(i)}(t') \rangle \langle \mathcal{J}_3^{(j)}(t) \rangle \right\}. \tag{4.73}$$

Now, we can perform standard calculations, whose details are given in Appendix G, in order to evaluate all the terms appearing in Eq. (4.72). In this way, the total heat noise in the double-drive configuration can be obtained. Interestingly, double-drive heat noise is not equivalent to the one generated in a single-drive configuration with an effective drive $V_-(t) = V_R(t) - V_L(t)$, contrarily to charge noise (see Eq. (3.45)). Indeed, one finds that

$$\mathcal{S}_{Q,23}(V_R, V_L) = \mathcal{S}_{Q,23}(V_-, 0) + \Delta\mathcal{S}_{Q,23}(V_R, V_L), \tag{4.74}$$

where

$$\mathcal{S}_{Q,23}(V_-, 0) = |\lambda|^2 \int_0^{\mathcal{T}} \frac{dt}{\mathcal{T}} \int dt' \Big\{ \cos\left(\nu e \int_t^{t'} d\tau V_-(\tau)\right) \Re\left[\mathcal{P}_\nu(t'-t)\partial_t^2 \mathcal{P}_\nu(t'-t)\right] +$$
$$+ \frac{\nu e \upsilon}{\pi} \int dt'' V_-(t') \mathcal{K}\left(t', t, t''\right) \sin\left(\nu e \int_t^{t'} d\tau V_-(\tau)\right) \Im\left[\partial_{t''} \mathcal{P}_{2\nu}(t''-t)\right] \Big\}, \tag{4.75}$$

$$\Delta\mathcal{S}_{Q,23}(V_R, V_L) = \nu^2 e^2 |\lambda|^2 \int_0^{\mathcal{T}} \frac{dt}{\mathcal{T}} \int dt' \gamma_{RL} \cos\left(\nu e \int_t^{t'} d\tau V_-(\tau)\right) \times$$
$$\times \left(\alpha_{RL}(t, t') \Re\left[\mathcal{P}_{2\nu}(t'-t)\right] + \beta_{RL}(t, t') \Im\left[\mathcal{P}_{2\nu}(t'-t)\right]\right), \tag{4.76}$$
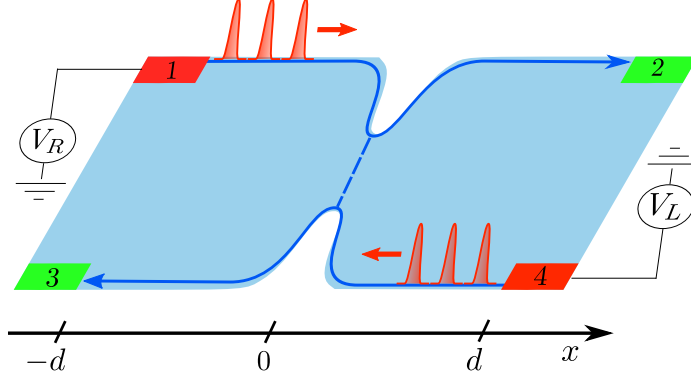
Figure 4.7: Four-terminal setup for Hong-Ou-Mandel interferometry in the FQH regime. Contact 1 and 4 are used as input terminals, while contact 2 and 3 are the output terminals where current and noise are measured.

where we defined the following functions

$$\mathcal{K}(t_1, t_2, t_3) = \frac{\pi\theta}{v}\left(\coth\left(\pi\theta(t_1 - t_3)\right) - \coth\left(\pi\theta(t_1 - t_2)\right)\right) =$$

$$= \frac{\pi\theta}{v}\frac{\sinh\left(\pi\theta(t_2 - t_3)\right)}{\sinh\left(\pi\theta(t_1 - t_3)\right)\sinh\left(\pi\theta(t_1 - t_2)\right)}, \tag{4.77}$$

$$\alpha_{RL}(t, t') = \left(V_R(t)V_L(t') - V_L(t)V_R(t')\right), \tag{4.78}$$

$$\beta_{RL}(t, t') = \frac{v}{\pi}\int dt'' \mathcal{K}(t'', t, t')V_R(t'')\left[V_L(t') - V_L(t)\right]. \tag{4.79}$$

The result of Eq. (4.74) arises because heat noise is sensitive to the energy distribution of the injected particles, thus leading to different outcomes in single-drive and double-drive configurations. In this light, we expect this to hold true for general energy-dependent phenomena occurring at the QPC. For instance, any similarity between charge noises generated in the two setups discussed previously would disappear for more complicated tunneling geometry, such as multiple QPC or extended contacts, where transmission functions become energy-dependent [57, 58, 119, 178]. Eq. (4.74) further indicates that the double-drive and the single-drive configurations are completely distinct setups and that the relation in Eq. (3.45) is solely a contingent effect of the single local QPC geometry.

It is useful to express heat correlation noise in energy space, by introducing the following Fourier series

$$\nu e V_{R/L}(t) = \sum_k c_{k,R/L}e^{ik\omega t}, \tag{4.80}$$

$$e^{i\nu e \int_0^t d\tau V_-(\tau)} = \sum_l \tilde{p}_l e^{-i(l + q_R - q_L)\omega t}, \tag{4.81}$$

where we recall that

$$q_{R/L} = -\frac{e}{2\pi}\int_0^{\mathcal{T}} dt\, V_{R/L}(t) = -\frac{\nu e V_{R/L,dc}}{\omega} \tag{4.82}$$

is the number of particles excited by $V_{R/L}$ along the system in a period and the Fourier transform of $\mathcal{P}_g(t)$ in Eq. (3.30)

$$\tilde{\mathcal{P}}_g(E) = \int_{-\infty}^{+\infty} dt \mathcal{P}_g(t)e^{iEt}. \tag{4.83}$$

114

By exploiting these results, the two contributions to $\mathcal{S}_{Q,23}$ become

$$\mathcal{S}_{Q,23}(V_-,0) = -|\lambda|^2 \sum_l \left\{ \frac{2\nu^2\pi^2\theta^2 + (1+\nu)\left((l+q_R-q_L)\omega\right)^2}{1+2\nu} |\tilde{p}_l|^2 \, \tilde{\mathcal{P}}_{2\nu}((l+q_R-q_L)\omega) + \right.$$

$$-\frac{1}{4}\sum_{k\neq0}(c_{k,R}-c_{k,L})(\tilde{p}_{l-k}\tilde{p}_l^* - \tilde{p}_l\tilde{p}_{l+k}^*)(l+q_R-q_L)\omega\coth\frac{k\omega}{2\theta}\times$$

$$\left. \times \left(\tilde{\mathcal{P}}_{2\nu}((l+q_R-q_L)\omega) - \tilde{\mathcal{P}}_{2\nu}(-(l+q_R-q_L)\omega)\right)\right\}, \tag{4.84}$$

$$\Delta\mathcal{S}_{Q,23}(V_R,V_L) = \frac{|\lambda|^2}{2}\sum_{k,p,l}(c_{k,R}c_{p,L}-c_{k,L}c_{p,R})\,\tilde{p}_{l+k+p}\tilde{p}_l^*\frac{\mathcal{W}_{(l+q_R-q_L),k,p} + \mathcal{W}_{(l+q_R-q_L),p,k}}{2}, \tag{4.85}$$

where the coefficients $\mathcal{W}_{l,k,p}$ encodes all the effects due to temperature and interaction on $\mathcal{S}_Q^{(+-)}$ and reads

$$\mathcal{W}_{l,k,p} = \frac{\omega_c}{4\pi}\int_{-\infty}^{+\infty}\frac{dE}{2\pi}\left\{\tilde{\mathcal{P}}_1(E)\tilde{\mathcal{P}}_1(k\omega-E)\Big[\tilde{\mathcal{P}}_{2\nu-1}(E-l\omega) + \right.$$

$$\left. + \tilde{\mathcal{P}}_{2\nu-1}(-E-(l+k+p)\omega) + \tilde{\mathcal{P}}_{2\nu-1}(-E+l\omega)\Big] + \tilde{\mathcal{P}}_{2\nu-1}(E+(l+k+p)\omega)\right\} +$$

$$-\frac{1}{2}\left(\tilde{\mathcal{P}}_{2\nu}((l+k)\omega) + \tilde{\mathcal{P}}_{2\nu}(-(l+k))\right). \tag{4.86}$$

Let us observe that the contribution $\Delta\mathcal{S}_Q$ exists only in the double-drive configurations. Indeed, in the configuration with a single drive, where $V_L = 0$, one obtains that $c_{k,L} = 0$ for each k, and the contribution in Eq. (4.85) vanishes.

4.4.1 Hong-Ou-Mandel noise

Among all the possible choice for the configuration involving the two voltages V_R and V_L, one of the most interesting, even from the experimental point of view, is the Hong-Ou-Mandel (HOM) setup, where two identical voltage drives are applied to reservoirs 1 and 4 and delayed by a constant time t_D. This experimental configuration corresponds to set $V_R(t) = V(t)$ and $V_L(t) = V(t+t_D)$, with $V(t)$ a generic periodic drive. In this situation the charge excited by each drive along the edge channels are equal, such that $q_R = q_L = q$.

For notational convenience, we define the single-drive and the HOM heat noises as

$$\mathcal{S}_Q^{sd} = \mathcal{S}_{Q,23}(V_-(t),0), \tag{4.87}$$

$$\mathcal{S}_Q^{HOM} = \mathcal{S}_{Q,23}(V(t),V(t+t_D)). \tag{4.88}$$

According to Eq. (4.74) and using the above definitions, the HOM heat noise can be expressed as

$$\mathcal{S}_Q^{HOM} = \mathcal{S}_Q^{sd} + \Delta\mathcal{S}_{Q,23}. \tag{4.89}$$

Before entering into the details of our discussion, we would like to prove analytically that the HOM heat noise $\mathcal{S}_Q^{HOM}$ reduces to its equilibrium value for null time delay t_D, independently of the choice of any parameter. The photo-assisted amplitude in Eq. (4.81) reduces to $\tilde{p}_l = \delta_{l,0}$ and the Fourier coefficients $c_{k,-}$ vanish for all k. Let us start by looking at the HBT contribution. By substituting this analytical simplification in Eq. (4.84), we obtain

$$\mathcal{S}_Q^{sd}(t_D = 0) = -|\lambda|^2\frac{\nu^2\pi^2\theta^2}{1+2\nu} \equiv \mathcal{S}_Q^{vac}, \tag{4.90}$$

115

which is independent of the injected particles and correspond simply to the equilibrium noise $\mathcal{S}_Q^{vac}$ due to thermal fluctuations. This can be clearly understood given the fact that $V_-(t) = 0$ for $t_D = 0$ and the HBT contribution corresponds to the noise generated in a driveless configuration.

Concerning the remaining part in Eq. (4.89), one has for $t_D = 0$

$$\Delta\mathcal{S}_{Q,23} = \frac{|\lambda|^2}{4} \sum_k c_{k,R} c_{-k,R} \left(\mathcal{W}_{0,k,-k} + \mathcal{W}_{0,-k,k} \right), \qquad (4.91)$$

where

$$\mathcal{W}_{0,k,-k} = \frac{\tilde{\mathcal{P}}_{2\nu}(k\omega) - \tilde{\mathcal{P}}_{2\nu}(-k\omega)}{2}. \qquad (4.92)$$

From Eq. (4.92), we can clearly deduce that $\mathcal{W}_{0,k,-k} = -\mathcal{W}_{0,-k,k}$, which enforces the vanishing of $\Delta\mathcal{S}_Q$ in Eq. (4.91). This is enough to prove that HOM heat noise always reaches its equilibrium value at $t_D = 0$, such that

$$\mathcal{S}_Q^{HOM}(t_D = 0) = \mathcal{S}_Q^{sd}(t_D = 0) = \mathcal{S}_Q^{vac}. \qquad (4.93)$$

Let us note that this is not a trivial result since $\mathcal{S}_Q^{HOM}$ does not depend effectively on the single drive V_- as $\mathcal{S}_Q^{sd}$, but on both V_R and V_L and even at $t_D = 0$ the system is still driven by these two voltages.

4.4.2 Results and discussions

In this section, we discuss the results concerning the heat correlation noises in the HOM interferometer. In particular, we focus our discussion on the specific case of levitons. The Fourier coefficients for this specific drive are given in Appendix C.

In the HOM setup, a state composed by $q_L = q_R = q$ levitons [125] is injected by each driven contact and collide at the QPC, separated by a controllable time delay. In analogy with the previous literature on charge noise, we introduce the following ratio [30, 100, 108, 115]

$$\mathcal{R}_Q^{HOM} = \frac{\mathcal{S}_Q^{HOM} - \mathcal{S}_Q^{vac}}{2\mathcal{S}_Q^R - 2\mathcal{S}_Q^{vac}}, \qquad (4.94)$$

where we subtracted the equilibrium noise $\mathcal{S}_Q^{vac}$ and we normalize with respect to $\mathcal{S}_Q^R \equiv \mathcal{S}_Q(V_R, 0)$, which is the noise expected for the random partitioning of a single source of levitons, i.e. when $V_R(t) = V_{lor}(t)$ and $V_L(t) = 0$. The latter reads

$$\mathcal{S}_Q^R = -|\lambda|^2 \sum_l \left\{ \frac{2\nu^2\pi^2\theta^2 + (1+\nu)(l\omega)^2}{1 + 2\nu} |p_l|^2 \tilde{\mathcal{P}}_{2\nu}((l+q)\omega) + \right.$$
$$\left. - \sum_{k\neq 0} c_k \left(p_{l-k}p_l^* - p_l p_{l+k}^* \right)(l+q)\omega \frac{\tilde{\mathcal{P}}_2(k\omega)}{2k\omega} \left(\tilde{\mathcal{P}}_{2\nu}((l+q)\omega) - \tilde{\mathcal{P}}_{2\nu}(-(l+q)\omega) \right) \right\}, \qquad (4.95)$$

where $c_k = \nu e \int_0^{\mathcal{T}} \frac{dt}{\mathcal{T}} V_{lor}(t) e^{ik\omega t}$ are the Fourier coefficients for a single Lorentzian voltage and $p_l = \int_0^{\mathcal{T}} \frac{dt}{\mathcal{T}} e^{-i\nu e \int_0^t d\tau V_{lor}(\tau)} e^{i(l+q)\omega t}$ (see Appendix C).

In addition, we define an analogous ratio for the single-drive heat noise as

$$\mathcal{R}_Q^{sd} = \frac{\mathcal{S}_Q^{sd} - \mathcal{S}_Q^{vac}}{2\mathcal{S}_Q^R - 2\mathcal{S}_Q^{vac}}, \qquad (4.96)$$

in order to asses its relative contribution to the overall HOM heat noise.

Let us notice that, according to Eqs (4.90) and (4.93) both ratios, $\mathcal{R}_Q^{HOM}$ and $\mathcal{R}_Q^{sd}$ vanishes for $t_D = 0$. In the specific case of levitons, which are single-electron excitations, at $\nu = 1$ the physical explanation for the total dip at $t_D = 0$ involves the anti-bunching effect of identical fermions: electron-like excitations colliding at the QPC at the same time are forced to escape on opposite channels, thus leading to a total suppression of fluctuations at $t_D = 0$ and generating the so called Pauli dip [14, 15, 106]. For fractional filling factors, it is remarkable that this total dip is still present despite the presence of anyonic quasi-particle in the system, which do not obey Fermi-Pauli statistics [56, 115]. Anyway, this single QPC geometry does not allow for the braiding of one quasi-particle around the other, thus excluding any possible effect due to fractional statistics.

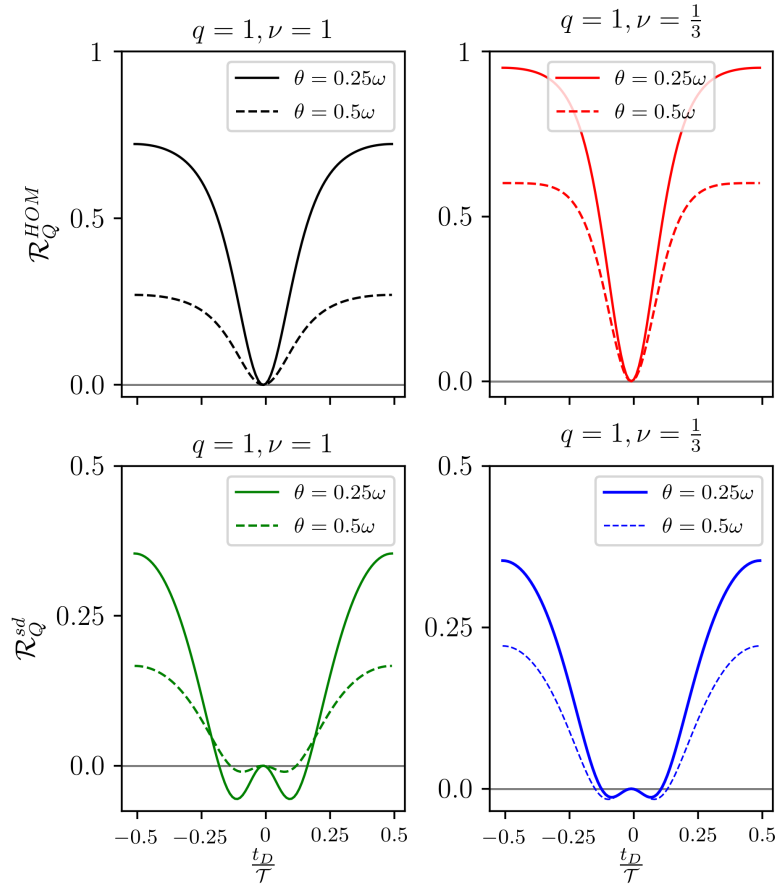In the following, we exploit the full generality of our derivation by performing the

Figure 4.8: HOM heat ratio $\mathcal{R}_Q^{HOM}$ (upper panels) and single-drive heat ratio $\mathcal{R}_Q^{sd}$ (lower panels) as a function of the time delay t_D for $q = 1$ and temperatures $\theta = 0.25\omega$ (solid lines) and $\theta = 0.5\omega$ (dashed lines). The integer case (left panel) and the fractional case for $\nu = \frac{1}{3}$ (right panel) are compared. The other parameters are $W = 0.1\mathcal{T}$ and $\omega = 0.01\omega_c$.

analysis for different values of q.

We start by considering the regime where thermal and quantum fluctuations are comparable.

As a beginning, we focus on the relevant case of $q = 1$, where states formed by a

single Leviton are injected from both sources [173]. The collision of identical single-Leviton states is very interesting because previous work on fluctuations of charge current proved that in this case the ratio of HOM charge noise is independent of filling factors and temperatures, acquiring an universal analytical expression [31, 115]. In order to perform a similar comparison for the heat noise, we present in Fig. 4.8 the HOM heat ratio (upper panels) considering two temperatures $\theta = 0.25\omega$ (solid line) and $\theta = 0.5\omega$ (dashed lines) for the both integer and fractional case. Contrarily to the charge case, these curves are all clearly distinct. This means that this universality does not extend also to heat fluctuations. This fact can be explained by the dependence of heat HOM noise on the energy distribution of particles injected by the drives, which in turn is significantly affected by the temperature and by the strength of correlations encoded in the filling factor ν. In particular, as the temperature is further increased, the thermal fluctuations tend to hide the effect of the voltages, resulting in a reduction of $\mathcal{R}_Q^{HOM}$ for both filling factors.

Interestingly, we also note that the single-drive ratio can switch sign as t_D is tuned, independently of the filling factor. Since $\mathcal{S}_Q^R$ is independent of t_D, the change of sign of the HBT ratio is entirely due to $\mathcal{S}_Q^{sd}$ itself. This is a remarkable difference with respect to the charge noise generated in the same configurations, since charge conservation fixes the sign of current-current correlations. On the contrary, it should be pointed out that the sign of heat noise is not constrained by any conservation law [160].

In Fig. 4.9, we start looking at the collision of states composed by multiple levitons and compare the HOM charge and heat ratios (dashed and solid lines, respectively) for $q = 2$ and $q = 4$. In the fermionic case, presented in the two upper panels, the qualitative behavior of the two ratios is very similar, showing no particular features. It is interesting to point out that in an interval of time delays t_D, heat noise is less suppressed that charge noise. This means that, if levitons overlap only partially, then the heat carried by them fluctuates more than their charge. These additional fluctuations could be attributed to the fact that, in the case of heat, the quantum-statistical exchange is not constrained by the conservation law per particle as in the case of charge. Therefore, we can conclude that the different nature of heat and charge single-electron transport can be extracted in heat interferometric experiments by observing the fluctuations of heat current. Remarkably, the curves for the HOM heat ratio in the fractional case display instead some unexpected side peaks and dips in addition to the central dip, which appear for the same value of t_D as in charge noise. In particular, the number of these maxima and minima increases for states composed by more levitons. On the contrary, in the analogous curves for the effective single-drive ratio at fractional filling factors, these features are completely absent. In order to understand this remarkable result, we recall the crystallization of multiple levitons states discussed in Chapter 3. Based on this argument, we can infer that the HOM heat noise is affected by the crystallization induced in the propagating levitons, thus giving rise to the features observed in the lower panel of Fig. 4.9.

We conclude by noticing that strong correlation of the fractional regime can increase the value of the HOM heat ratio even above 1. Once again, since this is not the case for the effective single-drive contribution, this is due to the presence of $\Delta\mathcal{S}_{Q,23}$, which is peculiar to collision between levitons incoming from different reservoirs.

Now, we consider the regime of very low temperature $\theta \ll \omega$, where the quantum effects should be largely enhanced with respect to the thermal fluctuations.
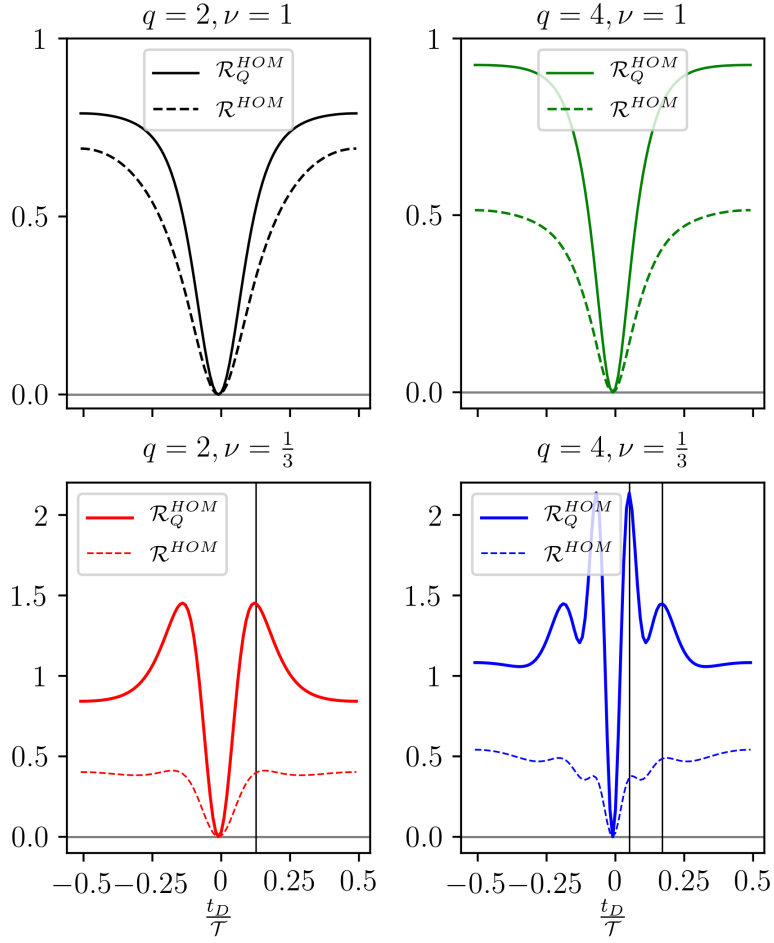
Figure 4.9: (HOM heat ratio $\mathcal{R}_Q^{HOM}$ (solid lines) and charge HOM ratio $\mathcal{R}_C^{HOM}$ (dashed lines) as a function of the time delay t_D for $\nu = 1$ (upper panel) and $\nu = \frac{1}{3}$ (lower panel) for $q = 2$ or $q = 4$. The other parameters are $\theta = 0.25\omega, W = 0.1\mathcal{T}$ and $\omega = 0.01\omega_c$.

The plots for $\mathcal{R}_Q^{HOM}$ in the integer and in the fractional case are compared in Fig. 4.10 for different values of q. In the integer case, a single smooth dip is present for all the values of q, confirming the phenomenology described for the finite temperature case. For the strongly correlated case, at $q = 1$ one observes a smooth profile, except for a small decreasing close to $t_D = 0.5$. Intriguingly, the oscillations observed in Fig. 3.7 for $q > 1$ are widely enhanced in this regime, such that the HOM ratio displays zeros, whose number increases with q, in addition to the central one and can reach also negative values.
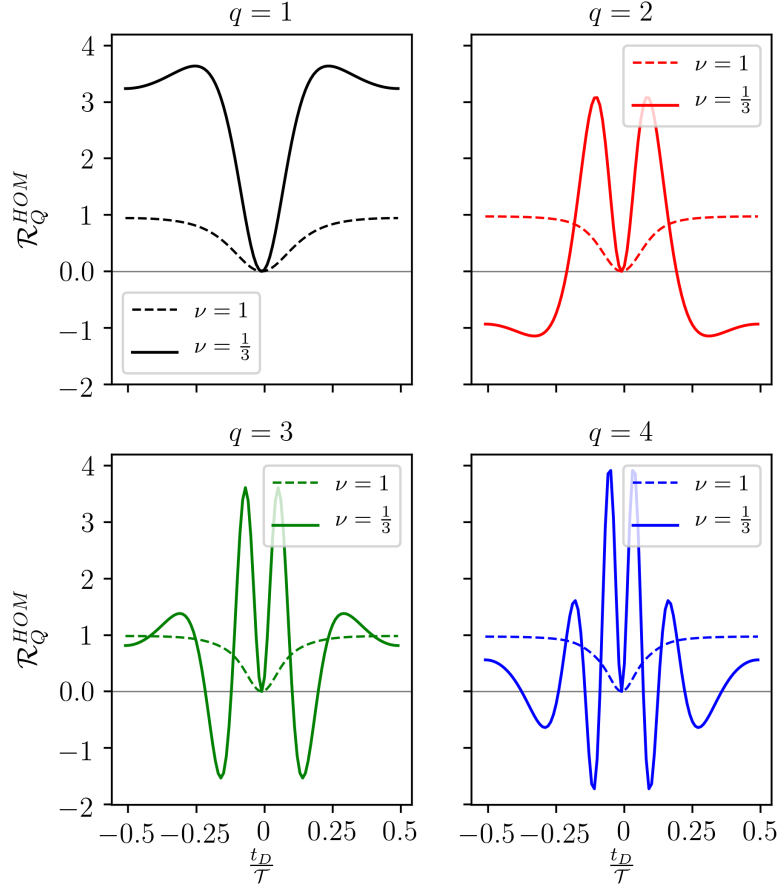
Figure 4.10: HOM heat ratio $\mathcal{R}_Q^{HOM}$ as a function of the time delay t_D for $q = 1$, $q = 2$, $q = 3$, $q = 4$. The integer case (dashed lines) and the fractional case for $\nu = \frac{1}{3}$ (solid lines) are compared. The other parameters are $W = 0.1\mathcal{T}$, $\theta = 10^{-4}\omega$ and $\omega = 0.01\omega_c$.

Summary

In this thesis, we have investigated charge and heat transport in integer and fractional quantum Hall systems in the presence of time-dependent external voltages. Quantum Hall systems are one of the most famous and important example of topological states, which are exotic phases of matter, whose properties are described by quantities that do not depend on the details of a specific system. The hallmark of quantum Hall systems is the emergence of one-dimensional conducting channels at the boundary. These edge states are topologically protected against backscattering, thus ensuring a coherence length of several μm. In **Chapter 1**, we reviewed the phenomenology of integer and fractional quantum Hall states, with a particular emphasis of the theoretical description of their edge states. To this end, we have derived a chiral Luttinger liquid model, which is the most suitable tool to inspect both non-interacting and strongly correlated states of quantum Hall systems.

The discovery of quantum Hall states of matter and their protected edge states has triggered a huge number of theoretical proposals and cutting-edge experiments. Several analogies can be drawn between the propagation of electrons in quantum Hall edge channels and photons in vacuum. This observation opened the way to a new research field, known as electron quantum optics (EQO). The main purpose of EQO is to reproduce conventional optics experiments using electronic wave-packets propagating in condensed matter systems instead of photons traveling along waveguides. In **Chapter 2**, we revisited the main concepts of electron quantum optics. Here, we introduced the idea of single-electron sources, that can be exploited to emit purely electronic excitations into quantum Hall edge states. In particular, we focused on the case of Lorentzian pulses carrying an integer number of particles, the so-called levitons, which are one of the main building blocks of EQO. By partitioning a periodic train of levitons traveling along quantum Hall edge states against a quantum point contact, which is the analogue of a photonic beam splitter for electrons, we showed that levitons are minimal excitation states for integer filling factors of the Laughlin sequence. Finally, we presented the HOM interferometry with levitons, where electrons impinge on the opposite side of a QPC with a tunable delay. By performing such interferometric experiments, it is possible to observe the anti-bunching effect typical of particle obeying Fermi statistics.

Chapter 3 is devoted to the study of correlation effects. Here, we consider a fractional liquid and we have shown that the strongly correlated phase of FQH systems is able to crystallize levitons, soliton-like excitations in the realm of condensed matter, after their tunneling at a QPC. This process rearranges the excess density of levitons in a regular oscillating pattern, showing as many peaks as the number of injected particles. The amplitude of oscillations gets enhanced by increasing the strength of interactions. The crystallization of levitons represents an electronic counterpart of soliton crystals realized with photons in optical fiber setups. Exper-

imental evidence of this effect can be found in a Hong-Ou-Mandel interferometer, where unexpected dips in the noise reveal the crystallization mechanism. This kind of experiment is within reach for nowadays technology.

Despite several challenging and fascinating results concerning charge transport properties, electric charge is far from being the only interesting degree of freedom in the framework of electron quantum optics. For this reason, we consider heat transport properties of levitons in **Chapter 4**. Even though the experimental investigation of heat transport properties remains quite challenging, the problem of heat conduction and manipulation at the nanoscale has become more actual than ever, as demonstrated by some recent groundbreaking results.

In **Chapter 4**, we have shown that mixed and heat noises measured in one of the output arms of a Hanbury-Brown-Twiss interferometer all reach their minimal value (set by the respective poissonian dc relations) when levitons impinge on the beam splitter, that is when the voltage drive generates Lorentzian pulses carrying an integer amount of electronic charge along the edge states of the quantum Hall system. These results extend the notion of leviton as a minimal excitation state in the Laughlin sequence to the heat transport domain. Furthermore, we demonstrated the robustness of this result even in the presence of an arbitrary overlap between multiple levitons, regardless of the nonlinear dependence on the voltage bias typical of heat-transport-related quantities.

Finally, we investigated heat current fluctuations in a Hong-Ou-Mandel interferometer in the fractional quantum Hall regime. Here, two identical leviton excitations impinge at a quantum point contact with a given time delay. We showed that single-drive configuration and HOM interferometer implemented with voltage sources are two physically distinct experimental configurations. Interestingly, unexpected side dips emerged only in the fractional regime which can be related to the crystallization mechanism discussed in **Chapter 3** for levitons.

Perspectives

The generation and control of levitons and, more in general, of single- to few-electronic excitations in one-dimensional ballistic conductors have attracted a huge interest in recent years and is actually at the forefront of research in condensed matter physics, and may lead to fascinating applications in quantum communication and quantum information. However, several important issues, including for instance the role of decoherence or screening in the dynamics of single-electron excitations [30, 87, 109], are yet to be fully understood and will certainly deserve a lot of attention in years to come. Further interesting developments could also involve the investigation of pseudo-random emission of levitons, as recently proposed for the free fermion case [95]. Besides closing the conceptual gap between time-periodic injection and individual wave-packet emission this newly proposed emission protocol opens important perspectives for the FQH case, as it promises to strongly magnify the side dip features discussed in Chapter 3.

Possible extensions include the investigations of related setups as optimal sources for fractionally charged single-anyons. On one side, it would be extremely interesting to investigate whether related setups can serve as optimal sources for fractionally charged single-anyons. In this sense, it has been proposed that a quantum point contact may be used to break the leviton into a coherent quasi-particle reflected off the barrier and a pair of Laughlin quasi-particles transmitted [88]. The outcome of such a setup should then be used as the input of a Hanbury-Brown-Twiss interferometer, in order to investigate the cleanliness of such a state. On the other hand, multiple-QPC setups such as Fabry-Perot interferometers could be investigated in an attempt to reveal signatures of the fractional statistics through Hong-Ou-Mandel interferometry.

Moreover, the exotic physics of the quantum Hall effect allows for the existence of peculiar neutral edge modes for some values of the filling factor [179–182]. While they cannot contribute to charge transport, they do carry a finite amount of energy, which often flows in opposite direction with respect to the charged modes. An application of EQO paradigms to FQH states supporting neutral modes let us envisage an exciting setup were single-particle charge and energy are separated on-demand into different output terminals, exploiting the composite edge structure of two-dimensional systems in the QH regime.

Other possibilities may involve two-dimensional topological insulators, where a pair of counter-propagating gapless and one-dimensional channels appears on each edge, in the absence of a magnetic field [183–185]. Interestingly, the direction of propagation of electrons belonging to these edge channel is linked to their spin by a property called helicity. The injection of levitons in these helical edge states might open up interesting application where a single spin-polarized electron can be manipulated for applications in the field of spintronic.

Very remarkably, some experiment in the presence of time-dependent voltages are starting to be realized in the fractional regime [186]. These preliminary results might pave the way for the emission of levitons in states with a fractional filling factor, thus leading to the possibility of an experimental verification of the many fascinating phenomena that arise due to the interplay between the properties of levitons and strong correlations of fractional quantum Hall systems.

Appendix A

Bosonic commutators

In this appendix, we compute bosonic commutators introduced in the main text (see Eqs. (1.111) and Eqs. (1.112) in Chapter 1) . In addition, we will show the connection between bosonic and fermionic formalism at $\nu = 1$.

A.1 Bosonic commutators

Before starting this calculation, we recall the form of bosonic field appearing in the main text in Eq. (1.109)

$$\Phi_{R/L}(x) = i\sqrt{\frac{2\pi}{L}} \sum_{k>0} \frac{e^{-\frac{ak}{2}}}{\sqrt{k}} \left(e^{\pm ikx} b_{R/L,k} - e^{\mp ikx} b_{R/L,k}^\dagger \right), \qquad (A.1)$$

where bosonic operators $b_{k,R/L}$ satisfy $\left[b_{k,R/L}, b_{R/L}^\dagger \right] = \delta_{k,q}$. Bosonic fields in Eq, (A.1) can be splitted into two conjugate fields $\varphi_{R/L}(x)$ and $\varphi_{R/L}^\dagger(x)$ as

$$\Phi_{R/L}(x) = \varphi_{R/L}(x) + \varphi_{R/L}^\dagger(x), \qquad (A.2)$$

where

$$\varphi_{R/L}(x) = i\sqrt{\frac{2\pi}{L}} \sum_{q>0} \frac{e^{-\frac{aq}{2}}}{\sqrt{q}} e^{\pm iqx} b_{q,R/L}. \qquad (A.3)$$

Here, parameter a indicates the lattice spacing and corresponds to an ultra-violet length cut-off. In the end of calculations, one has to take the limit $a \to 0^+$ in order to find the final expressions of commutators.

Let us evaluate commutators for fields $\varphi_{R/L}(x)$ and $\varphi_{R/L}^\dagger(x)$

$$\left[\varphi_{R/L}(x), \varphi_{R/L}^\dagger(x') \right] = \frac{2\pi}{L} \sum_{k,q>0} \frac{e^{-\frac{a(k+q)}{2}}}{\sqrt{q}\sqrt{k}} e^{\pm ikx} e^{\mp iqx'} =$$

$$= \frac{2\pi}{L} \sum_{q>0} \frac{1}{q} e^{-q[\pm i(x'-x)+a]} =$$

$$= -\ln \left[1 - e^{-\frac{2\pi}{L}[\pm i(x'-x)+a]} \right], \qquad (A.4)$$

where, in the last step, we used the series $\sum_{n=1}^{\infty} \frac{x^n}{n} = -\ln(1-x)$. By taking the lowest order in the expansion over $\frac{1}{L}$ (which corresponds to the limit $L \to \infty$), one has that

$$\left[\varphi_{R/L}(x), \varphi_{R/L}^\dagger(x') \right] = \ln \left[-\frac{2\pi}{L} r[i(x'-x) + ar] \right]. \qquad (A.5)$$

At this stage, one can directly obtain the commutators in Eq. (1.111), by resorting to Eq. (A.2), thus finding

$$\left[\Phi_{R/L}(x), \Phi_{R/L}(x')\right] = \left[\varphi_{R/L}(x), \varphi_{R/L}^{\dagger}(x')\right] + \left[\varphi_{R/L}^{\dagger}(x), \varphi_{R/L}(x')\right] =$$

$$= -\ln\left[\frac{1 - e^{-\frac{2\pi}{L}[\pm i(x'-x)+a]}}{1 - e^{-\frac{2\pi}{L}r[\pm i(x-x')+a]}}\right]. \tag{A.6}$$

In the limit $L \to +\infty$, one has

$$\left[\Phi_{R/L}(x), \Phi_{R/L}(x')\right] \simeq -\ln\left[\frac{1 - 1 \pm \frac{2\pi}{L}[i(x'-x)+a]}{1 - 1 \pm \frac{2\pi}{L}[i(x-x')+a]}\right] =$$

$$= -\ln\left[\pm\frac{\frac{x-x'}{a} + i}{\mp\frac{x-x'}{a} + i}\right]. \tag{A.7}$$

By using the identity $z = \frac{i}{2}\ln\left(\frac{z+i}{-z+i}\right)$ [110], the commutators become

$$\left[\Phi_{R/L}(x), \Phi_{R/L}(x')\right] = \mp\frac{2}{i}\arctan\left(\frac{x-x'}{a}\right). \tag{A.8}$$

Since the limit $a \to 0$ is now well-defined, one can perform it, thus getting rid of the short-length cut-off and finally finding

$$\left[\Phi_{R/L}(x), \Phi_{R/L}(x')\right] = \pm i\pi\text{sign}(x - x'). \tag{A.9}$$

The commutators with density operator, appearing in Eq. (1.112), can be easily calculated by taking the derivative with respect to x of both members in Eq. (A.9) and inserting the proper prefactor. Indeed, one has

$$\left[\rho_{R/L}(x), \Phi_{R/L}(x')\right] = -i\sqrt{\nu}\delta(x - x'). \tag{A.10}$$

A.2   Fermionic formalism at $\nu = 1$

In the following, we show that a low-energy bosonic theory of a one-dimensional non-interacting system is equivalent to a fermionic model with linear spectrum. The corresponding hamiltonian is

$$H_{R/L} = \int_{-\infty}^{+\infty} dx : \Psi_{R/L}^{\dagger}(x)(\mp iv\partial_x - \mu)\Psi_{R/L}(x) :, \tag{A.11}$$

where $\mu = vk_F$ and the fermionic fields $\Psi_{R/L}$ are given by

$$\Psi_{R/L}(x) = \frac{1}{\sqrt{2\pi v}}\int_{-\infty}^{\infty} d\epsilon e^{\pm i\frac{\epsilon}{v}x}a_{R/L}(\epsilon). \tag{A.12}$$

For the following calculations, we will consider for simplicity the discrete version of these fermionic fields, which reads

$$\Psi_{R/L}(x) = \frac{1}{\sqrt{L}}\sum_{k=-\infty}^{k=\infty} e^{\pm ik_F x}c_{R/L,k}. \tag{A.13}$$

Note that the second contribution in Eq. (A.11) is proportional to the chemical potential μ, which is fundamental to fix the ground state charge and energy [83].

The notation $: \cdots :$ stands for normal ordering of operators with respect to the fermionic ground state, i.e. the filled Fermi sea. It means that all operators that destroy the ground state are moved to the right of all other operators [35, 36].

Fermionic fields obey the following anti-commutation relations

$$\left\{ \Psi_{R/L}(x), \Psi_{R/L}^\dagger(y) \right\} = \delta(x - y). \tag{A.14}$$

Charge and energy density operators can be defined in terms of these fields as

$$\rho_{R/L}(x) =: \Psi_{R/L}^\dagger(x)\Psi_{R/L}(x) :, \tag{A.15}$$

$$\mathcal{H}_{R/L}(x) = \mp iv : \Psi_{R/L}^\dagger(x)\partial_x \Psi_{R/L}(x) : -vk_F \rho_{R/L}(x). \tag{A.16}$$

The relation between fermionic and bosonic descriptions relies on the bosonization approach at $\nu = 1$. In this case, the bosonization identity is

$$\Psi_{R/L}(x) = \frac{\mathcal{F}_{R/L}}{\sqrt{2\pi a}} e^{\pm ik_F x} e^{-i\Phi_{R/L}(x)}. \tag{A.17}$$

We will show that the bosonic form for Eqs. (A.11), (A.15) and (A.16) will lead us to

$$\rho_{R/L}(x) = \mp \frac{1}{2\pi}\partial_x \Phi_{R/L}(x),$$

$$\mathcal{H}_{R/L}(x) = \frac{v}{4\pi} : \left[\partial_x \Phi_{R/L}(x)\right]^2 : . \tag{A.18}$$

A.2.1 Particle density

Let us first consider the density operator ρ_R. We focus again on the case of right-moving excitations, and drop the label R for brevity. We also drop for the moment the factor $e^{ik_F x}$ in the definition of $\Psi_R(x)$ (see Eq. (A.17)) which will be reinstated at the end of calculations. We thus consider the field

$$\tilde{\Psi}(x) = \frac{\mathcal{F}}{\sqrt{L}} e^{-i\varphi^\dagger(x)} e^{i\varphi(x)} = \frac{\mathcal{F}}{\sqrt{2\pi a}} e^{-i\Phi(x)}. \tag{A.19}$$

Note that the operator in the middle of Eq. (A.19) is normal ordered, while the right-hand side if the equation is not, hence the presence of the diverging factor $(\sqrt{2\pi a})^{-1}$ [35, 36]. We can now work out the bosonized expression for the density $\tilde{\rho}(x) =: \tilde{\Psi}^\dagger(x)\tilde{\Psi}(x) :$. We use the point splitting technique to regularize such a diverging quantity, using $\delta = ia$ as the splitting parameter and taking the limit $a \to 0$ at the end of calculation [36]. Using $e^A e^B = e^B e^A e^{[A,B]}$, we have

$$\tilde{\Psi}^\dagger(x+ia)\tilde{\Psi}(x) = \frac{1}{L} e^{i\varphi^\dagger(x+ia)} e^{i\varphi(x+ia)} \mathcal{F}^\dagger \mathcal{F} e^{-i\varphi^\dagger(x)} e^{-i\varphi(x)} =$$

$$= \frac{1}{L} e^{i\varphi^\dagger(x+ia)} e^{-i\varphi^\dagger(x)} e^{i\varphi(x+ia)} e^? {-i\varphi(x)} e^{\left[\varphi(x+ia),\varphi^\dagger(x)\right]}. \tag{A.20}$$

The commutator in the exponential gives

$$e^{\left[\varphi(x+ia),\varphi^\dagger(x)\right]} = e^{-\ln\frac{2\pi a}{L}} = \frac{L}{2\pi a}. \tag{A.21}$$

Eq. (A.20) now reads

$$\tilde{\Psi}^\dagger(x+ia)\tilde{\Psi}(x) = \frac{1}{2\pi a} e^{i\left[\varphi^\dagger(x+ia)-\varphi^\dagger(x)\right]} e^{i\left[\varphi(x+ia)-\varphi(x)\right]}. \tag{A.22}$$

We now expand the exponentials in powers of a

$$\tilde{\Psi}^\dagger(x+ia)\tilde{\Psi}(x) = \frac{1}{2\pi a}\left[1 + i\partial_x\varphi^\dagger(x)ia + \mathcal{O}(a^2)\right]\left[1 + i\partial_x\varphi(x)ia + \mathcal{O}(a^2)\right] =$$

$$= \frac{1}{2\pi a} - \frac{1}{2\pi}\left[\partial_x\varphi^\dagger(x) + \partial_x\varphi(x)\right] + \mathcal{O}(a) =$$

$$= \frac{1}{2\pi a} - \frac{1}{2\pi}\partial_x\Phi(x) + \mathcal{O}(a). \tag{A.23}$$

Finally, normal ordering the last expression and taking the limit $a \to 0$ we get the final result

$$\tilde{\rho}(x) = \lim_{a\to 0} \; : \tilde{\Psi}^\dagger(x+ia)\tilde{\Psi}(x) :=$$

$$= \lim_{a\to 0}\left[\tilde{\Psi}^\dagger(x+ia)\tilde{\Psi}(x) - \left\langle\tilde{\Psi}^\dagger(x+ia)\tilde{\Psi}(x)\right\rangle\right]_0 =$$

$$= -\frac{1}{2\pi}\partial_x\Phi(x), \tag{A.24}$$

where the notation $\langle\ldots\rangle_0$ stands for a quantum average over the ground state. Notice that the normal ordering allowed us to get rid of the diverging contribution $(2\pi a)^{-1}$.

A.2.2 Hamiltonian density

We proceed similarly for the energy density $\mathcal{H}(x)$. However, this calculation presents some tricky passages that need to be performed carefully. Consider the first term in Eq. (A.16) for the case of right-moving fermions, which we will denote as $\mathcal{H}_0$. We have

$$\mathcal{H}_0(x) = -iv : \Psi^\dagger(x)\partial_x\Psi(x) : . \tag{A.25}$$

Now, let us drop the exponential factor $e^{ik_F x}$ and work with the field $\tilde{\Psi} = e^{-ik_F x}\Psi$. We resort to the point splitting technique and write

$$\tilde{\Psi}^\dagger(x+ia)\partial_x\tilde{\Psi}(x) =$$

$$= \frac{1}{L}e^{i\varphi^\dagger(x+ia)}e^{i\varphi(x+ia)}\mathcal{F}^\dagger\mathcal{F}\partial_x\left[e^{-i\varphi^\dagger(x)}e^{-i\varphi(x)}\right] =$$

$$= \frac{1}{L}e^{i\varphi^\dagger(x)}e^{i\varphi(x+ia)}e^{-i\varphi^\dagger(x)}\left[-i\partial_x\varphi^\dagger(x)e^{-\varphi(x)} - ie^{-i\varphi(x)}\partial_x\varphi(x)\right] =$$

$$= \frac{1}{L}e^{i\varphi^\dagger(x)}e^{i\varphi(x+ia)}e^{-i\varphi^\dagger(x)}e^{-i\varphi(x)}\left\{-i\partial_x\varphi^\dagger(x) - i\partial_x\varphi(x) - \left[\partial_x\varphi^\dagger(x), \varphi(x)\right]\right\}. \tag{A.26}$$

It is worth noticing that we had to move the exponential $e^{-i\varphi(x)}$ to the left of $\partial_x\varphi^\dagger(x)$, thus generating an additional commutator. The latter is given by

$$\left[\partial_x\varphi^\dagger(x), \varphi(x)\right] = -\partial_y\left[\varphi(x), \varphi^\dagger(y)\right]_{x=y} \simeq \partial_y\ln\left[-i\frac{2\pi}{L}(x-y+ia)\right]_{x=y} =$$

$$= \left[\frac{i\frac{2\pi}{L}}{-i\frac{2\pi}{L}(x-y+ia)}\right]_{x=y} = \frac{i}{a}. \tag{A.27}$$

Then we obtain

$$\tilde{\Psi}^\dagger(x+ia)\partial_x\tilde{\Psi}(x) =$$

$$= \frac{1}{L}e^{i\left[\varphi^\dagger(x+ia)-\varphi^\dagger(x)\right]}e^{i\left[\varphi(x+ia)-\varphi(x)\right]}e^{\left[\varphi(x+ia),\varphi^\dagger(x)\right]}\left[-i\partial_x\varphi^\dagger(x) - i\partial_x\varphi(x) - \frac{i}{a}\right]. \tag{A.28}$$

128

At this stage, one should notice that the exponential of the commutator $\left[\varphi(x), \varphi^\dagger(x)\right]$ is proportional to $1/a$, and we also have a term $\sim 1/a$ in the square brackets. It follows immediately that we need to expand the exponential of φ and $\varphi^\dagger$ up to order a^2 to get the correct result. We have

$$e^{i\left[\varphi^\dagger(x+ia)-\varphi^\dagger(x)\right]} =$$

$$= 1 + a\left\{\partial_a e^{i\left[\varphi^\dagger(x+ia)-\varphi^\dagger(x)\right]}\right\}_{a=0} + \frac{a^2}{2}\left\{\partial_a^2 e^{i\left[\varphi^\dagger(x+ia)-\varphi^\dagger(x)\right]}\right\}_{a=0} + \mathcal{O}(a^3) =$$

$$= 1 - a\partial_x\varphi^\dagger(x) + \frac{a^2}{2}\partial_a\left\{-\partial_x\varphi^\dagger(x+ia)e^{i\left[\varphi^\dagger(x+ia)-\varphi^\dagger(x)\right]}\right\}_{a=0} + \mathcal{O}(a^3) =$$

$$= 1 - a\partial_x\varphi^\dagger(x) + \frac{a^2}{2}\left\{-i\partial_x^2\varphi^\dagger(x) + \left[\partial_x\varphi^\dagger(x)\right]^2\right\} + \mathcal{O}(a^3), \quad (A.29)$$

and we obtain similarly the expansion for $e^{i\left[\varphi(x+ia)-\varphi(x)\right]}$. Inserting both results into Eq. (A.28) we get

$$\tilde{\Psi}^\dagger(x+ia)\partial_x\tilde{\Psi}(x) =$$

$$= -\frac{i}{2\pi a}\left[\partial_x\Phi(x) + \frac{1}{a}\right]\left\{1 - a\partial_x\varphi^\dagger(x) - i\frac{a^2}{2}\partial_x^2\varphi^\dagger(x) + \frac{a^2}{2}\left[\partial_x\varphi^\dagger\right]^2\right\} \times$$

$$\times \left\{1 - a\partial_x\varphi(x) - i\frac{a^2}{2}\partial_x^2\varphi(x) + \frac{a^2}{2}\left[\partial_x\varphi(x)\right]^2 + \mathcal{O}(a^3)\right\} =$$

$$= -\frac{i}{2\pi a}\left[\partial_x\Phi(x) + \frac{1}{a}\right]\left\{1 - a\partial_x\varphi(x) - i\frac{a^2}{2}\partial_x^2\varphi(x) + \frac{a^2}{2}\left[\partial_x\varphi(x)\right]^2 - a\partial_x\varphi^\dagger(x) +\right.$$

$$\left.+ a^2\partial_x\varphi^\dagger(x)\partial_x\varphi(x) - i\frac{a^2}{2}\partial_x^2\varphi^\dagger(x) + \frac{a^2}{2}\left[\partial_x\varphi^\dagger(x)\right]^2 + \mathcal{O}(a^3)\right\} =$$

$$= -\frac{i}{2\pi a}\left[\partial_x\Phi(x) + \frac{1}{a}\right]\left\{1 - a\partial_x\Phi(x) - i\frac{a^2}{2}\partial_x^2\Phi(x) + \frac{a^2}{2} : \left[\partial_x\Phi(x)\right]^2 :\right\} + \mathcal{O}(a^3). \quad (A.30)$$

In the last step we recognized that

$$\frac{a^2}{2}\left\{\left[\partial_x\varphi^\dagger(x)\right]^2 + \partial_x\varphi^\dagger(x)\partial_x\varphi(x) + \left[\partial_x\varphi(x)\right]^2\right\} = \frac{a^2}{2} : \left[\partial_x\Phi(x)\right]^2 : \quad (A.31)$$

is a normal ordered expression, since the field $\varphi^\dagger$ is always on the left of φ. We are left with

$$\tilde{\Psi}^\dagger(x+ia)\partial_x\tilde{\Psi}(x) =$$

$$= -i\left\{\frac{1}{2\pi a^2} - \frac{1}{2\pi}\left[\partial_x\Phi(x)\right]^2 - i\frac{1}{4\pi}\partial_x^2\Phi(x) + \frac{1}{4\pi} : \left[\partial_x\Phi(x)\right]^2 :\right\} + \mathcal{O}(a). \quad (A.32)$$

We can drop the term $\sim \partial_x^2\Phi(x)$ which is a total derivative and vanishes as we integrate over x. Indeed, we should remember that the only meaningful physical quantity is proportional to $\int_{-\infty}^{\infty}\tilde{\Psi}^\dagger\partial_x\tilde{\Psi}$. Finally, we normal order the entire expression and take the limit $a \to 0$. This yields

$$: \tilde{\Psi}^\dagger(x)\partial_x\tilde{\Psi}(x) := \lim_{a\to 0}\left[\tilde{\Psi}^\dagger(x+ia)\partial_x\tilde{\Psi}(x) - \left\langle\tilde{\Psi}^\dagger(x+ia)\partial_x\tilde{\Psi}(x)\right\rangle_0\right] =$$

$$= \frac{i}{4\pi} : \left[\partial_x\Phi(x)\right]^2 : . \quad (A.33)$$

We only have to multiply by $-iv$ to get $\tilde{\mathcal{H}}_0$

$$\tilde{\mathcal{H}}_0(x) = -iv : \tilde{\Psi}^\dagger(x)\partial_x\tilde{\Psi}(x) := \frac{v}{4\pi} : \left[\partial_x\Phi(x)\right]^2 : . \quad (A.34)$$

129

Introducing the Fermi momentum

As a final step, we restore the oscillating exponential factor $e^{ik_F x}$ dropped at the beginning of the calculation. Considering a right-moving field, we have $\Psi(x) = e^{ik_F x}\tilde{\Psi}(x)$. The particle density in our formalism is left unchanged since

$$\rho(x) =: \Psi^\dagger(x)\Psi(x) :=: \tilde{\Psi}^\dagger(x)\tilde{\Psi}(x) := -\frac{1}{2\pi}\partial_x\Phi(x). \tag{A.35}$$

Differently, the energy density acquires an additional term due to the derivative acting on the exponential $e^{ik_F x}$

$$\mathcal{H}_0(x) = -iv : \Psi^\dagger(x)\partial_x\Psi(x) := -iv : \tilde{\Psi}^\dagger(x)\partial_x\tilde{\Psi}(x) : +vk_F : \Psi^\dagger(x)\Psi(x) :=$$
$$= \frac{v}{4\pi} : [\partial_x\Phi(x)]^2 : +vk_F\rho(x). \tag{A.36}$$

We finally get the result anticipated in Eq. (A.18), since

$$\mathcal{H}(x) = \mathcal{H}_0(x) - vk_F\rho(x) = \frac{v}{4\pi} : [\partial_x\Phi(x)]^2 : . \tag{A.37}$$

Appendix B

Gate voltages and gauge transformation

In this Appendix, we derive the time evolution of bosonic fields in the presence of external space- and time-dependent voltages introduced in the main text. Moreover, we show that there is no gauge transformation able to link the equations of motion for the configurations with two driving voltages V_R and V_L and the configuration with a single drive $V_- = V_R - V_L$, presented in the main text.

B.1 Bosonic fields in the presence of external gate voltages

In the main text, we investigated time-dependent transport properties of quantum Hall states in the Laughlin sequence in presence of external gate voltages. The effect of the gate potential on transport properties of the Hall bar can be inspected by finding the time evolution of bosonic fields $\Phi_R(x,t)$. Let us start by considering a right-moving channel emerging on the edge of quantum Hall bar connected to a reservoir, as in Fig. 2.1 of the main text. The coupling to an external potential is implemented in the hamiltonian description of the edge channel by capacitively coupling the charge density, given by $-e\rho_R(x)$, to the space- and time- dependent gate voltages $\mathcal{V}_R(x,t)$. In the remainder of this thesis, we will always consider semi-infinite contacts, namely restricted to $x < -d$ (for the right-moving channel) or to $x > d$ (for left-moving channel). Nevertheless, for the present discussion, we keep a generic spatial dependence for $\mathcal{V}_R(x,t)$. The corresponding gate hamiltonian is

$$H_g = -e \int_{-\infty}^{+\infty} dx \left\{ \mathcal{V}_R(x,t) \rho_R(x) \right\} =$$
$$= \frac{e\sqrt{\nu}}{2\pi} \int_{-\infty}^{+\infty} dx \left\{ \mathcal{V}_R(x,t) \partial_x \Phi_R(x) \right\}. \tag{B.1}$$

The equation of motion for bosonic fields from the total hamiltonian $H = H_R + H_g$ reads

$$\left(\partial_t + v \partial_x \right) \Phi_R(x,t) = -e\sqrt{\nu} \mathcal{V}_R(x,t). \tag{B.2}$$

These inhomogeneous transport equations can be solved by resorting to the Green's function method for first order partial differential equations [187]. The first step is

to find the solution of the homogeneous equation

$$(\partial_t + v\partial_x)\,\phi_R(x,t) = -e\sqrt{\nu}\mathcal{V}_R(x,t), \tag{B.3}$$

where ϕ_R is the time-evolved bosonic field without external voltage. Eq. (B.3) is solved by a generic function of the form $F_R(x,t) = F_R(x - vt)$. Indeed, since these solutions should coincide at $t = 0$ with bosonic field $\Phi_R(x)$ in Eq. (1.109), they read

$$\phi_R(x,t) = \Phi_R(x - vt). \tag{B.4}$$

In the presence of the inhomogeneous terms $\mathcal{V}_R(x,t)$, it can be easily shown that the solution to Eq. (B.2) is given by

$$\Phi_R(x,t) = \phi_R(x,t) + \tilde{\phi}_R(x,t), \tag{B.5}$$

where

$$\tilde{\phi}_R(x,t) = -e\sqrt{\nu} \int_{-\infty}^{+\infty} dx' \int_{-\infty}^{+\infty} dt' \mathcal{V}_R(x',t') G(x,t;x',t'). \tag{B.6}$$

Here, the function G is called Green's function and it is defined by the requirement that it satisfy the following equation

$$(\partial_t \pm v\partial_x)\,G(x,t;x',t') = \delta(x - x')\delta(t - t'). \tag{B.7}$$

For the differential operator $(\partial_t + v\partial_x)$, the Green's function is

$$G(x,t;x',t') = \Theta(t - t')\delta(v(t - t') - (x - x')), \tag{B.8}$$

which, substituted into Eq. (B.6) gives the full solution for the right-moving bosonic field in presence of gate voltage $\mathcal{V}_R(x,t)$, which reads

$$\Phi_R(x,t) = \phi_R(x,t) - e\sqrt{\nu} \int_{-\infty}^{t} dt' \mathcal{V}_R(x - v(t - t'), t'). \tag{B.9}$$

Similarly, one can repeat the same procedure for an external potential $\mathcal{V}_L(x,t)$ applied to the left-moving channel. In this case, the solution for the left-moving bosonic field is

$$\Phi_L(x,t) = \phi_L(x,t) - e\sqrt{\nu} \int_{-\infty}^{t} dt' \mathcal{V}_L(x + v(t - t'), t'). \tag{B.10}$$

By means of bosonization identities in Eqs. (1.113) and (1.124), the time evolution of electron and quasi-particle field operators is given by

$$\Psi_{R/L}^{(el)}(x,t) = \psi_{R/L}^{(el)}(x,t) \exp\left\{ ie \int_{-\infty}^{t} dt' \mathcal{V}_{R/L}(x \mp v(t - t'), t') \right\}, \tag{B.11}$$

$$\Psi_{R/L}^{(qp)}(x,t) = \psi_{R/L}^{(qp)}(x,t) \exp\left\{ i\nu e \int_{-\infty}^{t} dt' \mathcal{V}_{R/L}(x \mp v(t - t'), t') \right\}, \tag{B.12}$$

where we introduced time-dependent electronic and quasi-particle field operators at the equilibrium, i.e. $\mathcal{V}_R = \mathcal{V}_L = 0$

$$\psi_{R/L}^{(el)}(x,t) = \frac{\mathcal{F}_{R/L}^{(el)}}{\sqrt{2\pi a}} e^{\pm i k_F x} e^{-\frac{i}{\sqrt{\nu}}\phi_{R/L}(x,t)}, \tag{B.13}$$

$$\psi_{R/L}^{(qp)}(x,t) = \frac{\mathcal{F}_{R/L}^{(qp)}}{\sqrt{2\pi a}} e^{\pm i k_F x} e^{-i\sqrt{\nu}\phi_{R/L}(x,t)}. \tag{B.14}$$

As anticipated, for the following discussion, we specialize to the case of semi-infinite contacts, which perfectly model usual experimental configurations. For this reason, the gate potentials are assumed to factorize as

$$\mathcal{V}_{R/L}(x,t) = \Theta\left(\mp x - d\right) V_{R/L}(t), \tag{B.15}$$

where $x = \pm d$ are position of the interfaces between reservoirs 1/4 and the edge states. In the regions downstream of each contacts, namely $x \geq -d$ for right-movers and $x \leq d$ for left-movers, the time-dependent bosonic fields read

$$\Phi_{R/L}(x,t) = \phi_{R/L}(x,t) - e\sqrt{\nu}\int_{-\infty}^{t} dt' \Theta\left[\left(t \mp \frac{x}{v} - \frac{d}{v}\right) - t'\right] V_{R/L}(t') = \tag{B.16}$$

$$= \phi_{R/L}(x,t) - e\sqrt{\nu}\int_{-\infty}^{t \mp \frac{x}{v} - \frac{d}{v}} dt' V_{R/L}(t'). \tag{B.17}$$

The factor $\frac{d}{v}$ is a simple constant shift that could be canceled out by re-setting the origin of time axis. In the remainder of this thesis, we can safely neglect it, since it would not play any significant role in our discussion.

Field operators for electrons and quasi-particles are

$$\Psi_{R/L}^{(el)}(x,t) = \psi_{R/L}^{(el)}(x,t) e^{ie\int_{-\infty}^{t \mp \frac{x}{v}} dt' V_{R/L}(t')}, \tag{B.18}$$

$$\Psi_{R/L}^{(qp)}(x,t) = \psi_{R/L}^{(qp)}(x,t) e^{i\nu e\int_{-\infty}^{t \mp \frac{x}{v}} dt' V_{R/L}(t')}. \tag{B.19}$$

The electron density can be obtained as well from Eq. (B.17)

$$\rho_{R/L}(x,t) = \mp\frac{\sqrt{\nu}}{2\pi}\partial_x\phi_{R/L}(x,t) - \frac{\nu e}{2\pi} V_{R/L}\left(t \mp \frac{x}{v}\right). \tag{B.20}$$

The theta functions in the above equations preserve the causality of the emitted signal. In the remainder of this thesis, we assume that they are always satisfied.

Let us comment that the the deformation induced in the densities with respect to the equilibrium condition has the same shape of the applied voltages. Since edge states are chiral, the charge current operators can be simply expressed in terms of density operators as

$$J_{R/L}(x,t) = \mp ev\rho_{R/L}(x,t) = e\frac{\sqrt{\nu}}{2\pi}\partial_x\phi_{R/L}(x,t) \pm \frac{\nu e^2}{2\pi} V_{R/L}\left(t \mp \frac{x}{v}\right). \tag{B.21}$$

The average value over the equilibrium configuration is

$$\langle J_{R/L}(x,t)\rangle = \pm\frac{\nu e^2}{2\pi} V_{R/L}\left(t \mp \frac{x}{v}\right), \tag{B.22}$$

since $\langle\partial_x\phi_{R/L}(x,t)\rangle = 0$.

Finally, let us comment that, for the filling factor $\nu = 1$, according to Eq. (1.125), one has that

$$\Psi_{R/L}(x,t) \equiv \Psi_{R/L}^{(el)}(x,t) = \Psi_{R/L}^{(qp)}(x,t) = \psi_{R/L}(x,t) e^{ie\int_{-\infty}^{t \mp \frac{x}{v}} dt' V_{R/L}(t')}, \tag{B.23}$$

where $\psi_{R/L}(x,t)$ is the time-evolution of fermionic fields in Eq. (1.127) in the absence of external potentials and reads

$$\psi_{R/L}(x,t) = \frac{1}{\sqrt{2\pi v}}\int_{-\infty}^{+\infty} d\epsilon\, e^{-i\epsilon\left(t \mp \frac{x}{v}\right)} a_{R/L}(\epsilon). \tag{B.24}$$

B.2 Applying gauge transformations to the HOM setup

In the double-drive setup a voltage drive is applied both to right-moving and left-moving excitations. We consider a situation in which the vector potentials $\mathcal{A}_{R/L}(x,t)$ are absent. The Lagrangian density is

$$\mathcal{L} = \frac{1}{4\pi}\Big\{ -\partial_x\Phi_R(x,t)\big[\partial_t\Phi_R(x,t) + v\partial_x\Phi_R(x,t)\big] + $$

$$+ \partial_x\Phi_L(x,t)\big[\partial_t\Phi_L(x,t) - v\partial_x\Phi_L(x,t)\big]\Big\} \tag{B.25}$$

$$- \frac{e\sqrt{\nu}}{2\pi}\Big[\partial_x\Phi_R(x,t)\mathcal{V}_R(x,t) - \partial_x\Phi_L(x,t)\mathcal{V}_L(x,t)\Big]. \tag{B.26}$$

The Euler-Lagrange equations

$$\partial_t\frac{\delta\mathcal{L}}{\delta\partial_t\Phi_\alpha} + \partial_x\frac{\delta\mathcal{L}}{\delta\partial_x\Phi_\alpha} - \frac{\delta\mathcal{L}}{\delta\Phi_\alpha} = 0 \tag{B.27}$$

with $\alpha = R, L$, give rise to the following equation of motions for the bosonic fields:

$$(\partial_t + v\partial_x)\Phi_R(x,t) = -e\sqrt{\nu}\mathcal{V}_R(x,t) \tag{B.28}$$

$$(\partial_t - v\partial_x)\Phi_L(x,t) = -e\sqrt{\nu}\mathcal{V}_L(x,t). \tag{B.29}$$

In order to model the system presented in B.1, the form for the voltage drives is

$$\mathcal{V}_R(x,t) = f_R(x)V_R(t), \tag{B.30}$$

$$\mathcal{V}_L(x,t) = f_L(x)V_L(t), \tag{B.31}$$

where $f_{R/L}(x)$ are time-independent, while $V_{R/L}(t)$ are space-independent. In this case equation of motions for the double-drive setup are

$$(\partial_t + v\partial_x)\Phi_R(x,t) = -e\sqrt{\nu}f_R(x)V_R(t), \tag{B.32a}$$

$$(\partial_t - v\partial_x)\Phi_L(x,t) = -e\sqrt{\nu}f_L(x)V_L(t). \tag{B.32b}$$

We also consider a single-drive setup with an effective voltage drive $\mathcal{V}_R(x,t) = f_R(x)[V_R(t) - V_L(t)]$ on the right side, and the left side grounded $[\mathcal{V}_L(x,t) = 0]$. We still consider that the magnetic potential is zero on both edges. It is immediate to show that the equation of motions are now

$$(\partial_t + v\partial_x)\Phi_R(x,t) = -e\sqrt{\nu}f_R(x)[V_R(t) - V_L(t)], \tag{B.33a}$$

$$(\partial_t - v\partial_x)\Phi_L(x,t) = 0. \tag{B.33b}$$

Here we show that a gauge transformation that operates in the following way on the voltage drives

$$\begin{cases} \mathcal{V}_R(x,t) = f_R(x)V_R(t), \\ \mathcal{V}_L(x,t) = f_L(x)V_L(t), \end{cases} \longrightarrow \begin{cases} \mathcal{V}'_R(x,t) = f_R(x)[V_R(t) - V_L(t)], \\ \mathcal{V}'_L(x,t) = 0, \end{cases} \tag{B.34}$$

does not transform Eqs. (B.32) into Eqs. (B.33), but leaves them unchanged.
Since these equations involve spatial-dependent functions, we expect that non-zero

magnetic potentials arise as a consequence of the gauge transformation. In particular we have

$$\mathcal{V}'_R(x,t) = f_R(x)V_R(x) - \partial_t\chi_R(x,t) = f_R(x)[V_R(t) - V_L(t)], \qquad (B.35)$$
$$\mathcal{V}'_L(x,t) = f_L(x)V_L(x) - \partial_t\chi_L(x,t) = 0 \qquad (B.36)$$

for the right-moving and left-moving sector respectively. The transformation is evidently implemented by the choice

$$\chi_R(x,t) = f_R(x)\int_0^t d\tau V_L(\tau), \qquad (B.37a)$$

$$\chi_L(x,t) = f_L(x)\int_0^t d\tau V_L(\tau). \qquad (B.37b)$$

As expected, in the new gauge we get non-zero magnetic potentials given by

$$\mathcal{A}'_R(x,t) = \partial_x f_R(x)\int_0^t d\tau V_L(\tau), \qquad (B.38)$$

$$\mathcal{A}'_L(x,t) = \partial_x f_L(x)\int_0^t d\tau V_L(\tau), \qquad (B.39)$$

and the Lagrangian density now reads

$$\mathcal{L}' = \frac{1}{4\pi}\Bigg\{ -\partial_x\Phi_R(x,t)\big[\partial_t\Phi_R(x,t) + v\partial_x\Phi_R(x,t)\big] +$$
$$+ \partial_x\Phi_L(x,t)\big[\partial_t\Phi_L(x,t) - v\partial_x\Phi_L(x,t)\big]\Bigg\} +$$
$$- \frac{e\sqrt{\nu}}{2\pi}\Bigg\{ \partial_x\Phi_R(x,t)f_R(x)[V_R(t) - V_L(t)] +$$
$$+ \big[\partial_t\Phi_R(x,t)\partial_x f_R(x) - \partial_t\Phi_L(x,t)\partial_x f_L(x)\big]\int_{t_0}^t d\tau V_L(\tau)\Bigg\}, \qquad (B.40)$$

where the last term accounts for the presence of $\mathcal{A}'_R(x,t)$ and $\mathcal{A}'_L(x,t)$. We now look for the equation of motions in this new configuration. From Euler-Lagrange equations one gets

$$(\partial_t + v\partial_x)\Phi_R(x,t) =$$
$$= -e\sqrt{\nu}f_R(x)[V_R(t) - V_L(t)] + e\sqrt{\nu}f_R(x)V_L(t) =$$
$$= -e\sqrt{\nu}f_R(x)V_R(t), \qquad (B.41)$$
$$(\partial_t - v\partial_x)\Phi_L(x,t) = e\sqrt{\nu}f_L(x)V_L(t). \qquad (B.42)$$

Note that we have not recovered the equation of motions for the single drive setup, Eqs. (B.33), as one may naively expect. On the contrary, we have found the equations of motion for the double-drive setup, Eqs. (B.32).

Appendix C

Photo-assisted coefficients

C.1 Single source

The application of a spatially homogeneous time-dependent voltage $V(t)$ to quantum Hall channels at filling factor ν is manifested in the phase ($\hbar = 1$)

$$e^{i\nu e \int_0^t dt' V(t')} \tag{C.1}$$

acquired by particle with charge νe.

For voltage periodic in time, it is convenient to separate dc and ac part of the signal, as $V(t) = V_{dc} + V_{ac}(t)$, where V_{ac} is a function with period $\mathcal{T}$ whose average over one period is zero. The dc part is linked to the number of particle q emitted along the edge state in a period, as

$$q = -\frac{\nu e}{\omega} V_{dc}. \tag{C.2}$$

The total phase in Eq. (C.1) can be written as

$$e^{i\nu e \int_0^t dt' V(t')} = e^{i\phi_{ac}(t)} e^{-iq\omega t}, \tag{C.3}$$

where $\omega = \frac{2\pi}{\mathcal{T}}$ and

$$\phi_{ac}(t) = \nu \int_0^t V_{ac}(t')dt'. \tag{C.4}$$

The phase given by $e^{-i\phi_{ac}(t)}$ is a periodic function of time and can be written in Fourier series as

$$e^{i\phi_{ac}(t)} = \sum_l p_l e^{-il\omega t}, \tag{C.5}$$

where we introduced the photo-assisted coefficient

$$p_l = \int_{-\frac{\mathcal{T}}{2}}^{\frac{\mathcal{T}}{2}} \frac{dt}{\mathcal{T}} e^{il\omega t} e^{i\phi_{ac}(t)}. \tag{C.6}$$

C.1.1 Cosine drive

In the case of a cosine drive

$$V_{sin}(t) = V_{dc}(1 - \cos(\omega t)), \tag{C.7}$$

one finds

$$
\begin{aligned}
p_l &= \int_{-\frac{\mathcal{T}}{2}}^{\frac{\mathcal{T}}{2}} \frac{dt}{\mathcal{T}} e^{il\omega t} e^{-i\nu eV_{dc}\int_0^t dt' \cos(\omega t')} = \int_{-\frac{\mathcal{T}}{2}}^{\frac{\mathcal{T}}{2}} \frac{dt}{\mathcal{T}} e^{il\omega t} e^{iq\sin(\omega t)} = \\
&= \int_{-\pi}^{\pi} d\tau \left\{ \cos\left[q\sin\left(\tau\right)+l\tau\right] + i\sin\left[q\sin\left(\tau\right)+l\tau\right]\right\} = \\
&= \frac{1}{\pi}\int_0^{\pi} d\tau \cos\left[q\sin\left(\tau\right)+l\tau\right] = J_{-l}(q),
\end{aligned}
\tag{C.8}
$$

where in the last step we used the integral representation of the Bessel function of the first kind $J_{-l}(q)$ [110].

C.1.2   Square drive

For a square drive, oscillating each period between 0 and $2V_{dc}$

$$
V_{sqr}(t) = 2V_{dc} \sum_{k=-\infty}^{+\infty} \Theta(t-k\mathcal{T})\Theta\left(\frac{\mathcal{T}}{2}-t+k\mathcal{T}\right),
\tag{C.9}
$$

the photo-assisted coefficient is

$$
\begin{aligned}
p_l &= \int_{-\frac{\mathcal{T}}{2}}^{\frac{\mathcal{T}}{2}} \frac{dt}{\mathcal{T}} e^{il\omega t} e^{-iq\omega|t|} = \int_{-\frac{\mathcal{T}}{2}}^{0} \frac{dt}{\mathcal{T}} e^{i(l+q)\omega t} + \int_0^{\frac{\mathcal{T}}{2}} \frac{dt}{\mathcal{T}} e^{i(l-q)\omega t} = \\
&= \frac{1}{2\pi i}\left[\frac{1-e^{-i\pi(l+q)}}{l+q} + \frac{e^{-i\pi(l+q)-1}}{l+q}\right] = \\
&= \frac{i}{\pi}\frac{q}{l^2-q^2}\left[1-(-1)^l e^{-i\pi q}\right].
\end{aligned}
\tag{C.10}
$$

The corresponding probability to absorb or emit l photons is

$$
P_l = |p_l|^2 = \left(\frac{q}{l+q}\frac{\sin\left[\frac{\pi}{2}(l-q)\right]}{\frac{\pi}{2}(l-q)}\right)^2.
\tag{C.11}
$$

C.1.3   Lorentzian drive

A periodic train of Lorentzian pulses with a mid-height width W and period $\mathcal{T} = \frac{2\pi}{\omega}$ is described by the function

$$
V_{lor}(t) = \frac{V_{dc}}{\pi} \sum_{k=-\infty}^{+\infty} \frac{W}{W^2+(t-k\mathcal{T})^2}.
\tag{C.12}
$$

The calculation for photo-assisted coefficient is a little more cumbersome for the Lorentzian drive than for cosine and square drives. It is useful to recast the phase ϕ_{ac} as

$$
\begin{aligned}
\phi_{ac}(t) &= \nu V_{dc} \int_0^t dt'\left[\sum_{k=-\infty}^{\infty} \frac{W}{W^2+(t-k\mathcal{T})^2} - 1\right] = \\
&= -2q \sum_{k=-\infty}^{\infty} \int_{-\frac{k\mathcal{T}}{W}}^{\frac{t}{W}-\frac{k\mathcal{T}}{W}} d\tau \frac{1}{1+\tau^2} + q\omega t = \\
&= -2q \sum_{k=-\infty}^{\infty} \left[\arctan\left(\frac{t}{W}-\frac{k\mathcal{T}}{W}\right) - \arctan\left(-\frac{k\mathcal{T}}{W}\right)\right] + q\omega t.
\end{aligned}
\tag{C.13}
$$

Since arctan is an odd function of its argument, the second term in the bracket is zero and one can rearrange the remaining terms as

$$\phi_{ac}(t) - q\omega t = -2q \sum_{k=-\infty}^{\infty} \left[\arctan\left(\frac{t}{W} - \frac{k\mathcal{T}}{W}\right) - \arctan\left(-\frac{k\mathcal{T}}{W}\right) \right] =$$

$$= -iq \sum_{k=-\infty}^{\infty} \ln\left(\frac{i + \frac{t}{W} - \frac{k\mathcal{T}}{W}}{i - \frac{t}{W} + \frac{k\mathcal{T}}{W}}\right) =$$

$$= -iq \left[\sum_{k=-\infty}^{\infty} \ln\left(k - i\frac{W+t}{\mathcal{T}}\right) - \sum_{k=-\infty}^{\infty} \ln\left(k - i\frac{W-t}{\mathcal{T}}\right) \right] =$$

$$= -iq \ln\left[\frac{\sin\left(i\pi\frac{W+t}{\mathcal{T}}\right)}{\sin\left(i\pi\frac{W-t}{\mathcal{T}}\right)} \right], \tag{C.14}$$

where the following identities have been exploited

$$\arctan(z) = \frac{i}{2} \ln\left(\frac{i+z}{i-z}\right), \tag{C.15}$$

$$\sum_{k=-\infty}^{\infty} \ln(k+\gamma) = \ln\left[\sin(\pi\gamma)\right] + \sum_{k=-\infty}^{\infty} \ln\left(k+\frac{1}{2}\right). \tag{C.16}$$

It is convenient to switch to write p_l as a complex integral with the substitution $z = e^{i\omega t}$

$$p_l = \int_{-\frac{\mathcal{T}}{2}}^{\frac{\mathcal{T}}{2}} \frac{dt}{\mathcal{T}} e^{il\omega t} e^{i\phi_{ac}(t)} =$$

$$= \int_{-\frac{\mathcal{T}}{2}}^{\frac{\mathcal{T}}{2}} \frac{dt}{\mathcal{T}} e^{i(l+q)\omega t} \left[\frac{\sin\left(i\pi\frac{W+t}{\mathcal{T}}\right)}{\sin\left(i\pi\frac{W-t}{\mathcal{T}}\right)} \right]^q =$$

$$= \frac{1}{2\pi i} \oint_{|z|=1} \frac{dz}{z} z^{l+q} \left(\frac{1-\gamma z}{z-\gamma}\right)^q, \tag{C.17}$$

where $\gamma = e^{-2\pi\eta}$. In the disc $|\xi| \leq 1$, the following generalized binomial series is valid [188]

$$(1-\xi)^\beta = 1 - \beta\xi + \cdots + (-1)^n \frac{\beta(\beta-1)\cdots(\beta-n+1)}{n!} \xi^n + \cdots =$$

$$= \sum_{n=0}^{\infty} (-1)^n \frac{\Gamma(\beta+1)}{\Gamma(\beta-n+1)} \frac{\xi^n}{n!}. \tag{C.18}$$

Since $|z| = 1$ and $\gamma < 1$, one can exploit it to recast p_l as

$$p_l = \frac{1}{2\pi i} \oint_{|z|=1} dz \sum_{n,m=0}^{\infty} (-1)^{n+m} \frac{\Gamma(1+q)}{\Gamma(1-n+q)} \frac{\Gamma(1-q)}{\Gamma(1-m-q)} \frac{z^{l+n-m-1}\gamma^{n+m}}{n!m!} \tag{C.19}$$

By using the fact that $\Gamma(m+1) = m!$ for $m \geq 0$ and $\frac{1}{\Gamma(m+1)} = 0$ for $m \leq -1$, the two sums can be extended to include negative values of m [110] as

$$p_l = \frac{1}{2\pi i} \oint_{|z|=1} dz \sum_{n}^{\infty} \sum_{m=-\infty}^{\infty} (-1)^{n+m} \frac{\Gamma(1+q)}{\Gamma(1-n+q)} \frac{\Gamma(1-q)}{\Gamma(1-m-q)} \frac{z^{l+n-m-1}\gamma^{n+m}}{n!\Gamma(m+1)}. \tag{C.20}$$

According to Cauchy's theorem, the only non-vanishing contribution to this integral comes from $l + n - m$, thus obtaining

$$p_l = \frac{1}{2\pi i} \oint_{|z|=1} dz \sum_{n}^{\infty} \sum_{m=-\infty}^{\infty} \delta_{m,l+n} (-1)^{n+m} \frac{\Gamma(1+q)}{\Gamma(1-n+q)} \frac{\Gamma(1-q)}{\Gamma(1-m-q)} \frac{\gamma^{n+m}}{n!\Gamma(m+1)} =$$

$$= \sum_{n=0}^{\infty} (-1)^l \frac{\Gamma(1+q)}{\Gamma(1-n+q)} \frac{\Gamma(1-q)}{\Gamma(1-n-l-q)} \frac{\gamma^{2n+l}}{n!\Gamma(n+l+1)} =$$

$$= \sum_{n=0}^{\infty} (-1)^l \frac{\Gamma(1+q)}{\Gamma(l+n+q)} \frac{\Gamma(1-q)}{\Gamma(1-n-l-q)} \frac{\Gamma(l+n+q)}{\Gamma(1-n+q)} \frac{\gamma^{2n+l}}{n!\Gamma(n+l+1)}. \qquad (C.21)$$

The property $\Gamma(\xi)\Gamma(1-\xi) = \frac{\pi}{\sin(\pi\xi)}$, which is valid for $\xi \neq 0, \pm 1, ...$, implies that

$$\frac{\Gamma(1+q)\Gamma(1-q)}{\Gamma(l+n+q)\Gamma(1-n-l-q)} = (-1)^{l+n}q, \qquad (C.22)$$

which can be exploited to finally find

$$p_l = q\gamma^l \sum_{n=0}^{\infty} (-1)^n \frac{\Gamma(l+n+q)}{\Gamma(1-n+q)} \frac{\gamma^{2n}}{n!\Gamma(n+l+1)} \qquad (C.23)$$

for non integer values of q. This last equation can be used for integer values of q as well, given the fact that $\lim_{q \to i} p_l$ with $i \in \mathbb{N}$ is well defined.

With the help of Eq. (C.17) one also realizes the uniqueness of the Lorentzian drive with integer q. Under this assumption the integrand function in Eq. (C.17) does not have any singularity outside the unit circle for $l < q$, even at infinity. This automatically translates into $p_l = 0$ for $l < q$.

C.1.4 Single leviton

In the following, we specialize to the case of $q = 1$, which is the simplest case that allows to evaluate explicitly the sum in Eq. (C.23). By plugging $q = 1$ into Eq. (C.23), one has

$$p_l = \frac{1}{2\pi i} \oint_{|z|=1} dz z^l \frac{1-z\gamma}{z-\gamma}. \qquad (C.24)$$

According to the value of l, there are three different cases.

1): $l \geq 0$. In this case, the function

$$f_l(z) = z^l \frac{1-z\gamma}{z-\gamma} \qquad (C.25)$$

has a single pole of order 1 in $z = \gamma$. By using Cauchy's theorem, we know that the only residue contributing to the integral is inside the unit circle and gives

$$p_l = \text{Res}\,[f_l(z), \gamma] = z^l(1-z\gamma)\Big|_{z=\gamma} = \gamma^l(1-\gamma^2). \qquad (C.26)$$

2): $l \leq -2$. The two poles $z = \gamma$ and $z = 0$ lie inside the unit circle, thus implying that the integrand is analytic everywhere outside the unit circle. For this reason, $p_l = 0$ for $l \leq -2$.

3): $l = -1$. For this value of l, $f_{-1}(z)$ has two poles in $z = \gamma$ and $z = 0$. According to Cauchy's theorem, one has

$$p_{-1} = \text{Res}\,[f_{-1}(z), \gamma] + \text{Res}\,[f_{-1}(z), 0] = \frac{1}{\gamma}(1-\gamma^2) - \frac{1}{\gamma} = -\gamma. \qquad (C.27)$$

Finally, the result for each value of l is

$$p_l(q = 1) = \begin{cases} \gamma^l(1 - \gamma^2) & \text{if } l \geq 0, \\ -\gamma & \text{if } l = -1, \\ 0 & \text{if } l \leq -2. \end{cases} \tag{C.28}$$

C.2 Hong-Ou-Mandel setup

Here, we consider the phase

$$e^{i\nu e \int_0^t dt' V_-(t')}, \tag{C.29}$$

with $V_-(t) = V_R(t) - V_L(t)$, which appears for charge noise and for a contribution to heat noise in a double-drive setup. This can be written in terms of a series as

$$e^{i\nu e \int_0^t dt' V_-(t')} = \sum_{l=-\infty}^{\infty} \tilde{p}_l e^{-i(l+q_R-q_L)\omega t}, \tag{C.30}$$

where we defined

$$\tilde{p}_l = \int_{-\frac{\mathcal{T}}{2}}^{\frac{\mathcal{T}}{2}} \frac{dt}{\mathcal{T}} e^{i(l+q_R-q_L)\omega t} e^{i\nu e \int_0^t dt' V_R(t')} e^{-i\nu e \int_0^t dt' V_L(t')} = \sum_{m=-\infty}^{\infty} p_{l+m+q_R-q_L,R} p_{m,L}^*. \tag{C.31}$$

In a Hong-Ou-Mandel setup, one has that $V_R(t) = V(t)$ and $V_L(t) = V(t+t_D)$, such that the photo-assisted coefficients become

$$\tilde{p}_l(t_D) = e^{i\nu e \int_0^{t_D} dt' [V(t') - V(t'+t_D)]} \sum_{m=-\infty}^{\infty} p_{l+m+q_R-q_L} p_m^* r^{im\omega t_D}. \tag{C.32}$$

Lorentzian drive

In the case of a periodic train of Lorentzian pulses in the HOM setup, one can find a simpler expression for photo-assisted coefficients

$$\tilde{p}_l = e^{i\nu e \int_0^{t_D} dt' [V_R(t') - V_R(t'+t_D)]} e^{-iq\omega t} \int_{-\frac{\mathcal{T}}{2}}^{\frac{\mathcal{T}}{2}} \frac{dt}{\mathcal{T}} e^{i2\pi l \frac{t}{\mathcal{T}}} \left[\frac{\sin\left(i\pi \frac{W+t}{\mathcal{T}}\right)}{\sin\left(i\pi \frac{W-t}{\mathcal{T}}\right)} \right]^q \left[\frac{\sin\left(i\pi \frac{W-t-t_D}{\mathcal{T}}\right)}{\sin\left(i\pi \frac{W+t+t_D}{\mathcal{T}}\right)} \right]^q =$$

$$= e^{i\nu e \int_0^{t_D} dt' [V_R(t') - V_R(t'+t_D)]} \frac{1}{2\pi i} \oint_{|z|=1} \frac{dz}{z} z^{l+q} \left(\frac{1 - \gamma z}{z - \gamma} \right)^q \left(\frac{\gamma\phi - z}{\gamma z - \phi} \right)^q, \tag{C.33}$$

with $\phi = e^{-i2\pi \frac{t_D}{\mathcal{T}}}$. For $q = 1$, one can simply use Cauchy theorem to evaluate $\tilde{p}_l$. One has to distinguish between three cases.

1): $l \geq 1$. The integrand function

$$\tilde{f}_l(z) = z^{l-1} \frac{(1 - z\gamma)\left(\phi - \frac{z}{\gamma}\right)}{(z - \gamma)\left(z - \frac{\phi}{\gamma}\right)} \tag{C.34}$$

has a pole at $z = \gamma$ and another one at $z = \frac{\phi}{\gamma}$ Since $|\phi| = 1$ and $\gamma < 1$, the only contribution to $\tilde{p}_l$ is

$$\tilde{p}_l = e^{-i\nu e \int_0^{t_D} dt' [V_R(t') - V_R(t'+t_D)]} \phi \text{Res}\left[\tilde{f}_l(z), \gamma\right] =$$

$$= e^{-i\nu e \int_0^{t_D} dt' [V_R(t') - V_R(t'+t_D)]} \phi \gamma^l \frac{(1 - \gamma^2)(1 - \phi)}{\phi - \gamma^2}. \tag{C.35}$$

2): $l \leq -1$. Under this condition, we can either look for the residues at $z = 0$ and $z = \gamma$ inside the circle or evaluate the residue at $z = \frac{\phi}{\gamma}$ outside the circle, with a change of sign. The latter gives

$$\tilde{p}_l = -e^{-i\nu e \int_0^{t_D} dt' [V_R(t') - V_R(t'+t_D)]} \phi \mathrm{Res}\left[\tilde{f}_l(z), \frac{\phi}{\gamma}\right] =$$
$$= e^{-i\nu e \int_0^{t_D} dt' [V_R(t') - V_R(t'+t_D)]} \phi^{l+1} \gamma^{-l} \frac{(1-\gamma^2)(1-\phi)}{\phi - \gamma^2}. \tag{C.36}$$

3): $l = 0$. The function $\tilde{f}_0(z)$ has residues at $z = 0$ and at $z = \gamma$ inside the unit circle. Thus

$$\tilde{p}_l = e^{-i\nu e \int_0^{t_D} dt' [V_R(t') - V_R(t'+t_D)]} \phi \mathrm{Res}\left[\tilde{f}_0(z), 0\right] +$$
$$+ e^{-i\nu e \int_0^{t_D} dt' [V_R(t') - V_R(t'+t_D)]} \phi \mathrm{Res}\left[\tilde{f}_0(z), \gamma\right] =$$
$$= e^{-i\nu e \int_0^{t_D} dt' [V_R(t') - V_R(t'+t_D)]} \left[1 + \frac{(1-\gamma^2)(1-\phi)}{\phi - \gamma^2}\right]. \tag{C.37}$$

C.3 Multiple pulses

Finally, let us briefly discuss the case of multiple pulses of Sec. 4.3.3. The phase accumulated for the periodic signal $V_N(t) = \sum_{j=0}^{N-1} \tilde{V}\left(t - j\frac{\alpha}{N}\mathcal{T}\right)$ is given by

$$\varphi_N(t) = \nu e \int_0^t dt' \left[\sum_{j=0}^{N-1} \tilde{V}\left(t' - j\frac{\alpha}{N}\mathcal{T}\right) - \tilde{V}_{dc}\right]$$
$$= \sum_{j=0}^{N-1} \left[\tilde{\varphi}\left(t - j\frac{\alpha}{N}\mathcal{T}\right) - \tilde{\varphi}\left(-j\frac{\alpha}{N}\mathcal{T}\right)\right], \tag{C.38}$$

where $\tilde{\varphi}(t) = \nu e \int_0^t dt' \left[\tilde{V}(t') - \tilde{V}_{dc}\right]$. Each phase factor $e^{-i\tilde{\varphi}(t)}$ can be written as

$$e^{i\tilde{\varphi}(t)} = \sum_l p_l\left(\frac{q}{N}\right) e^{-il\omega t}, \tag{C.39}$$

since each pulse $\tilde{V}$ involves only a fraction of the total charge q. The corresponding Fourier coefficients for $e^{-i\varphi_N(t)}$ read

$$p_l^{(N)}(q) = e^{\left[i\sum_{j=0}^{N-1} \tilde{\varphi}\left(-j\frac{\alpha}{N}\mathcal{T}\right)\right]} \int_0^{\mathcal{T}} \frac{dt}{\mathcal{T}} e^{il\omega t} \prod_{j=0}^{N-1} e^{i\tilde{\varphi}\left(t - j\frac{\alpha}{N}\mathcal{T}\right)} =$$
$$= e^{\left[i\sum_{j=0}^{N-1} \tilde{\varphi}\left(-j\frac{\alpha}{N}\mathcal{T}\right)\right]} \int_0^{\mathcal{T}} \frac{dt}{\mathcal{T}} e^{(il\omega t)} \sum_{m_0=-\infty}^{+\infty} \sum_{m_1=-\infty}^{+\infty} \cdots \sum_{m_{N-1}=-\infty}^{+\infty} e^{(-im_0\omega t)} p_{m_0}\left(\frac{q}{N}\right)$$
$$\times e^{\left\{-im_1\omega\left[t - \frac{\alpha}{N}\mathcal{T}\right]\right\}} p_{m_1}\left(\frac{q}{N}\right) \cdots e^{\left\{-im_{N-1}\omega\left[t - (N-1)\frac{\alpha}{N}\mathcal{T}\right]\right\}} p_{m_{N-1}}\left(\frac{q}{N}\right) =$$
$$= e^{\left[i\sum_{j=0}^{N-1} \tilde{\varphi}\left(-j\frac{\alpha}{N}\mathcal{T}\right)\right]} \sum_{m_1=-\infty}^{+\infty} \cdots \sum_{m_{N-1}=-\infty}^{+\infty} \exp\left\{i\frac{2\pi}{N}\alpha\left[m_1 + \cdots + (N-1)m_{N-1}\right]\right\}$$
$$\times p_{l-m_1-\ldots-m_{N-1}}\left(\frac{q}{N}\right) p_{m_1}\left(\frac{q}{N}\right) \cdots p_{m_{N-1}}\left(\frac{q}{N}\right). \tag{C.40}$$

As an example, coefficients for $N = 2$ are given by

$$p_l^{(2)}(q) = e^{-i\widetilde{\varphi}\left(-\frac{\alpha\mathcal{T}}{2}\right)} \sum_{m=-\infty}^{+\infty} e^{i\pi\alpha m} p_{l-m}\left(\frac{q}{2}\right) p_m\left(\frac{q}{2}\right). \tag{C.41}$$

Note that the time-independent phase $e^{i\widetilde{\varphi}\left(-\frac{\alpha\mathcal{T}}{2}\right)}$ has been omitted in Eq. (4.67) of the main text, as it is washed out as soon as we compute the squared modulus of $p_l^{(2)}$. Finally it is worth remarking that in the case of Lorentzian pulses with $q = N$ one should require $m_i \geq -1$ to prevent the vanishing of $p_l^{(N)}$.

C.4   Useful sum rule

In this section we prove the following sum rule for photo-assisted coefficients p_l

$$\sum_{l=-\infty}^{\infty} l^s |p_l|^2 = \left(\frac{\nu e}{\omega}\right)^s \int_{-\frac{\mathcal{T}}{2}}^{\frac{\mathcal{T}}{2}} \frac{dt}{\mathcal{T}} V_{ac}^s(t), \tag{C.42}$$

where s is an integer number. Firstly, we recast the sum as

$$\sum_{l=-\infty}^{\infty} l^s |p_l|^2 = \sum_{l=-\infty}^{\infty} l^s \int_{-\frac{\mathcal{T}}{2}}^{\frac{\mathcal{T}}{2}} \frac{dt}{\mathcal{T}} \int_{-\frac{\mathcal{T}}{2}}^{\frac{\mathcal{T}}{2}} \frac{dt'}{\mathcal{T}} e^{il\omega(t-t')} e^{i\phi_{ac}(t')-i\phi_{ac}(t)} =$$

$$= \int_{-\frac{\mathcal{T}}{2}}^{\frac{\mathcal{T}}{2}} \frac{dt}{\mathcal{T}} \int_{-\frac{\mathcal{T}}{2}}^{\frac{\mathcal{T}}{2}} \frac{dt'}{\mathcal{T}} \sum_{l=-\infty}^{\infty} l^s e^{il\omega(t-t')} e^{i\phi_{ac}(t')-i\phi_{ac}(t)} =$$

$$= \int_{-\frac{\mathcal{T}}{2}}^{\frac{\mathcal{T}}{2}} \frac{dt}{\mathcal{T}} \int_{-\frac{\mathcal{T}}{2}}^{\frac{\mathcal{T}}{2}} \frac{dt'}{\mathcal{T}} \sum_{l=-\infty}^{\infty} \left(\frac{i}{\omega}\right)^s \partial_{t'}^s e^{il\omega(t-t')} e^{i\phi_{ac}(t')-i\phi_{ac}(t)} =$$

$$= \int_{-\frac{\mathcal{T}}{2}}^{\frac{\mathcal{T}}{2}} \frac{dt}{\mathcal{T}} \int_{-\frac{\mathcal{T}}{2}}^{\frac{\mathcal{T}}{2}} \frac{dt'}{\mathcal{T}} \sum_{l=-\infty}^{\infty} \left(-\frac{i}{\omega}\right)^s \delta(t-t') e^{-i\phi_{ac}(t)} \partial_{t'}^s e^{i\phi_{ac}(t')} =$$

$$= \int_{-\frac{\mathcal{T}}{2}}^{\frac{\mathcal{T}}{2}} \frac{dt}{\mathcal{T}} \left(-\frac{i}{\omega}\right)^s e^{-i\phi_{ac}(t)} \partial_t^s e^{i\phi_{ac}(t)}. \tag{C.43}$$

It is easy to verify that the s-th derivative of the phase factor has the following form

$$\partial_t^s e^{i\phi_{ac}(t)} = D[V_{ac}(t)] e^{i\phi_{ac}(t)} + (i\nu e)^s V_{ac}^s(t) e^{i\phi_{ac}(t)}, \tag{C.44}$$

where $D[V_{ac}(t)]$ contains only first- and higher-order derivatives of $V_{ac}(t)$. Thus, it is clear that

$$\int_{-\frac{\mathcal{T}}{2}}^{\frac{\mathcal{T}}{2}} \frac{dt}{\mathcal{T}} e^{-i\phi_{ac}(t)} \partial_t^s e^{i\phi_{ac}(t)} = (i\nu e)^s V_{ac}^s(t) e^{i\phi_{ac}(t)}, \tag{C.45}$$

which implies that

$$\sum_{l=-\infty}^{\infty} l^s |p_l|^2 = \left(\frac{\nu e}{\omega}\right)^s \int_{-\frac{\mathcal{T}}{2}}^{\frac{\mathcal{T}}{2}} \frac{dt}{\mathcal{T}} V_{ac}^s(t). \tag{C.46}$$

Notice in particular that $\sum_l |p_l|^2 = 1$ and $\sum_l l|p_l|^2 = 0$. One can also add the dc component $q = \frac{\nu e}{\omega} V_{dc}$, in order to find that

$$
\begin{aligned}
\sum_{l=-\infty}^{+\infty} |p_l|^2 (q+l)^2 &= \sum_l |p_l|^2 \sum_{k=0}^{s} \binom{s}{k} q^{s-k} l^k = \\
&= \sum_{k=0}^{s} \binom{s}{k} \left(\frac{\nu e V_{dc}}{\omega}\right)^{s-k} \left(\frac{\nu e}{\omega}\right)^k \int_{-\frac{T}{2}}^{\frac{T}{2}} \frac{dt}{T} V_{ac}^k(t) = \\
&= \left(\frac{\nu e}{\omega}\right)^s \int_{-\frac{T}{2}}^{\frac{T}{2}} \frac{dt}{T} \left[\sum_{k=0}^{s} \binom{s}{k} V_{dc}^{s-k} V_{ac}^k\right] = \\
&= \left(\frac{\nu e}{\omega}\right)^s \int_{-\frac{T}{2}}^{\frac{T}{2}} \frac{dt}{T} [V_{dc} + V_{ac}] = \left(\frac{\nu e}{\omega}\right)^s \int_{-\frac{T}{2}}^{\frac{T}{2}} \frac{dt}{T} V^s(t). \quad \text{(C.47)}
\end{aligned}
$$

Appendix D

Second order expansion in tunneling

In this Appendix, we deal with the description of tunneling processes in the presence of a QPC in the FQH regime. In strongly correlated systems, we cannot rely on scattering matrix approach, presented in Chapter 2, which is valid solely for non-interacting electrons. In order to describe tunneling processes in the FQH regime, we introduced in the main text the following tunneling hamiltonians [36, 116]

$$H_T^{(qp)} = \Lambda \Psi_R^{(qp)\dagger}(0)\Psi_L^{(qp)}(0) + \text{h.c.}, \tag{D.1}$$

$$H_T^{(el)} = \Lambda \Psi_R^{(el)\dagger}(0)\Psi_L^{(el)}(0) + \text{h.c.}. \tag{D.2}$$

In the weak backscattering regime, tunneling amplitude Λ is assumed to be very small. Therefore, tunneling hamiltonian can be treated as a small perturbation with respect to the hamiltonian $H_0 + H_g$ (see Eqs. (3.1) and (3.2)). In the following, we will construct the time evolution of a generic quantum operator O in terms of perturbative series in the parameter Λ. This expansion is exploited in the main text for the specific case of charge and heat transport properties (see Eqs. (D.16) and (4.5)).

The time evolution for an operator O with respect to the total hamiltonian $H_0 + H_g + H_T^{(qp/el)}$ can be written in terms of the time evolution operator $U_I(t, -\infty) = Te^{-i\int_{-\infty}^t dt'\, H_T^{(qp/el)}(t')}$, with T time ordering operator, as

$$O(x,t) = U_I^\dagger(t, -\infty)O_I(x,t)U_I(t, -\infty). \tag{D.3}$$

Here, the operator $O_I(x,t)$ and the hamiltonians $H_T^{(qp/el)}(t)$ evolve in time in an interaction picture according to $H_0 + H_g$.

According to Eqs. (B.11) and (B.12), the time-dependent tunneling hamiltonians are

$$H_T^{(qp)} = \Lambda \Psi_R^{(qp)\dagger}(0,t)\Psi_L^{(qp)}(0,t) + \text{h.c.} =$$
$$= \Lambda e^{i\nu e \int_0^t d\tau (V_R(\tau) - V_L(\tau))} \psi_R^{(qp)\dagger}(0,t)\psi_L^{(qp)}(0,t) + \text{h.c.}, \tag{D.4}$$

and

$$H_T^{(el)} = \Lambda \Psi_R^{(el)\dagger}(0,t)\Psi_L^{(el)}(0,t) + \text{h.c.} =$$
$$= \Lambda e^{i\nu e \int_0^t d\tau (V_R(\tau) - V_L(\tau))} \psi_R^{(el)\dagger}(0,t)\psi_L^{(el)}(0,t) + \text{h.c.}. \tag{D.5}$$

Time evolution operators in Eq. (D.3) can be expanded with respect to tunneling hamiltonians. We truncate this perturbative expansion at second order, since it corresponds to the lowest order for the transport properties we are interested in. One finds for time evolution operator that

$$
U_I(t, -\infty) = \mathbf{1} + i \int_{-\infty}^{t} dt' \, H_T^{(qp/el)}(t') +
$$
$$
- \int_{-\infty}^{t} dt'' \int_{-\infty}^{t} dt' \, \Theta(t'' - t') H_T^{(qp/el)}(t') H_T^{(qp/el)}(t'') + \mathcal{O}(|\Lambda|^3). \quad \text{(D.6)}
$$

By inserting this result into Eq. (D.3), the operator $O(x, t)$ at second order in tunneling amplitude is

$$
O(x, t) =
$$
$$
= \left(\mathbf{1} + i \int_{-\infty}^{t} dt' \, H_T^{(qp/el)}(t') + \right.
$$
$$
\left. - \int_{-\infty}^{t} dt'' \int_{-\infty}^{t} dt' \, \Theta(t'' - t') H_T^{(qp/el)}(t') H_T^{(qp/el)}(t'') \right) O_I(x, t) \times
$$
$$
\times \left(\mathbf{1} - i \int_{-\infty}^{t} dt' \, H_T^{(qp/el)}(t') + \right.
$$
$$
\left. - \int_{-\infty}^{t} dt'' \int_{-\infty}^{t} dt' \, \Theta(t' - t'') H_T^{(qp/el)}(t') H_T^{(qp/el)}(t'') \right) + \mathcal{O}\left(|\Lambda|^3\right) =
$$
$$
= O_I(x, t) + i \int_{-\infty}^{t} dt' \left[H_T^{(qp/el)}(t') O_I(x, t) - O_I(x, t) H_T^{(qp/el)}(t') \right] +
$$
$$
+ \int_{-\infty}^{t} dt'' \int_{-\infty}^{t} dt' \, H_T^{(qp/el)}(t') O_I(x, t) H_T^{(qp/el)}(t'') +
$$
$$
- \int_{-\infty}^{t} dt'' \int_{-\infty}^{t} dt' \, \Theta(t'' - t') H_T^{(qp/el)}(t') H_T^{(qp/el)}(t'') O_I(x, t) +
$$
$$
- \int_{-\infty}^{t} dt'' \int_{-\infty}^{t} dt' \, \Theta(t' - t'') O_I(x, t) H_T^{(qp/el)}(t') H_T^{(qp/el)}(t'') + \mathcal{O}\left(|\Lambda|^3\right).
$$
$$
\text{(D.7)}
$$

In the last two lines a tunneling hamiltonian can be commuted with the operator O_I, in order to write both of them in the same form of the fourth line of Eq. (D.7)

In this way one obtains

$$
\begin{aligned}
O(x,t) = O_I(x,t) + i \int_{-\infty}^{t} dt' \; \left[H_T^{(qp/el)}(t'), O_I(x,t) \right] + \\
+ \int_{-\infty}^{t} dt'' \int_{-\infty}^{t} dt' \; H_T^{(qp/el)}(t') O_I(x,t) H_T^{(qp/el)}(t'') + \\
- \int_{-\infty}^{t} dt'' \int_{-\infty}^{t} dt' \; \Theta(t'' - t') H_T^{(qp/el)}(t') O_I(x,t) H_T^{(qp/el)}(t'') + \\
- \int_{-\infty}^{t} dt'' \int_{-\infty}^{t} dt' \; \Theta(t' - t'') H_T^{(qp/el)}(t') O_I(x,t) H_T^{(qp/el)}(t'') + \\
- \int_{-\infty}^{t} dt'' \int_{-\infty}^{t} dt' \; \Theta(t'' - t') H_T^{(qp/el)}(t') \left[H_T^{(qp/el)}(t''), O_I(x,t) \right] + \\
- \int_{-\infty}^{t} dt'' \int_{-\infty}^{t} dt' \; \Theta(t' - t'') \left[O_I(x,t), H_T^{(qp/el)}(t') \right] H_T^{(qp/el)}(t'') + \mathcal{O}\left(|\Lambda|^3 \right).
\end{aligned}
\tag{D.8}
$$

We notice that when the addends in the third and fourth lines are summed up, they cancel exactly the second line, thus finding

$$
\begin{aligned}
O(x,t) = O_I(x,t) + i \int_{-\infty}^{t} dt' \; \left[H_T^{(qp/el)}(t'), O_I(x,t) \right] + \\
- \int_{-\infty}^{t} dt'' \int_{-\infty}^{t} dt' \; \Theta(t'' - t') H_T^{(qp/el)}(t') \left[H_T^{(qp/el)}(t''), O_I(x,t) \right] + \\
- \int_{-\infty}^{t} dt'' \int_{-\infty}^{t} dt' \; \Theta(t' - t'') \left[O_I(x,t), H_T^{(qp/el)}(t') \right] H_T^{(qp/el)}(t'') + \mathcal{O}\left(|\Lambda|^2 \right) = \\
= O_I(x,t) + i \int_{-\infty}^{t} dt' \; \left[H_T^{(qp/el)}(t'), O_I(x,t) \right] + \\
- \int_{-\infty}^{t} dt'' \int_{-\infty}^{t} dt' \; \Theta(t' - t'') H_T^{(qp/el)}(t'') \left[H_T^{(qp/el)}(t'), O_I(x,t) \right] + \\
+ \int_{-\infty}^{t} dt'' \int_{-\infty}^{t} dt' \; \Theta(t' - t'') \left[H_T^{(qp/el)}(t'), O_I(x,t) \right] H_T^{(qp/el)}(t'') + \mathcal{O}\left(|\Lambda|^3 \right),
\end{aligned}
\tag{D.9}
$$

where we exchanged times in the second line and the order of operators in the last commutator. Finally, noticing that the terms in the last line add up to form a commutator and using that $-1 = i^2$, we get

$$
\begin{aligned}
O(x,t) = O_I(x,t) + i \int_{-\infty}^{t} dt' \; \left[H_T^{(qp/el)}(t'), O_I(x,t) \right] + \\
+ i \int_{-\infty}^{t} dt' \int_{-\infty}^{t} dt'' \; \Theta(t' - t'') \left[H_T^{(qp/el)}(t''), i \left[H_T^{(qp/el)}(t'), O_I(x,t) \right] \right] + \mathcal{O}(|\Lambda|^3).
\end{aligned}
\tag{D.10}
$$

Finally, we can put this expression in the form of a perturbative series in powers of Λ as

$$
O(x,t) = O(x,t)^{(0)} + O(x,t)^{(1)} + O(x,t)^{(2)} + \mathcal{O}(\Lambda^3),
\tag{D.11}
$$

147

where

$$O^{(0)}(x,t) = O_I(x,t), \tag{D.12}$$

$$O^{(1)}(x,t) = +i \int_{-\infty}^{t} dt' \left[H_T^{(qp/el)}(t'), O_I(x,t) \right], \tag{D.13}$$

$$O^{(2)}(x,t) = +i \int_{-\infty}^{t} dt' \int_{-\infty}^{t} dt'' \, \Theta(t'-t'') \left[H_T^{(qp/el)}(t''), i \left[H_T^{(qp/el)}(t'), O_I(x,t) \right] \right]. \tag{D.14}$$

D.1 Perturbative expansion of charge current operators

Charge current operators for right- and left-moving modes are defined as (see Eq. (3.7) of the main text)

$$J_{R/L}(x,t) = \mp ev\rho_{R/L}(x,t), \tag{D.15}$$

where $\rho_{R/L}(x,t)$ are density operators evolving with respect to the whole hamiltonian $H_0 + H_g + H_T^{(qp)}$. In order to treat perturbatively charge currents, one has simply to write down the second order expansion of density operators in the parameter Λ, which can be obtained by considering Eq. (D.11) in the case of operators $\rho_{R/L}(x,t)$ and reads (see Eq. (D.11))

$$\rho_{R/L}(x,t) = \rho_{R/L}^{(0)}(x,t) + \rho_{R/L}^{(1)}(x,t) + \rho_{R/L}^{(2)}(x,t) + \mathcal{O}(\Lambda^3), \tag{D.16}$$

where

$$\rho_{R/L}^{(0)}(x,t) = \mp \frac{\sqrt{\nu}}{2\pi} \partial_x \Phi_{R/L}(x,t), \tag{D.17}$$

$$\rho_{R/L}^{(1)}(x,t) = +i \int_{-\infty}^{t} dt' \left[H_T^{(qp)}(t'), \rho_{R/L}^{(0)}(x,t) \right], \tag{D.18}$$

$$\rho_{R/L}^{(2)}(x,t) = +i \int_{-\infty}^{t} dt' \int_{-\infty}^{t} dt'' \, \Theta(t'-t'') \left[H_T^{(qp)}(t''), i \left[H_T^{(qp)}(t'), \rho_{R/L}^{(0)}(x,t) \right] \right]. \tag{D.19}$$

It is extremely useful to further simplify the commutator in Eq. (D.18)

$$\left[H_T^{(qp)}(t'), \rho_{R/L}^{(0)}(x,t) \right] = \mp \frac{\sqrt{\nu}}{2\pi} \left[\Lambda \Psi_R^{(qp)\dagger}(0,t') \Psi_L^{(qp)}(0,t') + \text{h.c.}, \partial_x \Phi_{R/L}(x,t) \right]. \tag{D.20}$$

For the sake of simplicity, we consider only right-moving modes and we quote the results for left-movers in the end. We should pay attention that the commutator in Eq. (D.18) involves two different times t and t' and, therefore, usual commutation relations are not directly applicable. The trick is to exploit chirality of edge states to recast it as

$$\left[H_T^{(qp)}(t'), \rho_R^{(0)}(x,t) \right] =$$
$$= -\Lambda \frac{\sqrt{\nu}}{2\pi} e^{i\nu e \int_0^{t'} d\tau (V_R(\tau) - V_L(\tau))} \left[\psi_R^{(qp)\dagger}(-vt',0), \partial_x \Phi_R(x-vt,0) \right] \psi_L^{(qp)}(-vt',0) + \text{h.c.}. \tag{D.21}$$

Now, the commutator $\left[\psi_R^{(qp)\dagger}(-vt',0), \partial_x \Phi_R(x-vt,0) \right]$ can be evaluated by the help of bosonization identity and Baker-Hausdorff theorem [36]

$$\left[e^A, B \right] = [A,B]e^A \tag{D.22}$$

148

as

$$\left[\psi_R^{(qp)\dagger}(-vt',0), \partial_x\Phi_R(x-vt,0)\right] = \frac{\mathcal{F}_R^\dagger}{\sqrt{2\pi a}}e^{ik_F vt'}\left[e^{i\sqrt{\nu}\Phi_R(-vt',0)}, \partial_x\Phi_R(x-vt,0)\right] =$$

$$= i\sqrt{\nu}\left[\Phi_R(-vt',0), \partial_x\Phi_R(x-vt,0)\right]\psi_R^{(qp)\dagger}(-vt',0) =$$

$$= \sqrt{\nu}2\pi\delta(x-v(t-t'))\psi_R^{(qp)\dagger}(-vt',0), \tag{D.23}$$

where in the intermediate step we used the relation

$$\left[\Phi_{R/L}(x), \partial_y\Phi_{R/L}(y)\right] = \mp i2\pi\delta(x-y). \tag{D.24}$$

By inserting Eq. (D.23) into Eq. (D.21) , one finds

$$\left[H_T^{(qp)}(t'), \rho_R^{(0)}(x,t)\right] =$$

$$= -\Lambda e\nu\Theta(x)\Psi_R^{(qp)\dagger}\left(0, t-\frac{x}{v}\right)\Psi_L^{(qp)}\left(0, t-\frac{x}{v}\right)\delta\left(x-v(t-t')\right) + \text{h.c.}. \tag{D.25}$$

Similarly for left-moving particle, one finds

$$\left[H_T^{(qp)}(t'), \rho_L^{(0)}(x,t)\right] =$$

$$= -\Lambda e\nu v\Theta(-x)\Psi_R^{(qp)\dagger}\left(0, t+\frac{x}{v}\right)\Psi_L^{(qp)}\left(x-vt,0\right)\delta\left(x+v(t-t')\right) + \text{h.c.}. \tag{D.26}$$

By using the result for this commutator, the tunneling-dependent contributions to current in Eq. (D.18) and Eq. (D.19) can be simplified to

$$\rho_{R/L}^{(1)}(x,t) = -i\Theta(\pm x)\frac{\Lambda\nu}{v}\Psi_R^{(qp)\dagger}\left(0, t\mp\frac{x}{v}\right)\Psi_L^{(qp)}\left(0, t\mp\frac{x}{v}\right) + \text{h.c.}, \tag{D.27}$$

$$\rho_{R/L}^{(2)}(x,t) = -i\Theta(\pm x)\int_{-\infty}^{t\mp\frac{x}{v}}dt''\left[H_T^{(qp)}(t''), +i\frac{\Lambda\nu}{v}\Psi_R^{(qp)\dagger}\left(0, t\mp\frac{x}{v}\right)\Psi_L^{(qp)}\left(0, t\mp\frac{x}{v}\right) + \text{h.c.}\right]. \tag{D.28}$$

Let us observe that this contribution exist only for $x > 0$, in accordance with the fact that the effects of tunneling on right-moving particles exist solely downstream of the QPC. A similar result holds true for left-moving particle, where, in that case, tunneling affects transport only for $x < 0$.

Operators for charge current entering reservoir 2 and 3 are

$$J_{2/3}(t) = J_{R/L}(\pm d, t). \tag{D.29}$$

The expansion of $J_{2/3}$ in terms of the parameter Λ can be obtained from Eq. (D.16)

$$J_{2/3}(t) = J_{2/3}^{(0)}(t) + J_{2/3}^{(1)}(t) + J_{2/3}^{(2)}(t) + \mathcal{O}(\Lambda^3), \tag{D.30}$$

where

$$J_{2/3}^{(0)}(t) = \frac{ev\sqrt{\nu}}{2\pi}\left(\partial_x\Phi_{R/L}(x,t)\right)_{x=\pm d}, \tag{D.31}$$

$$J_{2/3}^{(1)}(t) = \pm i\Lambda e\nu\Psi_R^\dagger\left(0, t-\frac{d}{v}\right)\Psi_L\left(0, t-\frac{d}{v}\right) + \text{h.c.}, \tag{D.32}$$

$$J_{2/3}^{(2)}(t) = \pm i\int_{-\infty}^{t-\frac{d}{v}}dt''\left[H_T^{(qp)}(t''), +i\Lambda e\nu\Psi_R^{(qp)\dagger}\left(0, t-\frac{d}{v}\right)\Psi_L^{(qp)}\left(0, t-\frac{d}{v}\right) + \text{h.c.}\right]. \tag{D.33}$$

Appendix E

Bosonic correlator and Green's functions

In this Appendix, we evaluate the bosonic correlation function,

$$\mathcal{W}_{R/L}(x,t) = \left\langle \phi_{R/L}(x,t)\phi_{R/L}(0,0) \right\rangle - \left\langle \phi_{R/L}^2(0,0) \right\rangle, \tag{E.1}$$

where the bosonic fields $\phi_{R/L}(x,t)$ evolve accordingly to the edge hamiltonian

$$H = \frac{v}{4\pi} \int_{-\infty}^{+\infty} dx \left[(\partial_x \Phi_R(x))^2 + (\partial_x \Phi_L(x))^2 \right], \tag{E.2}$$

and their expression in terms of bosonic annihilation and creation operators $b_{q,R/L}$ and $b_{q,R/L}^\dagger$ read

$$\phi_{R/L}(x,t) = i\sqrt{\frac{2\pi}{L}} \sum_{q>0} \frac{e^{-\frac{aq}{2}}}{\sqrt{q}} \left[e^{-iq(vt\mp x)} b_{q,R/L} - e^{iq(vt\mp x)} b_{q,R/L}^\dagger \right]. \tag{E.3}$$

The average in Eq. (E.1) is taken with respect to the equilibrium density matrix $\rho_{eq} = e^{-\frac{H}{\theta}}$, where θ is the system temperature and we assumed $k_B = 1$. For the evaluation of Eq. (E.1), it is useful to write down the following average values over ρ_{eq} satisfied by bosonic annihilation and creation operators

$$\langle b_{q,R/L} b_{q',R/L} \rangle = \langle b_{q,R/L}^\dagger b_{q',R/L}^\dagger \rangle = 0, \tag{E.4}$$

$$\langle b_{q,R/L}^\dagger b_{q',R/L} \rangle = \delta_{q,q'} \frac{1}{e^{\frac{vq}{\theta}} - 1}, \tag{E.5}$$

$$\langle b_{q,R/L} b_{q',R/L}^\dagger \rangle = \delta_{q,q'} \frac{e^{\frac{vq}{\theta}}}{e^{\frac{vq}{\theta}} - 1}. \tag{E.6}$$

By exploiting Eqs. (E.4),(E.5) and (E.6), one can obtain the following relation

$$\left\langle \phi_{R/L}(x,t)\phi_{R/L}(0,0) \right\rangle = \frac{2\pi}{L} \sum_{q>0} \frac{e^{-aq}}{q} \left[e^{-iq(vt\mp x)} \left(\frac{1}{e^{\frac{vq}{\theta}}} + 1 \right) + \frac{e^{iq(vt\mp x)}}{e^{\frac{vq}{\theta}}} \right]. \tag{E.7}$$

By taking the continuous limit $(L \to +\infty)$

$$\frac{2\pi}{L} \sum_{q>0} \to \int_0^{+\infty} dq, \tag{E.8}$$

and plugging the result into Eq. (E.1), one finds

$$\mathcal{W}_{R/L}(x,t) = \int_0^{+\infty} dq \, \frac{e^{-aq}}{q} \left[\frac{e^{\frac{vq}{\theta}}}{e^{\frac{vq}{\theta}}-1} \left(e^{-iq(vt\mp x)} - 1 \right) + \frac{1}{e^{\frac{vq}{\theta}}-1} \left(e^{iq(vt\mp x)} - 1 \right) \right].$$
(E.9)

It is convenient to recast this expression as a sum of a zero temperature and a finite temperature contributions as

$$\mathcal{W}_{R/L}(x,t) = \mathcal{W}_{R/L;0}(x,t) + \mathcal{W}_{R/L;\theta}(x,t),$$
(E.10)

where

$$\mathcal{W}_{R/L;0}(x,t) = -\int_0^{+\infty} dq \, \frac{e^{-aq}}{q} \left[(1 - \cos q(vt \mp x)) - i\eta \sin q(vt \mp x) \right],$$
(E.11)

$$\mathcal{W}_{R/L;\theta}(x,t) = -\int_0^{+\infty} dq \, \frac{e^{-aq}}{q} \left(1 - \cos q(vt \mp x) \right) \left(\coth \frac{vq}{2\theta} - 1 \right).$$
(E.12)

Let us observe that the last term vanishes at $\theta = 0$, since

$$\lim_{\theta \to 0} \left(\coth \frac{vq}{2\theta} - 1 \right) = \lim_{\theta \to 0} \left(\frac{e^{\frac{vq}{2\theta}} - e^{-\frac{vq}{2\theta}}}{e^{\frac{vq}{2\theta}} + e^{-\frac{vq}{2\theta}}} \right) = 0.$$
(E.13)

E.1 Correlation function at $\theta = 0$

The complex exponential in Eq. (E.11) can be written as a power series, thus finding

$$\mathcal{W}_{R/L;0}(x,t) = -\int_0^{+\infty} dq \, \frac{e^{-aq}}{q} \left(1 - e^{iq(x\mp vt)} \right) =$$

$$= \int_0^{+\infty} dq \, e^{-aq} \sum_{n=1}^{+\infty} \frac{(\pm i \, (vt \mp x))^n}{n!} q^{n-1},$$
(E.14)

By defining $y = aq$, one can write

$$\mathcal{W}_{R/L;0}(x,t) = \sum_{n=1}^{+\infty} \left(\frac{i\eta \, (vt \mp x)}{a} \right)^n \frac{1}{n!} \int_0^{+\infty} dy \, e^{-y} y^{n-1}.$$
(E.15)

Then, we use the integral representation of the Gamma function

$$\Gamma(n) = \int_0^{+\infty} dy \, e^{-y} y^{n-1} = (n-1)!,$$
(E.16)

in order to obtain

$$\mathcal{W}_{R/L;0}(x,t) = \sum_{n=1}^{+\infty} \frac{1}{n} \left(\frac{i\eta \, (x \mp vt)}{a} \right)^n.$$
(E.17)

Finally, by recalling the identity

$$\ln(1-x) = -\sum_{n=1}^{+\infty} \frac{x^n}{n},$$
(E.18)

one has

$$\mathcal{W}_{R/L;0}(x,t) = \ln \frac{1}{1 + \frac{i(vt\mp x)}{a}}.$$
(E.19)

E.2   Correlation function at finite temperature

We recast Eq. (E.12) as

$$\mathcal{W}_{R/L;\theta}(x,t) = \int_0^{+\infty} dq \, \frac{e^{-\frac{aq}{q}}}{q} \left(2 - e^{iq(vt\mp x)} - e^{-iq(vt\mp x)} \right) \frac{e^{-\frac{vq}{\theta}}}{1 - e^{-\frac{vq}{\theta}}}. \qquad (E.20)$$

By defining $y = \frac{vq}{\theta}$ and $\omega_c = \frac{v}{a}$, we can write the above equation in the following form

$$\mathcal{W}_{R/L;\theta}(x,t) = -\int_0^{+\infty} dy \, \frac{1}{y \, (1 - e^{-y})} \Bigg(2 e^{-\left(1+\frac{\omega_c}{\theta}\right)y} - e^{-\left(1+\frac{\omega_c}{\theta} - \frac{i\theta(vt\mp x)}{v}\right)y}$$

$$- e^{-\left(1+\frac{\omega_c}{\theta} + \frac{i\theta(vt\mp x)}{v}\right)y} \Bigg). \qquad (E.21)$$

Let us recall the definition of the Hurwitz Zeta function [110]

$$\zeta(\gamma, \delta) = \frac{1}{\Gamma(\gamma)} \int_0^{+\infty} dt \, \frac{e^{-\delta t}}{t^{1-\gamma} \, (1 - e^{-t})}, \qquad (E.22)$$

and let us write Eq. (E.20) as

$$W_{R/L;\theta}(x,t) = -\lim_{\gamma \to 0} \Gamma(\gamma) \tilde{\zeta}(\gamma), \qquad (E.23)$$

where

$$\tilde{\zeta}(\gamma) = 2\zeta \left(\gamma, 1 + \frac{\omega_c}{\theta} \right) - \zeta \left(\gamma, 1 + \frac{\omega_c}{\theta} - \frac{i\theta(vt\mp x)}{v} \right)$$

$$- \zeta \left(\gamma, 1 + \frac{\omega_c}{\theta} + \frac{i\theta(vt\mp x)}{v} \right). \qquad (E.24)$$

In the limit $\gamma \to 0$, the following asymptotic relations hold true [110]

$$\Gamma(\gamma) = \frac{1}{\gamma} + O \left(\frac{1}{\gamma^2} \right), \qquad (E.25)$$

$$\zeta(\gamma, \delta) = \frac{1}{2} - \delta + \left(\ln \Gamma(\delta) + \ln \frac{2\pi}{2} \right) \gamma + O \left(\gamma^2 \right). \qquad (E.26)$$

By exploiting Eqs. (E.25) and (E.26), the function in Eq. (E.23) becomes

$$\mathcal{W}_{R/L;\theta}(x,t) = \ln \frac{\left| \Gamma \left(1 + \frac{\theta}{\omega_c} - i\theta(vt\mp x) \right) \right|^2}{\Gamma^2 \left(1 + \frac{\theta}{\omega_c} \right)}. \qquad (E.27)$$

E.2.1   Correlation function at any temperature

Recasting together the two results according to Eq. (E.10), one obtains

$$\mathcal{W}_{R/L}(x,t) = \ln \left[\frac{\left| \Gamma \left(1 + \frac{\theta}{\omega_c} - i\theta(t\mp \frac{x}{v}) \right) \right|^2}{\Gamma^2 \left(1 + \frac{\theta}{\omega_c} \right) \left(1 + i\omega_c \left(t \mp \frac{x}{v} \right) \right)} \right]. \qquad (E.28)$$

In conclusion, let us observe that correlation function has the following dependence on x and t

$$\mathcal{W}_{R/L}(x,t) = \mathcal{W}_{R/L}(x \mp vt, 0). \tag{E.29}$$

Therefore, one can define a function with a single argument $z = t \mp \frac{x}{v}$ as

$$W(z) = \ln\left[\frac{\left|\Gamma\left(1 + \frac{\theta}{\omega_c} - i\theta z\right)\right|^2}{\Gamma^2\left(1 + \frac{\theta}{\omega_c}\right)(1 + i\omega_c z)}\right], \tag{E.30}$$

which appears in the main text in Eq. (3.27).

Since ω_c is the high-energy cut-off, we will always work in the limit $\omega_c \gg \theta$. In this regime, we can use the identity

$$|\Gamma(1 + iy)|^2 = \frac{\pi y}{\sinh(\pi y)}, \quad y \in \mathbb{R}, \tag{E.31}$$

so that Eq. (E.30) becomes

$$W(z) = \ln\left[\frac{\pi\theta z}{\sinh(\pi\theta z)} \frac{1}{1 + i\omega_c z}\right]. \tag{E.32}$$

Appendix F

Fourier transform of $\mathcal{P}_g(t)$

In this Appendix, we calculate the Fourier transform of $\mathcal{P}_g(t) = e^{gW(t)}$

$$\tilde{\mathcal{P}}_g(E) = \int_{-\infty}^{\infty} dt e^{iEt} \mathcal{P}_g(t) = \int_{-\infty}^{\infty} dt e^{iEt} e^{gW(t)}, \tag{F.1}$$

where

$$W(t) = \ln \frac{\left| \Gamma \left(1 + \frac{\theta}{\omega_c} - i\theta t \right) \right|}{\Gamma \left(1 + \frac{\theta}{\omega_c} \right) (1 + i\omega_c t)}. \tag{F.2}$$

In addition, we derive some useful formulas that involve $\tilde{\mathcal{P}}_g(E)$.

It is useful to recast the function $W(t)$ in the limit $\frac{\omega_c}{\theta} \gg 1$, as it appears in Eq. (E.32). For completeness, we report its expression

$$W(t) = \ln \left[\frac{\pi t \theta}{(1 + i\omega_c t) \sinh (\pi t \theta)} \right]. \tag{F.3}$$

By inserting Eq. (F.3) into (F.1), one finds

$$\tilde{\mathcal{P}}_g(E) = \int_{-\infty}^{+\infty} dt e^{iEt} \left[\frac{\pi t}{1 + i\omega_c t} \frac{\theta}{\sinh (\pi t \theta)} \right]^g. \tag{F.4}$$

First of all, let us switch variable of integration as $\tilde{t} = \omega_c t - i$

$$\tilde{\mathcal{P}}_g(E) = \frac{1}{\omega_c} \int_{-\infty-i}^{+\infty-i} d\tilde{t} e^{iE \frac{\tilde{t}+i}{\omega_c}} \left[\frac{\pi \frac{\tilde{t}+i}{\omega_c}}{i\tilde{t}} \frac{\theta}{\sinh \left(\pi \frac{\tilde{t}+i}{\omega_c} \theta \right)} \right]^g. \tag{F.5}$$

In the approximation $\omega_c t \gg 1$, $\tilde{t} + i \approx \tilde{t}$: then, by substituting $t' = \frac{\tilde{t}}{\omega_c}$, one obtains

$$\tilde{\mathcal{P}}_g(E) = e^{-\frac{E}{\omega_c}} \int_{-\infty-\frac{i}{\omega_c}}^{+\infty-\frac{i}{\omega_c}} dt' e^{iEt'} \left[\frac{\pi \theta}{\omega_c} \frac{1}{i \sinh (\pi t' \theta)} \right]^g. \tag{F.6}$$

Finally, let us substitute $t' = t - \frac{i}{2T}$, thus finding

$$\tilde{\mathcal{P}}_g(\omega) = e^{-\frac{E}{\omega_c}} e^{\frac{E}{2\theta}} \int_{-\infty-\frac{i}{\omega_c}+\frac{i}{2\theta}}^{+\infty-\frac{i}{\omega_c}+\frac{i}{2\theta}} dt e^{iEt} \left[\frac{\pi \theta}{\omega_c} \frac{1}{\cosh (\pi t \theta)} \right]^g, \tag{F.7}$$

since $i \sinh(x - \frac{i\pi}{2}) = \cosh(x)$.

Let us observe that, the integral can be restricted to the real axis: by calling $F(t)$ the integrand function in Eq. (F.7)

$$\int_{-\infty - \frac{i}{\omega_c} + \frac{i}{2T}}^{\infty - \frac{i}{\omega_c} + \frac{i}{2T}} dt \; F(t) = \int_{-\infty}^{\infty} dt \; F(t). \tag{F.8}$$

In order to check this formula, let us consider the left member of Eq. (F.8), assuming that t is a complex variable. Let us choose as integral contour the rectangle R with one side between $(-r, +r)$ and $(+r, -r)$, with $r \in \mathbb{R}$, and with the others joining the real axis $\Re(z)$ to the line $\Im t = +\frac{1}{\omega_c} - \frac{1}{2T}$, in correspondence of $-r$ e r on the imaginary axis $\Im(z)$. In the limit $r \to +\infty$, the integration over the two vertical lines gives a vanishing contribution. The integral over the contour R becomes

$$\oint_R F(t)dt = \int_{\infty - \frac{i}{\omega_c} + \frac{i}{2T}}^{-\infty - \frac{i}{\omega_c} + \frac{i}{2T}} dt \; F(t) + \int_{-\infty}^{\infty} dt \; F(t). \tag{F.9}$$

Since the integrand function is analytical in R, the above integral is zero according to Cauchy's theorem

$$\int_{\infty - \frac{i}{\omega_c} + \frac{i}{2T}}^{-\infty - \frac{i}{\omega_c} + \frac{i}{2T}} dt \; F(t) + \int_{-\infty}^{\infty} dt \; F(t) = 0, \tag{F.10}$$

thus proving the formula in Eq. (F.8).

According to this result, one can write $\tilde{\mathcal{P}}_g(E)$

$$\tilde{\mathcal{P}}_g(E) = e^{-\frac{E}{\omega_c}} e^{\frac{E}{2\theta}} \int_{-\infty}^{+\infty} dt \; e^{iEt} \left[\frac{\pi\theta}{\omega_c} \frac{1}{\cosh(\pi t\theta)} \right]^g. \tag{F.11}$$

Let us exploit the parity of the integrand function in order to write it as

$$\tilde{\mathcal{P}}_g(E) = 2e^{-\frac{E}{\omega_c}} e^{\frac{E}{2\theta}} \int_0^{+\infty} dt \; \cos iEt \left[\frac{\pi\theta}{\omega_c} \frac{1}{\cosh \pi t\theta} \right]^g. \tag{F.12}$$

Let us substitute $z = e^{-\pi t\theta}$ in the integral (F.12)

$$\tilde{\mathcal{P}}_g(E) = 2e^{-\frac{E}{\omega_c}} e^{\frac{E}{2\theta}} \left(\frac{2\pi\theta}{\omega_c} \right)^g \frac{1}{2\pi\theta} \int_0^1 dz \; z^{g-1} \frac{z^{\frac{iE}{\pi T}} + z^{-\frac{iE}{\pi\theta}}}{(z^2 + 1)^g}. \tag{F.13}$$

By using $s = \frac{z^2}{z^2+1}$, Eq. (F.13) becomes

$$\tilde{\mathcal{P}}_g(E) = e^{-\frac{E}{\omega_c}} e^{\frac{E}{2\theta}} \left(\frac{2\pi\theta}{\omega_c} \right)^g \frac{1}{2\pi\theta} \int_0^1 ds \; s^{\frac{g}{2}-1-i\frac{\omega}{2\pi T}} (1-s)^{\frac{g}{2}-1+i\frac{\omega}{2\pi T}}. \tag{F.14}$$

By introducing the definition of the Beta function[110]

$$\mathcal{B}[x, y] = \int_0^1 ds \; s^{x-1} (1-s)^{y-1}, \tag{F.15}$$

Eq. (F.14) becomes

$$\tilde{\mathcal{P}}_g(E) = e^{-\frac{E}{\omega_c}} e^{\frac{E}{2\theta}} \left(\frac{2\pi\theta}{\omega_c} \right)^g \frac{1}{2\pi\theta} \mathcal{B}\left[\frac{g}{2} - i\frac{E}{2\pi\theta}, \frac{g}{2} + i\frac{E}{2\pi\theta} \right]. \tag{F.16}$$

156

Another representation of the Beta function is

$$\mathcal{B}(z,w) = \frac{\Gamma(z)\Gamma(w)}{\Gamma(z+w)}, \tag{F.17}$$

which can be used to write(F.16) as

$$\tilde{\mathcal{P}}_g(E) = \left(\frac{2\pi\theta}{\omega_c}\right)^{g-1} \frac{e^{\frac{E}{2\theta}}}{\Gamma(g)\omega_c} \left|\Gamma\left(\frac{g}{2} + \frac{iE}{2\pi\theta}\right)\right|^2. \tag{F.18}$$

In the limit of zero temperature, one can exploit the asymptotic form of the Gamma function

$$|\Gamma(x+iy)| \sim \sqrt{2\pi}|y|^{x-\frac{1}{2}}e^{-\frac{\pi|y|}{2}}, \tag{F.19}$$

valid for $|y| \to +\infty$, to recast Eq. (F.18) as

$$\tilde{\mathcal{P}}_g(E) = \frac{2\pi}{\Gamma(g)\omega_c^g} E^{g-1}\Theta(E). \tag{F.20}$$

Finally, let us observe that $\tilde{\mathcal{P}}_g(E)$ is linked to the Fermi function $f(E) = \frac{1}{e^{\frac{E}{\theta}}}$, since $\tilde{\mathcal{P}}_g(E) = \mathcal{D}_g(E)f(-E)$, where

$$\mathcal{D}_g(E) = \frac{(2\pi)^g}{\Gamma(g)\omega_c}\left(\frac{\theta}{\omega_c}\right)^{g-1} \frac{\left|\Gamma\left(\frac{g}{2} + \frac{iE}{2\pi\theta}\right)\right|^2}{\left|\Gamma\left(\frac{1}{2} + \frac{iE}{2\pi\theta}\right)\right|^2}. \tag{F.21}$$

Appendix G

Complements to the calculation of charge, mixed and heat noises

In this Appendix, we present some complementary details of the perturbative calculations of charge, mixed and heat noises in Chapter 3 and Chapter 4. In particular, we derive the useful formulas employed for evaluating heat noise in the double-drive configuration in Sec. 4.4.

G.1   Charge noise

In the main text charge noise (α and β refer to reservoirs 2 or 3)

$$\mathcal{S}_{\alpha\beta} = \int_0^{\mathcal{T}} \frac{dt}{\mathcal{T}} \int_{-\infty}^{+\infty} dt' \left[\langle J_\alpha(t) J_\beta(t') \rangle - \langle J_\alpha(t) \rangle \langle J_\beta(t') \rangle \right], \tag{G.1}$$

has been written as a perturbative series in powers of Λ, as

$$\mathcal{S}_{\alpha\beta} = \mathcal{S}_{\alpha\beta}^{(02)} + \mathcal{S}_{\alpha\beta}^{(11)} + \mathcal{S}_{\alpha\beta}^{(20)} + \mathcal{O}\left(\Lambda^3\right), \tag{G.2}$$

with

$$\mathcal{S}_{\alpha\beta}^{(ij)} = \int_0^{\mathcal{T}} \frac{dt}{\mathcal{T}} \int_{-\infty}^{+\infty} dt' \left\langle J_\alpha^{(i)}(t) J_\beta^{(j)}(t') \right\rangle - \left\langle J_\alpha^{(i)} \right\rangle \left\langle (t) J_\beta^{(j)}(t') \right\rangle. \tag{G.3}$$

Here, the perturbative contribution to charge current operator are

$$J_{2/3}^{(0)}(t) = \frac{ev\sqrt{\nu}}{2\pi} \left(\partial_x \Phi_{R/L}(x,t) \right)_{x=\pm d}, \tag{G.4}$$

$$J_{2/3}^{(1)}(t) = \pm i\Lambda e\nu \Psi_R^\dagger \left(0, t - \frac{d}{v} \right) \Psi_L \left(0, t - \frac{d}{v} \right) + \text{h.c.}, \tag{G.5}$$

$$J_{2/3}^{(2)}(t) = \pm i \int_{-\infty}^{t-\frac{d}{v}} dt'' \left[H_T^{(qp)}(t''), +i\Lambda e\nu \Psi_R^{(qp)\dagger} \left(0, t - \frac{d}{v} \right) \Psi_L^{(qp)} \left(0, t - \frac{d}{v} \right) + \text{h.c.} \right]. \tag{G.6}$$

Let us observe that, since $J_2^{(2)}(t) = -J_3^{(2)}(t)$, auto-correlators and cross-correlators are connected as [104, 112]

$$\mathcal{S}_{22} = \mathcal{S}_{33} = -\mathcal{S}_{23} = -\mathcal{S}_{32}. \tag{G.7}$$

For this relation, we can focus on the auto-correlator of reservoirs 2, namely $\mathcal{S}_{22}$, and we use the shorthand notation $\mathcal{S}_C \equiv \mathcal{S}_{22}$. In Chapter 3, the contribution with $\mathcal{S}_C^{(11)}$ has been already evaluated. Here, we show that it is the only non-vanishing contribution. Let us start by writing explicitly the two contributions $\mathcal{S}_C^{(02)}$ and $\mathcal{S}_C^{(20)}$. They read

$$\mathcal{S}_C^{(02)} = -\frac{e^2 \nu \sqrt{\nu}}{2\pi} \int_{-\frac{\mathcal{T}}{2}}^{\frac{\mathcal{T}}{2}} \frac{dt}{\mathcal{T}} \int_{-\infty}^{+\infty} dt' \int_{-\infty}^{t'} dt'' \times$$

$$\times \left[\left\langle \partial_t \Phi_R(0,t) \left[\Lambda \Psi_R^{(qp)\dagger}(0,t'') \Psi_L^{(qp)}(0,t'') + \text{h.c.}, +i\Lambda \Psi_R^{(qp)\dagger}(0,t') \Psi_L^{(qp)}(0,t') + \text{h.c.} \right] \right\rangle + \right.$$

$$\left. - \langle \partial_t \Phi_R(0,t) \rangle \left\langle \left[\Lambda \Psi_R^{(qp)\dagger}(0,t'') \Psi_L^{(qp)}(0,t'') + \text{h.c.}, +i\Lambda \Psi_R^{(qp)\dagger}(0,t') \Psi_L^{(qp)}(0,t') + \text{h.c.} \right] \right\rangle \right] =$$

$$= -\frac{e^2 \nu \sqrt{\nu}}{2\pi} \int_{-\frac{\mathcal{T}}{2}}^{\frac{\mathcal{T}}{2}} \frac{dt}{\mathcal{T}} \int_{-\infty}^{+\infty} dt' \int_{-\infty}^{t'} dt'' \times$$

$$\times \left\langle \partial_t \phi_R(0,t) \left[\Lambda \Psi_R^{(qp)\dagger}(0,t'') \Psi_L^{(qp)}(0,t'') + \text{h.c.}, +i\Lambda \Psi_R^{(qp)\dagger}(0,t') \Psi_L^{(qp)}(0,t') + \text{h.c.} \right] \right\rangle,$$

$$\text{(G.8)}$$

$$\mathcal{S}_C^{(20)} = -\frac{e^2 \nu \sqrt{\nu}}{2\pi} \int_{-\frac{\mathcal{T}}{2}}^{\frac{\mathcal{T}}{2}} \frac{dt}{\mathcal{T}} \int_{-\infty}^{+\infty} dt' \int_{-\infty}^{t} dt'' \times$$

$$\times \left[\left\langle \left[\Lambda \Psi_R^{(qp)\dagger}(0,t'') \Psi_L^{(qp)}(0,t'') + \text{h.c.}, +i\Lambda \Psi_R^{(qp)\dagger}(0,t) \Psi_L^{(qp)}(0,t) + \text{h.c.} \right] \partial_{t'} \Phi_R(0,t') \right\rangle + \right.$$

$$\left. - \left\langle \left[\Lambda \Psi_R^{(qp)\dagger}(0,t'') \Psi_L^{(qp)}(0,t'') + \text{h.c.}, +i\Lambda \Psi_R^{(qp)\dagger}(0,t) \Psi_L^{(qp)}(0,t) + \text{h.c.} \right] \right\rangle \langle \partial_{t'} \Phi_R(0,t') \rangle \right] =$$

$$= -\frac{e^2 \nu \sqrt{\nu}}{2\pi} \int_{-\frac{\mathcal{T}}{2}}^{\frac{\mathcal{T}}{2}} \frac{dt}{\mathcal{T}} \int_{-\infty}^{+\infty} dt' \int_{-\infty}^{t} dt'' \times$$

$$\times \left\langle \left[\Lambda \Psi_R^{(qp)\dagger}(0,t'') \Psi_L^{(qp)}(0,t'') + \text{h.c.}, +i\Lambda \Psi_R^{(qp)\dagger}(0,t) \Psi_L^{(qp)}(0,t) + \text{h.c.} \right] \partial_{t'} \phi_R(0,t') \right\rangle.$$

$$\text{(G.9)}$$

Notice that the factor $\frac{d}{v}$ has been canceled out by a shift over t or t'.

In order to evaluate these contributions, we have to perform the following averages

$$\left\langle \partial_{t_1} \phi_R(0,t_1) \Psi_R^\dagger(0,t_2) \Psi_R(0,t_3) \right\rangle, \qquad \text{(G.10)}$$

$$\left\langle \partial_{t_1} \phi_R(0,t_1) \Psi_R(0,t_2) \Psi_R^\dagger(0,t_3) \right\rangle, \qquad \text{(G.11)}$$

$$\left\langle \Psi_R^\dagger(0,t_1) \Psi_R(0,t_2) \partial_{t_3} \phi_R(0,t_3) \right\rangle, \qquad \text{(G.12)}$$

$$\left\langle \Psi_R(0,t_1) \Psi_R^\dagger(0,t_2) \partial_{t_3} \phi_R(0,t_3) \right\rangle. \qquad \text{(G.13)}$$

We recall the bosonized expression for the fermionic field

$$\Psi_{R/L}^{(qp)}(x,t) = \psi_{R/L}^{(qp)}(x,t) \exp\left\{ -i\nu e \int_0^t dt' V_{R/L}(x \mp v(t-t'),t') \right\}, \qquad \text{(G.14)}$$

where we introduced time-dependent electronic and quasi-particle field operators at the equilibrium, i.e. $V_R = V_L = 0$

$$\psi_R^{(qp)}(x,t) = \frac{\mathcal{F}_R^{(qp)}}{\sqrt{2\pi a}} e^{ik_F x} e^{-i\sqrt{\nu}\phi_R(x,t)}. \qquad \text{(G.15)}$$

By using looking at the bosonization identity, it is clear that we can simply focus on the following quantities

$$C_1^\pm(t_1, t_2, t_3) = \langle \partial_{t_1}\phi(0, t_1)e^{\pm i\sqrt{\nu}\phi(0,t_2)}e^{\mp i\sqrt{\nu}\phi(0,t_3)}\rangle, \tag{G.16}$$

$$C_2^\pm(t_1, t_2, t_3) = \langle e^{\pm i\sqrt{\nu}\phi(0,t_1)}e^{\mp i\sqrt{\nu}\phi(0,t_2)}\partial_{t_3}\phi(0, t_3)\rangle. \tag{G.17}$$

For simplicity, we drop the chirality index R.

In order to evaluate C_1 and C_2, we start by considering the following general average value

$$E_1(\epsilon_1, \epsilon_2, \epsilon_3; t_1, t_2, t_3) = \langle e^{-i\epsilon_1\phi(0,t_1)}e^{-i\epsilon_2\phi(0,t_2)}e^{-i\epsilon_3\phi(0,t_3)}\rangle, \tag{G.18}$$

which is connected to C_1 and C_2 by this relation

$$C_1^\pm(t_1, t_2, t_3) = i\partial_{t_1}\left\{\lim_{\epsilon_1\to 0}\partial_{\epsilon_1}E_1(\epsilon_1, \epsilon_2, \epsilon_3; t_1, t_2, t_3)\right\}_{\epsilon_2=-\epsilon_3\mp\sqrt{\nu}}, \tag{G.19}$$

$$C_2^\pm(t_1, t_2, t_3) = i\partial_{t_3}\left\{\lim_{\epsilon_3\to 0}\partial_{\epsilon_3}E_1(\epsilon_1, \epsilon_2, \epsilon_3; t_1, t_2, t_3)\right\}_{\epsilon_1=-\epsilon_2=\mp\sqrt{\nu}}. \tag{G.20}$$

By using [36]

$$\langle e^{\chi(0,t_1)}e^{\chi(0,t_2)}e^{\chi(0,t_3)}\rangle = e^{\frac{1}{2}\sum_{i=1}^3\langle\chi(0,t_i)^2\rangle}e^{\sum_{i<j}\langle\chi(0,t_i)\chi(0,t_j)\rangle}, \tag{G.21}$$

we obtain from Eq. (G.18)

$$E_1(\epsilon_1, \epsilon_2, \epsilon_3; t_1, t_2, t_3) = e^{-\frac{1}{2}\sum_{i=1}^3\langle\epsilon_i^2\phi^2(0,t_i)\rangle}\times$$
$$\times e^{-\{\epsilon_1\epsilon_2\langle\phi(0,t_1)\phi(0,t_2)\rangle+\epsilon_1\epsilon_3\langle\phi(0,t_1)\phi(0,t_3)\rangle+\epsilon_2\epsilon_3\langle\phi(0,t_2)\phi(0,t_3)\rangle\}}. \tag{G.22}$$

Finally, we use Eqs. (G.19) and (G.20) to find $C_1^\pm$ and $C_2^\pm$

$$C_1^\pm(t_1, t_2, t_3) = \mp i\sqrt{\nu}\mathcal{K}(t_1, t_2, t_3)\mathcal{P}_\nu(t_2 - t_3), \tag{G.23}$$

$$C_2^\pm(t_1, t_2, t_3) = \mp i\sqrt{\nu}\mathcal{K}(-t_3, -t_1, -t_2)\mathcal{P}_\nu(t_1 - t_2), \tag{G.24}$$

where we defined (see Eq. (G.25) in the main text)

$$\mathcal{P}_g(t' - t) = \langle e^{i\sqrt{g}\phi_{R/L}(0,t')}e^{-i\sqrt{g}\phi_{R/L}(0,t)}\rangle =$$
$$= \left[\frac{\pi\theta(t' - t)}{\sinh\left(\pi\theta(t' - t)\right)\left(1 + i\omega_c(t' - t)\right)}\right]^g, \tag{G.25}$$

and

$$\mathcal{K}(t_1, t_2, t_3) = \partial_{t_1}\left\{\langle\phi(0, t_1)\phi(0, t_3)\rangle - \langle\phi(0, t_1)\phi(0, t_2)\rangle\right\} =$$
$$= \int d\tau\mathcal{P}_2(t_1 - \tau)\left(\Theta(\tau - t_3) - \Theta(\tau - t_2)\right). \tag{G.26}$$

Therefore, the averages we were interested in reads

$$\left\langle\partial_{t_1}\phi_R(0, t_1)\Psi_R^\dagger(0, t_2)\Psi_R(0, t_3)\right\rangle = i\sqrt{\nu}\mathcal{K}(t_1, t_2, t_3)G_R^<(t_2, t_3), \tag{G.27}$$

$$\left\langle\partial_{t_1}\phi_R(0, t_1)\Psi_R(0, t_2)\Psi_R^\dagger(0, t_3)\right\rangle = -i\sqrt{\nu}\mathcal{K}(t_1, t_2, t_3)G_R^<(t_2, t_3), \tag{G.28}$$

$$\left\langle\Psi_R^\dagger(0, t_1)\Psi_R(0, t_2)\partial_{t_3}\phi_R(0, t_3)\right\rangle = i\sqrt{\nu}\mathcal{K}(t_1, t_2, t_3)G_R^>(t_1, t_2), \tag{G.29}$$

$$\left\langle\Psi_R(0, t_1)\Psi_R^\dagger(0, t_2)\partial_{t_3}\phi_R(0, t_3)\right\rangle = -i\sqrt{\nu}\mathcal{K}(t_1, t_2, t_3)G_R^>(t_1, t_2). \tag{G.30}$$

Let us observe that one could find similar relation for left-movers

$$\left\langle \partial_{t_1} \phi_L(0, t_1) \Psi_L^\dagger(0, t_2) \Psi_L(0, t_3) \right\rangle = i\sqrt{\nu} \mathcal{K}(t_1, t_2, t_3) G_L^<(t_2, t_3), \tag{G.31}$$

$$\left\langle \partial_{t_1} \phi_L(0, t_1) \Psi_L(0, t_2) \Psi_L^\dagger(0, t_3) \right\rangle = -i\sqrt{\nu} \mathcal{K}(t_1, t_2, t_3) G_L^<(t_2, t_3), \tag{G.32}$$

$$\left\langle \Psi_L^\dagger(0, t_1) \Psi_L(0, t_2) \partial_{t_3} \phi_L(0, t_3) \right\rangle = i\sqrt{\nu} \mathcal{K}(t_1, t_2, t_3) G_L^>(t_1, t_2), \tag{G.33}$$

$$\left\langle \Psi_L(0, t_1) \Psi_L^\dagger(0, t_2) \partial_{t_3} \phi_L(0, t_3) \right\rangle = -i\sqrt{\nu} \mathcal{K}(t_1, t_2, t_3) G_L^>(t_1, t_2). \tag{G.34}$$

Exploiting the following average

$$\langle \partial_{t_1} \phi(0, t_1) \partial_t \phi(0, t) \rangle = -\frac{\pi^2 \theta^2}{v^2 \sinh^2 \left(\pi\theta(t_1 - t) \right)} \tag{G.35}$$

the function $\mathcal{K}$ can be further evaluated by using

$$\partial_{t_1} \langle \phi(0, t_1) \phi(0, t_2) \rangle = \int_{-\infty}^{t_2} dt \langle \partial_{t_1} \phi(0, t_1) \partial_t \phi(0, t) \rangle =$$
$$= \frac{\pi\theta}{v} \left[\coth\left(\pi\theta(t_1 - t_2) \right) - 1 \right]. \tag{G.36}$$

By using this result, one finds

$$\mathcal{K}(t_1, t_2, t_3) = \frac{\pi\theta}{v} \left(\coth\left(\pi\theta(t_1 - t_3) \right) - \coth\left(\pi\theta(t_1 - t_2) \right) \right) =$$
$$= \frac{\pi\theta}{v} \frac{\sinh\left(\pi\theta(t_2 - t_3) \right)}{\sinh\left(\pi\theta(t_1 - t_3) \right) \sinh\left(\pi\theta(t_1 - t_2) \right)}. \tag{G.37}$$

The contributions to charge noise in Eqs. (G.8) and (G.9) become

$$\mathcal{S}_C^{(02)} = -|\Lambda|^2 \frac{e^2 \nu \sqrt{\nu}}{2\pi} \int_{-\frac{\mathcal{T}}{2}}^{\frac{\mathcal{T}}{2}} \frac{dt}{\mathcal{T}} \int_{-\infty}^{+\infty} dt' \int_{-\infty}^{t'} dt'' \mathcal{K}(t, t'', t') \times$$

$$\times \left[G_R^<(t'', t') G_L^>(t'', t') + G_R^>(t'', t') G_L^<(t'', t') + \right.$$

$$\left. + G_R^<(t', t'') G_L^>(t', t'') + G_R^>(t', t'') G_L^<(t', t'') \right], \tag{G.38}$$

$$\mathcal{S}_C^{(20)} = -|\Lambda|^2 \frac{e^2 \nu \sqrt{\nu}}{2\pi} \int_{-\frac{\mathcal{T}}{2}}^{\frac{\mathcal{T}}{2}} \frac{dt}{\mathcal{T}} \int_{-\infty}^{+\infty} dt' \int_{-\infty}^{t'} dt'' \mathcal{K}(-t, -t'', -t') \times$$

$$\times \left[G_R^<(t'', t') G_L^>(t'', t') + G_R^>(t'', t') G_L^<(t'', t') + \right.$$

$$\left. + G_R^<(t', t'') G_L^>(t', t'') + G_R^>(t', t'') G_L^<(t', t'') \right]. \tag{G.39}$$

Notice that we exchanged t and t' in $\mathcal{S}^{(20)}$. Since $\mathcal{K}(-t, -t'', -t') = -\mathcal{K}(t, t'', t')$, it easy to see that $\mathcal{S}_C^{(02)} + \mathcal{S}_C^{(20)} = 0$, thus implying that $\mathcal{S}_C^{(11)}$ is the only non-vanishing contribution at lowest order to charge noise.

G.2 Mixed and heat noise in the HBT configuration

In this Section, we focus on charge-heat mixed and heat noises

$$\mathcal{S}_{X,\alpha\beta} = \int_0^{\mathcal{T}} \frac{dt}{\mathcal{T}} \int_{-\infty}^{+\infty} dt' \ \left[\langle J_\alpha(t')\mathcal{J}_\beta(t)\rangle - \langle J_\alpha(t')\rangle \langle \mathcal{J}_\beta(t)\rangle\right] \ , \tag{G.40}$$

$$\mathcal{S}_{Q,\alpha\beta} = \int_0^{\mathcal{T}} \frac{dt}{\mathcal{T}} \int_{-\infty}^{+\infty} dt' \ \left[\langle \mathcal{J}_\alpha(t')\mathcal{J}_\beta(t)\rangle - \langle \mathcal{J}_\alpha(t')\rangle \langle \mathcal{J}_\beta(t)\rangle\right] \ , \tag{G.41}$$

in the HBT configuration and at zero temperature, as discussed in Sec. 4.3. By assuming that the QPC is working in the weak-backscattering regime, noises can be expressed in terms of a perturbative series in powers of tunneling amplitude Λ as

$$\mathcal{S}_{X,\alpha\beta} = \mathcal{S}_{X,\alpha\beta}^{(02)} + \mathcal{S}_{X,\alpha\beta}^{(20)} + \mathcal{S}_{X,\alpha\beta}^{(11)} + \mathcal{O}\left(|\Lambda|^3\right), \tag{G.42}$$

$$\mathcal{S}_{Q,\alpha\beta} = \mathcal{S}_{Q,\alpha\beta}^{(02)} + \mathcal{S}_{Q,\alpha\beta}^{(20)} + \mathcal{S}_{Q,\alpha\beta}^{(11)} + \mathcal{O}\left(|\Lambda|^3\right), \tag{G.43}$$

where

$$\mathcal{S}_{X,\alpha\beta}^{(ij)} = \int_0^{\mathcal{T}} \frac{dt}{\mathcal{T}} \int_{-\infty}^{+\infty} dt' \ \left\{\langle J_\alpha^{(i)}(t')\mathcal{J}_\beta^{(j)}(t)\rangle - \langle J_\alpha^{(i)}(t')\rangle\langle \mathcal{J}_\beta^{(j)}(t)\rangle\right\}, \tag{G.44}$$

$$\mathcal{S}_{Q,\alpha\beta}^{(ij)} = \int_0^{\mathcal{T}} \frac{dt}{\mathcal{T}} \int_{-\infty}^{+\infty} dt' \ \left\{\langle \mathcal{J}_\alpha^{(i)}(t')\mathcal{J}_\beta^{(j)}(t)\rangle - \langle \mathcal{J}_\alpha^{(i)}(t')\rangle\langle \mathcal{J}_\beta^{(j)}(t)\rangle\right\}. \tag{G.45}$$

The perturbative expansion for heat current operator reads

$$\mathcal{J}_{2/3}^{(0)}(t) = \pm v \mathcal{Q}_{R/L}^{(0)}(\pm d, t), \tag{G.46}$$

$$\mathcal{J}_{2/3}^{(1)}(t) = \pm \dot{Q}_{R/L}\left(\pm d, t\right), \tag{G.47}$$

$$\mathcal{J}_{2/3}^{(2)}(t) = \pm i \int_{-\infty}^{t-\frac{d}{v}} dt'' \left[H_t(t''), \dot{Q}_{R/L}\left(\pm d, t\right)\right], \tag{G.48}$$

where

$$\mathcal{Q}_R^{(0)}(x,t) = \frac{v}{4\pi}\left[(\partial_x \phi_R(x,t))^2 \pm 2e\sqrt{\nu}\partial_x \phi_R(x,t) V_R\left(t \mp \frac{x}{v}\right) + \frac{e^2 \nu}{v} V_R^2\left(t \mp \frac{x}{v}\right)\right], \tag{G.49}$$

$$\mathcal{Q}_L^{(0)}(x,t) = \frac{v}{4\pi}\left(\partial_x \phi_L(x,t)\right)^2, \tag{G.50}$$

$$\dot{Q}_R\left(x,t\right) = v\Lambda\left(\partial_x + ik_F\right)\Psi_R^{(qp)\dagger}(x,t)\Psi_L^{(qp)}(x,t) + \text{H.c.}, \tag{G.51}$$

$$\dot{Q}_L\left(x,t\right) = -v\Lambda\Psi_R^{(qp)\dagger}(x,t)\left(\partial_x + ik_F\right)\Psi_L^{(qp)}(x,t) + \text{H.c.}. \tag{G.52}$$

As in the main text, we consider the auto-correlators of terminals 3, namely $\mathcal{S}_X \equiv \mathcal{S}_{X,33}$ and $\mathcal{S}_Q \equiv \mathcal{S}_{Q,33}$. In Chapter 4, we have already evaluated $\mathcal{S}_{X/Q}^{(11)}$. Here, we will show that these are the only non-vanishing contribution in our perturbative

approach. Indeed, the other contributions read

$$
\mathcal{S}_X^{(02)} = -\frac{e\sqrt{\nu}}{2\pi} \int_{-\frac{\mathcal{T}}{2}}^{\frac{\mathcal{T}}{2}} \frac{dt}{\mathcal{T}} \int_{-\infty}^{+\infty} dt' \int_{-\infty}^{t'} dt'' \times
$$

$$
\times \left[\langle \partial_t \phi_L(0,t) \Big[\Lambda \Psi_R^{(qp)\dagger}(0,t'') \Psi_L^{(qp)}(0,t'') + \text{h.c.}, \right.
$$

$$
\left. + i\Lambda \Psi_R^{(qp)\dagger}(0,t')(\partial_{t'} + ik_F v)\Psi_L^{(qp)}(0,t') + \text{h.c.}\Big] \rangle \right], \tag{G.53}
$$

$$
\mathcal{S}_X^{(20)} = \frac{e\nu}{4\pi v} \int_{-\frac{\mathcal{T}}{2}}^{\frac{\mathcal{T}}{2}} \frac{dt}{\mathcal{T}} \int_{-\infty}^{+\infty} dt' \int_{-\infty}^{t} dt'' \times
$$

$$
\times \left[\left\langle \Big[\Lambda \Psi_R^{(qp)\dagger}(0,t'') \Psi_L^{(qp)}(0,t'') + \text{h.c.}, \right.\right.
$$

$$
\left. + i\Lambda \Psi_R^{(qp)\dagger}(0,t)\Psi_L^{(qp)}(0,t) + \text{h.c.}\Big] \left(\partial_{t'}\phi_L(0,t')\right)^2 \right\rangle +
$$

$$
- \left\langle \Big[\Lambda \Psi_R^{(qp)\dagger}(0,t'') \Psi_L^{(qp)}(0,t'') + \text{h.c.}, \right.
$$

$$
\left.\left. + i\Lambda \Psi_R^{(qp)\dagger}(0,t)\Psi_L^{(qp)}(0,t) + \text{h.c.}\Big] \right\rangle \left\langle \partial_{t'}\left(\phi_L(0,t')\right)^2 \right\rangle \right], \tag{G.54}
$$

$$
\mathcal{S}_Q^{(02)} = \frac{1}{4\pi} \int_{-\frac{\mathcal{T}}{2}}^{\frac{\mathcal{T}}{2}} \frac{dt}{\mathcal{T}} \int_{-\infty}^{+\infty} dt' \int_{-\infty}^{t} dt'' \times
$$

$$
\times \left[\left\langle \left(\partial_t \phi_L(0,t)\right)^2 \Big[\Lambda \Psi_R^{(qp)\dagger}(0,t'') \Psi_L^{(qp)}(0,t'') + \text{h.c.}, \right.\right.
$$

$$
\left.\left. + i\Lambda \Psi_R^{(qp)\dagger}(0,t')(\partial_{t'} + ik_F v)\Psi_L^{(qp)}(0,t') + \text{h.c.}\Big] \right\rangle +
$$

$$
- \left\langle \partial_t \left(\phi_L(0,t)\right)^2 \right\rangle \left\langle \Big[\Lambda \Psi_R^{(qp)\dagger}(0,t'')(\partial_{t'} + ik_F v)\Psi_L^{(qp)}(0,t'') + \text{h.c.}, \right.
$$

$$
\left.\left. + i\Lambda \Psi_R^{(qp)\dagger}(0,t')\Psi_L^{(qp)}(0,t') + \text{h.c.}\Big] \right\rangle \right], \tag{G.55}
$$

$$
\mathcal{S}_Q^{(20)} = \frac{1}{4\pi} \int_{-\frac{\mathcal{T}}{2}}^{\frac{\mathcal{T}}{2}} \frac{dt}{\mathcal{T}} \int_{-\infty}^{+\infty} dt' \int_{-\infty}^{t} dt'' \times
$$

$$
\times \left[\left\langle \Big[\Lambda \Psi_R^{(qp)\dagger}(0,t'') \Psi_L^{(qp)}(0,t'') + \text{h.c.}, \right.\right.
$$

$$
\left. + i\Lambda \Psi_R^{(qp)\dagger}(0,t)(\partial_t + ik_F v)\Psi_L^{(qp)}(0,t) + \text{h.c.}\Big] \left(\partial_{t'}\phi_L(0,t')\right)^2 \right\rangle +
$$

$$
- \left\langle \Big[\Lambda \Psi_R^{(qp)\dagger}(0,t'')(\partial_{t'} + ik_F v)\Psi_L^{(qp)}(0,t'') + \text{h.c.}, \right.
$$

$$
\left.\left. + i\Lambda \Psi_R^{(qp)\dagger}(0,t)\Psi_L^{(qp)}(0,t) + \text{h.c.}\Big] \right\rangle \left\langle \partial_{t'}\left(\phi_L(0,t')\right)^2 \right\rangle \right], \tag{G.56}
$$

for mixed and heat noises.

In order to evaluate these expression, we need the values of the following averages

$$\left\langle (\partial_{t_1}\phi_L(0,t_1))^2\, \Psi_L^\dagger(0,t_2)\Psi_L(0,t_3) \right\rangle, \tag{G.57}$$

$$\left\langle (\partial_{t_1}\phi_L(0,t_1))^2\, \Psi_L(0,t_2)\Psi_L^\dagger(0,t_3) \right\rangle, \tag{G.58}$$

$$\left\langle \Psi_L^\dagger(0,t_1)\Psi_L(0,t_2)\, (\partial_{t_3}\phi_L(0,t_3))^2 \right\rangle, \tag{G.59}$$

$$\left\langle \Psi_L(0,t_1)\Psi_L^\dagger(0,t_2)\, (\partial_{t_3}\phi_L(0,t_3))^2 \right\rangle. \tag{G.60}$$

$$\tag{G.61}$$

As for charge, the above equations are linked through bosonization identity to the following quantities (we drop the chirality index L)

$$D_1^\pm(t_1,t_2,t_3) = \langle (\partial_{t_1}\phi(0,t_1))^2\, e^{\pm i\sqrt{\nu}\phi(0,t_2)} e^{\mp i\sqrt{\nu}\phi(0,t_3)} \rangle, \tag{G.62}$$

$$D_2^\pm(t_1,t_2,t_3) = \langle e^{\pm i\sqrt{\nu}\phi(0,t_1)} e^{\mp i\sqrt{\nu}\phi(0,t_2)}\, (\partial_{t_3}\phi(0,t_3))^2 \rangle, \tag{G.63}$$

where the thermal average is performed over the initial equilibrium density matrix, in absence of tunneling and driving voltage and bosonic fields evolve according to the edge Hamiltonian H_0. In order to evaluate $D_1^\pm$ and $D_2^\pm$, we start by considering the following general average value

$$E_2(\epsilon_1,\epsilon_2,\epsilon_3,\epsilon_4;t_1,t_2,t_3,t_4) =$$
$$= \langle e^{-i\epsilon_1\phi(0,t_1)} e^{-i\epsilon_2\phi(0,t_2)} e^{-i\epsilon_3\phi(0,t_3)} e^{-i\epsilon_4\phi(0,t_4)} \rangle, \tag{G.64}$$

which is connected to $D_1^\pm$ and $D_2^\pm$ by these relations

$$D_1^\pm(t_1,t_2,t_3) = -\partial_{t_1}\partial_{t_1'}\left\{ \lim_{\epsilon_1\to0,\epsilon_2\to0} \partial_{\epsilon_1}\partial_{\epsilon_2} E_2(\epsilon_1,\epsilon_2,\epsilon_3,\epsilon_4;t_1,t_2,t_3,t_3') \right\}_{\substack{\epsilon_1=-\epsilon_2=\mp\sqrt{\nu},\\ t_1'=t_1}}, \tag{G.65}$$

$$D_2^\pm(t_1,t_2,t_3) = -\partial_{t_3}\partial_{t_3'}\left\{ \lim_{\epsilon_1\to0,\epsilon_2\to0} \partial_{\epsilon_3}\partial_{\epsilon_4} E_2(\epsilon_1,\epsilon_2,\epsilon_3,\epsilon_4;t_1,t_1',t_2,t_3) \right\}_{\substack{\epsilon_4=-\epsilon_3=\pm\sqrt{\nu},\\ t_3'=t_3}}. \tag{G.66}$$

$$\tag{G.67}$$

By using Eq. (G.21), we obtain from Eq. (G.18)

$$E_2(\epsilon_1,\epsilon_2,\epsilon_3,\epsilon_4;t_1,t_2,t_3,t_4) = e^{-\frac{1}{2}\sum_{i=1}^{4}\epsilon_i^2\langle\phi^2(0,t_i)\rangle} \times \tag{G.68}$$

$$\times\, e^{-\{\epsilon_1\epsilon_2\langle\phi(0,t_1)\phi(0,t_2)\rangle + \epsilon_1\epsilon_3\langle\phi(0,t_1)\phi(0,t_3)\rangle + \epsilon_1\epsilon_4\langle\phi(0,t_1)\phi(0,t_4)\rangle\}} \times$$

$$\times e^{-\{\epsilon_2\epsilon_3\langle\phi(0,t_2)\phi(0,t_3)\rangle + \epsilon_2\epsilon_4\langle\phi(0,t_2)\phi(0,t_4)\rangle + \epsilon_3\epsilon_4\langle\phi(0,t_3)\phi(0,t_4)\rangle\}}. \tag{G.69}$$

Finally, we use Eq. (G.65) and (G.66) to find $D_1^\pm$ and $D_2^\pm$

$$D_1^\pm(t_1,t_2,t_3) = \left\{ \langle(\partial_{t_1}\phi(t_1))^2\rangle - \nu\,(\mathcal{K}(t_1,t_2,t_3))^2 \right\} P_\nu(t_2-t_3), \tag{G.70}$$

$$D_2^\pm(t_1,t_2,t_3) = \left\{ \langle(\partial_{t_3}\phi(t_3))^2\rangle - \nu\,(\mathcal{K}(-t_3,-t_1,-t_2))^2 \right\} P_\nu(t_1-t_2). \tag{G.71}$$

The average values we were looking for become

$$\left\langle (\partial_{t_1}\phi_L(0,t_1))^2 \, \Psi_L^\dagger(0,t_2)\Psi_L(0,t_3) \right\rangle = \left\{ \langle(\partial_{t_1}\phi(t_1))^2\rangle - \nu \left(\mathcal{K}(t_1,t_2,t_3)\right)^2 \right\} G_L^<(t_2,t_3),$$
(G.72)

$$\left\langle (\partial_{t_1}\phi_L(0,t_1))^2 \, \Psi_L(0,t_2)\Psi_L^\dagger(0,t_3) \right\rangle = \left\{ \langle(\partial_{t_1}\phi(t_1))^2\rangle - \nu \left(\mathcal{K}(t_1,t_2,t_3)\right)^2 \right\} G_L^<(t_2,t_3),$$
(G.73)

$$\left\langle \Psi_L^\dagger(0,t_1)\Psi_L(0,t_2) \, (\partial_{t_3}\phi_L(0,t_3))^2 \right\rangle = \left\{ \langle(\partial_{t_1}\phi(t_1))^2\rangle - \nu \left(\mathcal{K}(t_1,t_2,t_3)\right)^2 \right\} G_L^>(t_1,t_2),$$
(G.74)

$$\left\langle \Psi_L(0,t_1)\Psi_L^\dagger(0,t_2) \, (\partial_{t_3}\phi_L(0,t_3))^2 \right\rangle = \left\{ \langle(\partial_{t_1}\phi(t_1))^2\rangle - \nu \left(\mathcal{K}(t_1,t_2,t_3)\right)^2 \right\} G_L^>(t_1,t_2).$$
(G.75)

The expression for contributions to mixed and heat noises in Eqs. (G.53),(G.54),(G.56) and (G.56) become, respectively,

$$\mathcal{S}_X^{(02)} = |\Lambda|^2 \frac{e\sqrt{\nu}}{2\pi} \int_{-\frac{\mathcal{T}}{2}}^{\frac{\mathcal{T}}{2}} \frac{dt}{\mathcal{T}} \int_{-\infty}^{+\infty} dt' \int_{-\infty}^{t'} dt'' \times$$

$$\times \Big[(\partial_t + ik_F v)\left(\mathcal{K}(t',t'',t)G_L^>(t'',t)\right) G_R^<(t'',t)+$$

$$+ (\partial_t + ik_F v)\left(\mathcal{K}(t',t'',t)G_L^<(t'',t)\right) G_R^>(t'',t)+$$

$$- (\partial_t + ik_F v)\left(\mathcal{K}(t',t,t'')G_L^>(t,t'')\right) G_R^<(t,t'')+$$

$$- (\partial_t + ik_F v)\left(\mathcal{K}(t',t,t'')G_L^<(t,t'')\right) G_R^>(t,t'')\Big],$$
(G.76)

$$\mathcal{S}_X^{(20)} = |\Lambda|^2 \frac{e\nu}{4\pi v} \int_{-\frac{\mathcal{T}}{2}}^{\frac{\mathcal{T}}{2}} \frac{dt}{\mathcal{T}} \int_{-\infty}^{+\infty} dt' \int_{-\infty}^{t} dt'' \times$$

$$\times \Big[\left(\mathcal{K}^2(t',t'',t)G_L^>(t'',t)\right) G_R^<(t'',t)+$$

$$+ \left(\mathcal{K}^2(t',t'',t)G_L^<(t'',t)\right) G_R^>(t'',t)+$$

$$- \left(\mathcal{K}^2(t',t,t'')G_L^>(t,t'')\right) G_R^<(t,t'')+$$

$$- \left(\mathcal{K}^2(t',t,t'')G_L^<(t,t'')\right) G_R^>(t,t'')\Big],$$
(G.77)

and

$$\mathcal{S}_Q^{(02)} = |\Lambda|^2 \frac{1}{4\pi} \int_{-\frac{\mathcal{T}}{2}}^{\frac{\mathcal{T}}{2}} \frac{dt}{\mathcal{T}} \int_{-\infty}^{+\infty} dt' \int_{-\infty}^{t} dt'' \times$$

$$\times \left[(\partial_{t'} + ik_F v) \left(\mathcal{K}^2(t', t'', t) G_L^>(t'', t) \right) G_R^<(t'', t) + \right.$$
$$+ (\partial_t + ik_F v) \left(\mathcal{K}^2(t', t'', t) G_L^<(t'', t) \right) G_R^>(t'', t) +$$
$$- (\partial_t + ik_F v) \left(\mathcal{K}^2(t', t, t'') G_L^>(t, t'') \right) G_R^<(t, t'') +$$
$$\left. - (\partial_t + ik_F v) \left(\mathcal{K}^2(t', t, t'') G_L^<(t, t'') \right) G_R^>(t, t'') \right], \tag{G.78}$$

$$\mathcal{S}_Q^{(20)} = |\Lambda|^2 \frac{1}{4\pi} \int_{-\frac{\mathcal{T}}{2}}^{\frac{\mathcal{T}}{2}} \frac{dt}{\mathcal{T}} \int_{-\infty}^{+\infty} dt' \int_{-\infty}^{t'} dt'' \times$$

$$\times \left[(\partial_t + ik_F v) \left(\mathcal{K}^2(t', t'', t) G_L^>(t'', t) \right) G_R^<(t'', t) + \right.$$
$$+ (\partial_t + ik_F v) \left(\mathcal{K}^2(t', t'', t) G_L^<(t'', t) \right) G_R^>(t'', t) +$$
$$- (\partial_t + ik_F v) \left(\mathcal{K}^2(t', t, t'') G_L^>(t, t'') \right) G_R^<(t, t'') +$$
$$\left. - (\partial_t + ik_F v) \left(\mathcal{K}^2(t', t, t'') G_L^<(t, t'') \right) G_R^>(t, t'') \right]. \tag{G.79}$$

All these contributions vanish at zero temperature, according to the relations

$$\int_{-\infty}^{+\infty} dt_1 \mathcal{K}(t_1, t_2, t_3) = 0, \tag{G.80}$$

$$\int_{-\infty}^{+\infty} dt_1 \mathcal{K}^2(t_1, t_2, t_3) = 0, \tag{G.81}$$

that we will prove in the following.

Let us start by the first one: using the expression of $\mathcal{K}$ in Eq. (G.26), one finds

$$\int_{-\infty}^{+\infty} dt_1 \mathcal{K}(t_1, t_2, t_3) = \int_{-\frac{\mathcal{T}}{2}}^{\frac{\mathcal{T}}{2}} \frac{dt_1}{\mathcal{T}} \int_{-\infty}^{+\infty} d\tau \mathcal{P}_2(t_1 - \tau) \left(\Theta(\tau - t_3) - \Theta(\tau - t_2) \right) =$$

$$= \int_{-\infty}^{+\infty} d\tau \left(\int_{-\infty}^{+\infty} dt_1 \mathcal{P}_2(t_1 - \tau) \Theta(\tau) - \int_{-\infty}^{+\infty} dt_1 \mathcal{P}_2(t_1 - \tau) \Theta(\tau) \right) = 0. \tag{G.82}$$

For the second relation, let us notice that at zero temperature one has

$$\mathcal{K}(t_1, t_2, t_3) = \partial_{t_1} \left\{ \langle \phi(0, t_1) \phi(0, t_3) \rangle - \langle \phi(0, t_1) \phi(0, t_2) \rangle \right\} =$$
$$= -i\omega_c \left(\mathcal{P}_1(t_1 - t_3) - \mathcal{P}_1(t_1 - t_2) \right). \tag{G.83}$$

Using this expression for $\mathcal{K}$, Eq. (G.81) becomes

$$\int_{-\infty}^{+\infty} dt_1 \mathcal{K}^2(t_1, t_2, t_3) = 2 \int_{-\infty}^{+\infty} dt_1 \left\{ \mathcal{P}_1^2(t_1) - \mathcal{P}_1(t_1 - t_2) \mathcal{P}_1(t_1 - t_3) \right\} =$$

$$= 2 \int_{-\infty}^{+\infty} dt_1 \left\{ \int_{-\infty}^{+\infty} \frac{dE}{2\pi} e^{-iEt_1} \tilde{\mathcal{P}}_2(E) + \right.$$

$$\left. - \int_{-\infty}^{+\infty} \frac{dE_1}{2\pi} e^{-iE_1(t_1 - t_3)} \tilde{\mathcal{P}}_1(E_1) \int_{-\infty}^{+\infty} \frac{dE_2}{2\pi} e^{-iE_2(t_1 - t_2)} \tilde{\mathcal{P}}_1(E_2) \right\} =$$

$$= 2 \left\{ \int_{-\infty}^{+\infty} \frac{dE}{2\pi} \delta(E) \tilde{\mathcal{P}}_2(E) - \int_{-\infty}^{+\infty} \frac{dE}{2\pi} e^{-iE(t_2 - t_3)} \tilde{\mathcal{P}}_1(E) \tilde{\mathcal{P}}_1(-E) \right\} = 0, \tag{G.84}$$

where we introduced the Fourier transform of $\mathcal{P}_{1/2}(t)$

$$\tilde{\mathcal{P}}_g(E) = \frac{2\pi}{\Gamma(g)\omega_{\mathrm{c}}} \left| \frac{E}{\omega_{\mathrm{c}}} \right|^{g-1} \Theta(E). \tag{G.85}$$

In conclusion, we observe that similar average values hold true for right-movers

$$\left\langle (\partial_{t_1} \phi_R(0,t_1))^2 \Psi_R^\dagger(0,t_2) \Psi_R(0,t_3) \right\rangle = \left\{ \langle (\partial_{t_1} \phi(t_1))^2 \rangle - \nu \left(\mathcal{K}(t_1,t_2,t_3) \right)^2 \right\} G_R^<(t_2,t_3), \tag{G.86}$$

$$\left\langle (\partial_{t_1} \phi_R(0,t_1))^2 \Psi_R(0,t_2) \Psi_R^\dagger(0,t_3) \right\rangle = \left\{ \langle (\partial_{t_1} \phi(t_1))^2 \rangle - \nu \left(\mathcal{K}(t_1,t_2,t_3) \right)^2 \right\} G_R^<(t_2,t_3), \tag{G.87}$$

$$\left\langle \Psi_R^\dagger(0,t_1) \Psi_R(0,t_2) \left(\partial_{t_3} \phi_R(0,t_3) \right)^2 \right\rangle = \left\{ \langle (\partial_{t_1} \phi(t_1))^2 \rangle - \nu \left(\mathcal{K}(t_1,t_2,t_3) \right)^2 \right\} G_R^>(t_1,t_2), \tag{G.88}$$

$$\left\langle \Psi_R(0,t_1) \Psi_R^\dagger(0,t_2) \left(\partial_{t_3} \phi_R(0,t_3) \right)^2 \right\rangle = \left\{ \langle (\partial_{t_1} \phi(t_1))^2 \rangle - \nu \left(\mathcal{K}(t_1,t_2,t_3) \right)^2 \right\} G_R^>(t_1,t_2). \tag{G.89}$$

G.3 Noise in the double-drive configuration

In the following, we evaluate explicitly heat cross-correlator between reservoir 2 and 3 at lowest order in tunneling for the double-drive configuration considered in Sec. 4.4. Its perturbative expansion read

$$\mathcal{S}_{Q,23} = \mathcal{S}_{Q,23}^{(02)} + \mathcal{S}_{Q,23}^{(20)} + \mathcal{S}_{Q,23}^{(11)} + \mathcal{O}\left(|\Lambda|^2 \right), \tag{G.90}$$

where the different terms are given in Eqs. (G.4), (G.5) and (G.6).
Firstly, we start by deriving the term $\mathcal{S}_{Q,23}^{(11)}$, which reads

$$\mathcal{S}_{Q,23}^{(11)} = \int_0^{\mathcal{T}} \frac{dt}{\mathcal{T}} \int_{-\infty}^{+\infty} dt' \Big\{ \langle (\partial_{t'} - ik_F v) \Psi_R^\dagger(0,t') \Psi_L(0,t') (\partial_t + ik_F v) \Psi_L^\dagger(0,t) \Psi_R(0,t) \rangle +$$

$$+ \langle \Psi_L^\dagger(0,t') (\partial_{t'} + ik_F v) \Psi_R(0,t') \Psi_R^\dagger(0,t) (\partial_t - ik_F v) \Psi_L(0,t) \rangle \Big\}, \tag{G.91}$$

since $\langle \mathcal{J}_{2/3}^{(1)}(t) \rangle = 0$ (see Eq. (4.15)). By performing the thermal averages in the above equation, one can express it in terms of Green's functions in Eqs. (3.28) and (3.29). One has that

$$\mathcal{S}_{Q,23}^{(11)} = \int_0^{\mathcal{T}} \frac{dt}{\mathcal{T}} \int_{-\infty}^{+\infty} dt' \Big\{ \langle (\partial_{t'} - ik_F v) G_R^<(t',t) (\partial_t + ik_F v) G_L^>(t',t) \rangle +$$

$$+ \langle (\partial_{t'} + ik_F v) G_R^>(t',t) (\partial_t - ik_F v) G_L^<(t',t) \rangle \Big\}. \tag{G.92}$$

The relation between Green's functions and the correlators $\mathcal{P}_g$ in the double-drive configuration is

$$G_R^{</>}(t',t) = \frac{e^{\pm ik_F v(t'-t)}}{2\pi a} e^{\mp i\nu e \int_t^{t'} d\tau V_R(\tau)} \mathcal{P}_\nu(t'-t), \tag{G.93}$$

$$G_L^{</>}(t',t) = \frac{e^{\pm ik_F v(t'-t)}}{2\pi a} e^{\mp i\nu e \int_t^{t'} d\tau V_L(\tau)} \mathcal{P}_\nu(t'-t). \tag{G.94}$$

By inserting these equations into (G.92), one finds

$$\mathcal{S}_{Q,23}^{(11)} = 2\left|\lambda\right|^2 \int_0^{\mathcal{T}} \frac{dt}{\mathcal{T}} \int_{-\infty}^{+\infty} dt' \left\{ \cos\left(\nu e \int_{t'}^t dt'' V_R(t'') - V_L(t'')\right) \partial_t' \mathcal{P}_\nu(t'-t) \partial_t \mathcal{P}_\nu(t'-t) + \right.$$

(G.95)

$$+ \nu e V_R(t') \sin\left(\nu e \int_{t'}^t dt'' V_R(t'') - V_L(t'')\right) \frac{1}{2} \partial_t \mathcal{P}_{2\nu}(t'-t) +$$

$$+ \nu e V_L(t) \sin\left(\nu e \int_{t'}^t dt'' V_R(t'') - V_L(t'')\right) \frac{1}{2} \partial_{t'} \mathcal{P}_{2\nu}(t'-t) +$$

$$\left. - \nu^2 e^2 V_R(t') V_L(t) \cos\left(\nu e \int_{t'}^t dt'' V_R(t'') - V_L(t'')\right) \mathcal{P}_{2\nu}(t'-t) \right\},$$

where the contributions involving k_F have been canceled out as in the calculations in Sec. 4.3. The integration by parts of second and third line of Eq. (G.95) provides some useful eliminations, providing the final expression

$$\mathcal{S}_{Q,23}^{(11)} = 2\left|\lambda\right|^2 \int_0^{\mathcal{T}} \frac{dt}{\mathcal{T}} \int_{-\infty}^{+\infty} dt' \left\{ \cos\left(\nu e \int_{t'}^t dt'' \left(V_R(t'') - V_L(t'')\right)\right) \partial_t' \mathcal{P}_\nu(t'-t) \partial_t \mathcal{P}_\nu(t'-t) + \right.$$

(G.96)

$$\left. - \frac{1}{2} \nu^2 e^2 \left(V_R(t') V_R(t) + V_L(t') V_L(t)\right) \cos\left(\nu e \int_{t'}^t dt'' \left(V_R(t'') - V_L(t'')\right)\right) \mathcal{P}_{2\nu}(t'-t) \right\}.$$

(G.97)

We focus on the remaining contributions, starting from $\mathcal{S}_{Q,23}^{(02)}$: the calculations for the other term would be analogous. By plugging Eqs. (4.6) and (4.8) in the definition of $\mathcal{S}_{Q,23}^{(02)}$, one finds

$$\mathcal{S}_{Q,23}^{(02)} = -i\frac{\left|\lambda\right|^2}{4\pi} \int_{-\infty}^{+\infty} dt \int_0^{\mathcal{T}} \frac{dt'}{\mathcal{T}} \int_{-\infty}^{+\infty} dt'' \theta(t'-t'') \times$$

$$\times \left\{ \langle (\partial_t \phi_R(0,t))^2 \left[\Psi_R^\dagger(0,t'') \Psi_L(0,t''), (\partial_{t'} + ik_F v) \Psi_L^\dagger(0,t') \Psi_R(0,t') \right] \rangle + \right.$$

$$- 2\nu e V_R(t) \langle \partial_t \phi_R^\dagger(0,t) \left[\Psi_R(0,t'') \Psi_L(0,t''), (\partial_{t'} + ik_F v) \Psi_L^\dagger(0,t') \Psi_R(0,t') \right] \rangle +$$

$$\left. - \langle (\partial_t \phi_R(0,t))^2 \rangle \langle \left[\Psi_R(0,t'') \Psi_L(0,t''), (\partial_{t'} + ik_F v) \Psi_L^\dagger(0,t') \Psi_R(0,t') \right] \rangle \right\}.$$

(G.98)

The averages involving the commutators are a bit more complicated that those in $\mathcal{S}_{Q,23}^{(11)}$, which simply corresponded to quasi-particle Green's functions. Here, we quote the results for some useful formulas, derived in Appendix G, which allow to further evaluate Eq. (G.98). They read

$$\left\langle (\partial_{t_1} \phi_R(0,t_1))^2 \Psi_R^\dagger(0,t_2) \Psi_R(0,t_3) \right\rangle = \left\{ \left\langle (\partial_{t_1} \Phi_R(0,t_1))^2 \right\rangle - \nu \mathcal{K}^2(t_1,t_2,t_3) \right\} G_R^<(t_2,t_3),$$

(G.99)

$$\left\langle (\partial_{t_1} \phi_R(0,t_1))^2 \Psi_R(0,t_2) \Psi_R^\dagger(0,t_3) \right\rangle = \left\{ \left\langle (\partial_{t_1} \Phi_R(0,t_1))^2 \right\rangle - \nu \mathcal{K}^2(t_1,t_2,t_3) \right\} G_R^>(t_2,t_3),$$

(G.100)

$$\left\langle \partial_{t_1} \phi_R(0,t_1) \Psi_R^\dagger(0,t_2) \Psi_R(0,t_3) \right\rangle = -i\sqrt{\nu} \mathcal{K}(t_1,t_2,t_3) G_R^<(t_2,t_3),$$

(G.101)

$$\left\langle \partial_{t_1} \phi_R(0,t_1) \Psi_R(0,t_2) \Psi_R^\dagger(0,t_3) \right\rangle = i\sqrt{\nu} \mathcal{K}(t_1,t_2,t_3) G_R^>(t_2,t_3),$$

(G.102)

169

where we defined

$$\mathcal{K}(t', t, t'') = \int_{-\infty}^{+\infty} d\tau \mathcal{P}_2(t' - \tau) \left(\Theta(\tau - t'') - \Theta(\tau - t)\right) =$$

$$= \frac{\pi\theta}{v} \frac{\sinh\left(\pi\theta(t - t'')\right)}{\sinh\left(\pi\theta(t' - t)\right)\sinh\left(\pi\theta(t' - t'')\right)}. \tag{G.103}$$

By inserting these expressions into Eq. (G.98), one finds

$$\mathcal{S}_{Q,23}^{(02)} = -i\frac{|\lambda|^2}{4\pi} \int_{-\infty}^{+\infty} dt \int_0^{\mathcal{T}} \frac{dt'}{\mathcal{T}} \int_{-\infty}^{+\infty} dt'' \; \Theta\left(t' - t''\right) \left\{ - \left[\nu\partial_{t'}\mathcal{K}^2(t, t', t'') \cos\left(\nu e \int_{t''}^{t'} d\tau V_-(\tau)\right) + \right.\right.$$

$$\left. + \nu e V_L(t')\mathcal{K}^2(t, t', t'') \sin\left(\nu e \int_{t''}^{t'} d\tau V_-(\tau)\right)\right] \left(\mathcal{P}_{2\nu}(t'' - t') - \mathcal{P}_{2\nu}(t' - t'')\right) +$$

$$+ \mathcal{K}(t, t', t'')\left[2\nu e V_R(t) \sin\left(\nu e \int_{t''}^{t'} d\tau V_-(\tau)\right)\partial_{t'}\left[\mathcal{P}_{2\nu}\left(t'' - t'\right) - \mathcal{P}_{2\nu}\left(t' - t''\right)\right] +$$

$$\left.\left. - 4\nu^2 e^2 V_R(t)V_L(t') \cos\left(\nu e \int_{t''}^{t'} d\tau V_-(\tau)\right)\left[\mathcal{P}_{2\nu}\left(t'' - t'\right) - \mathcal{P}_{2\nu}\left(t' - t''\right)\right]\right]\right\}. \tag{G.104}$$

A similar calculation can be performed for the last contribution, given by

$$\mathcal{S}_{Q,23}^{(20)} = -i\frac{|\lambda|^2}{4\pi} \int_{-\infty}^{+\infty} dt \int_0^{\mathcal{T}} \frac{dt'}{\mathcal{T}} \int_{-\infty}^{+\infty} dt'' \theta(t' - t'')\times$$

$$\times \left\{ \langle\left[\Psi_R^\dagger(0, t'')\Psi_L(0, t''), (\partial_{t'} + ik_F v)\Psi_L^\dagger(0, t')\Psi_L(0, t')\right](\partial_t\phi_R(0, t))^2\rangle + \right.$$

$$- 2\nu e V_R(t)\left[\Psi_R(0, t'')\Psi_L(0, t''), (\partial_{t'} + ik_F v)\Psi_L^\dagger(0, t')\Psi_R(0, t')\right]\langle\partial_t\phi_L^\dagger(0, t)\rangle +$$

$$\left. - \langle\left[\Psi_R(0, t'')\Psi_L(0, t''), (\partial_{t'} + ik_F v)\Psi_L^\dagger(0, t')\Psi_R(0, t')\right]\rangle\langle(\partial_t\phi_L(0, t))^2\rangle\right\}. \tag{G.105}$$

Analogously to $\mathcal{S}_{Q,23}^{(02)}$, in Appendix G, we derived some formulas which allow to evaluate the average values in the above equation. Here, we report their expressions

$$\left\langle\Psi_L^\dagger(0, t_1)\Psi_L(0, t_2)(\partial_{t_3}\phi_L(0, t_3))^2\right\rangle = \left\{\left\langle(\partial_{t_3}\phi_L(0, t_3))^2\right\rangle - \nu\mathcal{K}^2(-t_3, -t_2, -t_1)\right\}G_L^<(t_1, t_2), \tag{G.106}$$

$$\left\langle\Psi_L(0, t_1)\Psi_L^\dagger(0, t_2)(\partial_{t_3}\phi_L(0, t_3))^2\right\rangle = \left\{\left\langle(\partial_{t_3}\phi_L(0, t_3))^2\right\rangle - \nu\mathcal{K}^2(-t_3, -t_2, -t_1)\right\}G_L^<(t_1, t_2), \tag{G.107}$$

$$\left\langle\Psi_L^\dagger(0, t_1)\Psi_L(0, t_2)\partial_{t_3}\phi_L(0, t_3)\right\rangle = i\sqrt{\nu}\mathcal{K}(-t_3, -t_2, -t_1)G_L^<(t_1, t_2), \tag{G.108}$$

$$\left\langle\Psi_L(0, t_1)\Psi_L^\dagger(0, t_2)\partial_{t_3}\phi_L(0, t_3)\right\rangle = -i\sqrt{\nu}\mathcal{K}(-t_3, -t_2, -t_1)G_L^<(t_1, t_2), \tag{G.109}$$

which can be exploited to recast Eq. (G.105) as

$$\mathcal{S}_{Q,23}^{(20)} = -i\frac{|\lambda|^2}{4\pi}\int_{-\infty}^{+\infty}dt\int_0^{\mathcal{T}}\frac{dt'}{\mathcal{T}}\int_{-\infty}^{+\infty}dt''\,\Theta\left(t'-t''\right)\left\{\left[\nu\partial_{t'}\mathcal{K}^2(t,t',t'')\cos\left(\nu e\int_{t''}^{t'}d\tau V_-(\tau)\right)+\right.\right.$$

$$+\nu e V_L(t')\mathcal{K}^2(t,t',t'')\sin\left(\nu e\int_{t''}^{t'}d\tau V_-(\tau)\right)\bigg]\left(\mathcal{P}_{2\nu}(t''-t')-\mathcal{P}_{2\nu}(t'-t'')\right)+$$

$$+\mathcal{K}(t,t'',t')\left[2\nu e V_L(t)\sin\left(\nu e\int_{t'}^{t''}d\tau V_-(\tau)\right)\partial_{t'}\left[\mathcal{P}_{2\nu}\left(t''-t'\right)-\mathcal{P}_{2\nu}\left(t'-t''\right)\right]+$$

$$-4\nu^2 e^2 V_R(t)V_L(t'')\cos\left(\nu e\int_{t''}^{t'}d\tau V_-(\tau)\right)\left[\mathcal{P}_{2\nu}\left(t'-t''\right)-\mathcal{P}_{2\nu}\left(t''-t'\right)\right]\bigg]\bigg\}.$$

Bibliography

[1]   B. Bernevig and T. Hughes, *Topological insulators and topological supercon-ductors* (Princeton University Press, 2013).

[2]   S. Shen, *Topological insulators: dirac equation in condensed matter*, Springer Series in Solid-State Sciences (Springer Singapore, 2017).

[3]   C. Chamon, G. Chamon, L. Cugliandolo, M. Goerbig, and R. Moessner, *Topo-logical aspects of condensed matter physics: lecture notes of the les houches summer school. august 2014. volume 103* (Oxford University Press, 2016).

[4]   C. Chamon, M. Goerbig, R. Moessner, and L. Cugliandolo, *Topological aspects of condensed matter physics: lecture notes of the les houches summer school: volume 103, august 2014*, Lecture Notes of the Les Houches Summer School (OUP Oxford, 2017).

[5]   D. Tong, "Lectures on the Quantum Hall Effect", ArXiv e-prints (2016), arXiv:1606.06687 [hep-th].

[6]   M. O. Goerbig, "Quantum Hall Effects", ArXiv e-prints (2009), arXiv:0909.1998 [cond-mat.mes-hall].

[7]   R. Prange and S. Girvin, *The quantum hall effect*, Graduate texts in contem-porary physics (Springer-Verlag, 1987).

[8]   S. Das Sarma and A. Pinczuk, *Perspectives in quantum hall effects: novel quantum liquids in low-dimensional semiconductor structures* (Wiley, 2008).

[9]   K. v. Klitzing, G. Dorda, and M. Pepper, "New method for high-accuracy de-termination of the fine-structure constant based on quantized hall resistance", Phys. Rev. Lett. **45**, 494–497 (1980).

[10]   K. von Klitzing, "Quantum hall effect: discovery and application", Annual Review of Condensed Matter Physics **8**, 13–30 (2017), eprint: https://doi.org/10.1146/annurev-conmatphys-031016-025148.

[11]   M. Büttiker, "Capacitance, admittance, and rectification properties of small conductors", J. Phys.: Condens. Matter **5**, 9361 (1993).

[12]   M. Büttiker, H. Thomas, and A. Prêtre, "Mesoscopic capacitors", Phys. Lett. A **180**, 364 (1993).

[13]   G. Fève et al., "An On-Demand Coherent Single-Electron Source", Science **316**, 1169 (2007).

[14]   J. Dubois et al., "Minimal-excitation states for electron quantum optics using levitons", Nature (London) **502**, 659 (2013).

[15]   E. Bocquillon et al., "Electron Quantum Optics: Partitioning Electrons One by One", Phys. Rev. Lett. **108**, 196803 (2012).

[16] E. Bocquillon et al., "Coherence and Indistinguishability of Single Electrons Emitted by Independent Sources", Science **339**, 1054 (2013).

[17] E. Bocquillon et al., "Electron quantum optics in ballistic chiral conductors", Ann. Phys. (Berlin) **526**, 1–30 (2014).

[18] C. K. Hong, Z. Y. Ou, and L. Mandel, "Measurement of subpicosecond time intervals between two photons by interference", Phys. Rev. Lett. **59**, 2044 (1987).

[19] R. Hanbury Brown and R. Q. Twiss, "Correlation between photons in two coherent beams of light", Nature **177**, 27 (1956).

[20] S. Haroche, J. Raimond, and O. U. Press, *Exploring the quantum: atoms, cavities, and photons*, Oxford Graduate Texts (OUP Oxford, 2006).

[21] L. S. Levitov, H. Lee, and G. B. Lesovik, "Electron counting statistics and coherent states of electric current", J. Math. Phys. **37**, 4845 (1996).

[22] D. A. Ivanov, H. W. Lee, and L. S. Levitov, "Coherent states of alternating current", Phys. Rev. B **56**, 6839 (1997).

[23] J. Keeling, I. Klich, and L. S. Levitov, "Minimal Excitation States of Electrons in One-Dimensional Wires", Phys. Rev. Lett. **97**, 116403 (2006).

[24] B. J. van Wees, H. van Houten, C. W. J. Beenakker, J. G. Williamson, L. P. Kouwenhoven, D. van der Marel, and C. T. Foxon, "Quantized conductance of point contacts in a two-dimensional electron gas", Phys. Rev. Lett. **60**, 848–850 (1988).

[25] C. W. J. Beenakker and M. Büttiker, "Suppression of shot noise in metallic diffusive conductors", Phys. Rev. B **46**, 1889–1892 (1992).

[26] M. Reznikov, M. Heiblum, H. Shtrikman, and D. Mahalu, "Temporal correlation of electrons: suppression of shot noise in a ballistic quantum point contact", Phys. Rev. Lett. **75**, 3340–3343 (1995).

[27] D. A. Wharam et al., "One-dimensional transport and the quantisation of the ballistic resistance", Journal of Physics C: Solid State Physics **21**, L209 (1988).

[28] T. Jullien, P. Roulleau, B. Roche, A. Cavanna, Y. Jin, and D. C. Glattli, "Quantum tomography of an electron", Nature (London) **514**, 603 (2014).

[29] V. Freulon, A. Marguerite, J.-M. Berroir, B. Plaçais, A. Cavanna, Y. Jin, and G. Fève, "Hong-Ou-Mandel experiment for temporal investigation of single-electron fractionalization", Nat. Commun. **6**, 6854 (2015).

[30] A. Marguerite et al., "Decoherence and relaxation of a single electron in a one-dimensional conductor", Phys. Rev. B **94**, 115311 (2016).

[31] D. C. Glattli and P. Roulleau, "Hanbury-Brown Twiss noise correlation with time controlled quasi-particles in ballistic quantum conductors", Phys. E **76**, 216 (2016).

[32] R. J. Glauber, "The Quantum Theory of Optical Coherence", Phys. Rev. **130**, 2529 (1963).

[33] C. Grenier, R. Hervé, G. Fève, and P. Degiovanni, "Electron quantum optics in quantum Hall edge channels", Mod. Phys. Lett. B, 1053 (2011).

[34] T. Giamarchi, *Quantum physics in one dimension* (Oxford University Press, Oxford, 2003).

[35] E. Miranda, "Introduction to bosonization", Braz. J. Phys. **33**, 3 (2003).

[36] J. von Delft and H. Schoeller, "Bosonization for beginners - refermionization for experts", Ann. Phys. (Leipzig) **7**, 225 (1998).

[37] J. P. Eisenstein and H. L. Stormer, "The fractional quantum hall effect", Science **248**, 1510–1516 (1990), eprint: `http://science.sciencemag.org/content/248/4962/1510.full.pdf`.

[38] D. C. Tsui, H. L. Stormer, and A. C. Gossard, "Two-dimensional magneto-transport in the extreme quantum limit", Phys. Rev. Lett. **48**, 1559–1562 (1982).

[39] C. Nayak, S. H. Simon, A. Stern, M. Freedman, and S. Das Sarma, "Non-abelian anyons and topological quantum computation", Rev. Mod. Phys. **80**, 1083–1159 (2008).

[40] L. Saminadayar, D. C. Glattli, Y. Jin, and B. Etienne, "Observation of the $e/3$ Fractionally Charged Laughlin Quasiparticle", Phys. Rev. Lett. **79**, 2526 (1997).

[41] R. de-Picciotto, M. Reznikov, M. Heiblum, V. Umansky, G. Bunin, and D. Mahalu, "Direct observation of a fractional charge", **389**, 162–164 (1997).

[42] M. Reznikov, R. D. Picciotto, T. G. Griffiths, M. Heiblum, and V. Umansky, "Observation of quasiparticles with one-fifth of an electron's charge", **399**, 238–241 (1999).

[43] F. Wilczek, "Quantum mechanics of fractional-spin particles", Phys. Rev. Lett. **49**, 957–959 (1982).

[44] B. I. Halperin, "Statistics of quasiparticles and the hierarchy of fractional quantized hall states", Phys. Rev. Lett. **52**, 1583–1586 (1984).

[45] D. Arovas, J. R. Schrieffer, and F. Wilczek, "Fractional statistics and the quantum hall effect", Phys. Rev. Lett. **53**, 722–723 (1984).

[46] X. G. Wen, "Chiral Luttinger liquid and the edge excitations in the fractional quantum Hall states", Phys. Rev. B **41**, 12838 (1990).

[47] X.-G. Wen, "Topological orders and edge excitations in fractional quantum Hall states", Adv. Phys. **44**, 405 (1995).

[48] A. M. Chang, "Chiral luttinger liquids at the fractional quantum hall edge", Rev. Mod. Phys. **75**, 1449–1505 (2003).

[49] E. Wigner, "On the interaction of electrons in metals", Phys. Rev., 1002 (1934).

[50] F. Giazotto and M. J. Martínez-Pérez, "The Josephson heat interferometer", Nature (London) **492**, 401 (2012).

[51] S. Jezouin, F. D. Parmentier, A. Anthore, U. Gennser, A. Cavanna, Y. Jin, and F. Pierre, "Quantum Limit of Heat Flow Across a Single Electronic Channel", Science **342**, 601 (2013).

[52] M. Banerjee, M. Heiblum, A. Rosenblatt, Y. Oreg, D. E. Feldman, A. Stern, and V. Umansky, "Observed quantization of anyonic heat flow", Nature (London) **545**, 75 (2017).

175

[53] M. Banerjee, M. Heiblum, V. Umansky, D. E. Feldman, Y. Oreg, and A. Stern, "Observation of half-integer thermal hall conductance", Nature **559**, 205 (2018).

[54] L. Vannucci, F. Ronetti, J. Rech, D. Ferraro, T. Jonckheere, T. Martin, and M. Sassetti, "Minimal excitation states for heat transport in driven quantum Hall systems", Phys. Rev. B **95**, 245415 (2017).

[55] F. Ronetti, L. Vannucci, D. Ferraro, T. Jonckheere, J. Rech, T. Martin, and M. Sassetti, "Crystallization of levitons in the fractional quantum hall regime", Phys. Rev. B **98**, 075401 (2018).

[56] D. Ferraro et al., "Hong-ou-mandel characterization of multiply charged levitons", European Physics Journal (2018).

[57] L. Vannucci, F. Ronetti, G. Dolcetto, M. Carrega, and M. Sassetti, "Interference-induced thermoelectric switching and heat rectification in quantum Hall junctions", Phys. Rev. B **92**, 075446 (2015).

[58] F. Ronetti, L. Vannucci, G. Dolcetto, M. Carrega, and M. Sassetti, "Spin-thermoelectric transport induced by interactions and spin-flip processes in two-dimensional topological insulators", Phys. Rev. B **93**, 165414 (2016).

[59] F. Ronetti, M. Carrega, D. Ferraro, J. Rech, T. Jonckheere, T. Martin, and M. Sassetti, "Polarized heat current generated by quantum pumping in two-dimensional topological insulators", Phys. Rev. B **95**, 115412 (2017).

[60] L. Vannucci, F. Ronetti, D. Ferraro, J. Rech, T. Jonckheere, T. Martin, and M. Sassetti, "Photoassisted shot noise spectroscopy at fractional filling factor", Journal of Physics: Conference Series **969**, 012143 (2018).

[61] D. Ferraro, F. Ronetti, J. Rech, T. Jonckheere, M. Sassetti, and T. Martin, "Enhancing photon squeezing one leviton at a time", Phys. Rev. B **97**, 155135 (2018).

[62] R. B. Laughlin, "Anomalous Quantum Hall Effect: An Incompressible Quantum Fluid with Fractionally Charged Excitations", Phys. Rev. Lett. **50**, 1395 (1983).

[63] L. Landau and E. Lifshitz, *Statistical physics*, v. 5 (Elsevier Science, 2013).

[64] L. Landau and E. Lifshitz, *Quantum mechanics: non-relativistic theory*, Course of Theoretical Physics (Elsevier Science, 1981).

[65] B. I. Halperin, "Quantized hall conductance, current-carrying edge states, and the existence of extended states in a two-dimensional disordered potential", Phys. Rev. B **25**, 2185–2190 (1982).

[66] H. Bruus, K. Flensberg, and O. U. Press, *Many-body quantum theory in condensed matter physics: an introduction*, Oxford Graduate Texts (OUP Oxford, 2004).

[67] M. Büttiker, Y. Imry, R. Landauer, and S. Pinhas, "Generalized many-channel conductance formula with application to small rings", Phys. Rev. B **31**, 6207–6215 (1985).

[68] D. C. Tsui, "Nobel lecture: interplay of disorder and interaction in two-dimensional electron gas in intense magnetic fields", Rev. Mod. Phys. **71**, 891–895 (1999).

[69] P. W. Anderson, "Absence of diffusion in certain random lattices", Phys. Rev. **109**, 1492–1505 (1958).

[70] D. J. Thouless, M. Kohmoto, M. P. Nightingale, and M. den Nijs, "Quantized hall conductance in a two-dimensional periodic potential", Phys. Rev. Lett. **49**, 405–408 (1982).

[71] M. Kohmoto, "Topological invariant and the quantization of the Hall conductance", Annals of Physics **160**, 343–354 (1985).

[72] R. B. Laughlin, "Nobel lecture: fractional quantization", Rev. Mod. Phys. **71**, 863–874 (1999).

[73] H. L. Stormer, D. C. Tsui, and A. C. Gossard, "The fractional quantum Hall effect", Rev. Mod. Phys. **71**, S298 (1999).

[74] E. Y. Andrei, G. Deville, D. C. Glattli, F. I. B. Williams, E. Paris, and B. Etienne, "Observation of a magnetically induced wigner solid", Phys. Rev. Lett. **60**, 2765–2768 (1988).

[75] A. Zee, "Quantum hall fluids", in Field theory, topology and condensed matter physics, edited by H. B. Geyer (1995), pp. 99–153.

[76] G. V. Dunne, "Aspects of chern-simons theory", in Aspects topologiques de la physique en basse dimension. topological aspects of low dimensional systems, edited by A. Comtet, T. Jolicœur, S. Ouvry, and F. David (1999).

[77] E. Witten, "Three lectures on topological phases of matter", Riv. Nuovo Cimento **39**, 313 (2016).

[78] A. Lopez and E. Fradkin, "Universal structure of the edge states of the fractional quantum hall states", Phys. Rev. B **59**, 15323 (1999).

[79] V. G. Kac, *Infinite-dimensional lie algebras*, 3rd ed. (Cambridge University Press, 1990).

[80] S. Tomonaga, "Remarks on bloch's method of sound waves applied to many-fermion problems", Progress of Theoretical Physics **5**, 544–569 (1950), eprint: `/oup/backfile/content_public/journal/ptp/5/4/10.1143/ptp/5.4.544/2/5-4-544.pdf`.

[81] J. M. Luttinger, "An exactly soluble model of a many-fermion system", J. Math. Phys. **4**, 1154 (1963).

[82] D. C. Mattis, "Exact solution of a many-fermion system and its associated boson field", J. Math. Phys. **6**, 304 (1965).

[83] F. D. M. Haldane, "Luttinger liquid theory of one-dimensional quantum fluids. i. properties of the luttinger model and their extension to the general 1d interacting spinless fermi gas", J. Phys. C: Solid State Phys. **14**, 2585 (1981).

[84] C. de C. Chamon, D. E. Freed, and X. G. Wen, "Nonequilibrium quantum noise in chiral Luttinger liquids", Phys. Rev. B **53**, 4033 (1996).

[85] J. Dubois, T. Jullien, C. Grenier, P. Degiovanni, P. Roulleau, and D. C. Glattli, "Integer and fractional charge Lorentzian voltage pulses analyzed in the framework of photon-assisted shot noise", Phys. Rev. B **88**, 085301 (2013).

[86] C. Grenier, J. Dubois, T. Jullien, P. Roulleau, D. C. Glattli, and P. Degiovanni, "Fractionalization of minimal excitations in integer quantum Hall edge channels", Phys. Rev. B **88**, 085302 (2013).

[87] M. Misiorny, G. Fève, and J. Splettstoesser, "Shaping charge excitations in chiral edge states with a time-dependent gate voltage", Phys. Rev. B **97**, 075426 (2018).

[88] D. C. Glattli and P. Roulleau, "Levitons for electron quantum optics", Phys. Status Solidi B **254**, 1600650 (2017).

[89] C. Bauerle et al., "Coherent control of single electrons: a review of current progress", Rep. Prog. Phys. **81**, 056503 (2018).

[90] M. Moskalets, "Noise of a single-electron emitter", Phys. Rev. B **88**, 035433 (2013).

[91] F. D. Parmentier et al., "Current noise spectrum of a single-particle emitter: theory and experiment", Phys. Rev. B **85**, 165438 (2012).

[92] D. Ferraro, J. Rech, T. Jonckheere, and T. Martin, "Single quasiparticle and electron emitter in the fractional quantum Hall regime", Phys. Rev. B **91**, 205409 (2015).

[93] M. Moskalets, "Fractionally Charged Zero-Energy Single-Particle Excitations in a Driven Fermi Sea", Phys. Rev. Lett. **117**, 046801 (2016).

[94] M. Moskalets, "First-order correlation function of a stream of single-electron wave packets", Phys. Rev. B **91**, 195431 (2015).

[95] D. C. Glattli and P. Roulleau, "Pseudorandom binary injection of levitons for electron quantum optics", Phys. Rev. B **97**, 125407 (2018).

[96] D. Dasenbrook and C. Flindt, "Dynamical generation and detection of entanglement in neutral leviton pairs", Phys. Rev. B **92**, 161412 (2015).

[97] D. Dasenbrook, J. Bowles, J. B. Brask, P. Hofer, C. Flindt, and N. Brunner, "Single-electron entanglement and nonlocality", New J. Phys. **18**, 043036 (2016).

[98] D. Dasenbrook and C. Flindt, "Dynamical Scheme for Interferometric Measurements of Full-Counting Statistics", Phys. Rev. Lett. **117**, 146801 (2016).

[99] C. Grenier et al., "Single-electron quantum tomography in quantum Hall edge channels", New J. Phys. **13**, 093007 (2011).

[100] D. Ferraro et al., "Wigner function approach to single electron coherence in quantum Hall edge channels", Phys. Rev. B **88**, 205303 (2013).

[101] D. Ferraro, B. Roussel, C. Cabart, E. Thibierge, G. Fève, C. Grenier, and P. Degiovanni, "Real-Time Decoherence of Landau and Levitov Quasiparticles in Quantum Hall Edge Channels", Phys. Rev. Lett. **113**, 166403 (2014).

[102] S. Ol'khovskaya, J. Splettstoesser, M. Moskalets, and M. Büttiker, "Shot noise of a mesoscopic two-particle collider", Phys. Rev. Lett. **101**, 166802 (2008).

[103] G. Rosselló, F. Battista, M. Moskalets, and J. Splettstoesser, "Interference and multiparticle effects in a mach-zehnder interferometer with single-particle sources", Phys. Rev. B **91**, 115438 (2015).

[104] T. Martin, "Noise in mesoscopic physics", in *Nanophysics: coherence and transport. les houches session lxxxi*, edited by H. Bouchiat, Y. Gefen, S. Guéron, G. Montambaux, and J. Dalibard (Elsevier, Amsterdam, 2005), pp. 283–359.

[105] M. Moskalets, "Single-particle shot noise at nonzero temperature", Phys. Rev. B **96**, 165423 (2017).

[106] T. Jonckheere, J. Rech, C. Wahl, and T. Martin, "Electron and hole Hong-Ou-Mandel interferometry", Phys. Rev. B **86**, 125425 (2012).

[107] D. Ferraro, C. Wahl, J. Rech, T. Jonckheere, and T. Martin, "Electronic hong-ou-mandel interferometry in two-dimensional topological insulators", Phys. Rev. B **89**, 075407 (2014).

[108] C. Wahl, J. Rech, T. Jonckheere, and T. Martin, "Interactions and Charge Fractionalization in an Electronic Hong-Ou-Mandel Interferometer", Phys. Rev. Lett. **112**, 046802 (2014).

[109] C. Cabart, B. Roussel, G. Fève, and P. Degiovanni, "Taming electronic decoherence in 1D chiral ballistic quantum conductors", ArXiv e-prints (2018), arXiv:1804.04054 [cond-mat.mes-hall].

[110] I. S. Gradshteyn and I. M. Ryzhik, *Table of integrals, series, and products*, 7th ed. (Academic Press, San Diego, 2007).

[111] D. Glattli and P. Roulleau, "Hanbury-brown twiss noise correlation with time controlled quasi-particles in ballistic quantum conductors", Physica E: Low-dimensional Systems and Nanostructures **76**, 216 –222 (2016).

[112] Y. M. Blanter and M. Büttiker, "Shot noise in mesoscopic conductors", Phys. Rep. **336**, 1–166 (2000).

[113] Y. Nazarov and Y. Blanter, *Quantum transport: introduction to nanoscience* (Cambridge University Press, 2009).

[114] G. B. Lesovik and I. A. Sadovskyy, "Scattering matrix approach to the description of quantum electron transport", Physics-Uspekhi **54**, 1007 (2011).

[115] J. Rech, D. Ferraro, T. Jonckheere, L. Vannucci, M. Sassetti, and T. Martin, "Minimal Excitations in the Fractional Quantum Hall Regime", Phys. Rev. Lett. **118**, 076801 (2017).

[116] C. L. Kane and M. P. A. Fisher, "Nonequilibrium noise and fractional charge in the quantum Hall effect", Phys. Rev. Lett. **72**, 724 (1994).

[117] C. L. Kane and M. P. A. Fisher, "Transport in a one-channel luttinger liquid", Phys. Rev. Lett. **68**, 1220–1223 (1992).

[118] C. L. Kane and M. P. A. Fisher, "Thermal Transport in a Luttinger Liquid", Phys. Rev. Lett. **76**, 3192 (1996).

[119] G. Dolcetto, S. Barbarino, D. Ferraro, N. Magnoli, and M. Sassetti, "Tunneling between helical edge states through extended contacts", Phys. Rev. B **85**, 195138 (2012).

[120] J. Voit, "One-dimensional Fermi liquids", Rep. Prog. Phys. **58**, 977 (1995).

[121] C. Chamon, D. E. Freed, S. A. Kivelson, S. L. Sondhi, and X. G. Wen, "Two point-contact interferometer for quantum Hall systems", Phys. Rev. B **55**, 2331 (1997).

[122] C. L. Kane and M. P. A. Fisher, "Quantized thermal transport in the fractional quantum hall effect", Phys. Rev. B **55**, 15832–15837 (1997).

[123] W. Schottky, "Über spontane Stromschwankungen in verschiedenen Elektrizitätsleitern", Ann. Phys. **362**, 541 (1918).

[124] R. de-Picciotto, M. Reznikov, M. Heiblum, V. Umansky, G. Bunin, and D. Mahalu, "Direct observation of a fractional charge", Nature (London) **389**, 162–164 (1997).

[125] M. Moskalets, "High-temperature fusion of a multi-electron leviton", arXiv:1801. 04787.

[126] D. C. Daniel, E. S. Lamb, P. Del'Haye, S. A. Diddams, and S. B. Papp, "Soliton crystals in kerr resonators", Nat. Photon. **11**, 671 (2017).

[127] G. Herink, F. Kurtz, B. Jalali, D. R. Solli, and C. Ropers, "Real-time spectral interferometry probes the internal dynamics of femtosecond soliton molecules", Science **356**, 50–54 (2017).

[128] K. Krupa, K. Nithyanandan, U. Andral, P. Tchofo-Dinda, and P. Grelu, "Real-time observation of internal motion within ultrafast dissipative optical soliton molecules", Phys. Rev. Lett. **118**, 243901 (2017).

[129] H. J. Schulz, "Wigner crystal in one dimension", Phys. Rev. Lett. **71**, 1864 (1993).

[130] V. V. Deshpande and M. Bockrath, "The one-dimensional Wigner crystal in carbon nanotubes", Nature Physics **4** (2008) `10.1038/nphys895`.

[131] J.-J. Wang, W. Li, S. Chen, X. Gao, M. Rontani, and M. Polini, "Absence of Wigner molecules in one-dimensional few-fermion systems with short-range interactions", Phys. Rev. B **86**, 075110 (2012).

[132] S. Pecker, F. Kuemmeth, A. Secchi, M. Rontani, D. C. Ralph, P. L. McEuen, and S. Ilani, "Observation and spectroscopy of a two-electron Wigner molecule in an ultraclean carbon nanotube", Nature Physics **9**, 576 (2013).

[133] N. Traverso Ziani, F. Cavaliere, and M. Sassetti, "Temperature-induced emergence of Wigner correlations in a STM-probed one-dimensional quantum dot", New J. Phys. **15**, 063002 (2013).

[134] V. V. Deshpande, M. Bockrath, L. I. Glazman, and A. Yacoby, "Electron liquids and solids in one dimension", Nature **464**, 209 (2010).

[135] K. A. Matveev, "Conductance of a Quantum Wire in the Wigner-Crystal Regime", Phys. Rev. Lett. **92**, 106801 (2004).

[136] M. Rontani and E. Molinari, "Imaging quasiparticle wave functions in quantum dots via tunneling spectroscopy", Phys. Rev. B **71**, 233106 (2005).

[137] I. Shapir, A. Hamo, S. Pecker, C. Pascu Moca, Ö. Legeza, G. Zarand, and S. Ilani, "Imaging the Wigner Crystal of Electrons in One Dimension", ArXiv e-prints (2018), arXiv:1803.08523 `[cond-mat.mes-hall]`.

[138] D. Glattli and S. Roulleau, *Method and device for phase modulation of a carrier wave and application to the detection of multi-level phase-encoded digital signals*, WO Patent App. PCT/FR2016/050,193, 2016.

[139] Let us notice that the excess density backscattered into the lower, left-moving channel propagates rigidly towards left. Therefore, the temporal profile of $\Delta\rho_L(x,t)$ is identical for all positions $x < 0$ (apart from a constant delay).

[140] N. Traverso Ziani, F. Cavaliere, and M. Sassetti, "Signatures of Wigner correlations in the conductance of a one-dimensional quantum dot coupled to an AFM tip", Phys. Rev. B **86**, 125451 (2012).

[141] F. M. Gambetta, N. T. Ziani, F. Cavaliere, and M. Sassetti, "Correlation functions for the detection of Wigner molecules in a one-channel Luttinger liquid quantum dot", Europhys. Lett. **107**, 47010 (2014).

[142] F. Giazotto, T. T. Heikkilä, A. Luukanen, A. M. Savin, and J. P. Pekola, "Opportunities for mesoscopics in thermometry and refrigeration: Physics and applications", Rev. Mod. Phys. **78**, 217 (2006).

[143] R. Landauer, "Condensed-matter physics: The noise is the signal", Nat. Phys. **1**, 118–123 (2015).

[144] M. Esposito, U. Harbola, and S. Mukamel, "Nonequilibrium fluctuations, fluctuation theorems, and counting statistics in quantum systems", Rev. Mod. Phys. **81**, 1665–1702 (2009).

[145] M. Campisi, P. Hänggi, and P. Talkner, "*Colloquium*: Quantum fluctuation relations: Foundations and applications", Rev. Mod. Phys. **83**, 771 (2011).

[146] G. Benenti, G. Casati, K. Saito, and R. S. Whitney, "Fundamental aspects of steady-state conversion of heat to work at the nanoscale", arXiv:`1608.05595`.

[147] N. Li, J. Ren, L. Wang, G. Zhang, P. Hänggi, and B. Li, "Colloquium: phononics: manipulating heat flow with electronic analogs and beyond", Rev. Mod. Phys. **84**, 1045–1066 (2012).

[148] R. Sánchez, B. Sothmann, and A. N. Jordan, "Chiral Thermoelectrics with Quantum Hall Edge States", Phys. Rev. Lett. **114**, 146801 (2015).

[149] R. Sánchez, B. Sothmann, and A. N. Jordan, "Heat diode and engine based on quantum Hall edge states", New J. Phys. **17**, 075006 (2015).

[150] P. Samuelsson, S. Kheradsoud, and B. Sothmann, "Optimal quantum interference thermoelectric heat engine with edge states", arXiv:`1611.02997`.

[151] H. Thierschmann et al., "Three-terminal energy harvester with coupled quantum dots", Nat. Nanotechnol. **10**, 854 (2015).

[152] S. Juergens, F. Haupt, M. Moskalets, and J. Splettstoesser, "Thermoelectric performance of a driven double quantum dot", Phys. Rev. B **87**, 245423 (2013).

[153] M. F. Ludovico, J. S. Lim, M. Moskalets, L. Arrachea, and D. Sánchez, "Dynamical energy transfer in ac-driven quantum systems", Phys. Rev. B **89**, 161306 (2014).

[154] M. F. Ludovico, M. Moskalets, D. Sánchez, and L. Arrachea, "Dynamics of energy transport and entropy production in ac-driven quantum electron systems", Phys. Rev. B **94**, 035436 (2016).

[155] M. F. Ludovico, L. Arrachea, M. Moskalets, and D. Sánchez, "Probing the energy reactance with adiabatically driven quantum dots", Phys. Rev. B **97**, 041416 (2018).

[156] M. Carrega, P. Solinas, A. Braggio, M. Sassetti, and U. Weiss, "Functional integral approach to time-dependent heat exchange in open quantum systems: general method and applications", New J. Phys. **17**, 045030 (2015).

[157] M. Carrega, P. Solinas, M. Sassetti, and U. Weiss, "Energy Exchange in Driven Open Quantum Systems at Strong Coupling", Phys. Rev. Lett. **116**, 240403 (2016).

[158] M. Campisi, P. Talkner, and P. Hänggi, "Fluctuation Theorem for Arbitrary Open Quantum Systems", Phys. Rev. Lett. **102**, 210401 (2009).

[159] M. Campisi, J. Pekola, and R. Fazio, "Nonequilibrium fluctuations in quantum heat engines: theory, example, and possible solid state experiments", New J. Phys. **17**, 035012 (2015).

[160] M. Moskalets, "Floquet Scattering Matrix Theory of Heat Fluctuations in Dynamical Quantum Conductors", Phys. Rev. Lett. **112**, 206801 (2014).

[161] D. V. Averin and J. P. Pekola, "Violation of the Fluctuation-Dissipation Theorem in Time-Dependent Mesoscopic Heat Transport", Phys. Rev. Lett. **104**, 220601 (2010).

[162] G. Granger, J. P. Eisenstein, and J. L. Reno, "Observation of Chiral Heat Transport in the Quantum Hall Regime", Phys. Rev. Lett. **102**, 086803 (2009).

[163] C. Altimiras, H. le Sueur, U. Gennser, A. Cavanna, D. Mailly, and F. Pierre, "Tuning energy relaxation along quantum hall channels", Phys. Rev. Lett. **105**, 226804 (2010).

[164] C. Altimiras, H. le Sueur, U. Gennser, A. Anthore, A. Cavanna, D. Mailly, and F. Pierre, "Chargeless Heat Transport in the Fractional Quantum Hall Regime", Phys. Rev. Lett. **109**, 026803 (2012).

[165] S. H. Simon, "Interpretation of thermal conductance of the $\nu = 5/2$ edge", Phys. Rev. B **97**, 121406 (2018).

[166] C. Wang, A. Vishwanath, and B. I. Halperin, "Topological order from disorder and the quantized hall thermal metal: possible applications to the $\nu = 5/2$ state", Phys. Rev. B **98**, 045112 (2018).

[167] D. F. Mross, Y. Oreg, A. Stern, G. Margalit, and M. Heiblum, "Theory of disorder-induced half-integer thermal hall conductance", Phys. Rev. Lett. **121**, 026801 (2018).

[168] A. Crépieux and F. Michelini, "Mixed, charge and heat noises in thermoelectric nanosystems", J. Phys.: Condens. Matter **27**, 015302 (2014).

[169] A. Crépieux and F. Michelini, "Heat-charge mixed noise and thermoelectric efficiency fluctuations", J. Stat. Mech. **2016**, 054015 (2016).

[170] F. Battista, M. Moskalets, M. Albert, and P. Samuelsson, "Quantum heat fluctuations of single-particle sources", Phys. Rev. Lett. **110**, 126602 (2013).

[171] F. Battista, F. Haupt, and J. Splettstoesser, "Energy and power fluctuations in ac-driven coherent conductors", Phys. Rev. B **90**, 085418 (2014).

[172] F. Battista, F. Haupt, and J. Splettstoesser, "Correlations between charge and energy current in ac-driven coherent conductors", J. Phys.: Conf. Ser. **568**, 052008 (2014).

[173] M. Moskalets and G. Haack, "Heat and charge transport measurements to access single-electron quantum characteristics", Phys. Status Solidi B **254**, 1600616 (2017).

[174] G. Cuniberti, M. Sassetti, and B. Kramer, "ac conductance of a quantum wire with electron-electron interactions", Phys. Rev. B **57**, 1515 (1998).

[175] D. Ferraro, A. Braggio, N. Magnoli, and M. Sassetti, "Neutral modes' edge state dynamics through quantum point contacts", New J. Phys. **12**, 013012 (2010).

[176] M. P. A. Fisher and L. I. Glazman, "Transport in a one-dimensional Luttinger liquid", in *Mesoscopic electron transport*, edited by L. L. Sohn, L. P. Kouwenhoven, and G. Schön, NATO ASI Series E (Kluwer Academic Publishers, Dordrecht, 1997), pp. 331–373.

[177] P. Eyméoud and A. Crépieux, "Mixed electrical-heat noise spectrum in a quantum dot", Phys. Rev. B **94**, 205416 (2016).

[178] D. Chevallier, J. Rech, T. Jonckheere, C. Wahl, and T. Martin, "Poissonian tunneling through an extended impurity in the quantum Hall effect", Phys. Rev. B **82**, 155318 (2010).

[179] J. K. Jain, "Composite-fermion approach for the fractional quantum hall effect", Phys. Rev. Lett. **63**, 199–202 (1989).

[180] R. Willett, J. P. Eisenstein, H. L. St
ormer, D. C. Tsui, A. C. Gossard, and J. H. English, "Observation of an even-denominator quantum number in the fractional quantum hall effect", Phys. Rev. Lett. **59**, 1776–1779 (1987).

[181] V. Venkatachalam, S. Hart, L. Pfeiffer, K. West, and A. Yacoby, "Local thermometry of neutral modes on the quantum Hall edge", Nat. Phys. **8**, 676 (2012).

[182] I. Gurman, R. Sabo, M. Heiblum, V. Umansky, and D. Mahalu, "Extracting net current from an upstream neutral mode in the fractional quantum Hall regime", Nat. Commun. **3**, 1289 (2012).

[183] B. A. Bernevig, T. L. Hughes, and S.-C. Zhang, "Quantum spin hall effect and topological phase transition in hgte quantum wells", Science **314**, 1757–1761 (2006), eprint: `http://science.sciencemag.org/content/314/5806/1757.full.pdf`.

[184] M. König et al., "Quantum spin hall insulator state in hgte quantum wells", Science **318**, 766–770 (2007), eprint: `http://science.sciencemag.org/content/318/5851/766.full.pdf`.

[185] M. König, H. Buhmann, L. W. Molenkamp, T. Hughes, C.-X. Liu, X.-L. Qi, and S.-C. Zhang, "The quantum spin hall effect: theory and experiment", Journal of the Physical Society of Japan **77**, 031007 (2008), eprint: `https://doi.org/10.1143/JPSJ.77.031007`.

[186] M. Kapfer, P. Roulleau, I. Farrer, D. A. Ritchie, and D. C. Glattli, "The Josephson frequency of fractionally charged anyons", ArXiv e-prints (2018), arXiv:1806.03117 `[cond-mat.mes-hall]`.

[187] M. N. Berberan-Santos, "Green's function method and the first-order linear differential equation", Journal of Mathematical Chemistry **48**, 175–178 (2010).

[188] P. Zanghì, *Appunti di metodi matematici della fisica* (Università degli studi di Genova).